Title	Effects of exogenous B-cell immunoglobulin binding protein (BIP) and BIP protein inducer X (BIX) on myelination
Author(s)	Bandla, Sravanthi
Publication Date	2019-12-12
Publisher	NUI Galway
Item record	http://hdl.handle.net/10379/15649

EFFECTS OF EXOGENOUS B-CELL IMMUNOGLOBULIN BINDING PROTEIN (BIP) AND BIP PROTEIN INDUCER X (BIX) ON MYELINATION

Sravanthi Bandla

Galway Neuroscience Centre and School of Natural Sciences

National University of Ireland, Galway

A thesis submitted to the National University of Ireland, Galway in fulfilment of the requirement for the degree of Doctor of Philosophy

November 2019

DECLARATION

This dissertation is the result of my own work and work done in collaboration as specifically mentioned in the text. It has not been previously submitted in part or whole to any university or institution for any degree, diploma or other qualification.

Signed:

_____

Nov-2019

Date:

_____

Sravanthi Bandla, MPharm, MSc

NUI Galway

Abstract

B-cell immunoglobulin binding protein (BiP) is an essential endoplasmic reticulum (ER) chaperone that belongs to the Hsp70 family, normally found in the ER lumen. However, BiP also has other extracellular and intracellular functions. As it is unclear whether peripheral BiP always has a signal and/or ER retention sequence and the possibility that different variants of BiP could have differing biochemical impacts, we produced and biochemically characterised four variants of BiP (see Chapter 3). The variants differed depending on the presence or the absence of signal and ER retention peptides. BiP variants were purified using nickel affinity chromatography, and protein size and quality were assessed using SDS/PAGE gels. In addition, we characterised the nucleotide-binding properties of variants in the absence and the presence of divalent cations $Mg2^+$, $Mn2^+$, and $Ca2^+$. Interestingly, in the absence of cations, ADP has a higher binding affinity for BiP than ATP. The presence of divalent cations results in a decrease of the K_d values of both ADP and ATP, indicating higher affinities of both nucleotides for BiP. ATPase assays were carried out to study the enzyme activity of these variants and to characterise kinetic parameters. Variants with the signal sequence had higher specific activities than those without. Both Mg^{2+} and Mn^{2+} efficiently stimulated the ATPase activity of these variants at low micromolar concentrations, whereas calcium failed to stimulate BiP ATPase. Our novel findings indicate the potential functionality of the BiP signal sequence, and also reveal the effect of physiological concentrations of cations on the nucleotide-binding properties and enzyme activities of all variants.

Studies have shown that BiP is essential for the survival of oligodendrocytes and is upregulated during developmental myelination. We hypothesized that the exogenous addition of BiP would enhance myelination in multiple sclerosis (Chapter 4). To address this, preliminary experiments to study the uptake of BiP by cells were conducted by adding FITC-labelled BiP to B104 neuroblastoma cells and spinal cord myelinating cultures. These experiments confirmed that

BiP was taken up by cells in a dose- and time-dependent manner. In addition, the dose-dependent effects of unlabelled BiP were assessed and a dose of 20 µg/ml was selected for all other experiments. BiP was found to have no effect on myelination but increased the microglia number 2.5 times. This effect could be possibly due to BiP acting on cells directly, however heat inactivation experiments of BiP should be conducted to differentiate the effects of the protein from the endotoxins. Our results suggest that BiP could be detrimental as well. In an alternative approach (described in Chapter 5), we induced the expression of BiP using a chemical inducer of BiP (BIX). As the use of BIX in spinal cord myelinating cultures is not established before, we performed dose-dependent effects using BIX and 5 µg/ml of dose was used for further experiments. Surprisingly BIX had a detrimental effect on the microglia, oligodendrocytes, and myelin. We performed RNA sequencing to study the differentially expressed genes and used the Reactome pathway browser to identify the pathways possibly involved in the BIX effects observed. The genes related to oligodendrocytes and microglia were found to be downregulated, confirming the observed toxicity of BIX towards these cell populations. Astrocytes and neurons related genes were also down regulated but they seem to be resistant compared to oligodendrocytes and microglia. Additionally, the top 25 most upregulated and downregulated pathways suggested that BIX interferes with the cell cycle, cell division, metabolism, and apoptosis. BIX exerted similar effects when added to organotypic slice cultures, suggesting that the effects of BIX are reproducible in a different model of myelination. Neither BiP nor BIX proved to be therapeutic in our culture models. The application of BIX as a therapeutic should be pursued with caution. Our results highlight the need for further investigation of BiP's therapeutic potential within the context of myelinating disorders.

Acknowledgements

List of Figures

List of tables

Abbreviations and Acronyms

ABCG2: Binding cassette subfamily G member 2

AGR2: Anterior gradient 2

ALDH1A1: Aldehyde dehydrogenase 1 family member A1

ANLN: Anillin actin-binding protein

AQP4: Aquaporin 4

ASK1: Apoptosis signal-regulating kinase 1

ASNS: Asparagine Synthetase (Glutamine-hydrolysing)

ATF2: Activating transcription factor 2

ATF4: Activated transcription factor 4

ATF6: Activating transcription factor 6

ATF6b: Activating transcription factor 6 beta

BAD: Bcl2 associated agonist of cell death

BAK1: Bcl2 antagonist/killer 1

BAPTA-AM: 1, 2-Bis (2-aminophenoxy) ethane-N, N, N, N-tetraacetic acid tetrakis (acetoxymethyl ester)

BAX: Bcl2 associated X

BBB: Blood-brain barrier

BID: BH3 interacting domain death agonist

BIP: B cell immunoglobulin binding protein

BIX: BiP inducer X

BMS: Benign multiple sclerosis

BOK: Bcl-2 related ovarian killer

C1QA: Complement C1q A chain

C1QB: Complement C1q B chain

C1QC: Complement C1q C chain

C3AR1: Complement C3a receptor 1

CBF: C-repeated binding factor

CCL4: C-C Motif chemokine ligand 4

CCNA2: Cyclin A2

CD: Cluster of differentiation

CD300A: Cluster of differentiation 300 a

CHOP: C/EBP homologous protein

CHRNA5: Cholinergic Receptor Nicotinic Alpha 5 subunit

CIS: Clinically isolated syndrome

COMP: Cartilage Oligomeric matrix protein

COPII: Cytoplasmic coat protein complex II

COPS5: COP9 Signalosome Subunit 5

CREB: cAMP-responsive element CRE-like

CREB3: Cyclic AMP responsive element-binding protein 3

CSF: Cerebrospinal fluid

CSF1R: Colony-stimulating factor 1 receptor

CX3CR1: CXC3 chemokine receptor 1

DAMP: Danger associated molecular pattern

DIV: Day *in-vitro*

DMSO: Dimethyl sulfoxide

EAE: Experimental autoimmune encephalomyelitis

EDEM: Endoplasmic reticulum degradation-enhancing alpha-mannosidase-like 1

EGFR: Epidermal growth factor tyrosine kinase

EIF2α: Eukaryotic translation initiation factor 2α

ENPP6: Ectonucleotide pyrophosphatase/phosphodiesterase 6

EP300: E1A Binding Protein P300

EP300: E1A binding protein P300

ER: Endoplasmic reticulum

ERAD: Endoplasmic reticulum-associated degradation

ERdj4: Endoplasmic reticulum localised DnaJ 4

FA2H: Fatty acid 2-hydroxylase

FADD: Fas-associated protein with death domain

FAM180a: Family with sequence similarity 180 member

FICD: FIC domain containing

GABRG2: Gamma-aminobutyric acid type A receptor gamma2 subunit

GADD153: Growth arrest and DNA-dependent damage 153

GADD153: Growth arrest and DNA-dependent damage 153

GCHFR: GTP cyclohydrolase 1 feedback regulator

GCs: Granule cells

GFAP: Glial Fibrillary acid protein

GJB6: Gap junction protein beta 6

GL: Granular layer

GPR17: G protein-coupled receptor 17

GPR183: G protein-coupled receptor 183

GRP: Glucose-regulated proteins

GRP17: Glycine rich protein 17

GRP170: Glucose-regulated protein 170

GRP94: Glucose-regulated protein 94

GTP: Guanosine triphosphate

HEDJ: Human endoplasmic reticulum-associated DNAJ

HEPES: N-(2-Hydroxyethyl) piperazine-N-(2-ethanesulfonic acid)

HM: Human monocytes

HMBC: Human peripheral blood monocytes

HRP: Horseradish peroxidase

HSP70: Heat shock protein 70

HSPA5: Heat Shock 70kDa protein 5

IFNγ: Interferon

Ig: Immunoglobulin

IGF-1R: Insulin-like growth factor receptor 1

IKK: I kappa B kinase

IL-: Interleukin

IRE1: Inositol requiring enzyme 1

JNK: c-Jun N-terminal kinase

K5: Kringle 5

KIF11: Kinesin family member 11

KLK6: Kallikrein related peptidase 6

LAPTM5: Lysosomal protein transmembrane 5

LDLR: low-density lipoprotein

LIMS2: LIM zinc finger domain containing 2

LPIN3: Lipin family member

LPS: Lipopolysaccharides

LRP: Low-density lipoprotein receptor-related protein

MAG: Myelin associated glycoprotein

MAIT: Mucosal-associated invariant T cells

MAPK: Mitogen-activated protein kinase

MBP: Myelin basic protein

MHC: Major histocompatibility complex

MICA: MHC1 class 1-related polypeptide 1

ML: Molecular layer

MOG: Myelin oligodendrocyte glycoprotein

MRI: magnetic resonance imaging

MS: Multiple Sclerosis

MT1: Metallothionein 1

MTJ1: J domain of the murine transmembrane protein

MTOR: mammalian target of rapamycin

NAGM: Normal appearing grey matter

NAWM: Normal appearing white matter

NBD: Nucleotide-binding domain

NCK1: NCK adapter protein 1

NCK2: NCK adapter protein 2

NELL1: Neural EGFL like 1

NFE212: Nuclear factor, erythroid 2 like 2

NF-Y: Nuclear transcription factor-Y

NF-κB: Nuclear factor light chain enhancer of activated B cells

NKG2D: Natural killer group 2D receptors

NMDA: N-methyl-D-aspartate

NMR: Nuclear magnetic resonance

NUSAP1: Nucleolar and spindle associated protein 1

OPALIN: Oligodendrocyte myelin paranodal and inner loop protein

P58IPK/DNAJC3: DnaJ heat shock protein family (HSP40) member c3

Par-4: Prostate apoptosis response- 4

PC: Purkinje cells

PCL: Purkinje cell layer

PDI: Protein disulphide-isomerase

PDIA6: Protein Disulfide Isomerase family A member 6

PERK: Protein kinase RNA (PKR)-like ER kinase

PFA: Paraformaldehyde

PI3K: Phosphoinositide 3-kinase

PLL: Poly-L-Lysine hydrobromide

PLP1: Proteolipid protein 1

PNLIP: Pancreatic lipase

PPM1J: Protein Phosphatase, Mg^{2+}/ Mn^{2+} dependent 1J

PPMS: Primary progressive multiple sclerosis

PTAFR: Platelet-activating factor receptor

PTPN1: Protein tyrosine phosphate non-receptor type 1

RAMP: Resolution-associated molecular pattern

RAMP: Ribosome-associated membrane protein 4

RIDD: Regulated Ire-1 dependent decay

RIS: Radiologically isolated syndrome

RRMS: Relapsing-remitting multiple sclerosis

S1P: site 1 protease

S2P: site 2 proteases

SBD: Substrate-binding domain

SDS: Sodium dodecyl sulfate

SLC25A18: Solute carrier family 25-member 18 protein-encoding gene

SMC2: Structural maintenance of chromosomes protein 2

SPMS: Secondary progressive multiple sclerosis

SRP: Signal recognition peptide

TAC3: Tachykinin-3

TACC3: Transforming acidic coiled-coil containing protein 3

TCF712: Transcription factor 7-like 2

TEMED: Tetramethylethylenediamine

TESC: Tescalcin

TF1: Tissue factor 1

TFB: Transformation buffer

TFII: General transcription factor II-I

TLR: Toll-like receptor

TMEM125: Transmembrane protein125

TMEM130: Transmembrane protein 130

TMEM33: Transmembrane protein 33

TNF: Tumor necrosis factor

TOP2: DNA topoisomerase II alpha

TRAF2: Tumour necrosis factor α receptor-associated factor 2

TRAIL- TNF-related apoptosis-inducing ligand

TREM2: Triggering receptor expressed on myeloid cells 2

TUNEL: Terminal deoxynucleotide transferase dUTP nick end labeling

UPAR: Urokinase plasminogen activator surface receptor
UPR: Unfolded protein response
VEP: Visual evoked potential
WFS1: Wolframin ER transmembrane glycoprotein
WML: White matter layer
WNT: Wingless-related integration site
XBP1: X-box Binding Protein-1
YB1: Y-box binding protein 1
YY1: Yin-Yang 1
PDIA5: Protein disulphide isomerase family a member 5
CALR3: Calreticulin 3

Chapter 1 : Introduction

1.1 Multiple sclerosis

Multiple sclerosis (MS) is one of the most debilitating chronic inflammatory disorders of the central nervous system (CNS) in which focal lymphocytic infiltration causes damage to myelin and axons. The lesions can develop in various parts of the CNS, spinal cord, brain stem, and optic nerve. The lesions can be easily identified in the white matter as areas of demyelination, inflammation and glial reaction (Reich et al., 2018). MS is the most common cause of non-traumatic neurological disability in young adults. The pathological hallmarks of MS include plaques of inflammatory demyelination and damage to axons. MS is not limited to white matter, it also involves the grey matter of the CNS (Wu and Alvarez, 2011). Muscular weakness, speech problems, visual impairment, bladder dysfunction, sexual dysfunction, trigeminal neuralgia, pain, Lhermitte's sign, and neuropathic pain are some of the symptoms of the MS. The MS symptoms vary from patient to patient depending on the location of the lesion (Figure 1.1) making its diagnosis and treatment difficult (Crayton and Rossman, 2006; DasGupta and Fowler, 2003).

1.1.1 MS Diagnosis and classification

Clinical and radiological investigations such as magnetic resonance imaging (MRI), cerebrospinal fluid (CSF) analysis and visual evoked potential (VEP) are diagnostic tools that can add important information when clinically relevant symptoms of a patient alone are not enough to make a positive MS diagnosis. Each of these tests provides different information and their weight of contribution towards an MS diagnosis depends on the context of diagnosis. Cerebrospinal fluid analysis can detect markers of inflammation, while VEP can provide supporting information when the MRI-detected lesions in the patient's brain are few and not informative. The 'dissemination in space' criteria is fulfilled by the presence of more than one symptomatic and/or asymptomatic lesion in more than 2 of the 4 regions of the CNS, the periventricular,

juxtacortical, infratentorial and spinal cord. The 'dissemination in time' criterion
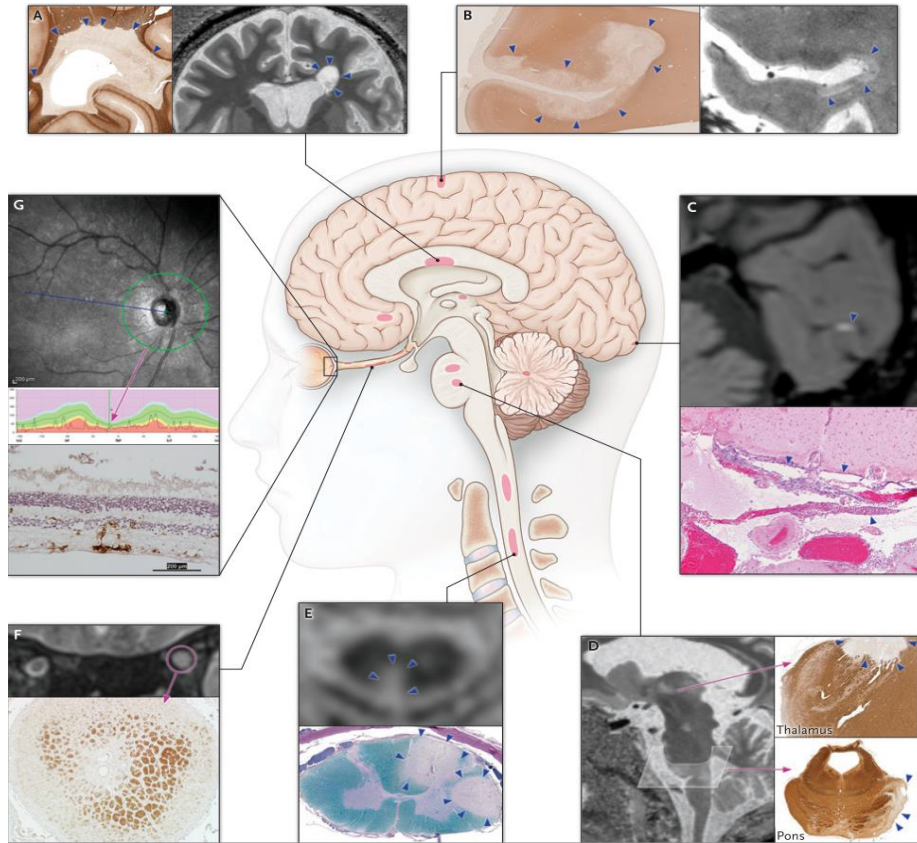
Figure 1.1: Topography of Multiple Sclerosis lesions.

Showing lesion locations in periventricular white matter (inset A), subpial cortex (B), leptomeninges (C), thalamus and pons (D), spinal cord (E), optic nerve (F) and retina (G). Insets A, B, and D show a 40 Tesla MRI scan lesions in relapsing-remitting MS patients and similar finding in other patients immunohistochemically stained for myelin basic protein. Inset C presents a 3-Tesla MRI scan of gadolinium lesion in secondary progressive MS and (Eosin and hematoxylin) staining of similar pathological finding in the meninges of a different patient. Inset E shows a 3-Tesla MRI scan of a relapsing-remitting MS patient and similar pathology in a different patient stained with (luxol fast blue-periodic acid and Schiff staining) Inset F shows a 3-Tesla MRI scan lesions in relapsing-remitting MS patients and similar finding in others patients immunohistochemically stained for proteolipid protein. Inset G presents spectral-domain optical coherence tomographic reconstruction illustrating thinning of the peripheral retinal nerve fibre layer. The normal retinal thickness was shown in green and the patient has a 99% reduction in the retina compared to the fibre layer thickness. The bottom panel of Inset G depicts similar finding in other patients immunohistochemically stained for microglia and macrophages (Iba1 and counterstained with hematoxylin counterstaining). Lesions are indicated with arrowheads or circles (Reich et al., 2018).Copy rights Massachusetts Medical Society.

is met when there exists the simultaneous presence of gadolinium-enhancing lesions and a nonenhancing T2-hyperintense lesion. Alternatively, evidence of

a second clinical occurrence of MS in the patient or the presence of T2 lesion and/or gadolinium-enhancing lesion on follow-up MRI, regardless of its timing. The revised version of McDonald's 2017 criteria (Thompson et al., 2018)(Figure 1.1) recommends the following:

1. Inclusion of cerebrospinal fluid oligoclonal bands for diagnosing MS in some of the patients.

2. Inclusion of the symptomatic lesion in giving confirmation for dissemination in space and time.

3. Cortical lesions are as important as juxtacortical lesions and should be incorporated into the MRI criteria for the dissemination of space criterion. However, care should be taken to identify the cortical lesions properly.

4. There is a slight change in the diagnostic criteria of progressive MS. The difference between symptomatic and asymptomatic MRI lesions was removed and cortical lesions were also included.

5. In addition to the revised MS clinical phenotype classification in 2013, the 2017 revised version further classified the disease course as active or not (depending on the recent clinical relapse and/or MRI lesion activity) and progressive or not (depending on the clinical assessment of disability).

Some of the future recommendations also suggest studying a variety of populations and the inclusion of effects on the anterior visual system (optic nerve) as diagnostic criteria. They also consider strict measures on avoiding misdiagnosis and to consider patients with non-classic presentations when applying the diagnostic criteria (Thompson et al., 2017).

1.1.2 Immunopathology of MS

MS is correlated to several genetic and environmental factors including vitamin D deprivation, viral pathogens, diet, smoking and obesity in patients (Oksenberg and Baranzini, 2010). The complex interplay between the immune system, glia (oligodendrocytes, oligodendrocyte precursors, microglia and astrocytes) and neurons causes the tissue damage in MS patients' brain. During the development of the disease dendritic cells travel from patient's bloodstream

through the blood-brain barrier (BBB) into the CNS and causes the differentiation of memory T cells into T helper 1 (Th1) and Th17 which are pro-inflammatory in nature and cause inflammation events in the CNS (Figure 1.2) (Ifergan et al., 2008; Pashenkov et al., 2001; Serafini et al., 2006). Following this, demyelination and axonal loss are caused by the proinflammatory cytokines, oxygen and nitric oxide radicals produced from the activated macrophages and microglia. Other participating factors inside the CNS of MS patients are as presented below and summarised in Figure 1.2:

CD4+T cells and Th1 cells produce IL-2, IL-12, TNF-alpha and IFN-gamma and are proinflammatory. Th2 cells are anti-inflammatory in nature and secrete IL-4, IL-5, IL-6, IL-10, IL-13, and IL-25. Th9 cells secrete large amounts of IL-9. Th17 cells produce IL-17A, IL-17F, IL-21 IL-22, IL-24 and IL-26 smaller amounts of IL-9 and IFN-gamma, and these cells are proinflammatory. Th22 cells secrete high amounts of IL-13, IL-22 and TNF alpha. In summary, Th 1, 9 and 17 cells are the main contributors to MS disease progression (Dargahi et al., 2017). The role of Th1 and Th17 cells in MS pathology is well established in EAE mouse models. Th17 cells increase the permeability of the BBB by causing the production of reactive oxygen species (ROS) (Huppert et al., 2010). Th17 cells also participate in the formation of ectopic lymphoid tissue (Peters et al., 2011). Due to a combination of genetic and environmental factors, memory T cells become activated in the periphery(Sospedra and Martin, 2005). The pro-inflammatory cells that penetrate the BBB become activated in response to unknown CNS antigens and cause the inflammatory response (summarised in several reviews (Compston and Coles, 2008; Grigoriadis and van Pesch, 2015; Hemmer et al., 2006)). A series of molecular events occur before demyelination and axonal loss, i.e., activated macrophages and microglia produces oxygen and nitric oxide radicals that cause the tissue damage (Das Sarma et al., 2009; Kawanokuchi et al., 2008; Murphy et al., 2010). Th1 cells are capable of identifying MOG, PLP and MBP peptide epitopes presented by the MHC class II become activated cross the blood-brain barrier and cause CNS autoimmunity.

An additional player in the development of MS requires CD8+ T cells, which are mostly present in the parenchyma, in contrast to CD4+T cells, which are

more concentrated in the perivascular cuff (Lassmann, 2014). CD8+ T cells isolated from MS patients react mainly against MOG, PLP, and MBP. The classic CD8+T cells secrete IFN-γ whereas new subsets Tc2 secrete IL-4, Tc10 secrete IL-10, Tc17 secrete IL-17, Tc21-secrete IL-21, and Tc22-secrete IL-22. CD8+ T cells are present in higher numbers than in MS patients CNS tissue and cerebrospinal fluid (Dargahi et al., 2017).

During MS disease development in patients, the macrophage activation has been found to be T cell-mediated. Microglia and macrophages play an important role in initiating and sustaining the inflammatory reaction in patients with MS (Trebst et al., 2001). In a marmoset Experimental Autoimmune Encephalomyelitis (EAE) model of the disease, during the early stages of inflammation microglia are present in the perivascular lesions and monocytes are associated with demyelination (Maggi et al., 2014). Apart from the participation in inflammation, microglial cells also remove cellular debris and dead cells which is essential for remyelination and decreasing inflammation in goldfish (Battisti et al., 1995; Napoli and Neumann, 2010). Microglia also release growth factors that benefit axons and neurons (Stadelmann et al., 2002).

In patients developing MS B cells act as antigen-presenting cells and stimulate antigen-specific CD4-T cell response via MHCII (Parker Harp et al., 2015). B cells participate in the formation of ectopic lymphoid tissue. The evidence of oligoclonal bands formed by immunoglobulins in the CSF proves that the antibody-producing function of the plasmablasts developed from the memory B cells is important in some lesions of MS (Lucchinetti et al., 2000; Reindl et al., 2009; von Büdingen et al., 2010). All these roles of B cells suggest that B cell depletion therapies would be very successful to treat MS in patients and such therapy using the anti-CD20-antibody ocrelizumab is well established now for the treatment of relapsing-remitting and primary progressive MS (Myhr et al., 2019). In the CNS, complement-mediated damage to myelin and activation of T cells are caused by reactivation of B cells. The accumulation of autoreactive B cell clones in the blood of MS patients happens due to the defective peripheral B cell tolerance caused by compromised T-regulatory function (Kinnunen et al.,

2013). B cells can promote and inhibit immune responses (Matsushita et al., 2008). Increased activation of macrophages and inflammatory T cells were observed in mice lacking IL-35 expressing B cells and the ability to recover from EAE was effected in these mice (Shen et al., 2014). Production of IL-10 from B cells is important for the recovery from EAE (Fillatreau et al., 2002).

Figure 1.2: Immune cells in Multiple sclerosis.

The different types of immune cells implicated in the pathology of Multiple Sclerosis in patients are illustrated along with the cytokine profile (Dargahi et al., 2017).

Another set of immune cells, Natural Killer cells, are also involved in the development of MS in patients. They stimulate the maturation of antigen-presenting cells such as dendritic cells and are important in cytokine production (Della Chiesa et al., 2006; Piccioli et al., 2002; Vitale et al., 2005). Natural Killer cells were classified into two subsets, variant and invariant Natural Killer cells. Markers such as CD25, CD44, and CD69 are expressed on the invariant Natural Killer cells along with characteristic markers such as CD161 and Ly49. Upon activation by binding to GalCer-CD1d complex Natural Killer cells secrete both proinflammatory and anti-inflammatory cytokines. Invariant Natural Killer cells regulate immune cells in three ways. Firstly, by secreting

IL-4 and IL-13, which aid in the differentiation of CD4$^+$ T cells into Th2 cells that are anti-inflammatory. Secondly, by stimulating the production of regulatory T cells by secreting IL-2 and tumour growth factor. Lastly by secreting IL-4, IL-10, IL-13, IFN-γ that activate suppressive myeloid-derived suppressor cells, dendritic cells, and macrophages which in turn secrete IL-10 to activate regulatory T cells. The Th2 cells and the regulatory T cells inhibit the Th17, Th1, CD8+ cells in the central nervous system, thereby having a protective role (Van Kaer et al., 2015). Variant Natural Killer cells on the other hand bind to the self-glycolipid, and sulphatide abundant proteins in myelin and participate and disease progression (Jahng et al., 2004).

Finally, mucosal-associated invariant T cells (MAIT) need to be discussed. These are a subset of T cells that defend against microbial infections (Napier et al., 2015). MAIT cells get activated by the presentation for microbial antigens and B vitamin metabolites by MHC-Class 1 related protein MR1 (Kjer-Nielsen et al., 2012). MAIT cells are involved in autoimmune disorders including MS. MAIT cells are highly present in the demyelinated areas and secrete Th1 cytokines such as IFN-γ, TNF-α and Th17 cytokines IL-17 and IL-22. However, the role of MAIT cells is not clear in the development of MS.

Regulatory T cells are a subset of CD4+T cells. The characteristic feature of regulatory T cells is the expression of Foxp3+CD25+CD4. In MS the number of regulatory T cells expressing Foxp3+CD25+CD4 is same as in healthy controls but their function, maturation, and migration are disturbed (Zozulya and Wiendl, 2008). Regulatory T cells secrete IL-10 and are responsible for preventing autoimmunity and increased tolerance. The impaired function of these cells could be one of the reasons causing MS (Diebold and Derfuss, 2016). Dendritic cells are the classic antigen-presenting cells responsible for the activation of CD4+ and CD8+ T cells. The expression of costimulatory molecules CD40 and CD80 increased in relapsing-remitting MS (RRMS) and secondary progressive MS (SPMS)(see section 1.1.3) patients indicating a proinflammatory role. Dendritic cells produce large amounts of TNF-α, IFN-γ, and IL-6 (Huang et al., 1999).

Finally, dysbiotic gut microbiome could play a role in the development of MS in patients and may aid in the progression of MS. Gut microbiome could be altered to control the effector and regulatory phase of demyelination in MS (Ochoa-Repáraz et al., 2018).

1.1.3 Types of MS

Clinically isolated syndrome (CIS) is the first appearance of a disease that displays features of inflammatory demyelination in the CNS that possibly will be MS but it still has to meet the dissemination in time criteria (Miller et al., 2005). In most cases, based on the natural history and MS, disease-modifying therapies have shown that CIS in combination with MRI lesions brings a high risk for fulfilling MS disease diagnostic criteria. RRMS is the most commonly occurring form of MS in patients. It involves new attacks or worsening of neurological symptoms followed by a period of partial or complete recovery. Approximately 85% of MS patients are diagnosed with RRMS initially. Primary progressive MS (PPMS) is the minimal inflammatory form of MS (Mahad et al., 2015). The gradual deterioration of neurological function from the initial onset of symptoms without the occurrence of early remissions or relapses is categorised as PPMS. The deterioration rate and disease progression of PPMS is similar to SPMS without relapses (Ebers, 2004, 2001, 2000). Most RRMS cases convert into SPMS eventually and there are no simple diagnostic tools such as imaging, clinical evidence, immunological or pathological tools available that can identify when this switch occurs. However, SPMS can be further differentiated at different time points as active or inactive (evidence of new MRI activity with/without relapses), and progressive or non-progressive (evidence of worsening of disease on an objective measure of change over time, with or without relapses) (Browne et al., 2014). Radiologically isolated syndrome (RIS) is a condition where there is a lack of clinical signs and symptoms, but demyelinated lesions are noticed through imaging (Lebrun et al., 2009; Okuda et al., 2009; Siva et al., 2009). RIS is not a subtype of MS as such due to the lack of clinical evidence of demyelinating disease. Based on the location and the morphology of the detected MRI lesion, RIS may create a

notion of MS in the future. Positive CSF findings or gadolinium-enhancing lesions, asymptomatic spinal cord lesions increase the chances of MS development in the future (D.T. et al., 2011; Giorgio et al., 2011). It is important to follow these patients with no clinical signs or symptoms of MS. The concept of Benign MS (BMS) is quite controversial and has several definitions. Benign MS is not a phenotype of MS on its own. The patients experience a milder course of a disease resembling mild RRMS in the initial decades. Nearly all study groups use an expanded disease status scale <3 for a disease period of 10, 15 or more years to categorize those patients as having BMS (Reynders et al., 2017)

1.1.4. Pathological Hallmarks of MS

The key pathological hallmarks of MS are extensive demyelination along with the relative conservation of axons in the white and grey matter (Grigoriadis and van Pesch, 2015). The degeneration of denuded axons gradually happens in chronic demyelinated lesions. The possible mechanisms include mitochondrial dysfunction and disturbed axonal transport (Mahad et al., 2015). Axonal loss is a prominent feature in type III cortical lesions of MS and normal-appearing white matter (NAWM) (Klaver et al., 2015). In chronic MS neocortical neuronal loss is up to 40 % and the reduction in cortical volume reflects the reduction in neurons (Carassiti et al., 2018). Neuronal loss up to 65% is noticed in patients with severe inflammatory phenotype of MS (Magliozzi et al., 2010). Synaptic loss is also one of the features of MS (Dutta and Trapp, 2011; Mandolesi et al., 2015). Meningeal inflammation and B-cell clusters are also responsible for neurodegeneration. Other mechanisms of neurodegeneration include mitochondrial dysfunction (Witte et al., 2014), glutamate excitotoxicity (Pitt et al., 2000) and iron deposition (Haider et al., 2014). Acute plaques in brains of MS patients are the initial forms of lesion formation with vigorous infiltration of inflammatory cells, demyelination spread across the lesion. Depending on the presence or absence of inflammation and demyelination the lesions are classified into various types (Figure 1.3).

White matter lesions

Acute lesions are common in the acute and relapsing-remitting forms of MS. They contain an enormous number of cells and are infiltrated by macrophages (Figure 1.3). These macrophages engulf myelin debris (Grajchen et al., 2018). The early active demyelination that happens within 1-3 days can be detected by the presence of macrophages containing degradation products of minor myelin proteins such as CNPase, MOG, and MAG in animal models of MS.

The late active lesion is characterised by the presence of degradation products of major myelin proteins in macrophages. The digestion of these major myelin proteins happens slowly, taking up to 10 days. Based on myelin loss, the location and extension of plaques, oligodendrocyte destruction and the immunopathological evidence of complement activation the MS lesions are classified into 4 major patterns (Lucchinetti et al., 2000)(Reich et al., 2018).

Pattern I: These lesions are characterised by demyelination and products related to macrophages. They are located close to a blood vessel and also have clearly defined perivascular lesions. The demyelination may be caused due to the toxic factors released by the activated macrophages. At the active lesion border, the number of oligodendrocytes is variable. The reappearance of oligodendrocytes in the inactive plaque centre is possible and the incidence of remyelinated lesions are high. Immunoglobulin deposition and complement activation are absent in pattern I lesions.

Pattern II: These lesions share most of the features of pattern 1 lesions except antibody and complement deposition on myelin. Tissue injury and demyelination are antibody and complement-mediated. Macrophages are also involved in the phagocytosis of complement-opsonized myelin debris.

Pattern III: Oligodendrocyte dysfunction and apoptosis are the key features of pattern III lesions with ill-defined lesion borders. There is an absence of complement and immunoglobulins, however, there exists an early loss of myelin-associated glycoproteins. The loss of oligodendrocytes spreads from the active lesion border to the normal periplaque. There is no remyelination in these lesions and the centre of the lesions lack oligodendrocytes.

Pattern IV: The lesion biopsy tissue of MS patients show a non-apoptotic loss of oligodendrocytes in the periplaque white matter occurs due to metabolic

disturbance making them more susceptible to damage caused by inflammatory mediators.

Chronic lesions are more often seen in patients with progressive MS than active plaques. Chronic active lesions are defined as demyelinated lesions with macrophages present at the edges in large numbers, contributing to the progression of the lesion. Macrophages are absent in the inactive centre of the lesion, which is hypocellular. Chronic inactive lesions are characterised by loss of oligodendrocytes, axons, astrogliosis, with minimal infiltration of macrophages/microglia and lymphocytes. These lesions are absolutely demyelinated, demarcated and hypocellular in nature.

Cortical lesions

One of the important components of MS is demyelinated lesions in the cerebral cortex. Lesions that involve the cerebral cortex are four types (Figure 1.3). To visualise these lesions techniques such as double inversion recovery, phase-sensitive inversion recovery and magnetisation-prepared rapid acquisition with gradient echo sequences are employed (Filippi et al., 2016, 2010; Preziosa et al., 2018).

Type 1 Leucocortical lesions: Leucocortical lesions in superficial cortical layers are excluded in these lesions and include both deeper layers of grey matter and white matter below at the grey matter-white matter junction.

Type 2 Intracortical lesions: These lesions are located within the cortex without touching the outermost cortex and the neighbouring white matter.

Type 3 Subpial lesions: These lesions spread from the pial surface to the third or fourth layer of the cortex. They may spread across the cortex and include several gyri, but do not touch the white matter.

Type 4 Subpial lesions: They include all layers of the grey matter without touching the underlying white matter.
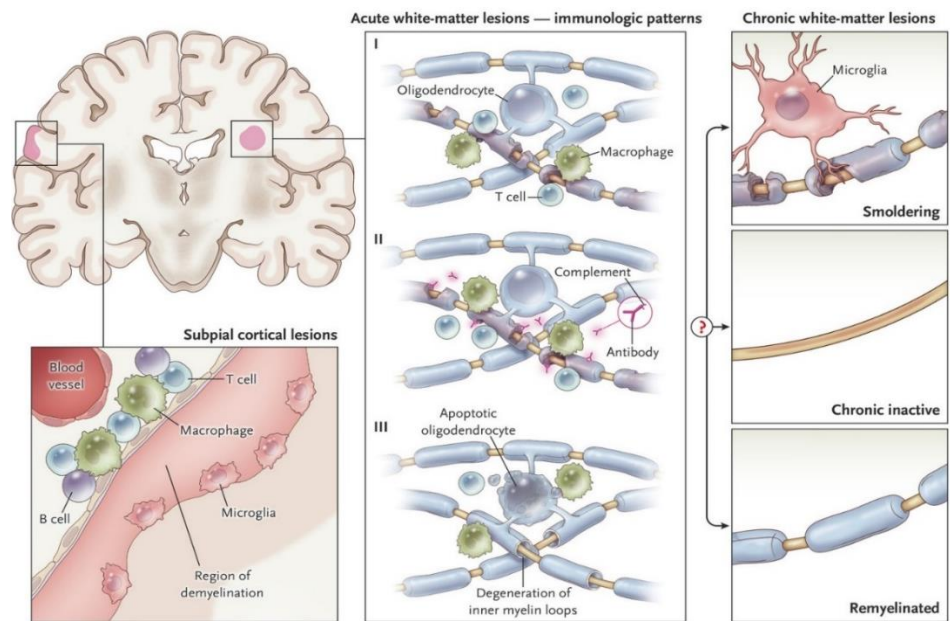
Figure 1.3: White and Grey matter lesions.

Acute white matter lesions are classified into three types. Pattern I, II and III. Pattern I and II have mononuclear phagocytes along with perivascular and parenchymal T cell infiltration. In addition, pattern II lesions also have immunoglobulin and complement deposition. Pattern III lesions have dying oligodendrocytes and degeneration of the inner myelin loop. Post-acute phase, the survival of axons relies on the extent of myelin formation (remyelination), resolution of inflammation without remyelination (chronic inactive) or very slow degeneration of myelin and progression of inflammation (smoldering) (Reich et al., 2018). Copy rights Massachusetts Medical Society.

Cell signalling pathways involved in the pathogenesis of MS

Neuronal injury and cell death in several chronic and acute disorders involve oxidative stress. Oxidative stress can cause changes in mitochondria, endoplasmic reticulum, cell organelles and can lead to a plethora of cell death paradigms such as apoptosis, necrosis, and autophagy. One of the major factors driving tissue injury in multiple sclerosis is mitochondrial injury followed by energy failure (Dutta et al., 2006; Lu et al., 2000). Alterations of mitochondrial respiratory chain proteins were noticed in active MS lesions. Pathological features such as demyelination, oligodendrocyte apoptosis (Veto et al., 2010), and arrest of oligodendrocyte differentiation, failure to remyelinate (Ziabreva et al., 2010), axonal damage (Mahad et al., 2008) and astrocyte dysfunction (Sharma et al., 2010) could be due to mitochondrial changes. Mitochondrial DNA and proteins are susceptible to oxidative damage (Higgins et al., 2010).

The Wnt-signalling pathway has a dual role in terms of myelination. Myelin formation is controlled by Tcf712 transcription factor (Fu et al., 2012). Oligodendrocyte precursor cells (OPC) differentiation and remyelination are controlled by the expression levels of Wnt molecules and other pathways that interact with the Wnt pathway (Xie et al., 2014). Nuclear factor kappa-light-chain-enhancer of activated B cells (NF-κB) is another molecule associated with immune responses in MS pathogenesis. NF-κB proteins are present in the cytoplasm of the cells along with their inhibitors (IkBs). IkB proteins undergo phosphorylation, ubiquitylation followed by proteasomal degradation in the presence of inducers that activate NF-κB. In the following degradation of IkB permits the translocation of NF-κB into the nucleus and the latter binds to NF-κB-specific DNA binding sites in promoters regulating the transcription of multiple proteins, polypeptides, and cell signalling molecules such as cytokines, chemokines, antimicrobial peptides, stress response and anti-apoptotic proteins (Li and Verma, 2002; Yamamoto and Gaynor, 2004). NF-κB is vital for the development, proliferation, and survival of T and B cells. Antibody class switching in B cells, as well as CD4c T cell differentiation and cytokine production, require NF-κB functions. NF-κB also influences the antigen processing and presentation in macrophages and production of inflammatory mediators by antigen-presenting cells such as dendritic cells. Moreover, production of proinflammatory cytokines and neurotoxic mediators in microglia and astrocytes is mediated by NF-κB (Yan and Greer, 2008) and therefore, enhanced expression of NF-κB could promote proinflammatory responses. In MS increased nuclear localisation of NF-κB was noticed in microglia, lymphocytes and a subset of astrocytes (Gveric et al., 1998). In active lesions of MS, NF-κB was found in the oligodendrocytes at the edges of the lesions and microglia throughout the lesion but not in silent lesions or healthy white matter (Biancotti et al., 2008)

1.1.5 ER stress and multiple sclerosis

Accumulating evidence suggests that ER stress pathways could be therapeutic targets in neurodegenerative disorders such as MS. The unfolded protein

response (UPR) as a stress pathway of the ER is regulated by three stress signalling molecules inositol requiring enzyme 1 (IRE1), Activating transcription factor 6 (ATF6) and Protein kinase RNA (PKR)-like ER kinase (PERK) (discussed later in this document) and activation of these pathways causes the induction of proteins and chaperones that assist in restoring the normal ER function. UPR can be either beneficial or detrimental for a cell-based on whether it is supporting survival or apoptosis. When prolonged ER stress overtakes the protective mechanisms, the signals become proapoptotic (Oyadomari and Mori, 2004). Inflammatory demyelination and neurodegeneration in MS are related to ER stress (Deslauriers et al., 2011). Published work from our group showed the upregulation of ER stress-associated molecules such as C/EBP homologous protein (CHOP), XBP-1 and BiP in MS lesions. Increased expression of BiP was also observed in acute lesions of MS patients compared to non-MS controls and edges of the chronic active lesions displayed the increased expression of CHOP (Mháille et al., 2008). The raised D-110 (hypoxia marker) matched the ER stress response in active lesions. Increased expression of CHOP, BiP and ATF4 were also observed in the normal-appearing white matter (NAWM) compared to Non-MS controls. The presence of increased levels of CHOP was observed in the peri-lesional areas of the active lesions (Cunnea et al., 2011). ER stress molecules were upregulated in the grey matter lesions and high number of D110 (hypoxia marker)-positive cells were also noticed in the grey matter lesions (McMahon et al., 2012). Microarray analysis indicated the upregulated for HSP gene in the active lesion of MS (Graumann et al., 2006; Mycko et al., 2012).

1.2 The Endoplasmic reticulum

The Endoplasmic reticulum (ER) is a subcellular organelle comprised of an interconnected network of membranous tubules, sacs, and flattened cisternae. It is involved in different cellular functions including synthesis of secretory and membrane proteins, biosynthesis of phospholipids, steroids, cholesterol and degradation of glycogen (Braakman and Bulleid, 2011; Zimmermann et al., 2011). The ER also regulates calcium homeostasis in mammalian cells. High levels of Ca^{2+}, ATP and the oxidising environment present in the ER lumen are

required for the proper functioning of the chaperones and glycosylating enzymes that support the folding and oxidising enzymes engaged in protein folding (Braakman and Bulleid, 2011; Zimmermann et al., 2011).

To perform these functions ER consists of cisternae and tubules and is connected to the nuclear envelope. The peripheral ER is composed of flat cisternal sheets and reticulated tubules which originate from the outer nuclear membrane. The ER sheets are flat and contain two membrane layers with the ER lumen being situated between the opposing two layers (Bernales et al., 2006; English et al., 2009). It is important to note that the cisternal flat sheets are less curved than the tubules and the tubules have a higher surface-to-volume ratio compared to the flat sheets. Therefore, the tubules are appropriate for the surface-dependent functions and cisternal sheets are more suited for luminal processes. The tubules originate from both the nuclear envelope and the sheets to form a network-like structure in cells that connects all the parts of the ER (Friedman and Voeltz, 2012). From the electron microscope images, it is clear that sheets are likely to be rough due to the presence of ribosomes whereas tubules are smooth due to the lack of ribosomes (Shibata et al., 2006; Voeltz et al., 2002). Depending on the requirement of the cell, the sheets-to-tubules ratio varies. The cells that are meant to secrete a large amount of proteins such as pancreatic cells were found to have large numbers of layers of sheets embedded with ribosomes. On the other hand, cells, which are involved secreting fewer proteins such as neurons, muscle cells, and epithelial cells, possess large tubular networks (Baumann and Walz, 2001; Shibata et al., 2006; Terasaki et al., 2013).

Translocation of proteins into the ER membrane can happen in two ways: Co-translationally and post-translationally. In the former, the entry of the protein into the membrane happens in parallel with the protein translation. In the latter, the protein is completely translated before it is inserted into the ER membrane. Both mechanisms have to follow four major steps: 1) recognising and directing the proteins to the ER, which is a signal recognition peptide (SRP) -dependent or -independent; 2) pairing up with the ER translocation machinery and the pore that acts as a gateway for the entry of the proteins into the ER. 3) energy-dependent protein import into the ER lumen or membrane; 4) completion of

folding and maturation of proteins in the ER. Cytosol- and ER lumen-located chaperones aid in the translocation, protein folding, and assembly of these proteins (Fewell and Brodsky, 2009).

Misfolded proteins normally get exported to the cytoplasm where they are degraded by proteasomes in a process called ER-associated degradation (ERAD) and this transport to the cytoplasm for degradation is called dislocation (Meusser et al., 2005).

1.2.1 Interactions of BiP with polypeptides

BiP binds to the newly synthesised polypeptides and is involved in the translocation of polypeptides into the ER. BiP interacts with the J-domain of the Sec63p, a component of the Sec complex which plays a vital role in the translocation of polypeptides across the ER membrane (Misselwitz et al., 1999). BiP in the ADP-bound confirmation blocks the translocon and prevents protein translocation and Ca^{2+} leakage, whereas BiP in the ATP-bound state opens the translocon and assists in translocation (Alder et al., 2005). Here it is important to note that BiP has more preference towards aliphatic amino acids Alanine, Valine, Leucine and Proline. Leucine is the most preferred amino acid for binding to BiP (Flynn et al., 1991a). Due to the presence of six leucines in the signal sequence of BiP and the hydrophobic nature of the signal sequence itself, there exists a possibility of intermolecular or intramolecular binding, leading to an enhanced ATPase activity of BiP variants with the signal sequence.

BiP binds to surfaces with alternate aromatic and hydrophobic amino acids and it is the earliest chaperone to bind a nascent polypeptide chain in the ER. Various partners involve in its substrate-binding and the modulation of its activity to hydrolyse ATP to ADP. ER-resident J domain proteins, homologs of yeast Sec63 (Otero et al., 2010) and P58 (IPK) (Tao and Sha, 2011) stimulate the ATP hydrolysis by BiP. Interestingly in the ADP-bound state BiP has a higher affinity for substrates. Then the ADP-bound closed state is reopened by the binding of ATP and this binding is simulated by nucleotide exchange factors GRP170 and Sil1 (Määttänen et al., 2010). Importantly BiP is involved in the macroautophagy of the misfolded proteins. In addition, BiP plays a vital role in

the translocation of proteins into the ER in an ATPase-dependent manner. Any mutations in the NBD that hinders the ATPase activity of BiP has a detrimental effect on the translocation of several proteins into the ER lumen such as invertase, immunoglobulin, carboxypeptidase Y, and α-factor (Brodsky and Schekman, 1993; Nguyen et al., 1991; Vogel et al., 1990).

1.2.2 Usage of recombinant proteins in the treatment of MS.

A variety of recombinant proteins have been used since the 1990s to treat MS in patients. Recombinant erythropoietin has been used as a therapeutic agent in chronic progressive MS (Ehrenreich et al., 2007) but a phase II clinical trial proved that recombinant erythropoietin is not effective in patients with moderately advanced progressive MS (Schreiber et al., 2017). Interferon Beta-1b (Betaferon) the popular drug used in the treatment of MS is a recombinant protein produced in bacteria. The formulation is given subcutaneously every alternative day. Interferon-beta 1a is a 23 kDa polypeptide produced in Chinese hamster ovarian cells is available as two formulations: Rebif (subcutaneous route of administration) and Avonex (intramuscular route of administration)(Huang, 2015). Recombinant IL-6 prevented a Theiler's murine encephalomyelitis virus-induced demyelination in a murine model of MS (Rodriguez et al., 1994) and protracted relapsing experimental allergic encephalomyelitis. Natalizumab which is a recombinant humanised IgG4k mAb acts on the $\alpha_4\beta_1$ and $\alpha_4\beta_7$-integrin (Gensicke et al., 2012), Natalizumab prevents the entry of activated T-cell into the CNS via the BBB but when the treatment is discontinued the T-cell infiltration resumes (Kivisäkk et al., 2009). Ofatumumab a humanised recombinant protein, the anti-CD20 antibody (IgG1k) acts via the complement-dependent cytotoxicity (Gensicke et al., 2012). Alemtuzumab is a human recombinant monoclonal antibody against the CD52 cell surface receptor on lymphocytes and aids in the elimination of T cells and B cells from the bone marrow (Cohen et al., 2008). Rituximab monoclonal antibody against CD-20 was developed using recombinant technologies and depletes B cells (Cohen et al., 2008). The current treatments such as disease-modifying drugs decrease the number and severity of attacks (Murray, 2006)

1.3 The Unfolded protein response (UPR)

In eukaryotes, the UPR is controlled by three ER membrane sensors: Ire1α, ATF6, and PERK (Figure 1.4). The UPR causes a reduction in protein translation, upregulation of genes encoding chaperones and other proteins associated with protein folding; it also prevents polypeptide misfolding and aggregation. Finally, the UPR traffics misfolded proteins to the cytosol for degradation (Cao et al., 2012; Walter, 2011).
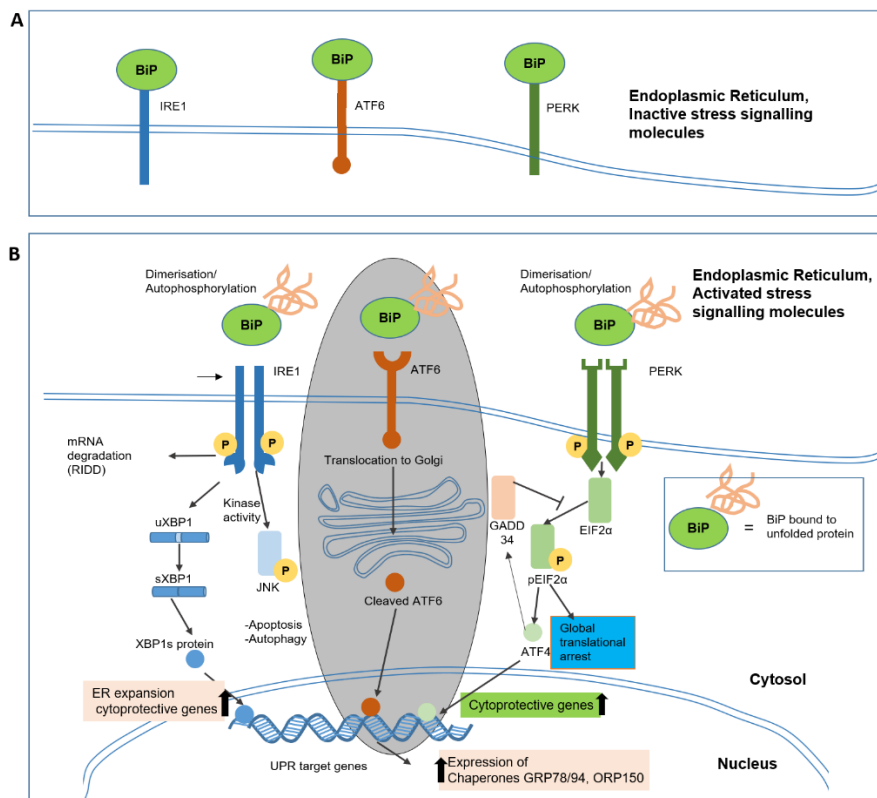
Figure 1.4: The unfolded protein response (UPR).

A. BiP binds to stress signalling molecules such as inositol requiring enzyme 1(IRE1), activating transcription factor (ATF6), protein kinase RNA (PKR)-like ER kinase (PERK) and maintains them in an inactive state. **B.** The accumulation of misfolded proteins in the ER causes ER stress, which leads to the dissociation of BiP from the stress signalling molecules such as IRE1, ATF6, and PERK. Activation of IRE1 causes splicing of X-box binding protein 1 (XBP1). Spliced XBP1 activate several unfolded protein response target genes that are cytoprotective, involved in ER expansion and ER-associated degradation. ATF6 gets transported from the ER to the Golgi complex where site 1 protease (S1P) and site 2 proteases (S2P) cleaves ATF6, followed by the trafficking of the cytosolic free domain to the nucleus causing the upregulation of ER chaperones such as glucose-regulated protein 94 (GRP94), BiP, CHOP, and protein disulphide-isomerase (PDI). PERK phosphorylates EIF2α resulting in the arrest of global protein translation and upregulates certain genes such as ATF4 and CHOP. BIX chemical inducer of BiP utilises the ATF6 pathway to induce the expression of BiP highlighted using grey-shaded oval (Source: Sravanthi Bandla).

1.3.1 The PERK Pathway

Accumulation of misfolded protein activates the UPR and this leads to the dimerization and autophosphorylation of PERK (Figure 1.4). Active PERK phosphorylates α- subunit of eukaryotic translation initiation factor 2α (EIF2α), which leads to the inactivation of EIF2α and inhibition of protein translation. Binding of phosphorylated EIF2-guanine nucleotide exchange factor decreases the EIF2-guanosine 5' triphosphate required for translation initiation, resulting in reduced translation (Spaan et al., 2019). The inactivation of EIF2α reduces

the protein load of the ER (Harding et al., 2000, 1999; Shi et al., 1998). Selected mRNA species, including activated transcription factor 4 (ATF4) are not affected by this translation block due to the presence of multiple open reading frames in the 5$'$-untranslated region (5$'$-UTR). In contrast, CHOP also known as growth arrest and DNA-dependent damage 153 (GADD153) is induced. CHOP is a transcription factor that promotes apoptosis (Li et al., 2014).

1.3.2 The ATF6 pathway

ATF6 resides in the ER lumen as an inactive precursor (Figure 1.4). When the UPR is triggered, ATF6 is transported from the ER to the Golgi apparatus where it undergoes intramembrane proteolysis by the site 1 protease (S1P) and site 2 proteases (S2P) resulting in a free cytosolic domain, which is further transported to the nucleus, causing the upregulation of ER chaperones and transcription factors such as glucose-regulated protein 94 (GRP94), BiP, CHOP, Protein disulphide-isomerase (PDI). These chaperones are involved in protein folding, secretion, and degradation. BiP also mediates apoptosis through the ATF6 pathway.

1.3.3 IRE1 pathway

The UPR also causes homodimerisation, auto-phosphorylation, and activation of Inositol requiring enzyme-1 (IRE1), which is both an ER-resident transmembrane serine/threonine kinase receptor and an endoribonuclease kinase (Figure 1.4). The preformed X-box Binding Protein-1 (XBP1) mRNA substrate of XBP1 is cleaved by the activated IRE1 through its endoribonuclease activity at two sites causing the removal of 26 nucleotide intron. Then tRNA ligase ligates the two parts of the mRNA which encodes for the transcription factor XBP1 (Patil and Walter, 2001; Sidrauski and Walter, 1997). XBP1 dependent target genes include ERdj4 (Shen et al., 2002), p58IPK (Melville et al., 1999), EDEM (Yu et al., 2000), RAMP4, PDI and HEDJ all of which has a role in the ER. EDEM is mainly involved in ERAD. Therefore, all the pathways ensure that the ER protein folding capacity is regulated properly (Lee et al., 2002; Tsunemi et al., 2010; Yoshida et al., 2001a).

In addition, Tumour necrosis factor α receptor-associated factor 2 (TRAF2), an adaptor protein in the TNF α signalling pathway, interacts with the phosphorylated cytosolic domain of the IRE1α under ER stress. I kappa B kinase (IKK) is recruited by the IRE1α-TRAF2 complex and causes the phosphorylation and degradation of IKB. This results in NF-κB activation and upregulation of its downstream inflammatory pathways. The IRE1α-TRAF2 complex also recruits apoptosis signalling kinase 1 (ASK1), which in turn activates c-Jun N-terminal kinase (JNK) that stimulates the proinflammatory response signalling by the phosphorylation of an AP1 transcription factor. The IRE1a-JNK complex is also involved in the activation of the proapoptotic pathways (Cao et al., 2012).

IRE1-dependent decay contributes to the apoptosis of cells by participating in the activating caspase 2 which is independent of the Xbp1 splicing under extreme stress conditions and it also promotes degradation of ER-resident proteins. RIDD also reduces the amount of proteins imported into the ER lumen. RIDD combines the ER targeted mRNA load with the ER folding capacity to preserve the ER homeostasis during ER expansion and cell differentiation (Coelho and Domingos, 2014).

1.4 Function of molecular chaperones in the ER

A molecular chaperone is defined as any protein that interacts with, stabilises or helps another protein to acquire its functionally active conformation, without being present in its final structure (Bracher and Hayer-Hartl, 2011; Ellis, 1993) (Figure 1.4). Molecular chaperones are induced by stress and participate in protein folding in association with co-chaperones, cofactors, and ATP, in order to regulate the binding and release cycles (Hartl, 1996).

1.4.1 B-cell immunoglobulin binding protein

Binding immunoglobulin protein, BiP, an HSP70 protein family member, was first discovered in 1977 when chick embryo fibroblast cells were deprived of glucose in the medium. The amount of specific proteins in the cells was dependent on the glucose availability in the medium and hence these proteins were named as glucose-regulated proteins (GRPs). One of them, a membrane protein with a molecular weight of 78,000 Dalton was called GRP78 and alternatively BiP due to its immunoglobulin binding activity (Shiu et al., 1977). The HSP5A gene encodes BiP (Wang et al., 2017). In contrast to the other heat shock proteins, BiP is not upregulated by heat shock because the heat shock element is absent in the BiP promoter (Wang et al., 2017). However, BiP expression is induced by the calcium ionophore A23187 (Resendez et al., 1985), thapsigargin, BAPTA-AM (Suzuki et al., 1991), and tunicamycin (Lee, 1987). Moreover, various cell stress-dependent factors upregulate the expression of BiP due to the preserved elements in the promoter of the HSP5A gene that include a CCAAT box (Resendez et al., 1988), a CREB (cAMP-responsive element CRE-like) (Alexandra et al., 1991), and an ER stress-responsive element ERSE (Resendez et al., 1988). Binding of the transcription factor such as CBF/NF-Y (Roy and Lee, 1995), CREB, ATF2 (Chen et al., 1997), YY1, YB1, SP1(Li et al., 1997), ATF4 (Luo et al., 2003), TFII (Parker et al., 2001), ATF6 (Yoshida et al., 2001c) and XBP1 (Yoshida et al., 2001b) to the regulatory elements in HSP5 gene controls its expression. Additionally, an internal ribosome entry sequence at the 5'-UTR of the BiP mRNA mediates the post-translation regulation of BiP (Macejak and Sarnow, 1991).
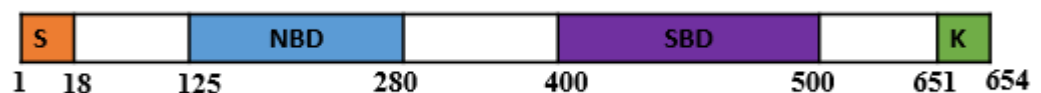
Figure 1.5: Structure of human full-length BiP illustrating the various domains.

The 654 amino acid protein contains a signal sequence (orange; S), nucleotide-binding domain (blue; NBD), substrate-binding domain (violet; SBD) and a KDEL ER retention sequence (green; K) (Wang et al., 2017; Zhang et al., 2010) (Image Source: Sravanthi Bandla).

BiP is a 654 amino acid long protein (Figure 1.5). The N-terminal signal sequence of BiP (amino acids 1-18) directs BiP to the ER and the C-terminal KDEL sequence is thought to retain BiP within the ER (Pidoux and Armstrong, 1993). The nucleotide-binding domain (NBD) is divided into two large globular domains (A and B) (Figure 1.6). Each of these domains is further divided into two subdomains IA, IB, and IIA, IIB. The substrate-binding domain (SBD) is also divided into two subdomains α and β. The β subdomain helps as a binding pocket for the nascent proteins/ peptides. The α- subdomain acts as a lid covering the binding pocket. The nucleotide-binding domain in the N-terminus binds to ATP or ADP, and the substrate-binding domain in the C-terminus aids in the attachment of nascent protein chains. A flexible linker connects the N terminus and the C terminus of BiP (Awad et al., 2008; Mayer and Bukau, 2005) (Figure 1.6). The main functions of BiP in the ER are protein folding, prevention of aggregation of protein intermediates during their translation process, calcium-binding, and trafficking of misfolded proteins in ER-associated protein degradation pathways (ERAD (Lee, 2007)). BiP depends on several partners, co-chaperones, nucleotide exchange factors, and signal transducers to carry out its diverse functions. When the BiP protein sequence of the Homosapiens and

Rattus norvegicus were compared, there is a 98% identity. They only varied in few amino acids mostly in the signal sequence (3, 4, 5, 9, 14, 16) and a few others at (313, 587, 638 and 649) (As illustrated in the Appendix Figure A1.1). No variation was noticed in the nucleotide binding domain and substrate binding domain when amino acids were compared. When the nucleotide sequences of human and rat were compared there was a 91% identity. The differences are illustrated in (Appendix Figure A2.1). BiP sequence were highly conserved among mammalian species, however, this slight variation in sequences could possibly lead to immune reactions when human protein was added to rat cultures.
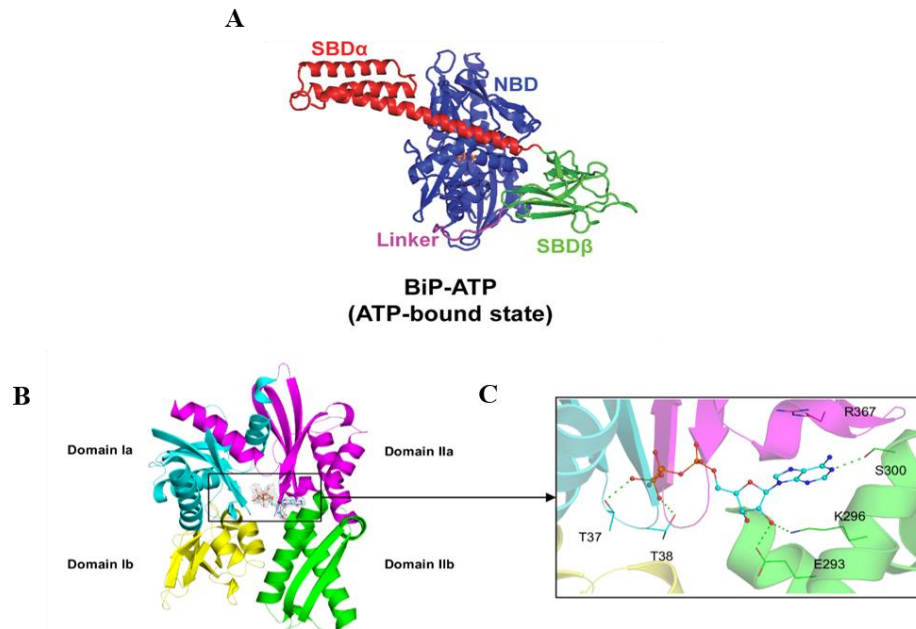
Figure 1.6: Nucleotide and substrate-binding domains of BiP.

(A) Ribbon diagram of BiP in its ATP bound state depicting nucleotide-binding domain (NBD) and substrate-binding domain (SBD) and linker. Domain colouring NBD- Blue, SBD-red and green, Linker-purple, Orange-ATP. (Yang et al., 2015) reproduced with permission from Elsevier's copy clearance center. (B) Subdomains of NBD, domains Ia-teal, Ib- yellow, IIa-purple and IIb-green. (C) Key interacting sites of the nucleotide-binding domain (Hughes et al., 2016).

1.4.2 Role of BiP in ERAD

Degradation of misfolded proteins takes place in the cytoplasm via the ubiquitin-proteosome system. BiP assists in the degradation of misfolded/unfolded proteins in multiple ways, it identifies the substrates, increases the solubility of the substrates and then dissociates from the substrates upon translocation into the cytoplasm (Wang et al., 2017). In the ER, BiP in association with soluble J domain proteins such as Jem1p and Scj1p assists in the export of substrates to the cytosol for ERAD thereby preventing protein aggregation in the ER lumen (Nishikawa et al., 2001). The binding of BiP to misfolded proteins is extended in the ER lumen and functions in cell signalling pathways (Sörgjerd et al., 2006). This extended contact acts as a signal for the

degradation of the bound protein (Petrova et al., 2008). BiP along with the other ER chaperones initiates the ERAD. Collectively, these chaperones lead to the deglycosylation and dissembling of the misfolded proteins (Printsev et al., 2017).

1.4.3 Mechanisms of BiP translocation from the ER to multiple cellular and extracellular locations

While BiP is primarily considered to be an ER-residential protein, it has also been reported to be present within the cytoplasm, nucleus, mitochondria and on the cell surface (Wang et al., 2017). BiP is also released into the cell culture medium by the oviductal epithelial cells (Marín-Briggiler et al., 2010a). BiP was also released in the cell culture medium from the intact human rabdomiosarcoma cells post-treatment with 500 nM of thapsigargin (Delpino and Castelli, 2002). Immunogold electron microscopic analysis of rat pancreatic cells confirms that BiP having KDEL is transported from the ER to the other parts of the cell and into the extracellular spaces via the secretory mechanism (Takemoto et al., 1992). Tumour cells secrete BiP into the tumour microenvironment and develop resistance to antiangiogenic activity of Bortezomib (Kern et al., 2009). Under certain conditions, BiP is released into the extracellular space or outside the cell (Ni et al., 2011). Moreover, BiP was also reported in the synovial fluid of Rheumatic arthritis (Tsunemi et al., 2010), in sera of gastric cancer patients (Giusti et al., 2010a) and its precursor is found in the saliva of Rheumatic arthritis patients.

The secretion of the proteins having the signal sequence starts in the ER where the nascent polypeptide undergoes proper folding before exiting via the ER exit site in a COPII-dependent manner (Grieve and Rabouille, 2011). The COPII-dependent manner is considered as the conventional secretory pathway in which most of the vesicles are transferred to the Golgi complex for further modification and secretion. Conversely, some proteins leave the ER independently bypassing the conventional pathway. These proteins follow the unconventional pathway. Utilising the unconventional mechanism HSP70 and annexin translocates from the cytosol to the cell surface (Deora et al., 2004). Brefeldin A treatment is generally exploited to understand whether a protein

utilises the conventional pathway or unconventional pathway. It is a fungal metabolite that inhibits the GTP-exchange factors of ADP ribosylation factor 1 and prevents protein transport from ER to Golgi (Popoff et al., 2011). Different cells use different routes to secrete BiP. For example, the cell surface expression of GRP78/BiP in HeLa Cells is interrupted by Brefrelin A but not in HCT116 cells (Tsai et al., 2015). The presence of GRP78/BiP in the exosomes indicates a new mechanism for the transport of GRP78/BiP to the cell surface for subsequent secretion (Xiao et al., 2012).

The ATPase domain also participates in the protein-protein interactions of BiP. For example, the interactions of BiP with caspase 7 was stopped when the amino acids 175-201 in the ATPase-binding domain were deleted (Reddy et al., 2003). The substitution of the Arginine 197 in the ATPase domain with histidine abolished the binding of BiP to DnaJ co-chaperones (Awad et al., 2008). The substrate-binding domain is important for the cell surface expression of BiP. A T453D defect in the substrate-binding domain decreased the cell surface expression on BiP whereas R197H or G227D substitutions in the ATP binding domain had not affected the cell surface expression of the BiP. Therefore SBD appears to be more important for the cell surface expression of BiP when compared to ATP binding domain (Tsai et al., 2015).

Several possible mechanisms for the appearance of extracellular BiP have been proposed. BiP has a C-terminal tetrapeptide KDEL, which is thought to be responsible for retaining BiP within the ER lumen. During ER stress BiP is up-regulated, but the expression of the KDEL receptor remains the same, which leads to a situation where the KDEL retrieval capacity is surpassed making BiP translocate outside the ER and even to reach the cell surface despite it still has the KDEL retention sequence (Zhang et al., 2013). Moreover, chaperone proteins with KDEL have been described to appear on the cell surface due to their association with membrane proteins during the latter maturation and folding (Wiest et al., 1997; Xiao et al., 1999; Zhang et al., 2010) An additional possibility could be that the KDEL motif is disguised due to glycosylation or other post-translational modifications. Further, the interaction of BiP with protein partners such as DnaJ-like transmembrane protein MTJ-1 in

macrophages and Par-4 in PC3 cells was observed and it is believed that these interactions help in translocation of BiP to the cell surface (Ni et al., 2011). Alternatively, the ER is fused with the plasma membrane in phagocytic cups, thus providing easy access for ER-resident proteins to the cell surface. While BiP found on the cell surface may still have a KDEL sequence, enzymatic cleavage of the KDEL retention moiety could also be a reason for the secretion of BiP from the cell into the extracellular spaces. *Escherichia coli* subtilase cytotoxin has a catalytic subunit (SubA) that cleaves the C-terminal 28kDa fragment of cell surface BiP (Ray, 2018). Sub A cleaves GRP78/BiP between the amino acid Leu[416] and Leu[417] (Paton et al., 2006). Due to this cleavage, BiP loses its function and the cells experience lethal consequences (Morinaga et al., 2008). Alternatively, possible alternative splicing of BiP without KDEL also allows BiP to escape from the cell (Corrigall et al., 2004; Zhang et al., 2010). Several cancer cells exhibit BiP on their cell surface, which includes breast cancer, prostate cancer, lung cancer, hepatocellular and gastric cancer. Tumours of prostate cancer that are vigorous in nature exhibited increased levels of BiP on the cell surface as well as intracellularly (Rauschert et al., 2008).

1.4.4 BiP on the cell surface

It has been reported that BiP interacts with various cells surface ligands and receptors (Figure 1.7 and Figure 1.8) (Wang et al., 2017). Various extracellular ligands such as activated alpha 2-macroglobulin, Kringle 5 (K5) domains containing proteins (e.g., plasminogen), prostate apoptosis response- 4 (Par-4), and istmin (Xiang et al., 2011) interact with cell surface BiP and multiple cellular signalling pathways become modulated. Interestingly, by forming complexes with proteinases such as PSA, alpha 2-macroglobulin converts itself into its BiP receptor recognised form(s), binds to the cell surface BiP in 1-LN prostate cancer cells, and undergoes autophosphorylation, which activates downstream events that include RAS/MAPK, and PI 3-kinase/AKT/mTOR pathways. These signalling pathways cause cell proliferation and encourage cell survival (Misra et al., 2005; Tsai and Lee, 2018).

Another example for these cell surface functions of BiP is the high-affinity interaction of plasminogen Kringle-5 domain with cell surface BiP, which plays an important role in the antiangiogenic and antitumor activity of K5 domains in tumour and proliferating endothelial cells (Davidson et al., 2005). When Par-4 and BiP combine, it leads to apoptosis by ER stress and the commencement of the FADD/caspase-8/caspase-3 pathway. TNF-related apoptosis-inducing ligand (TRAIL) also relies on the Par-4 signalling to trigger apoptosis (Burikhanov et al., 2009). Inhibition of TGF-signalling by the complex of Cripto and BiP on the cell surface causes tumour growth (Gonzalez–Gronow et al., 2009). Cell surface-anchored proteins such as Cripto and T-cadherin also interacts with BiP causing activation of pro-survival or pro-apoptotic pathways in tumour and endothelial cells. Cell surface BiP is essential for Cripto signaling in human tumor, mammary epithelial and embryonic stem cells. Cripto signalling via MAPK/PI3K and Smad 2/3 pathways can be prevented by inhibiting the binding of Cripto to cell surface BiP (Kelber et al., 2009; Shani et al., 2008). It has been shown that inhibiting the interaction of Cripto with BiP on the cell surface prevents Cripto from enhancing cellular proliferation, reducing cell adhesion, downregulating E-Cadherin and encouraging pro-proliferative responses to activin-A and Nodal (Kelber et al., 2009). BiP also has the potential to control the coagulation cascade by interaction with tissue factor 1 (TF1). The effect of BiP on TF-mediated procoagulant activity in murine brain endothelial cells (bEND.3) and macrophage-like cells (RAW) cells was reported (Gaurabh batacharya, 2005). It was demonstrated, that the C-terminal of BiP physically interacts with the extracellular domain of TF1 and negatively affects its procoagulant activity. In addition, visceral adipose tissue-derived serine protease inhibitor (Vaspin) is a ligand for cell surface BiP/MTJ-1 complex, the downstream effects are protective against ER stress-induced metabolic dysfunction (Nakatsuka et al., 2012). Natural killer cells and T cells express activating receptor natural killer group 2D receptors (NKG2D) and MHC1 class 1-related polypeptide 1 (MICA) is a ligand for these receptors. Cells surface BiP interacts with MICA participating in immune evasion in chronic lymphocytic leukaemia (Huergo-Zapico et al., 2012). Transthyretin is a functional protein in pancreatic pancreatic-β cells. The internalisation of

transthyretin into pancreatic-β cells happens through its interaction with cell surface BiP (Dekki et al., 2012).

Pep42-cyclic oligopeptide that binds to the cell surface BiP was used for targeted drug delivery in cancer cells (Ying Liu et al., 2007). BiP interacts with α2 macroglobulin at the cell surface and low-density lipoprotein receptor-related protein (LRP) acts as a coreceptor. Urokinase plasminogen activator surface receptor (UPAR) interacts with cell surface BiP to degrade the extracellular matrix and facilitate cancer cell invasion (Li et al., 2013). Alpha-synuclein interacts with cell surface BiP to dysregulate actin turnover causing synaptic dysfunction that follows neurodegeneration (Bellani et al., 2014). Additionally, secreted BiP interacts with epidermal growth factor tyrosine kinase (EGFR) to activate cancer cells in hepatocellular carcinoma via the SRC pathway. Insulin-like growth factor receptor 1 (IGF-1R) interacts with cell surface BiP and involves in the proliferation and migration through the phosphatidylinositol 3-kinase (PI3K) and mitogen-activated protein kinase (MAPK) pathways (Yin et al., 2017). In atherosclerotic lesions, monocyte/macrophage-like cells and endothelium have been shown to exhibit BiP on the cell surface (Bhattacharjee, 2005).

Interestingly BiP also facilitates the internalisation of several viruses such as Dengue virus and Coxsackie virus. For the internalisation of the Coxsackie A9 virus, its interaction with Integrin $\alpha_v\beta3$ itself is not sufficient. It also needs BiP on the cell surface, which forms a complex with MHC-I and acts as a co-receptor for the Coxsackie A9 virus and, which is further internalized via the MHC-I-mediated endocytosis in mammalian cells (Gonzalez–Gronow et al., 2009; Triantafilou et al., 2002). Cell surface BiP interacts with the Bornavirus at the cell surface (Honda et al., 2009). BiP on the cell surface acts as a ligand to extracellular soluble BiP (Vig et al., 2019).
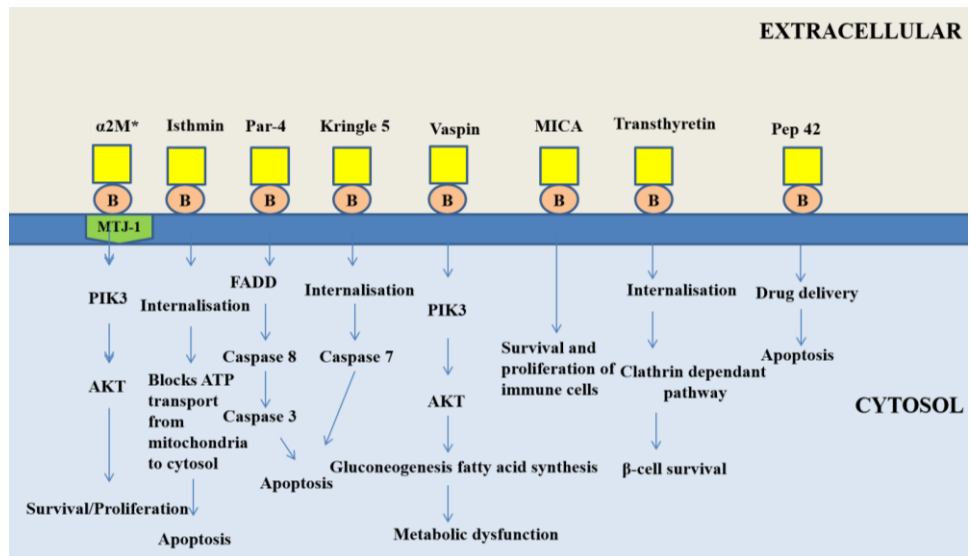
Figure 1.7: Cell surface BiP reacts with various extracellular ligands.

Various extracellular ligands such as isthmin, activated alpha 2-macroglobulin (alpha2M), Kringle 5 domain-containing proteins, Par-4, vaspin, (MHC1 class 1-related polypeptide 1 (MICA), transthyretin and pep42-containing proteins interact with cell surface GRP78 (Source: adapted from Gonzalez–Gronow et al., 2009).
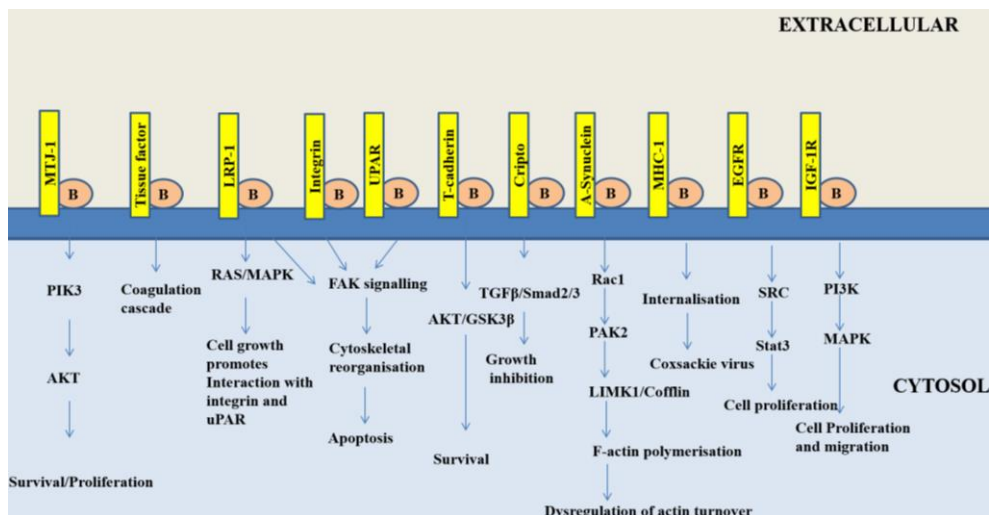
Figure 1.8: Cell surface BiP reacts with various surface receptors.

Various cell surface receptors such as murine DnaJ-like protein (MTJ1), tissue factor 1 (TF1), LRP1 (low density lipoprotein receptor-related protein), integrin, Urokinase plasminogen activator surface receptor (UPAR), T-cadherin, Cripto, A-synuclein, MHC1, epidermal growth factor tyrosine kinase (EGFR), Insulin-like growth factor receptor 1 (IGF-1R) interact with cell surface GRP78 (Source :adapted from Gonzalez–Gronow et al., 2009).

To verify that BiP is a true cell surface protein a combination of protein biotinylation with sodium carbonate extraction followed by avidin pull-down was used to separate the cell surface BiP, ER and plasma membrane-embedded form of BiP, BiP in the ER and transmembrane protein complex or GPI anchored BiP. Different fractions contained different forms of BiP. Under normal conditions, most of the BiP was proved to be an ER-luminal resident protein, whereas membrane-embedded form and cell surface form were noticed only under cell stress conditions. After inducing the ER stress, small amounts of membrane-embedded form was identified and the majority of the protein was present in the eluate indicating cell surface BiP is in the peripheral form (Tsai et al., 2015).

1.4.5 Effect of BiP on immune cells

BiP has been shown to suppress T cells by inducing regulatory B cells that secrete IL-10 and express programmed death-ligand 1 and FAS ligand (Tang et al., 2016). Dendritic cells express low levels of human leukocyte antigen-DR isotype (HLA-DR) and cluster of differentiation 86 (CD86) and increased expression of intracellular indoleamine 2, 3-dioxygenase upon treatment with BiP (Corrigall et al., 2009). BiP maintains the myeloid antigen-presenting cells to be in the tolerogenic state, even after stimulation with LPS (Yang et al., 2016). BiP was also shown to reduce the secretion of cytokines by facilitating the internalisation of TLR-4 by interacting with CD14 when stimulated with LPS (Qin et al., 2017).

Under certain conditions, BiP is thought to behave as a resolution-associated molecular pattern (RAMP) protein. RAMPS are released along with danger-associated molecular pattern (DAMP) molecules from necrotic cells and they antagonize proinflammatory mediators, aiding the reestablishment of homeostasis in the immune system. Therefore, BiP in the extracellular environment can have anti-inflammatory and immune-modulatory characteristics. BiP exhibits these properties by directing the T cell development towards the Th2 profile with the production of IL-4, IL-5, and IL-10, which are regulatory cytokines and also by stimulating human monocytes (HM). The possible mechanisms for the induction of regulatory T cells by BiP are as follows: The direct effect on T cells was achieved through the receptor-mediated process and the induction of dendritic cells (DC) of a tolerogenic phenotype. Increased amounts of BiP expression also protects the HeLa cells from cytotoxic T cells (Bläβ et al., 2001). BiP specific peptide presentation may lead to an increase in the number of regulatory T cells in a peptide-dependent manner (Shields et al., 2012, 2011). Binding of BiP to an unknown receptor on human peripheral blood monocytes (HMBC) causes changes identical to deactivated macrophages. The major outcome of this interaction is inhibition of TNF-α, a decrease in the IL-1b: IL-1 receptor antagonist ratio, an increase in the release of IL-10, and an increase in levels of the soluble TNF receptor II. Intracellular BiP and extracellular BiP may function to reduce the pro-inflammatory effects

of NF-κB, thus facilitating the reduction of acute inflammation. BiP also prevents the differentiation of immature dendritic cells (Panayi and Corrigall, 2006). BiP *in-vitro* encourages human monocytes to differentiate to mature DCs that have a stable anti-inflammatory phenotype. Interaction of T cells with these BiP-treated mature dendritic cells leads to regulatory T-cell development (Corrigall et al., 2009). The production of inhibitors of IL-1β and TNF-α such as IL-1Ra and sTNFRII was increased by BiP thereby reducing the inflammatory potential. BiP treated monocytes have a reduced ability for antigen presentation. Moreover, BiP can alter mouse B cells into the $CD_{19}^{hi}FASL^+$/PD-L1$^+$ IL-10- producing B cells that suppress T cell proliferation (Tang et al., 2016).

1.4.6 Chemical inducers of chaperone

Heat shock proteins have a very essential function in protecting the cells from various forms of stresses (Parsell and Lindquist, 1993) and also in processing the proteins (Hartl and Hayer-Hartl, 2002). Both in *in-vivo* and *in-vitro* studies it is proved that molecular chaperones inhibit the aggregate formation of partially denatured proteins. Due to these protective features, chaperones are considered as the lifeguards of the proteome (Jäättelä, 1999; Michels et al., 1997; Minami et al., 1996). Molecular chaperones offer organisms protective functions at both tissue and cellular level. For instance, hyperthermia or gene transfer induced chaperone expression can protect the brain and heart tissue from ischemia based injury (Brown and Sharp, 1999; Carroll and Yellon, 1999). Prevention of formation of protein aggregates was proved to be beneficial in several neurodegenerative diseases such as spinal and bulbar muscular atrophy (Kobayashi et al., 2000), familial amyotrophic lateral sclerosis (Takeuchi et al., 2002), spinocerebellar ataxia type 1 (Cummings et al., 1998) and Huntington's disease (Jana et al., 2000). In *Caenorhabditis elegans* and fruit fly, a modest amount of increase in chaperone expression extended their life span (Hsu et al., 2003; Tatar et al., 1997). The idea of substituting chaperones with wild proteins or normal proteins or inducing the expression of proteins originated from these beneficial effects of chaperones.

Various molecules added to cells and intracellular factors such as A23187, brefeldin A, thapsigargin, tunicamycin, and AIF_4 disrupt ER homeostasis, which leads to the accumulation of unfolded or misfolded proteins. Upregulation of glucose-regulated proteins (GRPs) could be a result of the accumulation of misfolded proteins. These compounds enhance the expression of GRP78 (BiP) and GRP94 (Price et al., 1992). Ethanol also upregulates the expression of BiP mRNA at the transcriptional level by utilising promoter sequences and pathways which differ from the ones utilised by classic GRP78 inducers such as A23187, brefeldin A and thapsigargin also has an additive effect on the expression of BiP when co-treated with these inducers. Ethanol also enhanced the induction of BiP by A23187, brefeldin, and thapsigargin (Potentiates et al., 1996). $\Delta^{12}PGJ_2$ cyclopentenone utilises the unfolded protein response to increases the expression of BiP gene (Odani et al., 1996).

1.4.7 Chemical Inducer of BiP (BIX)

BIX is a chemical inducer of BiP was discovered in 2008 in screening for compounds that selectively induced ER chaperone BiP (Kudo et al., 2008). BIX utilises the ATF6 pathway of the unfolded protein response to induce the expression of BiP preferentially (Kudo et al., 2008). The chemical name of this compound is (1-(3, 4-dihydroxyphenyl) -2-thiocyanate-ethanone) (Figure 1.9). It preferentially induces BiP, along with a slight induction of GRP94, CHOP, and Calreticulin through the ATF6 pathway of UPR. It is proved to be therapeutic against ER stress-induced cell death in neuroblastoma cell lines and retinal ganglion cells. Pre-treating the *in-vivo* models of cerebral infarction and forebrain ischemia with BIX reduced cell death. The effects of BIX in experimental models are summarised in Table 5.1.

Solubility: DMSO
Molecular weight: 209.22 g/mol
Chemical Formula: $C_9H_7NO_3S$
Synonyms: 2-(3, 4-Dihydroxyphenyl)-2-oxoethyl ester thiocyanic acid
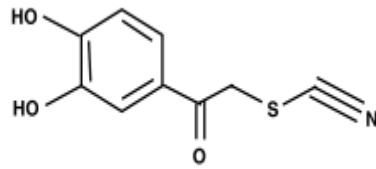
Figure 1.9: Structure of BIX (1-(3,4-dihydroxyphenyl)-2-thiocyanate-ethanone) (Kudo et al., 2008).
BIX is a member of thiocyanates that is 3, 4-dihydroxyacetophenone. One of the methyl hydrogen group of 3, 4-dihydroxyacetophenone is replaced by sulfur of a cyanosulfanediyl (-SC♯N) (https://pubchem.ncbi.nlm.nih.gov/compound/16656807).

BiP has been shown to be significantly upregulated during normal myelination (Naughton et al., 2015) and BiP's presence enhances the survival of myelinating oligodendrocytes in an EAE model of inflammatory demyelination (Hussien et al., 2015). Therefore, it is hypothesised that the induction of BiP using BIX could enhance myelination in *in-vitro* models of myelination.

1.5 Myelinating culture systems

1.5.1 *In-vitro* myelinating cultures

To study the therapeutic potential of BiP or BiP chemical inducer, *in-vitro* myelinating cultures were utilised. One model of myelination *in-vitro* involves the dissociation of cerebral hemispheres from mouse embryos prior to culturing *in-vitro*, allowing the interactions of neurons and oligodendrocytes in the presence of other CNS cells. Oligodendrocytes start myelinating axons *in-vitro* after 13-14 days (Lubetzki et al., 1993). Alternatively, embryonic rat cerebellar cultures with enhanced axonal ensheathment were developed which myelinate continuously for up to 3 months (Svenningsen et al., 2003). Oligo cortical spheroids which are 3D cultures developed from the human pluripotent stem cells were used to study the essential cellular interaction during myelination in the developing central nervous system (Madhavan et al., 2018). In a study conducted to study the genes involved in Wallerian degeneration *in-vitro*, a small explant culture developed from the sciatic nerve of young adult rats were used. They demonstrated myelination similar to *in-vivo* (Thomson et al., 1993).

Later, embryonic mouse spinal cord myelinating cultures were placed in a defined medium instead of serum, which has undefined components. (Thomson et al., 2006). Astrocytes in these cultures act as a scaffold on which axonal development and myelination happen, simulating the natural conditions. These protocols were further altered to prepare rat embryonic spinal cord cultures from E15 embryonic Sprague Dawley rats. A confluent monolayer of astrocytes derived from the corpus striata of the P1 rat pups brain was used as a scaffold in these cultures and it supports the formation of nodes of Ranvier and myelin sheaths by spinal cord cells (Sorensen et al., 2008). The astrocyte monolayer also influences neuronal survival and axonal density. The explant cultures have the advantages of complex cellular interactions and paracrine signalling. They simulate the *in-vivo* situation more closely. The spinal cord-derived myelinating cultures were used to study the glial axonal interaction during myelination (Ioannidou et al., 2012), mitochondria distribution in small diameter CNS axons (Edgar et al., 2008), the effect of dietary cholesterol on remyelination (Berghoff et al., 2017), and pathogenesis of Zika virus system (Cumberworth et al., 2017). These spinal cord myelination cultures were adapted to a multiwell plate for semi high throughput screening compounds and onto the microelectrode array to study the electrical activity (Bijland et al., 2019).

1.5.2 Organotypic Slice cultures

Different parts of the brain have been exploited by researchers in ex vivo models of myelination. For example, Barria et al used the hippocampus to study the function of the glutamate receptor (Barria, 2019). Quick *et al.*, used the spinal cord slice cultures prepared from neonatal 5-6 day old Swiss Webster mice to study the effects of minocycline against the West Nile virus (Quick et al., 2017) and brain slices were prepared from postnatal 8-9 days from 3XTg-AD mice to study Alzheimer disease (Croft and Noble, 2018). However, due to the prominent white matter tracts present in the sagittal sections of the cerebellum (see section 1.6 for a summary of the anatomy of the cerebellum), this brain region is the one that is most frequently used to study developmental and reparative myelination ex vivo. For example, organotypic cerebellar slices from mouse were developed and used for studying myelination and remyelination

using immunohistochemistry (Sekizar and Williams, 2019; Thetiot et al., 2019). Slice cultures prepared from P8 mouse forebrain and cerebellum retain the morphology and intercellular spatial relationship of oligodendrocyte lineage cells, microglia, astrocytes and neurons (Sherafat et al., 2018). The cerebellar slices prepared from P10 Wistar rats were used for studying anti-viral agents against tick-borne encephalitis (Lenz et al., 2018). As myelination in postnatal differs from that of the adults, to exclude the age factor while interpreting the data to MS, adult rodent cerebellar slice cultures were also developed (Tan et al., 2018). More recently, the application of live imaging to mouse organotypic slice cultures was carried out to study the trauma induced-cell death and loss of myelin (Llufriu-Dabén et al., 2019).

1.6 Rationale

Binding immunoglobulin protein/glucose-regulated protein 78 (BiP/GRP78) is a chaperone protein that functions within a subcellular organelle called the endoplasmic reticulum (ER). Under certain disease conditions, for example, chronic neurodegenerative disorders such as Alzheimer's disease, Parkinson's disease and multiple sclerosis (MS), BiP may end up being secreted out of the cell, leading to its detection in body fluids. While in circulation, BiP has been reported by others to have a protective or anti-inflammatory role, through interactions with dendritic cells. On discovering that recombinant BiP is currently in human clinical trials for the treatment of rheumatoid arthritis, we hypothesised that BiP might have therapeutic potential in multiple sclerosis another autoimmune disorder. During MS, the fatty nerve insulation (myelin) is attacked by immune cells. When we recently discovered significant upregulation of BiP during the production of myelin in the brain we speculated that BiP could be a 'super-therapeutic'. In addition to affecting immune cells, BiP could, if taken up by oligodendrocytes, have a positive impact on myelination. To test these ideas, we produced and characterised recombinant human full-length BiP and variants. The available literature on extracellular BiP did not describe the presence or absence of signal sequence (S) and KDEL (K) properly, therefore we produced and characterised four variants of human BiP (S^+/K^+, S^+/K^-, S^-/K^+, and S^-/K^-). Then we collaborated with Prof Chris Linington of the University of Glasgow to study the effect of BiP on myelin production by oligodendrocytes in spinal cord myelinating cultures *in vitro*. Later, organotypic slice cultures prepared from P10 rat pups cerebellum were used to study if the effects noticed in spinal cord myelinating cultures were reproducible.

Hypothesis

Recombinant BiP or chemical induction of BiP expression can enhance myelination in multiple sclerosis.

Aims

The over-arching aim of the study was to establish the therapeutic potential of recombinant BiP or BiP induction in MS.

Specific aims

- To produce endotoxin-free 'full length' and variant forms of recombinant human BiP.

- Analyse the translocation of exogenous recombinant BiP within different cell cultures.

- To test the therapeutic potential or detrimental effects of recombinant BiP or a chemical inducer of BiP (BIX) in multiple sclerosis.

- To perform RNA-seq to study the differentially expressed genes between different treatment groups and to perform pathway analysis from the differentially expressed gene data to investigate the pathways involved.

Chapter 2 : Materials and Methods

2.1 Materials

Table 2.1: General Chemicals

Material	Code	Supplier
NdeI	R0111S	New England Biolabs
XhoI	R0146S	New England Biolabs
Agarose	A9539	Sigma Aldrich
10X Fast digest green buffer	FD0274	Thermo Fisher Scientific
6X loading dye	R0611	Thermo Fisher Scientific
1Kb Gene ruler ladder	SM0313	Thermo Fisher Scientific
GenElute™ HP Plasmid Miniprep Kit	NA0150	Sigma Aldrich
Genejet Dna Cleanup Microkit	13253149	Thermo Fisher Scientific
Gel Red	BT41003	Cambridge Bioscience
LB Agar	L2897	Sigma Aldrich
LB Broth	L3022	Sigma Aldrich
Kanamycin	K4000	Sigma Aldrich
pGEM-T Easy vector system	I-A1360	MyBio Ltd
Ampicillin sodium salt	A0104	Melford Laboratories Ltd
pET22b vector	69744-3	Merck
Ethylene diamine tetra acetic acid, disodium salt dihydrate	E5134	Sigma Aldrich
Glacial Acetic acid	A/0360/PB17	Thermo Fisher Scientific
Trizma base	T6066	Sigma Aldrich
Bromophenol blue	44305	Electran, BDH
Endotoxin-free PBS	TMS-012-A	Sigma Aldrich
Magnesium Chloride Hexahydrate	M2393	Sigma Aldrich
Magnesium Sulfate Heptahydrate	M2773	Sigma Aldrich
Tryptone	TRP03	Formedium
Yeast extract powder	YEA01	Formedium

Material	Code	Supplier
Isopopyl-β-D-1-thiogalactopyranoside	MB1008	Melford Laboratories Ltd
KCL	P9541	Sigma Aldrich
MOPS sodium salt	M5789	Sigma Aldrich
Potassium acetate	P5708	Sigma Aldrich
Rubidium chloride	R2252	Sigma Aldrich
Magnesium chloride dihydrate	M8266	Sigma Aldrich
Manganese II chloride tetra hydrate	M3634	Sigma Aldrich
Calcium chloride dihydrate	C3306	Sigma Aldrich
Glycerol	G5516	Sigma Aldrich
Acetic Acid	A6283	Sigma Aldrich
DH5 alpha cells	Made in-house	Heinz P. Nasheuer's Lab (NUIG)
BL21-CodonPlus (DE3) RIL cells	230245	Agilent Technologies
Rosetta 2(DE3) pLysS cells	Made in-house	Andrew Flaus lab (NUIG)
GoTaq Green Master Mix 100	M7122	MyBio Ltd
PFU DNA polymerase	M7741	MyBio Ltd
PCR tube polypropylene natural 0.2ml flat cap	11889241	Thermo Fisher Scientific
dNTPs	U1511	MyBio Ltd
Pierce 1-Step^{TM} Transfer Buffer	84731	Thermo Fisher Scientific
Super Signal West Pico Chemiluminescent Substrate	34080	Thermo Fisher Scientific
Milk powder		Marvel original, Premier foods
Tween 20	P1379	Sigma Aldrich
DMEM	D6429	Sigma Aldrich
Amersham Hybond 0.45µm PVDF 300mmx 4mm roll	15259894	Thermo Fisher Scientific
Acrylamide/ Bis-Acrylamide 30%	A3699	Sigma Aldrich
Brilliant blue R 250	27816	Sigma Aldrich
Trizma base	T6066	Sigma Aldrich
Glycine	G7126	Sigma Aldrich
Methanol	34860	Sigma-Aldrich

Material	Code	Supplier
Glacial Acetic acid	A/0360/PB17	Thermo Fisher Scientific
NNNN-Tetra methyl ethylene diamine	T9281	Sigma-Aldrich
SDS	71725	Sigma-Aldrich
Whatman blotting paper	WHA10426892	Sigma-Aldrich
Konica Minolta medical imaging films	APlus 1824	Konica Minolta
Adenosine Triphosphate	272056-0251M	Lifesciences
Deoxyribonuclease I, lyophilized powder	DN25	Sigma Aldrich
Lysozyme from hen egg white	62971	Sigma Aldrich
Nonidet P40 substitute (NP40)	74385	Sigma Aldrich
Cuvettes	FB55147	Thermo Fisher Scientific
NaCl	S3014	Sigma Aldrich
Pierce Disposable 5 ml columns	29922	Thermo Fisher Scientific
His-Select Nickel affinity gel	P6611	Sigma Aldrich
Viva spin turbo, 15,5kDa, PES,48PK	VS15T12	Sartorius
X 30 Column PD10 Desalting, 30 columns	15497374	Thermo Fisher Scientific
Chloramphenicol	C0378	Sigma Aldrich
KOH	P1767	Sigma Aldrich
Imidazole	I2399	Sigma Aldrich
Sigmafast protease inhibitor cocktail	S8830	Sigma Aldrich
HEPES	B2001	Melford Laboratories Ltd
FG, Optical adhesive covers pack size pk100	4311971	Thermo Fisher Scientific
96-well Fast Thermal Cycling Plates	4346907	Thermo Fisher Scientific
Sypro Orange Protein G	S6650	Biosciences Ireland
HCL	07102	Sigma Aldrich
Nuclease free water	129115	Qiagen
RIPA buffer	R0278	Sigma Aldrich
RNAse ZAP	R2020	Sigma Aldrich

Material	Code	Supplier
RNA easy plus microkit	74034	Qiagen
Tris base	BP152-5	Thermo Fisher Scientific
Mowiol 4-88	81381	Sigma Aldrich
Triton X	T9284/T8787	Sigma Aldrich
Paraformaldehyde	158127	Sigma Aldrich
Dulbecco's PBS	D8662	Sigma Aldrich
Qiashredder	79654	Qiagen
Sodium azide	S2002	Sigma Aldrich
Flourshield with DAPI	F6057	Sigma Aldrich
Adenosine diphosphate	A2754	Sigma Aldrich
Endotoxin Elisa kit	OKEH02559	Aviva Biological Systems
AnaTag FITC protein labelling kit	AS-72059	Anaspec

Table 2.2: Primary and secondary antibodies used for western blotting and immunofluorescent microscopy

Material	Dilution	Code	Supplier
BiP-anti rabbit	1:5000 (WB)	Ab32618	Abcam
Z2-mouse IgG2A	1:200	Made in house	Linington's lab (University of Glasgow)
SMI31-mouse IgG1	1:1000	801601	Biolegend
Olig 2-mouse IgG2A	1:200	MABN50	Sigma Aldrich
AA3-rat IgG	1:100	Made in house	Linington's lab (University of Glasgow)

Material	Dilution	Code	Supplier
Iba1- rabbit IgG	1:500	019-19741	Wako
Ed1-mouse IgG 1	1:200	Ab31680	Abcam
Nestin-mouse IgG1	1:200	MAB353	Millipore
GFAP- mouse IgG1	1:500	Z0334	Dako, Agilent Technologies
MAP2-rabbit IgG	1:200	Ab32454	Abcam
SOX2	1:500	Ab97959	Abcam
Peroxidase-Conjugated affinity Pure donkey anti-rabbit	1:10000 (WB)	111-035-144	Jackson labs
Alexaflour 488 goat anti-mouse IgG2a(ɣ2a)	1:400	A21131	Thermo Fisher Scientific
Alexaflour 568 goat anti-mouse IgG2a(ɣ2a)	1:400	A21134	Thermo Fisher Scientific
Alexaflour 488 goat anti-rat IgG (H+L)	1:400	A11006	Thermo Fisher Scientific
Alexaflour 488 goat anti-rabbit IgG (H+L)	1:400	A11008	Thermo Fisher Scientific
Alexaflour 568 goat anti-mouse IgG1(ɣ1)	1:400	A21124	Thermo Fisher Scientific
Alexa flour 568 goat anti-rabbit IgG(H+L)	1:400	A11036	Thermo Fisher Scientific
Rhodamine phalloidin	1:200	R415	Thermo Fisher Scientific
Texas red phalloidin	1:200	T7471	Thermo Fisher Scientific
DAPI	1:1000	D3571	Thermo Fisher Scientific

Table 2.3: Tissue culture reagents

Chemical	Code	Supplier
BiP inducer X	SML-1073	Sigma Aldrich
Penicillin/streptomycin	P4458/ P0781	Sigma Aldrich
Minimum essential medium	51200-046	Thermo Fisher Scientific
Minimum essential medium eagle	M2279	Sigma Aldrich
Hank's Balanced Salt Solution	H6648	Sigma Aldrich
L-glutamine	g7513	Sigma Aldrich
L-ascorbic acid	A8960	Sigma Aldrich
N-acetyl L-Cysteine	A9165	Sigma Aldrich
Primocin	Ant-pm 1	Invivogen
Glucose	G7021	Sigma Aldrich
Tris (hydroxymethyl) aminomethane,	252859	Sigma Aldrich
Formalin, neutral buffered, 10%	HT501320	Sigma Aldrich
DMSO	D2650	Sigma Aldrich
Millicell cell culture inserts	PICMORG50	Millipore
Poly-L-lysine	P1274	Sigma Aldrich
Coverslips,13 mm	631-0150	VWR
Hydrocortisone	H0396	Sigma Aldrich
Biotin	B4501	Sigma Aldrich
Insulin	I1882	Sigma Aldrich
Collagenase type I	17100-017	Thermo Fisher Scientific
Soybean Trypsin Inhibitor	T9003	Sigma Aldrich

Chemical	Code	Supplier
Dnase I-bovine pancreas	D4263	Sigma Aldrich
BSA fraction V	A 3059-10mg	Sigma Aldrich
Trypsin EDTA	T3924-100ml	Sigma Aldrich
Glucose	G7021	Sigma Aldrich
NaHCO$_3$	S5761	Sigma Aldrich
HEPES	H4034	Sigma Aldrich
Transferrin human	T1147	Sigma Aldrich
Recombinant human Insulin	I-9278	Sigma Aldrich
Putrescine	P7505	Sigma Aldrich
Selenium	S9133	Sigma Aldrich
Progesterone	P-6149	Sigma Aldrich
DMEM/F12 media	21331-020	Thermo Fisher Scientific
N1 media supplement(100x)	N6530-5ml	Sigma Aldrich
Recombinant murine EGF	315-09	Peprotech
DMEM 1X high glucose with Glutmax	61965-026	Thermo Fisher Scientific
DMEM Glutmax Pyruvate (Low glucose)	21885-025	Thermo Fisher Scientific
Horse serum	26050-088	Thermo Fisher Scientific
L-glutamine	G7513-250ml	Sigma Aldrich
HBSS	14170-088 500ml	Thermo Fisher Scientific
Fetal bovine serum	F9665	Sigma Aldrich
Leibovitz L-15 media	11415-049	Thermo Fisher Scientific

2.2 Production of recombinant BiP variants
2.2.1 Polymerase chain reaction

To synthesise and amplify the DNA sequences of interest, two forward and two reverse primers were used: one forward primer with signal sequence 5′-CAGGATCCACATATGAAGCTCTCCCTGGTGGCCGCGATGCTGCTGC TGCTCAGCGCGGCGCGGGCCGAGGAGGAGGACAAGAAGGAGGAC GTG-3′ (to amplify full-length BiP (BiP S$^+$/K$^+$) and BiP S$^+$/K$^-$) and one forward primer without signal sequence 5′-CAGGATCCACATATGGAGGAGGAG GACAAGAAGGAGGACGTG-3′ (to amplify BiP S$^-$/K$^+$ and BiP S$^-$/K$^-$); one reverse primer with KDEL sequence 5′-GGTCTCGAGCAACTCATCTTTTCTGCTGTATCCTCTTCACCAGTTG G-3′ (amplifying BiP S$^+$/K$^+$ and BiP S$^-$/K$^+$) and the other reverse primer without KDEL sequence 5′-GGTCTCGAGTTCTGCTGTATCCTCTTCACCAGTTGG-3′ (amplifying BiP S$^+$/K$^-$ and BiP S$^-$/K$^-$). The PCR reactions were carried out on an Eppendorf PCR machine (Eppendorf AG 22331, Hamburg, Germany). For BiP S$^+$/K$^+$ and BiP S$^+$/K$^-$, the Gotaq green master mix was used, which produces A tails that can be ligated into pGEM-T Easy vector. For BiP S$^-$/K$^+$ and BiP S$^-$/K$^-$, Pfu DNA polymerase was used, which produces blunt ends at the PCR products. Therefore, A-tails were subsequently added by treating these PCR products with Gotaq green master mix by incubating at 70°C for 20 minutes. The PCR products were purified in cases where there was a single band and gel extractions were performed in cases where there were nonspecific bands using Genejet DNA Cleanup Microkit as per manufacturer's instructions.

2.2.2 Ligation of cDNA into pGEM-T easy vector
The purified PCR inserts were ligated to the pGEM-T Easy vector (Figure 2.1) using T4 DNA ligase. The ligation reaction was performed using the pGEM-T Easy vector kit as per the manufacturer's instructions. The ligation mixture consisted of 5 μl of 2x rapid ligation buffer, 1 μl pGEM-T Easy vector, DNA (as per the formula below), 1 μl T4 DNA ligase, MilliQ water (make up the final volume to 10 μl). To ensure a proper ligation the reaction mixtures were stored

at 4°C overnight. The below formula was used to calculate the amount of PCR product required for 50 ng of the vector.

Amount of PCR product = 50 ng Vector x KB insert/KB Vector (Insert: vector ratios of 1:1) was used for both pGEM-T Easy vector and pET22b expression vector.
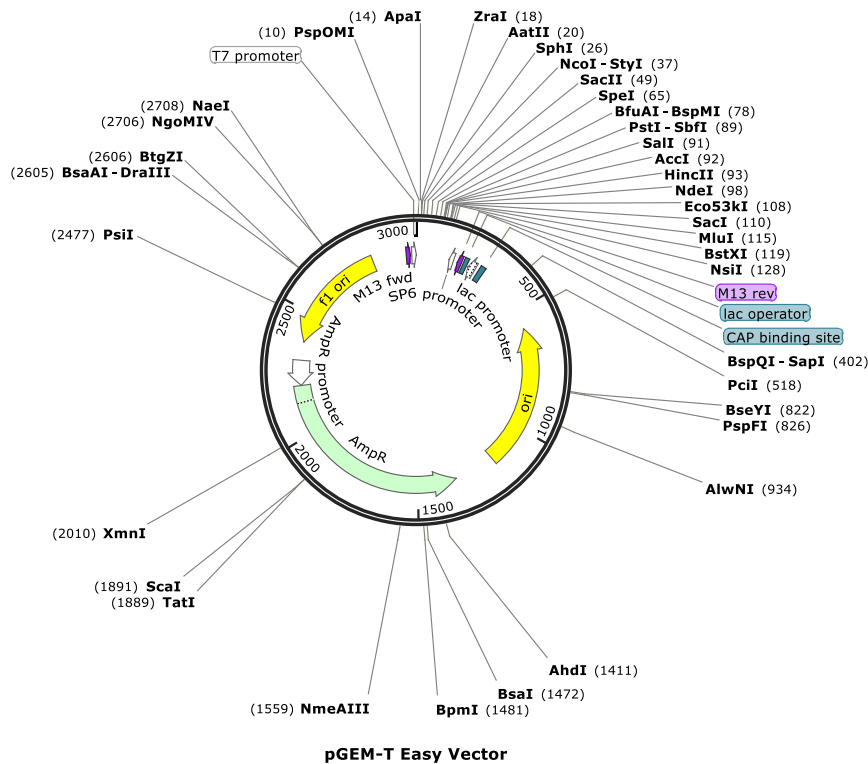
Figure 2.1: pGEM-T Easy Vector map generated using the Snap gene Viewer.

BiP PCR products were ligated to the T-tailed pGEM-T easy cloning vector (3015 bp).

2.2.3 Preparation of competent cells

First, SOB broth was prepared according to the following protocol. To 990 ml of MilliQ water 20 g of Tryptone, 5 g of yeast extract, 0.6 g of NaCl ad 0.5 g of KCl were added and sterilized using an autoclave. Ten ml of sterile-filtered 2 M Mg^{2+} solution was then added. A 2 M Mg^{2+} solution was prepared by adding 20.3 g of $MgCl_2$ and 24.7 g of $MgSO_4$ to a final volume of 100 ml MilliQ water.

DH5 alpha cells, Rosetta 2 (DE3) pLysS cells or BL21-CodonPlus (DE3)-RIL competent parent cells 10 µl were added to 40 ml of SOB broth and incubated overnight at 37°C at 180 rpm. Chloramphenicol (25 µg/ml) was added to the media while making Rosetta 2 (DE3) pLysS cells or BL21-CodonPlus (DE3)-RIL cells. The 8 ml overnight culture was added to 200 ml of SOB broth and further incubated at 37°C at 180 rpm until the OD at 590 nm reached 0.3. The cultures were then pelleted by centrifugation at 4500 rpm, 4°C for 30 min. The supernatant was discarded and 16 ml of transformation Buffer 1 (TFB1) (see Table 2.4 for details) was added to every 50 ml of the initial culture. The cell pellet was resuspended in TFB1 and incubated on ice for 15 min, followed by centrifugation at 4500 rpm, 4°C for 30 min. The supernatant was discarded and 4 ml of transformation Buffer 2 (TFB2) (see Table 2.4 for details) was added to every 50 ml of the initial culture. TFB1 and TFB2 additions were carried out on the ice. It was critical to ensure that, under no circumstances, the cells would be removed from the ice. Heat shock of calcium chloride-treated competent cells allows bacterial cells to uptake exogenous DNA (Mandel and Higa, 1970). The possible mechanism includes the attachment of DNA to the cell surface and uptake of this attached DNA during heat shock (Bergmans et al., 1981) (Chang et al., 2017). The calcium ions act as a bridge between the negatively charged lipopolysaccharide and the DNA. Increasing the permeability of the cell membrane by $CaCl_2$ is the key step in the process of transformation. The cell pellet was resuspended in TFB2 and 50 µl aliquots of the cell suspension were made and transferred to dry ice for immediate freezing of the bacterial solutions which were then stored at -80°C.

Table 2.4: Buffers for preparing competent cells.

Buffer	Composition	Preparation
0.5 M MOPS, pH 6.8 (100 ml)	MOPS 11.56 g	11.56 g of MOPS was dissolved in MilliQ water. pH 6.8 was adjusted using NaOH. The final volume was made up to 100 ml and sterile filtered using a 0.22 µm disposable filter. **Note:** MOPS should be clear and colourless
1 M Potassium acetate (100 ml)	Potassium acetate 9.82 g	9.82 g of potassium acetate was dissolved in MilliQ water and pH 7.5 was adjusted using acetic acid. The final volume was made up to 100 ml and sterile filtered using 0.22 µm disposable filter or autoclaving.
Transformation Buffer 1 (TFB1, 500 ml)	Rubidium chloride, 6.0 g Manganese chloride anhydrous, 3.18 g 1 M Potassium acetate, pH 7.5, Calcium chloride dihydrate, 0.75 g Glycerol, 75.0 ml	All the ingredients were dissolved in MilliQ water. pH 5.8 was adjusted using 0.2 M acetic acid. The volume was made up to 500 ml. And the resulting solution was sterile filtered using a Nalgene disposable bottle top filter. The buffer was stored at 4ºC.
Transformation Buffer 2 (TFB2, 500ml)	0.5 M MOPS Sodium salt, pH 6.8, 10 ml Rubidium Chloride 0.6 g Calcium chloride dihydrate 5.5 g Glycerol 75 ml	All the ingredients were dissolved in MilliQ water. The volume was made up to 500 ml. And the resulting solution was sterile filtered using a Nalgene disposable Bottle top filter. The buffer was stored at 4ºC.

2.2.4 Transformation of DH5 alpha cells

Competent cells have the potential to take up exogenously added plasmid DNA. The newly generated BiP constructs were transformed into competent DH5 alpha cells. Five µl of ligation mixture was added to 50 µl DH5 alpha competent cells and incubated on ice for 30 min. The cells were heat-shocked at 42ºC for 45 seconds in a water bath, followed by a 5 min incubation on ice. A 500 µl volume of SOC medium- was added and incubated at 37ºC on a rotary shaker at 180 rpm for 1 hour to allow the transformed cells to recover. Cells were plated onto an agar plate containing ampicillin at a concentration of 100 µg/ml (or the

necessary antibiotic(s) at indicated concentrations). The plates were incubated overnight at 37°C, in an inverted position, to avoid condensation.

2.2.5 Plasmid Isolation

Four to six single colonies were picked from the DH5 alpha-transformed plates. Each colony was inoculated in a separate tube and grown overnight at 37°C in 10 ml of LB broth with appropriate antibiotic concentration, at 180 rpm (for aeration) in 50 ml Falcon tubes. The transformed DH5 alpha cells grown overnight were centrifuged for 5 minutes at 4000 rpm in the 50 ml tubes. Plasmid isolation was performed according to the protocol provided in GenElute™ HP Plasmid Miniprep Kit. The pellets were resuspended in 200 µl of resuspension solution. The cells were then lysed by adding 200 µl of lysis buffer. The tubes were inverted 6-8 times and allowed to lyse for 3-5 minutes. Then 350 µl of neutralisation buffer was added and gently inverted 4-6 times. The contents of the 50 ml tube were transferred into 1.5 ml eppendorf and centrifuged at 13000 rpm in a microcentrifuge for 10 minutes in order to pellet the protein precipitate and the chromosomal DNA. The clear supernatant was transferred into the miniprep binding columns and centrifuged for 1 minute. The flow-through liquid was discarded and 500 µl of wash buffer 1 was added to the column and centrifuged for 1 minute, bound DNA washed twice using wash buffer. The column was transferred into clean 1.5 ml Eppendorf and 25 µl of elution buffer was added and centrifuged and for 1 minute. The same was repeated to get a final volume of 50 µl.

2.2.6 Restriction digestion of pGEM-T Easy vector, and ligation into pET22b

Table 2.5: Restriction digestion enzymes used for digesting pGEM-T easy vector and pET22b Vector.

Enzyme	Source		Recognition sequence	Cut
NdeI, New Biolabs	R0111S, England	*E. coli*	5´ CATATG 3´ 3´ GTATAC 5´	5´----CA▼TATG----3´ 3´----GTAT▲AC----5´
XhoI, New Biolabs	R0146S, England	*E. coli*	5´ CTCGAG 3´ 3´ GAGCTC 5´	5´----C▼TCGAG----3´ 3´----GAGCT▲C----5´

The series of steps carried out prior to the ligation of BiP inserts into pET22b was illustrated in the (Figure 2.3). Further to the ligation into the pGEM-T easy vector, the plasmid DNA was cut using high fidelity restriction enzymes Nde1 and Xho1 to separate the BiP insert from the pGEM-T Easy vector. The pET22b bacterial expression vector (Figure 2.2) was also digested with NdeI and XhoI. The purified gel extracted cDNAs were ligated into the pET22b vector as described in (section 2.2.2) (linearized pET22b vector was used instead of pGEM-T Easy vector). The ligated plasmids were transformed into DH5α-competent cells via heat shock method as described in (section 2.2.4) throughout the cloning process. Restriction digests were done according to manufacturer's instructions. Briefly, all the samples were run on 1% (w/v) agarose gels in 1X TAE (Tris –acetate-EDTA) buffer at 100 V. The bands were visualized using Protein simple-Alpha imager EC (San Jose, California, USA) in UV mode.
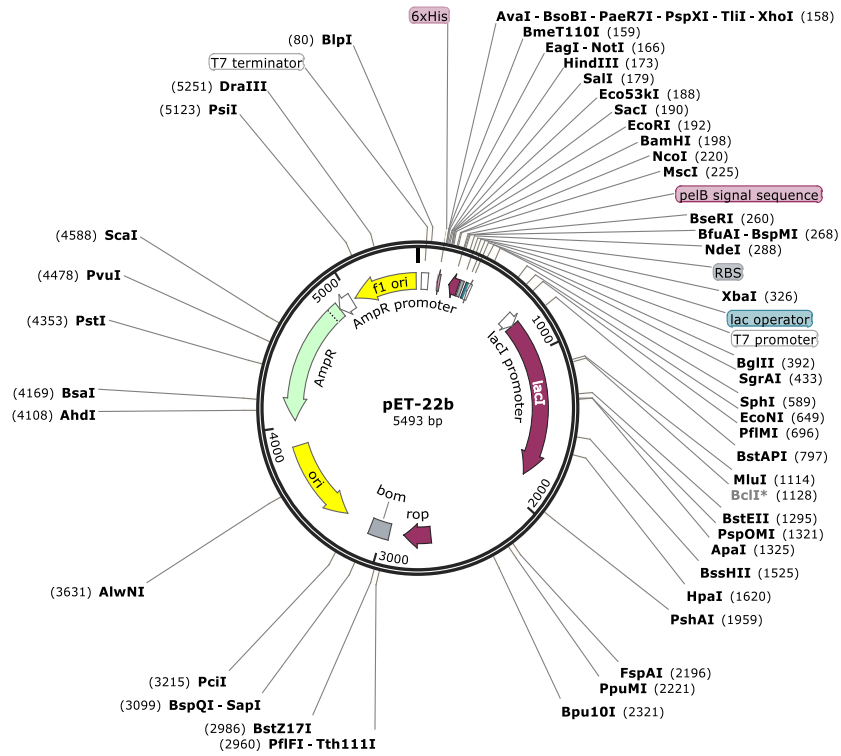
Figure 2.2: pET22b expression vector map generated using the Snap gene Viewer.

The vector was double digested using Nde1 and Xho1 restriction enzyme.

2.2.7 Sequencing of plasmid DNA

Sequencing was done at two stages. Initially, when the insert was in the pGEM-T Easy vector and finally when the insert was inserted into the pET22b plasmid under the control of T7 promoter region. Plasmid DNA samples were sent to Eurofins genomics (Dublin, Ireland) for sequencing along with primers suitable for amplifying internal sequences.

Table 2.6: Primers used for sequencing BiP variants.

Primers		Length	Melting temperature (°C)
T7 (Primer provided by Eurofins)	5'TAA TAC GAC TCA CTA TAG GG 3'	20	47.7
Internal sequence forward primer P0	5'GGTGGGCAAACAAAGACATTTGCTCCTG3'	28	61.4
Internal sequence forward primer P1	5'GCTTATGGCCTGGATAAGAGGGAGG3'	25	61
Internal sequence forward primer P2	5'CGTATGGTGCTGCTGTCCAGGC3'	22	60.4
Internal sequence forward primer P3	5'GCTGAGGAAGACAAAAAGCTCAAGGAGC3'	28	61.4
Internal sequence forward primer P4	5'GCTGGAAAGCCACCAAGATGCTGAC3'	25	61

2.2.8 Bacterial Strains

Rosetta2 (DE3) pLysS or BL21-CodonPlus (DE3)-RIL cell strains were used for protein expression experiments. Based on the level of protein expression and the absence of other unwanted proteins, protein purification was carried out in the BL21-CodonPlus (DE3)-RIL strain only. Competent BL21-CodonPlus (DE3)-RIL cells were transformed with 50 ng of recombinant plasmid DNA and streaked over an agar plate containing ampicillin (100 µg/ml) and chloramphenicol (25 µg/ml) and incubated at 37°C overnight.

2.2.9 Preparation of glycerol stocks

A single colony was inoculated into 10 ml of Luria-Bertani (LB) broth and incubated at 37 °C overnight at 180 rpm. Glycerol stocks were prepared by adding 200 µl of 100% glycerol to 800 µl of cell suspension (20% v/v). The stocks were stored at -80 °C.
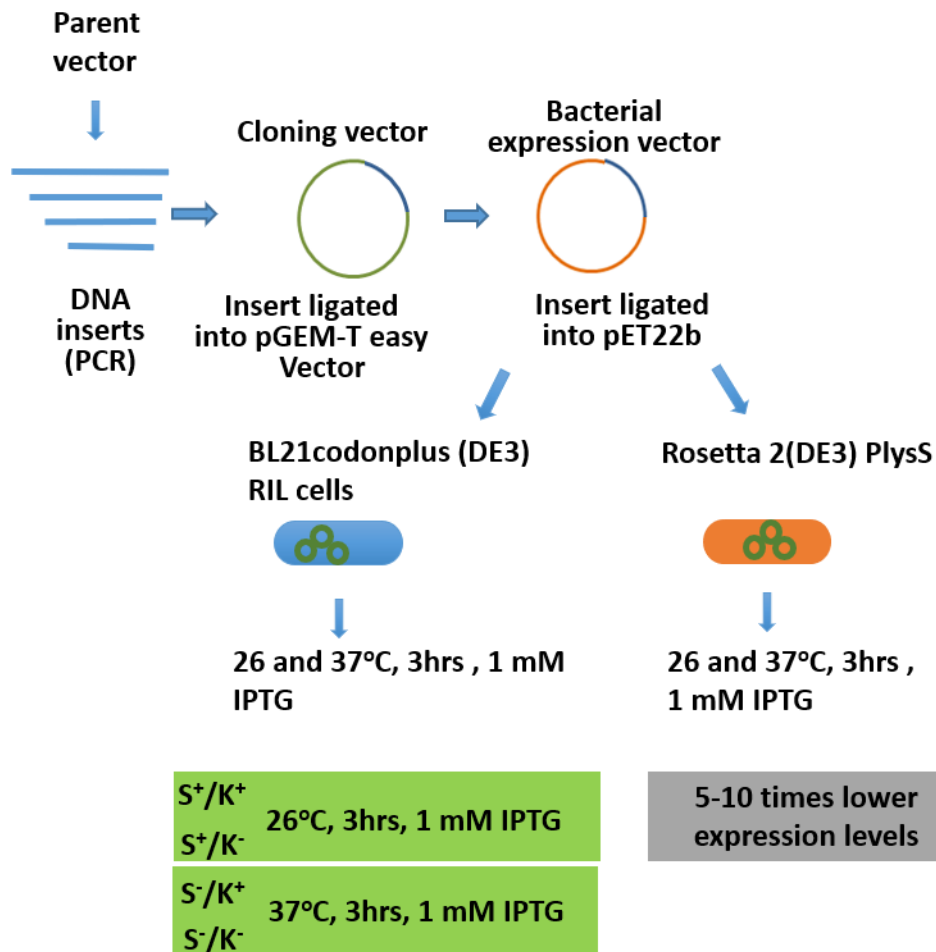
Figure 2.3: Protein Expression in Different Strains.

The parent vector having the BiP sequence was used as a template in the PCR reaction. Later the inserts were cloned into pGEM-T Easy vector and sent for sequencing. When the sequences were confirmed the insert was cleaved from the pGEM-T Easy vector using NdeI and XhoI restriction enzymes. In parallel the pET22b vector was also linearized using NdeI and XhoI restriction enzymes. The insert was ligated into pET22b expression vector and expanded in DH5 alpha cells. The protein expression was tested in BL21-CodonPlus (DE3)-RIL cells and Rosetta 2(DE3) pLysS cells at different temperatures. Finally, BL21-Codon Plus (DE3)-RIL cells were used for protein purifications.

2.2.10 Protein Expression and Purification

The presence of plasmid encoding BiP full length and variant genes was confirmed by restriction digestion. BL21-Codon plus (DE3)-RIL cells were transformed using BiP full length and variant plasmid DNA. A single colony of BL21-Codon plus (DE3)-RIL cells transformed with pET22b bacterial expression vector having the respective BiP gene (full length and variants) coding for a recombinant BiP having a His6 tag at its C-terminus was grown overnight in 100 ml of LB containing ampicillin (100 µg/ml) and chloramphenicol (25 µg/ml). The next day OD values of the cell cultures and medium (blank) were measured at 590 nm. The cells were diluted with fresh LB to adjust the OD to 0.5 to yield a total volume of 500 ml. In parallel, 50 ml of uninduced culture (negative control) was collected at this point and centrifuged at 4000 rpm for 30 min at 4°C and the pellet was frozen. The 500 ml cultures were induced using 1 mM IPTG for 3 h at 37°C. IPTG is similar to allolactose, a lactose metabolite that binds to the lac repressor and removes the tetrameric repressor from the Lac operator, causing the transcription of the gene under the lac operon (Brown et al., 1987). The induced culture was centrifuged at 4000 rpm for 30 min at 4°C in a centrifuge tube using Rotanta 460 R centrifuge (Hettich centrifuge, Tuttlingen, Germany). The supernatant was discarded, and the pellet frozen at -20°C. The buffers used for protein purification are described in (Table 2.7).

The pellet was lysed with lysis buffer (4 ml of buffer added for every gram of the pellet) containing 1 mg/ml lysozyme and incubated at 4°C on a rotary well for 3 h. Later 1 mg/ml DNase I was added and incubated for another hour at 4°C. Further, the lysed cells were centrifuged for 30 min at 14000 rpm at 4°C. Around 400 µl lysate was preserved to run on gels and the rest of the lysate was added to pre-equilibrated Nickel beads for metal affinity chromatography using the His-tag. Nickel has a total of 6 coordination sites and is immobilised on the nitriloacetic acid resin which has 4 chelation sites. The histidine in the his-tag of the proteins binds to the remaining 2 sites (Hochuli et al., 1987; Schmitt et al., 1993). The beads were equilibrated with 10 times the volume of wash buffer.

The wash buffer was removed and the lysate was added to the beads and incubated at 4ºC for 10 min rotating the tube containing resin and cell extract top over bottom. The column was prepared using 5 ml polypropylene tube into which a cotton swab was inserted to prevent the loss of beads during purification. The beads incubated with lysate were passed through the column. Later 5 ml of wash buffer was added ten times to wash the beads. Next, the protein was eluted using elution buffer containing imidazole. The protein eluted was first concentrated using Viva spin turbo concentrator tubes (5000 molecular weight cut-off), by spinning at 4000
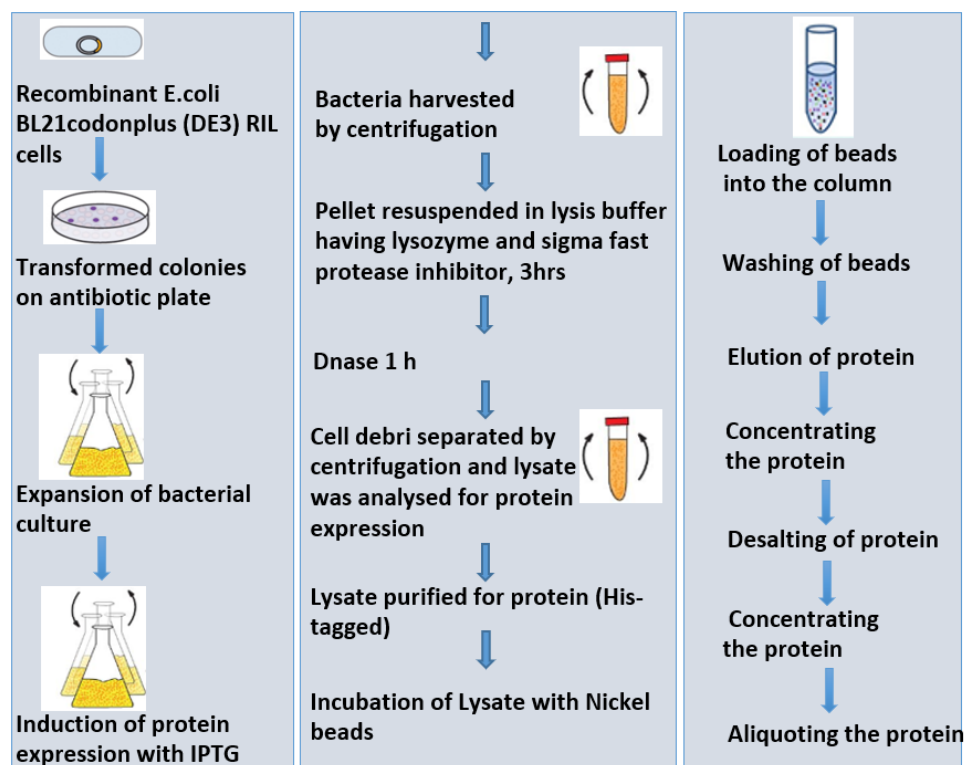
Figure 2.4: Flow chart of protein purification.

BL21-CodonPlus (DE3)-RIL cells were transformed using BiP full length and variant plasmid DNA. The transformed colonies were expanded, and the protein expression was induced with IPTG. The bacterial pellet was harvested and lysed with lysis buffer having lysozyme for 3h, followed by lysis buffer having lysozyme and DNase for 1 h. The lysate was incubated with nickel beads to perform affinity purification. The beads were washed, and the protein was eluted with eluted buffer. The protein was desalted using desalting columns and concentrated. The final purified protein was stored at -80ºC.

rpm, 4°C.The duration of centrifugation depends on the volume of the eluted protein solution. Once the volume is reduced to 3.5 ml it is passed through X30 Column PD10 desalting 30 column to remove imidazole from it. It is important to remove imidazole because it can cause the formation of protein aggregates and it interferes with the activity of the proteins, NMR studies, crystallisation studies (Hefti et al., 2001). The desalting column was equilibrated with wash buffer four times. Then the concentrated protein solution was passed through it and further eluted with 3.5 ml of wash buffer. Leave the eluted solution at 4°C. The desalted solution was passed through the concentrator tube to reduce the volume further to 400 µl. Protein was aliquoted and stored at -80°C (Figure 2.4). Protein concentrations were determined using a NanoDrop 2000 Spectro-photometer (Thermo Fisher Scientific) with 250 to 300 nm spectra collection and 280 nm reading.

The same protocol as above but upscaled was used to purify the protein from 20x1-litre culture. This batch of protein was made endotoxin-free using endotoxin removal high capacity kits for using in *in-vitro* and *in-vivo* experiments according to manufactures instructions.

Table 2.7: Buffers for protein purification.

Buffer	Recipe
Lysis Buffer	30 mM HEPES
	150 mM NaCl
	0.5% NP-40
	pH 7.8
Wash Buffer	30 mM HEPES
	150 mM NaCl
	pH 7.8
Elution buffer	30 mM HEPES
	150 mM NaCl
	250 mM Imidazole
	pH 7.8

2.2.11 SDS PAGE and Western blotting

The samples were denatured by adding 6x loading dye having (1.2 g SDS, 6 mg Bromophenol blue, 4.7 ml Glycerol, 1.2 ml 0.5 M Tris HCl pH 6.8, 2.1 ml water and 0.93 g DTT) and placed in a heating block for 5 minutes at 95°C. The treated samples were loaded onto 10% SDS-PAGE running gel having [30% acrylamide/bis acrylamide (3.3 ml), 1.5 M Tris HCl pH 8.8 (2.5 ml), 10% SDS (0.1 ml), 20% Ammonium persulphate (50 µl), Milli-Q water, TEMED (5 µl)] with a 4% stacking gel (composition see Table 2.8), and were run in 1X Tris-Glycine-SDS buffer (25 mM Tris, 0.192 M Glycine, 0.1% SDS) for 1 h at room temperature until the pre-stained protein ladder was resolved.

Table 2.8: SDS-PAGE gels.

Gel	Recipe	Volume
Running Gel (10%)	30% w/w acrylamide/bisacrylamide 37.5:1	3.3 ml
	1.5 M Tris HCl, pH 8.8	2.5 ml
	10% SDS	0.1 ml
	20% Ammonium persulphate	50 µl
	TEMED	5 µl
	ddH$_2$O	4.05 ml
Stacking Gel (4%)	30% w/w acrylamide/bisacrylamide 37.5:1	0.33 ml
	0.5 M Tris HCl, pH 6.8	0.63 ml
	10% SDS	25 µl
	20% Ammonium persulphate	12.5 µl
	TEMED	5 µl
	ddH$_2$O	1.5 ml

For western blotting, the gels were transferred onto the PVDF membrane using a Pierce power blotter (Thermo Fisher Scientific), according to the Fischer scientific G2 fast blotter instructions. The membrane was blocked using 5% milk in 1X PBS/0.1%Tween20 (PBST) for 1 h, at room temperature. The membrane was then incubated with rabbit polyclonal antibody against BiP (see Table 2.2), diluted 1 in 5,000 with 5% milk in PBST, for 2 h at RT (or overnight at 4°C), Followed by 3x5 min washes with PBST. The membrane was then incubated with secondary donkey anti-rabbit (see

Table 2.2), diluted 1 in 10,000 with 5% milk in PBST, for 1 h at RT. After 3x5 min washes with PBST, ECL solutions were added to the membrane according to the manufacturer's instructions. The membrane was placed in a developing cassette and medical film was placed over it and allowed to transfer for 30 s or until the bands were visible. The film was then developed using an AGFA automatic film processor in the darkroom.

To visualise proteins, separated proteins were stained in the gel with Coomassie Brilliant Blue R-250 (Coomassie Brilliant blue R-250 -2.5g, Methanol 450ml, Glacial Acetic Acid 100ml, Milli-Q water 450ml) for 1 h at RT. The gels were destained using a solution containing 45% methanol, 45% water, and 10% acetic acid (Table 2.9).

Table 2.9: Coomassie brilliant blue staining and destaining solutions.

Solution	Composition
Coomassie Brilliant Blue R-250 staining solution	Coomassie Brilliant Blue R-250 -2.5 g Methanol 450 ml Glacial Acetic Acid 100 ml Milli-Q water 450 ml
Coomassie Destaining Solution	Methanol 450 ml Milli-Q water 450 ml Acetic acid 100 ml

2.2.12 Native PAGE gel

Purified recombinant BiP was mixed with 6X native loading buffer (600 mM Tris HCl, pH 7.8, 50% glycerol, 0.02% bromophenol blue) and loaded onto 6% gel (using the stock solutions 30%,/0.8% w/v, Acrylamide/Bis-Acrylamide, 0.375 M Tris-HCl pH 8.8, 10% (w/v) ammonium persulfate, TEMED 1%). The gels were run in Tris-Glycine buffer 25 mM Tris, 192 mM glycine at 170 V for approximately 1 h. After electrophoresis, gels were stained with Coomassie Brilliant Blue and destained as discussed in the previous section, Table 2.10.

Table 2.10: Composition of native gels and associated buffers.

Gel	Recipe	Volume
Running gel (6%)	30% w/w acrylamide/bisacrylamide 37.5:1	2 ml
	0.375 M Tris-HCl, pH 8.8	7.89 ml
	10% (w/v) ammonium persulfate	100 µl
	TEMED 1%.	10 µl
Running gel (10%)	30% w/w acrylamide/bisacrylamide 37.5:1	3.4 ml
	0.375 M Tris-HCl, pH 8.8	6.49 ml
	10% (w/v) ammonium persulfate	100 µl
	TEMED 1%.	10 µl
Top gel	30% w/w acrylamide/bisacrylamide 37.5:1	4.275 ml
	0.375 M Tris-HCl, pH 8.8	0.67 ml
	10% (w/v) ammonium persulfate	50 µl
	TEMED 1%.	5 µl

2.2.13 ATPase activity measurements

ATPase assays were performed using a Malachite Green Phosphate Assay Kit according to the manufacturer's instructions. Reaction mixtures were prepared in triplicate in a final volume of 160 µl, using 10 µg of protein in 30 mM HEPES-KOH, pH 7.8, 150 mM NaCl, 20 µM ATP and 2 mM $MgCl_2$, and incubated for 60 min at 37°C (adapted from (Čiplys et al., 2014)). The samples were transferred into 96-well plates and the concentration of free phosphate was measured at 620 nm using a Varioskan flash plate reader (Thermo Fisher Scientific, Dublin, Ireland) with SkanIT software 2.4.3. For calculating the kinetic parameters such as K_M and V_{max}, the same protocol was used except that the concentrations of cations and nucleotides were varied. The resulting data were analysed and kinetic parameters calculated using the Michaelis-Menten equation with GraphPad Prism 6 software (GraphPad Software).

2.2.14 Differential Scanning Fluorimetry (DSF)

DSF was used to study the stability, nucleotide-binding and the effect of divalent cations on nucleotide-binding, as described elsewhere (Ericsson et al.,

2006; Vivoli et al., 2014). Experiments were performed using 1x fluorescent dye Sypro Orange in 30 mM HEPES-KOH, pH 7.8, 150 mM NaCl, with full-length huBiP and variants, set at a fixed concentration of 1 µM alone, or with titrations of cofactors (see Table 3.1). The samples were transferred to 96-well Fast Thermal Cycling Plates and subjected to a heating ramp of 1.0°C per min from 25 to 90°C, with fluorescence intensity readings at 470 nm and 550 nm of excitation and emission wavelengths, respectively, using a StepOnePlus System (Applied Biosystems). Data were analysed using Protein Thermal Shift Software v1.1 (Applied Biosystems) and GraphPad Prism 5 software (GraphPad Software) as described previously (Ericsson et al., 2006; Vivoli et al., 2014).

2.2.15 Endotoxin quantification

Endotoxin quantification was performed using the Aviva Endotoxin Elisa Kit as per the manufacturer's instructions. In brief, a series of standards were prepared with a concentration ranging from 0 EU/ml to 1 EU/ml. A volume of 50 μl of serially-diluted standards, diluted samples and a blank were added to the wells which were pre-coated with anti-endotoxin. To all the wells except absolute blank, 50 μl of 1X Endotoxin-Biotin complex was added and incubated for 60 min. Further to the incubation, the liquid was discarded, and any excess liquid was removed by flicking over a paper towel. The wells were washed thrice with 1X wash buffer for 2 min each. Once the washes were completed 100 μl of 1X-Avidine HRP conjugate was added to each well and the plate was incubated for 45 min. Later the 3 X 2 min washes were followed by 1X wash buffer treatment. Then 90 µl TMB substrate was added to each well and the samples were incubated for 15-30 min at 37 °C (blue colour develops). The reaction was stopped by adding stop solution (yellow colour develops) and the absorbance was measured at 540 nm**.** The endotoxin levels were quantified using competitive endotoxin quantification ELISA. These experiments were carried in association with Daniel O'Toole, REMEDI, National University of Ireland Galway.

2.2.16 ELISA for chemokines

BEAS-2B cells were cultured for 48 h cell with an initial seeding density of 100,000/ml. After 48 h, the cells were exposed to LPS or labelled and unlabelled BiP for 24 h. These cells proliferate and produce chemokines in response to LPS. The cell culture conditions were described in (J. Verspohl and Podlogar, 2012). Quantification of IL-8 was carried out using ELISA kits according to the manufacturer's instructions (R and D Systems, DY208, Duoset, R and D systems. Wiesbaden, Germany). These experiments were carried out by Daniel O'Toole and Sean Mc Carthy, REMEDI, National University of Ireland Galway.

2.2.17 Protein quantification

The molecular weight and molar extinction coefficient of the proteins were calculated using the Expasy Protparam tool. The concentration was calculated by measuring the absorption of purified proteins at 280 nm using a NanoDrop 2000 Spectrophotometer (Thermo Fisher Scientific).

2.3 Cellular response to BiP and BiP chemical inducer-X (BIX)

2.3.1 Fluorescent labelling of BiP

BiP was labelled according to the manufacturer's instruction using Anatag 5-FITC microscale protein labelling kit. In brief, the dye was dissolved in DMSO and the protein was incubated with the dye at 4°C for 2 h. Later the dye protein mixture was passed through the column. The mixture separates into two bands upper slow travelling free dye and the lower protein-dye conjugate. The protein-dye conjugate was collected, and the protein concentration was measured using NanoDrop 2000 Spectrophotometer at 280 nm.

2.3.2 B104 cell culture

The B104 neuroblastoma cell line (El Bitar et al., 1999) was used as a test cell line, to determine whether or not exogenously added BiP was taken up by cells. B104 cells were cultured in DMEM, 10% FBS, 0.1% p/s. T-25 flask having B104 cells was washed with PBS and to which 5ml of 1X trypsin was added

and incubated at 37º C. Trypsin was inactivated using fresh media. Cells were split 1 in 6 during culturing and while freezing, the cells were resuspended in 90% FBS, 10% DMSO. One million cells per vial or three vials per flask were frozen.

Coating coverslips with Poly-L-Lysine (1.33µg/ml)

Dissolve 25 mg of poly-L-Lysine hydrobromide (PLL) in 6.25 ml sterile water. Filter through a 0.22µm filter and store in 66 µl aliquots at -20ºC. Add one 66 µl aliquot in 20 ml sterile water for coating flasks/coverslips, incubate at least 1-2 h. Rinse with sterile water as PLL is toxic for cells.

2.3.3: Spinal cord myelinating cultures

Myelinating spinal cord cultures were generated by Paula Arseni and Lorna Hayden in the Prof. Christopher Linington's Lab, University of Glasgow, as described in (Thomson et al., 2008) (Figure 2.5).

2.3.3.1 Creation of Neurospheres: The corpus striatum from P1 *Sprague Dawley* rat brains was dissected and placed into a bijoux containing 1-2ml of Leibovitz L-15 media. The corpus striata were triturated using a glass It'Pasteur and transferred into a 15ml falcon tube. The cells were spun at 800 rpm for 5 min. The supernatant was removed and the pellet was resuspended in 2 ml of neurosphere media. The contents of the tube were transferred into a T75 flask containing 18 ml of neurosphere media to which 4 µl of EGF was added. The cultures were fed twice a week and usually take a week before they have neurosphere that can be plated. Four striata per Bijoux and one bijoux per flask were used.

2.3.3.2 Preparation of PLL coated coverslips: PLL was added to water and coverslips were added to the water and incubated at 37 ºC. Individual coverslips were placed into 24 well plates in an inclined position so that they do not stick to the bottom and then allowed to dry overnight in the hood.

2.3.3.3 Generation of astrocyte monolayer: The PLL coated coverslips were placed into 24 well plates. When neurospheres are large enough the contents of

the flask were transferred into a 50 ml falcon tube and were spun at 800 rpm for 5 min. The supernatant was removed and resuspended in 12 ml DMEM+10% FBS per plate. 0.5 ml of the cell suspension was added to each well and volume was made up to 1 ml when all the plates were done. The cultures were fed by removing half of the media and replacing with fresh media. It usually takes seven days for the astrocytes to form a uniform monolayer. I flask of neurospheres was sufficient for making 6 plates of astrocytes.

2.3.3.4 Myelinating Spinal cord cultures: The gravid uterus from Sprague Dawley female rats was collected on day E15.5 and placed into a dish containing cold HBSS. The embryos were removed from the embryonic sacs and transferred into a petri dish having HBSS. The embryos were decapitated without disturbing the cervical flexure. The top layer of the skin was removed and isolate the spinal cord from the embryo when it is exposed. The meninges and dorsal ganglia were removed starting at the cervical region. The spinal cords were placed into1ml HBSS. The spinal cords were enzymatically digested by adding 100µl of Trypsin and 100 µl of 1% collagenase-I per ml of HBSS. The spinal cords were incubated at 37 °C for 15 minutes. 2 ml of Soybean trypsin inhibitor was added and the cell suspension was shaken and placed back into the incubator for 2 minutes. The contents were transferred into a 15 ml tube and centrifuged for 5 min at 1200 rpm, 4 ° C. The supernatant was removed and resuspended in 1 ml of plating medium. The cells were passed through the cell strainer and washed with 10ml of media for all cells. The cells were counted and diluted to 3 million cells per ml. Three coverslips were placed in a small petri dish. 50 µl per coverslip was added and incubated for 2 h at 37 °C. For every dish, 600 µl of DMEM+ and 450 µl of plating medium was added. The cells were fed by removing 500 µl of media and by adding 600 µl of fresh media. DMEM+ was used until 12 days and DMEM- after 12 days.

 Use 50 µl per coverslip=150000 cells/coverslip.

Table 2.11: Media used for spinal cord myelinating cultures.

A. Neurosphere Media (NSM)

F12/DMEM	210 ml
Hormone Mix (10x)	25 ml
30% Glucose	5 ml
7.5%NaHCO$_3$	3.75 ml
1M HEPES	1.25 ml
L-Glutamine	2.5 ml
Pen/strep	2.5 ml
4% BSA in L15 media	0.625 ml

B. Astrocyte Media

DMEM (low glucose)	500 ml
FBS	50 ml
L-Glutamine	2.5 ml
P/S	5 ml

C. Plating Media

DMEM (high glucose)	25 ml
Horse serum	12.5 ml
HBSS	12.5 ml
L-Glutamine	0.5 ml

D. Differentiation Media DM- (suppl. P/S + Sodium Pyruvate)

DMEM (4.5g/l glucose)	49.5 ml
Biotin (10 µg/ml)	50 µl
N1 Supplement (100x)	250 µl
Hydrocortisone (10 µM)	250 µl

E. Differentiation Media plus INSULIN DM+

DMEM (4.5g/l glucose)	48.5 ml
Biotin (10 µg/ml)	50 µl
N1 Supplement (100x)	250 µl
Hydrocortisone (10 µM)	250 µl
Insulin	1 ml

Dose-dependent effect fluorescent BIP (S-/K-) by B104 cells

Cells (5000 per well) were seeded in an 8 well chamber slide. Cells were allowed to settle for 24 h. Varying doses of labelled BiP (1 µg, 5 µg, 10 µg, 20 µg, 30 µg, 40 µg) were added to cells in a final volume of 300 µl. Samples were incubated with labelled BiP for 24 h at 37°C. Stained with DAPI and Rhodamine phalloidin (1 in 200).

Staining of Fluorescently labelled BiP

The samples were removed from the incubator washed with PBS and fixed with 4% PFA for 15 minutes at room temperature. Later the cells were permeabilised with 200 µl of 0.2% Triton-X for 5 minutes, followed by a wash with PBS. The samples were incubated with Rhodamine Phalloidin (1:200) or Texas red phalloidin (1:200) for 1 h. The cells were rinsed with PBS and mounted using fluoroshield with DAPI or mowiol having 0.05 % DAPI.

2.3.4 B104 cells treated with labelled BiP

PLL-coated coverslips were placed in a 24 well plate and 40,000 cells were added per well. The cells were allowed to settle for 24 h and later 3 coverslips were transferred into a small petri dish, to which 1 ml of fresh medium was added along with 90 µg of labelled BiP. The cells on coverslips were fixed at different time points as indicated with 4% PFA for 15 min and then washed with PBS followed by immunofluorescence staining with Texas red-labelled phalloidin for Cytoskeleton staining.

2.3.5 Spinal Cord explant cultures treated with labelled BiP

Myelinating spinal cord cultures were generated by Paula Arseni and Lorna Hayden in the Prof. Christopher Linington's Lab, University of Glasgow, as described in (Thomson et al., 2008) (Figure 2.5). To the petri dish with three coverslips, 1 ml of media having 40 µg/ml of BiP was added and the cultures

were incubated. Cells were fixed at different time points and stained for GFAP, MAP2, IBA1, Olig2, Nestin, Sox2, NeuN.

2.3.6 Spinal cord explant cultures treated with recombinant BiP

The cultures were treated with recombinant BiP from DIV 18-28. A dose-response curve was performed using a dose range of 10, 20, 40 and 80 μg/ml. A dose of 20 μg/ml was selected for the subsequent experiment. The cultures were treated with the above-mentioned doses or a specific dose from DIV 18-28. Later the cultures were fixed with 4% paraformaldehyde and immunofluorescence staining was performed to quantify axonal density, myelination, microglia; astrocytes; neurons and cells of the oligodendrocyte lineage.
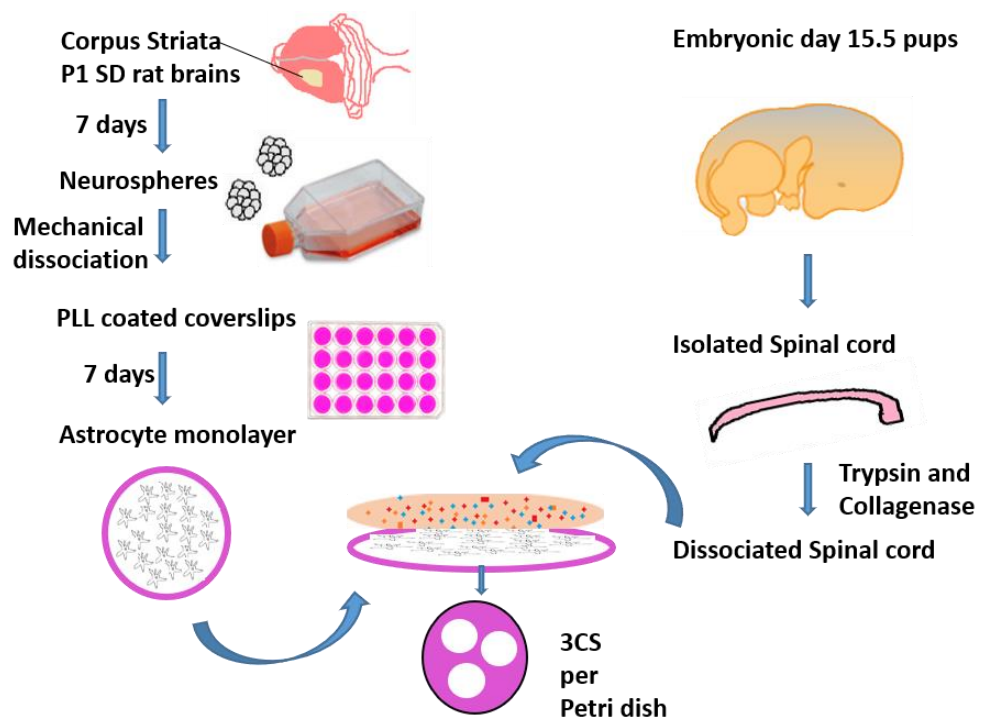
Figure 2.5: Preparation of rat myelinating cultures

Spinal cord myelinating cultures were prepared in two steps. The first step includes the preparation of neurospheres from corpus striatum of P1 Sprague Dawley rats for 7 days. The neurospheres are dissociated and added onto PLL coated coverslips and allowed to grow for 7 days to form the astrocyte monolayer. The second step includes the preparation of dissociated spinal cord cells from the embryonic 15.5 pups and these spinal cord cells were added onto the astrocyte monolayer.

2.3.7 Spinal cord explant cultures treated with BIX.

Once cultures reached DIV 18 and handed over for experimentation, the effect of explant exposure to different doses of BIX, including 0.05, 0.1, 0.5, 1, 2.5, 5 and 10 µg/ml, was assessed. For selected doses,

1. Cultures were treated with BIX or DMSO (vehicle control) from DIV 18-28 to study the effect on parameters such as axonal density, myelination, microglia; cells of the oligodendrocyte lineage and astrocytes.

2. The cultures were treated with BIX or DMSO (vehicle control) from DIV 28-38, to see the possible effects on myelination and microglia.

3. The cultures were treated with BIX or DMSO (vehicle control) from DIV 18-23 followed by withdrawal of BIX to see if the effects caused by BIX were reversible.

2.3.8 Immunofluorescence staining of the spinal cord explant cultures

The supernatant was removed, and cells were washed with PBS. Coverslips were then transferred to the staining tray and turned upside down onto 40 µl triton X, for 15 min. The coverslips were washed with PBS three times. Later the coverslips were transferred onto 50 µl blocking buffer (1% BSA and 10% horse serum in PBS) and incubated at room temperature for 30 min. They were then transferred onto 40 µl diluted primary antibodies (diluted as mentioned in Table 2.2) and incubated at RT for 1 h. Following 3XPBS wash, the coverslips were transferred onto 40 µl diluted secondary antibodies (see Table 2.2) and incubated at RT for 15 min. After another 3XPBS wash and 1X water rinse, the coverslips were placed on 10 µl of mowiol having 0.1 % DAPI. Mowiol hardens overnight at 4°C and the slides were ready to image next day. Care was taken not to introduce any air bubbles during mounting.

2.3.9 Imaging and quantitative analysis

Images were captured with an Olympus BX51 microscope and analysed using Ocular software version 2.0 and CellProfiler software version 2.1.1, (https://cellprofiler.org/). A minimum of thirty images/parameter were analysed from three independent cultures from at least three biological replicates per condition. For SMI31/Z2 and GFAP/MAP2 staining images were taken at 10x magnification. For IBA1/ED1 and Olig 2/AA3 (PLP) staining, a 20x magnification was used. IBA1-, ED1- and PLP-positive cells were counted manually. In spite of having an optimised pipeline for PLP-positive cells, they were counted manually because the software was identifying myelin debris of a certain size as a positive cell. Olig2-positive cells were analysed using a pipeline olig2-aa3.cp optimised for Olig2/PLP staining. The myelin.cp pipeline was used for measuring the myelination percentage and axonal density. The dapi.cp pipeline was used to measure the total cell nuclei counts. The fluorescent

intensity of the green channel was measured using pixel-int-g.cp pipeline and red channel were measured using pixel-int-r.cp in GFAP/MAP2 staining. These pipelines can be downloaded from https://github.com/muecs/cp. See appendix for more details.

2.3.10 RNA isolation

To prepare RNA lysates, the cultures were treated with BIX 5 μg/ml or DMSO for 24 h. The supernatant was removed from culture dishes. RLT lysis buffer 350 µl was added onto the coverslips. The cells were scraped using a sterile scraper. The contents of the dish were transferred into a Qiashredder and spun at 8000 g for 1 min at 25°C. Lysates were frozen at -80 °C.

Fresh or newly thawed RNA lysates were passed through a GDNA column at 8000 g for 30 s. The column was discarded and to the flow-through, an equal volume (350 µl +350 µl) of 70% ethanol was added and thoroughly mixed until no precipitate appeared. The mixture (700 µl) was transferred into RNAse easy micro spin column and centrifuged at 8000 g for 30 s. The flow-through was discarded and to the column, 700 µl of RW1 buffer was added and centrifuged at 8000 g for 0.5 min. The flow-through was discarded and 500 µl of the RPE was added to the column and centrifuged at 8000 g for 30 s. The flow-through was discarded and 500 µl of 80% ethanol was added and centrifuged at 8 g for 2 min. Later the column was centrifuged at 13.2 g for 5 min with the lid open. Next, the column was transferred into an RNA-free 1.5 ml collection tube and 14 µl of RNAse free water was added to elute the RNA. The concentration of RNA was measured using 260/280 absorbance.

2.3.11 RNA Sequencing
Data preparation: Samples were sent to Glasgow polyomics NGS for sequencing. Glasgow polyomics use Next Seq [TM] 500 platform for RNA sequencing. Paired-end 75 bp long reads (2X75 bp) sequencing with a sequencing depth of 25-40 million reads was used. TruSeq Stranded mRNA sample prep kit was used for Poly-A selection. These RNA libraries generated

were compatible with Illumina sequencing platforms for Next-Generation Sequencing.

The FASTQ files provide by Glasgow Polyomics were analysed by Siobhan Cleary, Bioinformatics group, National University of Galway, Ireland using the following software

The objectives of this analysis were to perform a quality control assessment of sequencing and alignment files and to perform gene expression analysis of the gene counts per sample. Differential gene expression analysis of BIX vs DMSO treated samples was also performed. FASTQC sequencing files were aligned to the rn6 rat reference genome using the hisat2 aligner. The analysis workflow is described in (Figure 2.6).
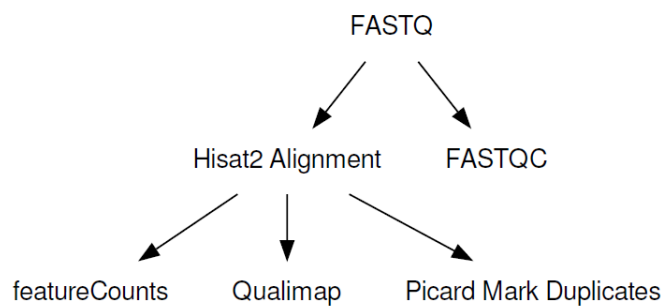
Figure 2.6: Analysis workflow of RNA sequencing data.

Quality control analysis of RNA sequencing included the following steps:

1. Prior to the alignment, the quality of the sequences within the FASTQs for read1 and read2 for each sample was analysed using FASTQC v0.11.8.

2. The alignment Statistics output was analysed using Hisat2 Aligner v2.1.0 (Kim et al., 2015)

3. Qualimap v2.2.1 was used to assess the quality of the alignment files (Okonechnikov et al., 2015).

4. Picard Mark Duplicates v2. 18. 17-SNAPSHOT was used to analyse the read duplication rates (http://broadinstitute.github.io/picard)
5. Feature Counts R package was used to assess the rRNA contamination (Liao et al., 2013).

6. MultiQC tool v1.6. tool was used to produce a single report of the steps from 1-4.

Differential Gene expression analysis was carried out using the DeSeq2 R package V1.18.1. in order to identify genes that are differentially expressed between the BIX treated group and the DMSO treated group.

Pathway analysis was carried out using the Reactome pathway browser version 3.6 (http://reactome.org). The pathway analysis was carried out by Prof. Christopher Linington, University of Glasgow.

2.4 Organotypic cerebellar slice cultures

2.4.1 Ethics
Under standard conditions, Sprague-Dawley rats were housed with a 12:12 hours light: dark cycle, room temperature of 21±2ºC, humidity of 55±10% with continuous access to food and water. The animals were either obtained from Charles River Laboratories or bred in the house. In order to breed, animals over two months of age male and female were placed in the same cage for approximately a week. Abdominal swelling or prominent nipples were considered as positive signs of pregnancy in the breeding female and also these symptoms confirm the success of mating. Female breeding animals were monitored daily to note the date of birth of the pups (postnatal day 0-P0). P10-P11 pups were anaesthetised using isoflurane followed by decapitation. All procedures were carried out in accordance to European directive 2010/62/EU by trained operators and were approved by the Animal care Research Ethics Committee of NUI Galway. All measures were followed to reduce the pain or distress experienced by the animals and also the tissue was shared with other researchers whenever possible to minimise the number of animals used.

2.4.2 Cerebellar dissection and slice culture conditions
The cerebella were isolated from the brains of P10 Sprague Dawley rats and the meninges removed by rolling on sterile Whatman filter paper. Sagittal sectioning of the cerebellum was done using a McIlwain tissue chopper (Gala Instrumente, Bad Schwalbach, Germany). The sectioned cerebellum was transferred into a petri dish containing cold dissection medium (500 ml MEM,

605 mg Tris (hydroxymethyl) aminomethane, Penicillin/Streptomycin 1%, L-glutamine 1%). The whole cerebellum was chopped, and the slices were separated gently in cold medium while viewing under a dissecting microscope using L shape bent glass capillaries (Drummond Scientific Company). Millipore inserts were pre-wet by placing them in 1.1 ml medium within a 6-well plate. Two-to-three slices were transferred using a p1000 tip or a Pasteur pipette that had been cut diagonally to produce a wide mouth, causing less mechanical damage. Slices were fed on DIV 0 with 1100 µl of culture medium (MEM 100 ml, MEME 50 ml, HBSS 44 ml, N-Acetyl amine 1%, Ascorbic acid 1%, L-glutamine 1%, Picromicin 0.2%, Glucose 1000 mg) on DIV 1and 4, with 1000 µl of fresh media. The five-day treatment with DMSO or BIX was started on DIV 7 and further doses were given on DIV 9 and DIV 11.

2.4.3 Slice immunohistochemistry

The slice cultures were fixed with 10% formalin for 2 h on DIV12 followed by 3X5 min washes with 1X PBS. For long-term storage, the slices were stored in 1XPBS/0.05% sodium azide, at 4°C. During fixation and storage, the membrane was also covered with liquid to avoid drying out. The slices were separated from the inserts and each slice was transferred into a well containing 50 µl of PBS in a 24-w plate. Once all the slices were transferred, PBS was removed and 350 µl of blocking buffer (10% Fetal bovine serum, 0.4% Triton X in 1X PBS) was added and incubated for 1 h at RT, with gentle agitation (50 rpm on a Stuart orbital shaker compact,model-SSM1, Fisher scientific). The blocking buffer was removed and 250 µl of diluted primary antibody prepared in diluent (2.5% Fetal bovine serum, 0.1% Triton in 1X PBS) was added. The slices were incubated with the primary antibody for 48 h at 4°C. The slices were washed with diluent 3X15min and followed by incubation with a secondary antibody according to the dilution indicated in Table 2.2. Overnight in dark at 4°C. The slices were washed three times in 1X PBS, for 15 min. The slices were removed from the well plates and transferred onto the glass slides membrane facing the glass for mounting. The slices were mounted with fluoroshield mounting medium and sealed with clear nail polish. The mounted slides were left in the

dark at 4 °C overnight before imaging.

2.4.4 Imaging of fluorescently stained slices

Slides were imaged using 20x magnification for quantification on an Olympus Fluoview1000 Shackleton confocal microscope and analysed using Cell Profiler software, (https://cellprofiler.org/). The Olympus Flourview version 4.2 b software was used. To quantify 4 random images per slice were taken from 5-6 slices per condition from three biological replicates per condition (n=3). The slices had an approximate diameter of 0.5 cm. The edges were avoided while capturing images to avoid the edge effect. The fluorescent intensity red channel was measured using pixel-int-r.cp in Iba1/Olig2 staining. Olig2-positive cells were analysed using a pipeline olig2-aa3.cp optimised for Olig2/PLP staining. These pipelines can be downloaded from https://github.com/muecs/cp. Additionally, slices were also stained for GFAP and PLP to study the effect on astrocytes and matured oligodendrocytes. The fluorescent intensity red channel was measured using pixel-int-r.cp in GFAP/PLP staining. PLP cells were counted manually.

2.4.5 Statistical Analyses

Statistical analyses were carried out using an unpaired T-test or one-way ANOVA with Dunnett's multiple comparisons or Two way ANOVA where applicable, A minimum of three experiments were performed unless otherwise mentioned and data depicted as SD ± mean. Results were considered significant when p values were <0.05.

Chapter 3 : Production and characterisation of recombinant BiP

3.1 Introduction

B-cell immunoglobulin binding protein (BiP), a heat shock protein 70 (HSP70) protein family member, is an indispensable endoplasmic reticulum (ER) chaperone normally present within the ER lumen (Wang et al., 2017). Classically, BiP functions to assist in protein folding, prevent the aggregation of intermediates, and aid calcium binding as well as the trafficking of misfolded protein to the ER-associated degradation system (Wang et al., 2017; Lee, 2007). BiP is comprised of multiple functional sequences (see Figure 3.6A). The N-terminal signal sequence of human BiP (huBiP, amino acids 1-18) directs the protein to the ER whereas the C-terminal KDEL sequence (amino acids 651-654) functions to retain BiP within the ER (Pidoux and Armstrong, 1993). The nucleotide-binding domain (amino acids 125-280) in the N-terminus binds to ATP and ADP in a cycle that controls protein substrate-binding and release, while the substrate-binding domain in the C-terminus (amino acids 420-500) aids in the interaction with substrate protein chains. In addition, a hydrophobic flexible linker region (amino acids 409-419) mediates BiP-BiP interactions and is exposed when BiP is in the ADP-bound state but is not accessible when BiP is in the ATP-bound state (Awad et al., 2008; Bertelsen et al., 2009; Mayer and Bukau, 2005). Cations act as cofactors in nucleotide-binding and Mg^{2+} is the chosen cation for BiP nucleotide-binding binding studies, although Mn^{2+} and Ca^{2+} may also affect ATPase activity (Kassenbrock and Kelly, 1989; Lamb et al., 2006).

Despite the presence of signal and KDEL sequences, BiP has also been detected in/at the nucleus, mitochondria, on the cell surface and extracellularly (Ni et al., 2011) , and *in vitro*, BiP release into the cell culture medium of oviductal epithelial cells has been reported (Marín-Briggiler et al., 2010b). In humans, BiP has also been found in the synovial fluid and its precursor was found in the saliva of individuals with Rheumatic arthritis (RA) (Tsunemi et al., 2010). Giusti et al also detected BiP in the sera of gastric cancer patients (Giusti et al., 2010b). In circulation, BiP may behave as a resolution associated molecular pattern (RAMP), by antagonizing proinflammatory mediators and re-

establishing homeostasis of the immune system (Shields et al., 2012). These properties led to clinical trials of recombinant BiP in therapies for RA (Brownlie et al., 2006; Kirkham et al., 2016; Tsunemi et al., 2010)

It is possible that malfunctioning protein trafficking or an aberrant ER retention process could lead to the extracellular distribution of BiP variants such as BiP with or without its signal and/or retention sequence. Therefore, we hypothesised that BiP variants could execute non-ER-associated physiological functions intra- or extra-cellularly, dictated in part by the presence or absence of signal or retention sequences. To test potential differences in the biochemical properties of huBiP variants, we completed an extensive characterisation of their stability and nucleotide-binding in the presence of different cations. From these studies, we conclude that the presence of the signal sequence influences the nucleotide-binding and ATPase activity of these proteins in the presence and absence of divalent cations.

3.2 Aims

Recombinant protein production and biochemical characterisation of full-length BiP and variants.

3.3 Specific aims

To establish the expression vectors for the production of recombinant human full-length BiP and variants thereof

To purify and characterise recombinant human full-length BiP and variants

To study the role of signal sequence in the enzyme activity of BiP

To study the nucleotide-binding properties of full-length BiP and variants

3.4 Summary of Methodology

Synthesis of BiP DNA sequences was carried out using PCR. These amplified DNA sequences were ligated into pGEM-T Easy vector (cloning vector) and upon sequence confirmation, the DNA sequences were transferred into pET22b vector (expression vector). In this work, we focused on production and

validation of full-length BiP, BiP without its signal sequence and without KDEL (S^-/K^-), BiP without its signal sequence, but with KDEL (S^-/K^+), and BiP with its signal sequence but without KDEL (S^+/K^-). Protein expression was optimised using BL21-CodonPlus (DE3)-RIL cells and Rossetta 2 (DE3) pLysS. Finally BL21-CodonPlus (DE3)-RIL cells were used for large scale protein purification of full length and variant BiPs.

Purification was carried out using His-select nickel affinity gel beads as described in 2.2.10. Each protein (full length and variants) was produced and purified in three independent processes under the same conditions. Molecular weights and molar extinction coefficient of the proteins, 30,495 $M^{-1}cm^{-1}$ at 280 nm, were calculated using the Expasy Protparam tool (https://web.expasy.org/protparam/) and the human amino acid sequence. To determine the concentration the absorption of purified proteins was measured at 280 nm using a NanoDrop 2000 Spectrophotometer.

Proteins were then characterised using SDS-PAGE, native PAGE, ATPase assays and DSF. The relative amounts of oligomeric species of the BiP variants in Coomassie-stained native polyacrylamide gels were quantified by scanning the native gels using an Epson Dual Lens system (model Epson perfection V700 photo, Digital Ice Technologies, Ireland) and band intensities were quantified using the Image J software (NIH, USA). All values were expressed relative to monomeric S^-/K^-.

The ATPase assay was used to investigate the effect of cations on ATPase activity of BiP full length and variants using Malachite Green Phosphate Assay Kit (POMG-25H; Bioassay system, California, USA) according to the manufacturer's instructions. Optimisation of cation concentration was also carried out using ATPase assays. For calculating the kinetic parameters such as K_M and V_{max} the ATPase assay was used except that the concentrations of cations and nucleotides were varied (see Table 3.2). The resulting data was analysed and the kinetic parameter calculated using the Michaelis-Menten equation with GraphPad Prism 5 software (GraphPad).

Differential Scanning Fluorimetry (DSF) was used to study the stability, nucleotide-binding and the effect of cations on the nucleotide-binding. The obtained data was analysed using Protein Thermal Shift Software v1.1 (Applied Biosystems) and GraphPad Prism 5 software (GraphPad). Statistical analysis was carried out using an unpaired T-test. A minimum of two experiments were performed in triplicate and data depicted as SD ± mean

3.5 Results:

3.5.1 Cloning of BiP:

The PCR products of BiP variants were run on a 1% agarose gel and the size of the products for all the variants was approximately around 2000bp (Figure 3.1). These PCR products were ligated into pGEM-T Easy vector and the success of the ligation was analysed using restriction digestions with restriction enzymes *Nde*I and *Xho*I. The size of the linearised pGEM-T Easy vector was approximately 3015 bp whereas the insert was approximately 2000 bp (Figure 3.2). Further, the DNA purified from positive clones were sent for sequencing and the sequence-verified BiP-coding DNAs were isolated and ligated into pET22b vector digested with *Nde*I and *Xho*I restriction enzymes. The success of the ligation into the pET22b vector was analysed using restriction digestion with restriction enzymes *Nde*I and *Xho*I (Figure 3.3). The inserted BiP-coding DNA sequences in the pET22b vector were then also verified by sequencing.
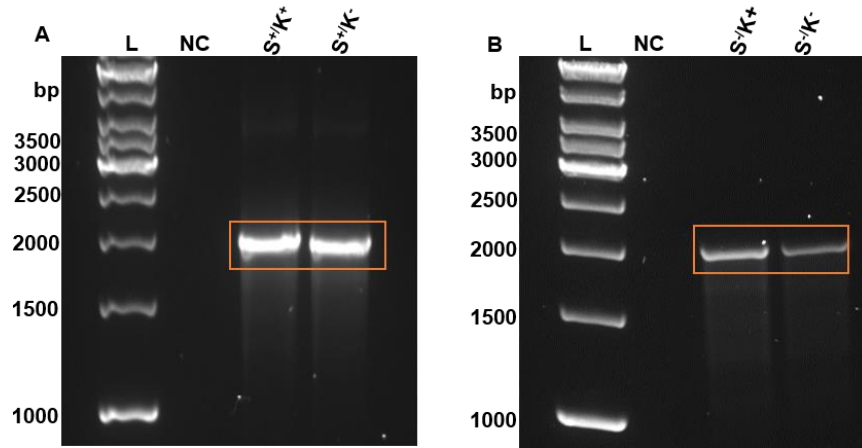
Figure 3.1: Gel electrophoresis images of BiP cDNA PCR products.

All the samples were run on 1% (w/v) agarose gels. The bands were visualized using Protein simple-Alpha imager EC in UV mode. BiP cDNA PCR products highlighted in a yellow box. DNA sequences of Nde1 and Xho1 restriction sites were included on the 5´ and 3´ end, respectively, of the inserted DNA construct. S^+/K^+ and S^+/K^- were produced using Go-Taq Green Master mix. S^-/K^+ and S^-/K^- were produced using Pfu DNA polymerase and A-tails were added by incubating with Go-tag green master mix. L -1kb Gene ruler DNA ladder, NC -control, S -signal and K –KDEL.

Challenges associated with cloning of the DNA inserts

The BiP signal sequence comprises the first 18 amino acids of the natural protein sequence (see Figure 3.6, (Wang et al., 2017) but is mostly cleaved off in the maturated BiP found in the ER. The BiP-encoding cDNA sequence obtained from the Polizzi lab does not contain this signal sequence. Therefore, a PCR-based approach was used to introduce back the signal sequence into the amplified coding sequence. Initially, Taq DNA polymerase (GoTaq Green Master Mix 100) was used for all PCR reactions, but when the cloned inserts were sequenced each construct had several mutations. Therefore, Pfu DNA polymerase was tried, as it is a high-fidelity DNA polymerase. Pfu DNA polymerase was successfully used to clone the BiP $S^-/K^+$and BiP S^-/K^- sequences, but it did not yield any PCR product when attempting to produce BiP S^+/K^+ and BiP S^+/K^- DNAs. Repeating the DNA amplifications with Taq DNA polymerase (GoTaq Green Master Mix 100 (MyBio Ltd)) to amplify BiP

83

S^+/K^+ and BiP S^+/K^- DNA, these two DNA sequences were successfully produced as verified by DNA sequencing of the obtained DNAs.
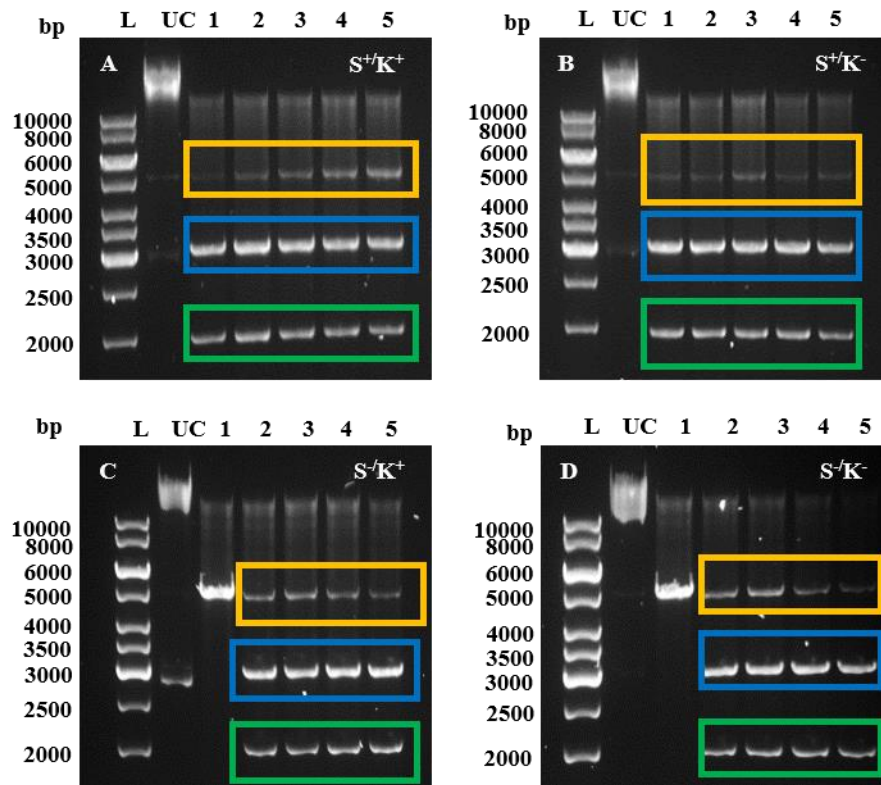
Figure 3.2: Gel electrophoresis images of restriction digestion of BiP constructs in pGEM-T Easy vector.

All the samples were run on 1% (w/v) agarose gels. The bands were visualized using Protein simple-Alpha imager EC in UV mode. A. Restriction digestion of BiP S^+/K^+ plasmid DNA (pGEM T Easy-Vector). B. Restriction digestion of BiP S^+/K^- plasmid DNA (pGEM-T Easy vector). C. Restriction digestion of BiP S^-/K^+ plasmid DNA (pGEM-T Easy vector). D. Restriction digestion of BiP S^-/K^- plasmid DNA (pGEM-T Easy vector). Undigested plasmid DNA highlighted in yellow boxes. Linearized pGEM-T Easy vector highlighted in blue boxes. BiP inserts highlighted in green boxes. The plasmid DNA was digested using *Nde*I and *Xho*I. L - 1kb Gene ruler DNA ladder, C - control. 1, 2, 3, 4, 5-bacterial colony number.
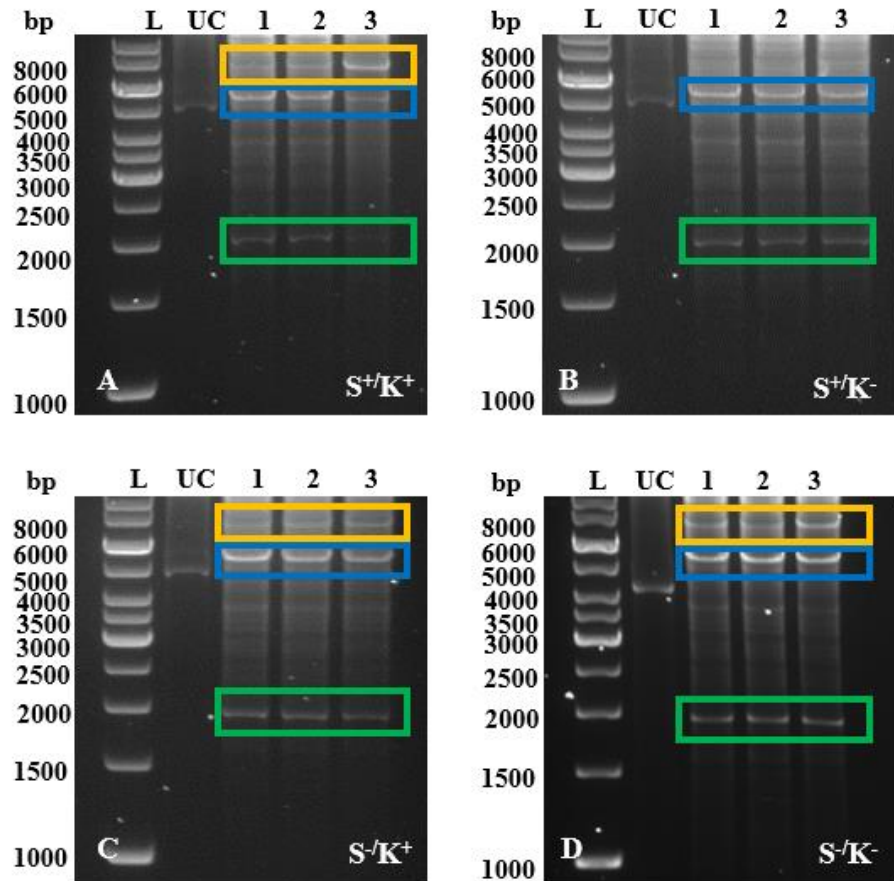
Figure 3.3: Gel electrophoresis images of restriction digestion of BiP constructs in pET22b.

All the samples were run on 1% (w/v) agarose gels. The bands were visualized using Protein simple-Alpha imager EC in UV mode. A. Restriction digestion of BiP S^+/K^+ plasmid DNA (pET22b vector). B. Restriction digestion of BiP S^+/K^- plasmid DNA (pET22b vector). C. Restriction digestion of BiP S^-/K^+ plasmid DNA (pET22b vector). D. Restriction digestion of BiP S^-/K^- plasmid DNA (pET22b vector). Undigested plasmid DNA highlighted in yellow boxes. Linearized pET22b vector highlighted in blue boxes. BiP inserts highlighted in green boxes. The plasmid DNA was digested using *Nde*I and *Xho*I. L-1kb Gene ruler DNA ladder, C-control. 1, 2, 3-colony number.

3.5.2 Human BiP expression, purification, and preliminary characterisation.

Various forms of BiP have been described to occur under physiological and pathological conditions including ER stress and on the cell surface of cancer cells (Corrigall et al., 2004; Ni et al., 2011; Rauschert et al., 2008; Zhang et al., 2010). To investigate biochemical activities of these BiP variants we cloned human BiP variants containing or lacking the signal and KDEL sequence (Figure 3.6) and produced them in *E. coli* cells BL21- (DE3) derivatives having a C-terminal 6x His-tag, enabling purification using immobilised metal affinity columns (Figures 3.5 to 3.6).

Protein expression of BiP variants was carried in *E. coli* strains BL21-CodonPlus (DE3)-RIL cells and Rosetta 2 (DE3) pLysS cells as described in section 2.2.10 and summarised in Figure 3.4. The proteins in the bacterial lysates were analysed by SDS PAGE followed by Coomassie Brilliant Blue staining of the separated proteins. These analyses of proteins in crude extracts reveal that expression of recombinant BiP was 5-10 times lower in Rosetta 2 (DE3) pLysS cells (Figure 3.4, panels B, D, F, and H) compared to BL21-CodonPlus (DE3)-RIL cells (Figure 3.4, panels A, C, E, and G; compare pairwise A-B, C-D, E-F, and G-H). Therefore, BL21-CodonPlus (DE3)-RIL cells were used for all protein purifications. Following optimisation of protein expression, three independent batches of protein of each of the variant were purified using 500 ml of bacterial culture. Representative Coomassie Brilliant blue-stained SDS PAGE gels and their respective western blots are presented in (Figure 3.5).
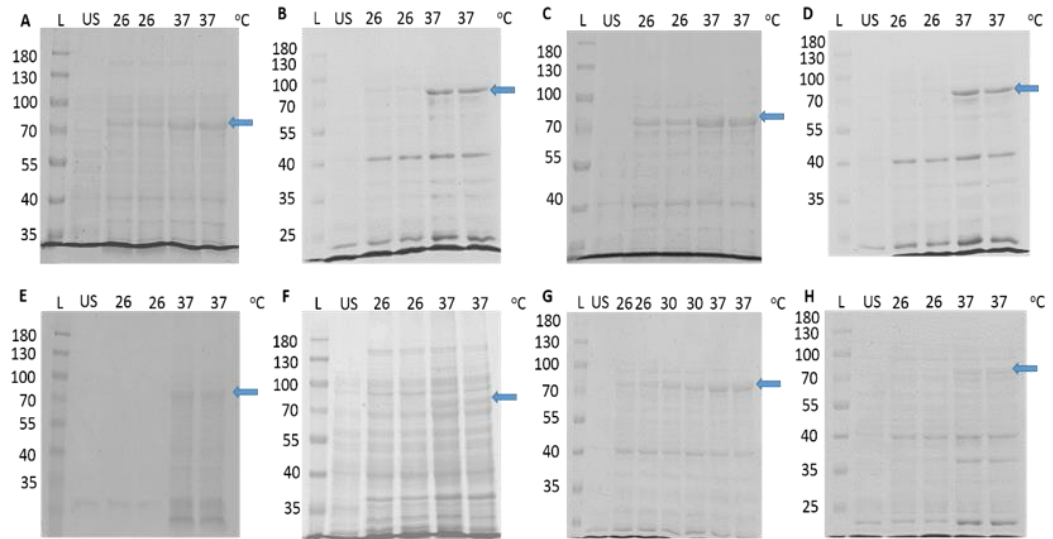
Figure 3.4: SDS-PAGE gels for analysing the protein expression of full-length human BiP and variants in two *E.coli* strains- BL21-CodonPlus (DE3)-RIL cells and Rosetta 2 (DE3) pLysS cells.

1mM IPTG was used for inducing protein expression. Cultures incubated for 3 h at the indicated temperatures.

A- BiP S$^+$/K$^+$ in BL21-CodonPlus (DE3)-RIL cells

B-BiP S$^+$/K$^+$ in Rosetta 2 (DE3) pLysS cells

C-BiP S$^+$/K$^-$ in BL21-CodonPlus (DE3)-RIL cells

D-BiP S$^+$/K$^-$ in Rosetta 2 (DE3) pLysS cells

E-BiP S$^-$/K$^+$ in BL21-CodonPlus (DE3)-RIL cells

F-BiP S$^-$/K$^+$ in Rosetta 2 (DE3) pLysS cells

G-BiP S$^-$/K$^-$ in BL21-CodonPlus (DE3)-RIL cells

H-BiP S$^-$/K$^-$ in Rosetta 2 (DE3) pLysS cells

L- Page rule prestained molecular weight ladder,

US- Uninduced supernatant, numbers 26, 30 and 37- indicate incubation temperatures in ºC, samples were collected from supernatants performed in duplicates.
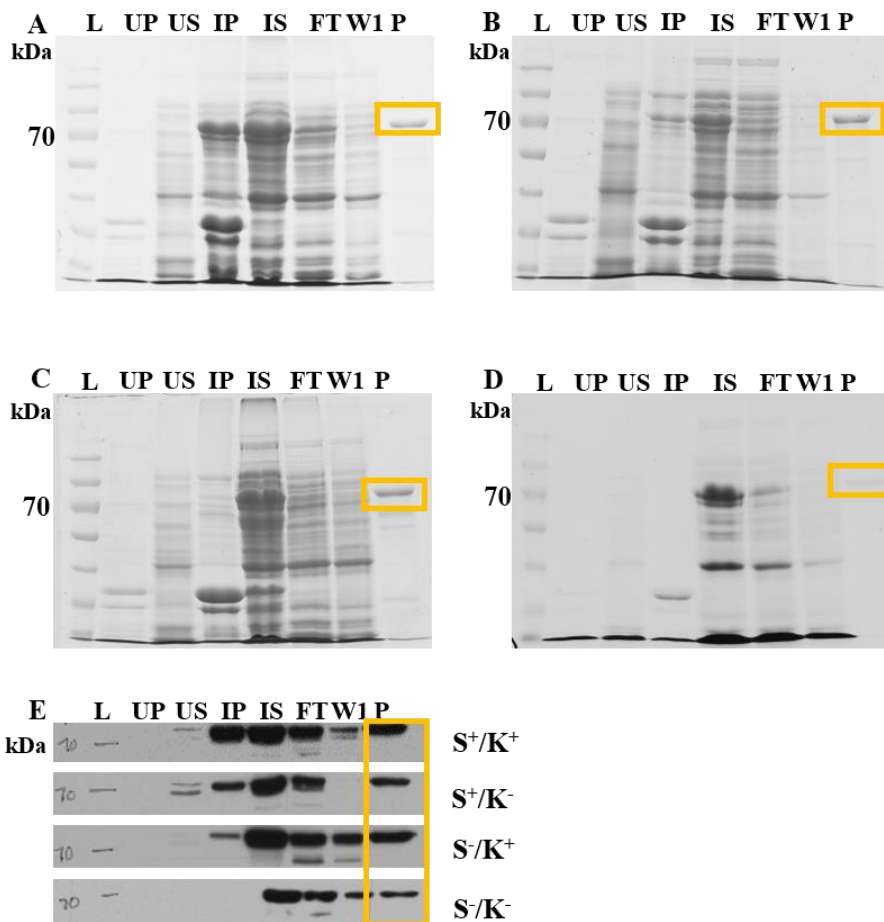
Figure 3.5: SDS-PAGE gels and western blots analyses of full-length human BiP and variants purifications using BL21-CodonPlus (DE3)-RIL cells.

The purification of BiP S^+/K^+, S^-/K^+, S^-/K^+ and S^-/K^- are shown in panel A, B, C, and D, respectively. Gels were stained with Coomassie Brilliant Blue R-250 for 1 h at room temperature and destained. L- Ladder, UP- uninduced pellet, US- uninduced supernatant, IP-Induced pellet, IS-Induced supernatant, FT-flow through nickel column, W1-Wash buffer having protein, P- purified protein of purified BiP protein variants (loading: 5 µg and 2.5 µg of purified BiP for Coomassie Brilliant Blue staining and western blotting, respectively). Panel E shows western blots of BiP variants as indicated on the right. The yellow box indicates purified protein. Primary antibody: Anti BiP (Abcam-ab32618) 1: 5000 (incubated overnight at 4°C). Blocking: 5% milk in PBST for 1 h at room temperature. Secondary antibody: Peroxidase-conjugated affinity Pure Donkey Anti-rabbit (Jackson labs 111-035-144) 1:10000 (Incubation: 1 hour at room temperature).

In the following, we demonstrate the feasibility of producing, from 500 ml cultures of *E. coli* BL21-CodonPlus (DE3)-RIL cells, 5-8 mg of full-length huBiP and its variants, at a concentration of 10-20 µg/µl. Batch quality was confirmed using SDS-PAGE. Coomassie Brilliant Blue-staining of gels showed that the size of the purified proteins was larger than 70 kDa, as expected (Figure 3.6B). The SDS PAGE also showed that the purified proteins were highly pure and had minimal contaminants or degradation. The estimated molecular weights of the proteins, derived from the cDNA sequences, were as follows; S^+/K^+, 73.4 kDa; S^+/K^-, 72.9 kDa; S^-/K^+, 71.7 kDa; S^-/K^-, 71.2 kDa. Thus the maximal difference between variants is about 2 kDa, an amount that is not detectable using SDS PAGE in a protein of this size.

To confirm the oligomeric state of the recombinant proteins, samples were separated on native PAGE gels. All variants were found to exist as monomers, dimers and higher oligomer forms (Figure 3.6C). For all variants, about 5% of the native protein was oligomeric, while between 20 and 30% was dimeric, and 60 to 70% monomeric protein. We also used the non-denaturing PAGE to study the effect of divalent cations and nucleotides on oligomerisation. In the presence of ATP alone or in combination with divalent cations, dimers were converted into monomers, whereas cations or ADP alone, or in combination, did not have an effect on oligomerisation (Figure 3.7) shows a representative experiment using BiP S^-/K^-.
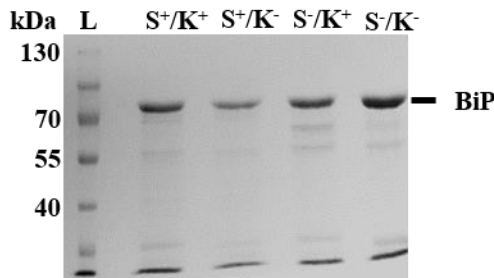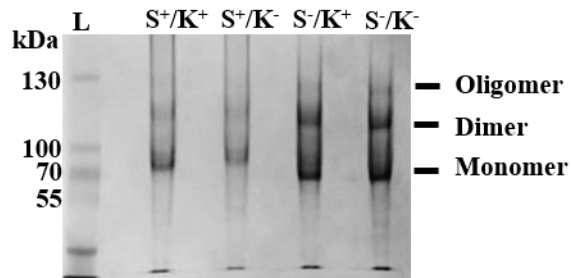
Figure 3.6: Expression, structure, and oligomerisation of full-length huBiP and variants.

 (A) Schematic illustration of recombinant human full-length BiP and its variants. Signal sequence (orange; S), nucleotide-binding domain (blue; NBD), substrate-binding domain (violet; SBD), KDEL sequence (green; K) [1, 23]. (B) SDS-PAGE of purified recombinant full-length huBiP and variant BiP proteins. Proteins were expressed in BL21-CodonPlus (DE3)-RIL cells and purified using metal chelate chromatography as described in the Methods part. A 10 % SDS polyacrylamide gel was used to separate the denatured protein. The Coomassie Brilliant Blue-stained gel is presented. On each lane of the SDS gel, 15 µg of either purified full-length BiP or variant proteins were loaded as indicated. (C) Native PAGE gel of purified full-length BiP and variants. 15 µg of purified full-length BiP and variant proteins were loaded on each lane of a 6 % polyacrylamide gel and native PAGE was performed using Tris-Glycine as running buffer. After the electrophoresis, the gel was stained with Coomassie Brilliant Blue.

A

250

100/130
70
55

S⁻/K⁻ · S⁻/K⁻+ATP · S⁻/K⁻+ATP+ MgCl₂ · S⁻/K⁻+ATP+MnCl₂ · S⁻/K⁻+ADP · S⁻/K⁻+ADP+ MgCl₂ · S⁻/K⁻+ADP+MnCl₂ · S⁻/K⁻+MgCl₂ · S⁻/K⁻+MnCl₂

B

250

100/130
70
55

S⁻/K⁻ · S⁻/K⁻+ATP · S⁻/K⁻+ATP+ MgCl₂ · S⁻/K⁻+ATP+MnCl₂ · S⁻/K⁻+ADP · S⁻/K⁻+ADP+ MgCl₂ · S⁻/K⁻+ADP+MnCl₂ · S⁻/K⁻+MgCl₂ · S⁻/K⁻+MnCl₂
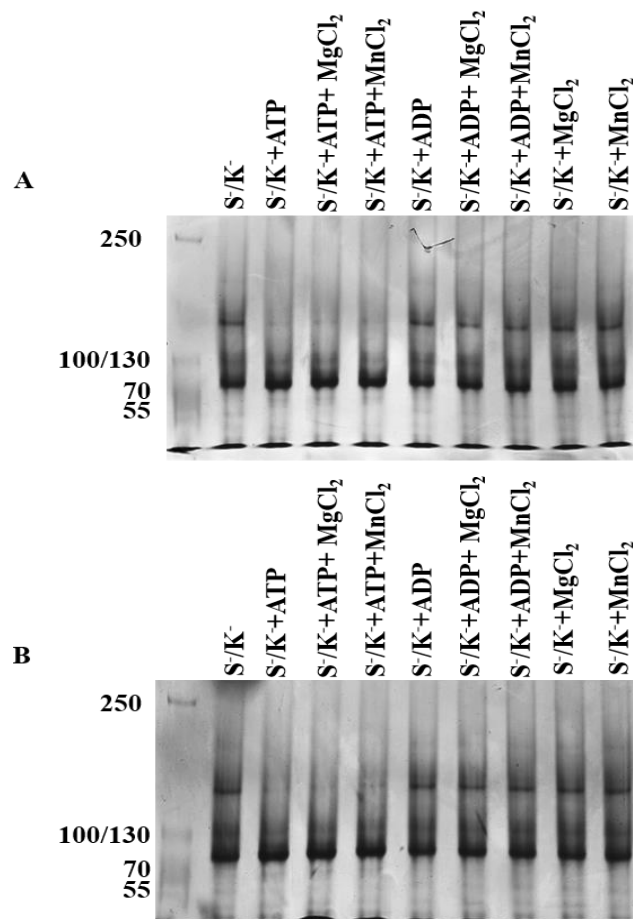
Figure 3.7: **Effect of nucleotides and cations on BiP oligomerization status.**

A. BiP S⁻/K⁻ (20 μg) in the presence of 2 mM of Mg^{2+} or Mn^{2+} or 1 mM of ATP or ADP and a combination of cations and nucleotides as indicated was incubated at 25°C for 10 minutes **B.** BiP S⁻/K⁻ (20 μg) in the presence of 50μM of Mg^{2+} or 25 Mm Mn^{2+} or 1 mM of ATP or ADP and a combination of cations and nucleotides as indicated was incubated at 25°C for 10 minutes and were loaded on a Bis-Tris 6% gel and native PAGE was performed using Tris-Glycine as running buffer. After electrophoresis, the gel was then stained with Coomassie Brilliant Blue.

3.5.3 Highest ATPase activity is associated with S⁺ BiP variants

The impact of the presence or absence of the signal sequence and/or KDEL on the ATPase activity of huBiP variants was tested using triplicate samples of independently purified protein batches. BiP that retained the signal sequences (BiP S⁺/K⁺ and S⁺/K⁻) had significantly higher ATPase activity than BiP S⁻/K⁺ and S⁻/K⁻ without the signal sequence (Figure 3.8). BiP S⁺/K⁻ lacking the KDEL

ER retention sequence also showed a trend towards a lower ATPase activity than full-length (S^+/K^+) BiP, but the difference was not found to be significant (Figure 3.8). These findings suggest that all recombinant proteins were produced and purified as functional proteins and that the signal sequence modulates ATPase activity.
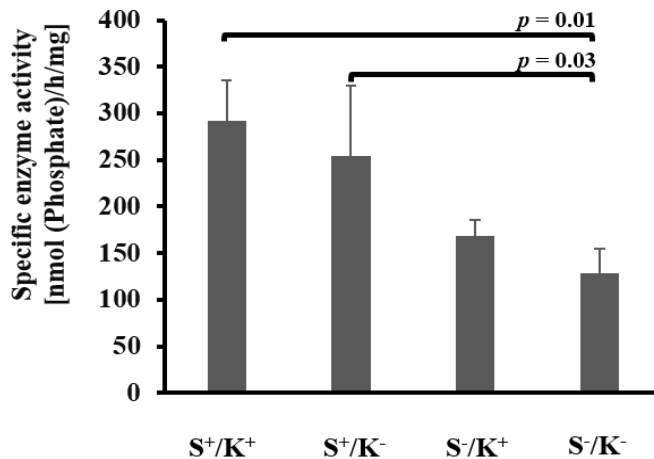
Figure 3.8: Biochemical characterisation of recombinant full-length BiP and variant proteins thereof

ATPase activity of recombinant full-length huBiP and three variant proteins was measured. ATPase activity assays were performed in a final volume of 160 µl containing 10 µg of protein with 30 mM HEPES-KOH, pH 7.8, 150 mM NaCl, 20 µM ATP, and 2 mM Mg^{2+}. The proteins with the signal sequence had the highest activity compared to the other variants with no signal sequence. An unpaired Student T-test was performed and significant differences were observed between full-length huBiP and variant S^-/K^- ($P=0.01$), as well as between variants S^-/K^+ and S^-/K^- ($P=0.03$). Specific enzyme activity and respective standard deviation (SD) values were calculated using data from three individual batches for each recombinant protein variant.

3.5.4 Low concentrations of divalent cations efficiently stimulate the ATPase activity of BiP

Initial experiments characterising the ATPase activity of huBiP variants were performed in the presence of millimolar concentrations of Mg^{2+}, as previously published (Kassenbrock and Kelly, 1989). While Mg^{2+} is considered the preferred divalent cation for stimulating BiP ATPase activity, the role of Mg^{2+} as co-factor may be substituted by Mn^{2+}. Therefore, we compared the effects of Magnesium and Manganese cations

on the ATPase activity of S^+/K^+ and S^-/K^- BiP over a wide range of concentrations (0-10 mM).

Concentrations of 10 µM and 30 µM Mg^{2+} efficiently stimulated the ATPase activity of S^+/K^+ and S^-/K^- BiP (approx. 175 nmol/h/mg protein, Figure 3.9A and 3.9B plus insets). Interestingly at these low concentrations, the stimulation of ATPase by Mn^{2+} was even more efficient than Mg^{2+}, provoking a specific enzyme activity of up to 250 nmol/h/mg of S^+/K^+ huBiP with Mn^{2+}. However, at 100 µM or above, Mn^{2+} stimulates the ATPase activity of huBiP less efficiently than at 10 µM to 30 µM concentrations. It is important to note that concentrations of 20-50 mM of Mn^{2+} were found in the normal brain whereas concentrations of 60-150 mM of Mn^{2+} may already represent pathological levels (Bowman and Aschner, 2014). Increasing the Mn^{2+} concentration reduced the stimulatory effect of the divalent cation even further, such that at 10 mM, Mn^{2+} stimulation of BiP ATPase was no longer detected (Figures 3.9A and 3.9B). In contrast, Mg^{2+} stimulated the ATPase in a very wide range from 10 µM to 10 mM concentrations and did not have any inhibitory effect (Figures 3.9A and 3.9B). Interestingly the concentration of free Mg^{2+} was determined to be 0.8 to 1.2 mM in the ER (Romani, 2011). It is important to note that the huBiP ATPase did not show a clear maximal activity in this wide concentration range of Mg^{2+}, and the difference between the ATPase activity at 100 µM, when compared to that measured at 10 mM, was only 15% (Figures 3.9A and 3.9B). Both Mg^{2+} and Mn^{2+} cations stimulated the ATPase activity of BiP with optimal concentrations of approximately 50 µM and 25 µM, respectively. Calcium did not have any stimulatory effect on the ATPase activity of BiP S^+/K^+ (Figures 3.9C).
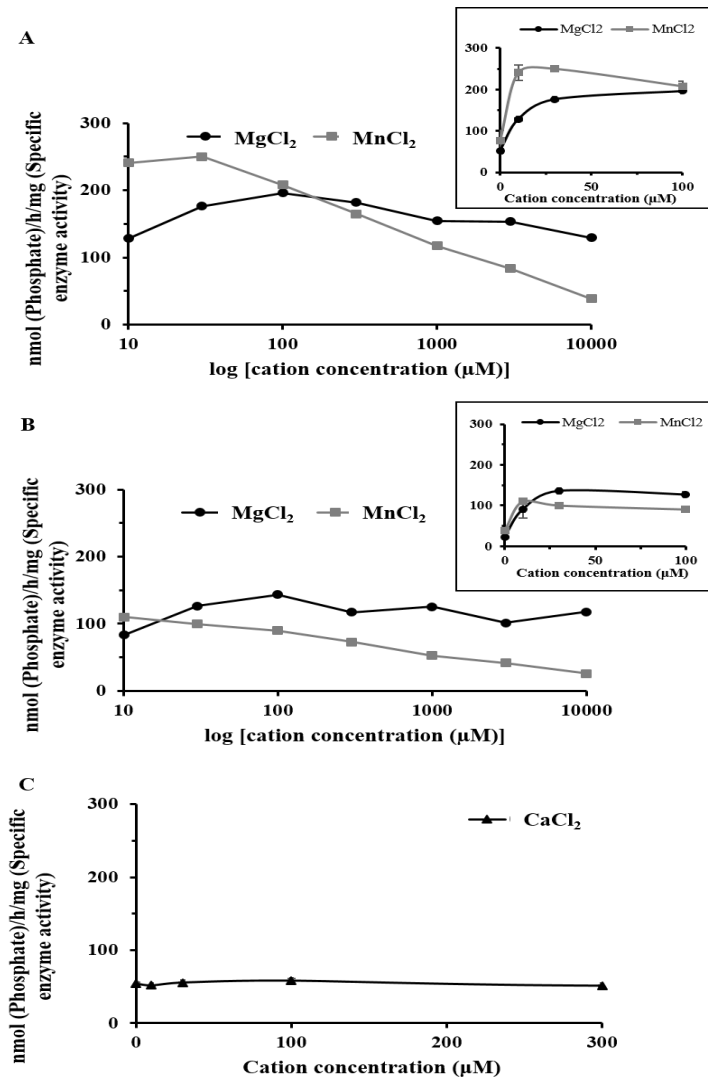
Figure 3.9: Effects of divalent cations on the ATPase activity of BiP S+/K+ and S-/K-.

To test the influence of divalent cations on the BiP ATPase activity increasing amounts of MgCl$_2$, MnCl$_2$ and CaCl$_2$ were added to the reaction mixture containing 20 µM ATP and 10 µg protein. ATPase assays were carried out in triplicate in a range from 0 to 10 mM of cations and representative results (mean of the values and standard deviation (SD)) of such analyses are presented. MgCl$_2$ and MnCl$_2$ stimulated the ATPase activity of BiP with optimal concentrations of 100 and 25 µM, respectively. At higher concentrations of $\geq$ 1 mM MgCl$_2$ still stimulated ATPase activity but to a slightly lesser extent, whereas MnCl$_2$ at concentration 1 mM failed to stimulate BiP ATPase activity and even inhibited it slightly. In contrast, Calcium did not stimulate or inhibit the ATPase activity of BiP S$^+$/K$^+$. (A) BiP S$^+$/K$^+$ ATPase activity in the presence of Mg^{2+} and Mn^{2+} using a logarithmic scale for the cation presentation. The small inset shows ATPase activity of BiP S$^+$/K$^+$ at lower concentrations (0-100 µM) of Mg^{2+} and Mn^{2+} presenting the cation concentrations as a linear scale. (B) BiP S$^-$/K$^-$ ATPase activity in the presence of Mg^{2+} and Mn^{2+} with a logarithmic scale for the cations being used. The inset is the close-up view of BiP S$^-$/K$^-$ ATPase activity at lower concentrations (0-100 µM) of Mg^{2+} and Mn^{2+} using a linear scale presentation of cation concentrations. (C) BiP S$^+$/K$^+$ ATPase activity in the presence of Ca^{2+}.

3.5.5 Preferential interaction of BiP variants with ADP rather than ATP

Physical interactions of proteins with their ligands, cofactors, and substrates can stabilize interacting protein domains and thus cause an increase in the melting temperature of proteins. In keeping with the methods of others (Niesen et al., 2007), DSF was used to analyse the melting temperature of all BiP variants in the presence or absence of nucleotides. In the absence of ADP or ATP, the melting temperatures of the BiP variants tested here ranged from 45.1 to 45.8°C (Figure 3.10A). Thermal denaturation profiles demonstrated the unfolding of the N-terminal (peak 1) and C-terminal (peak 2) of these proteins (Figure 3.10B) similar to previously published results (Lamb et al., 2006). The N-terminal denaturing temperatures were as follows: S^{+}/K^{+}: 46.6°C, S^{+}/K^{-}: 46.8°C, S^{-}/K^{+}: 46.8°C and S^{-}/K^{-}: 46.6°C, while C-terminal denaturing temperatures were: S^{+}/K^{+}: 62.8°C, S^{+}/K^{-}: 62.2°C, S^{-}/K^{+}: 63°C and S^{-}/K^{-}: 62.4°C.
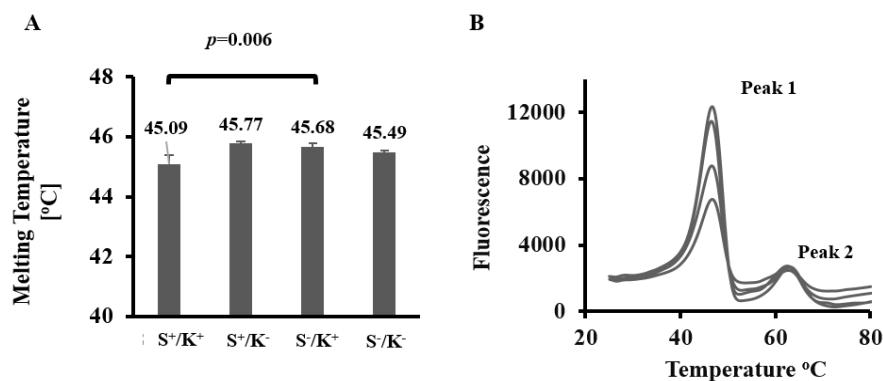
Figure 3.10: Biophysical characterisation of recombinant full-length huBiP and variant proteins thereof.

(**A**) Thermal stability analyses of recombinant full-length huBiP and three variant proteins thereof were performed using DSF. The reaction mixtures contained 1 μM protein in 30 mM HEPES-KOH, pH 7.8, 150 mM NaCl, and 1x Sypro orange. The melting temperatures of the full length and variant proteins are in the range of 45.1 - 45.8°C. The calculated T_m (e.g. the maximum of the first derivative of the raw data), is shown as a mean of triplicate experiments of three individual batches for each protein variants with respective standard deviation error bars. An unpaired Student T-test was performed and a significant difference was observed between S$^+$/K$^+$ and S$^-$/K$^-$ (P = 0.006). (**B**) Thermal denaturation profile of recombinant full-length huBiP and variants with omitted N- or C-terminal amino acids. The first peak (46.6°C for S$^+$/K$^+$, 46.8°C for S$^+$/K$^-$, 46.8°C for S$^-$/K$^+$, and 46.6°C for S$^-$/K$^-$) indicates the unfolding of the N terminus of these proteins whereas the second peak (62.75°C for S$^+$/K$^+$, 62.2°C for S$^+$/K$^-$, 63°C for S$^-$/K$^+$, and 62.4°C for S$^-$/K$^-$) represents the unfolding of the C-terminal domain of these proteins [8]. The thermal denaturation profiles of full-length huBiP and variant proteins suggest that the N- and C termini of these proteins are properly folded. Representative melting curves with calculated T_m are shown as a mean of three individual batches for each protein variant. Their low values of standard deviations of the melting temperatures suggest a very good reproducibility of the experiments (data not shown).

DSF was then used to study the binding affinity of ADP or ATP for BiP variants, in the absence of cations (Figure 3.11, summarized in Table 3.1). The K_d of ATP of all variants was as follows: S$^+$/K$^+$, 766 μM; S$^-$/K$^-$, 352 μM; S$^+$/K$^-$, 610 μM; S$^-$/K$^+$, 945 μM (Figures 3.11A to 3.11D, Table 3.1). ADP values were lower i.e., S$^+$/K$^+$, 138 μM; S$^-$/K$^-$, 107 μM; S$^+$/K$^-$, 188 μM; S$^-$/K$^+$, 98 μM. These findings indicate that in the absence of divalent cations, BiP variants have a higher binding affinity for ADP than for ATP.
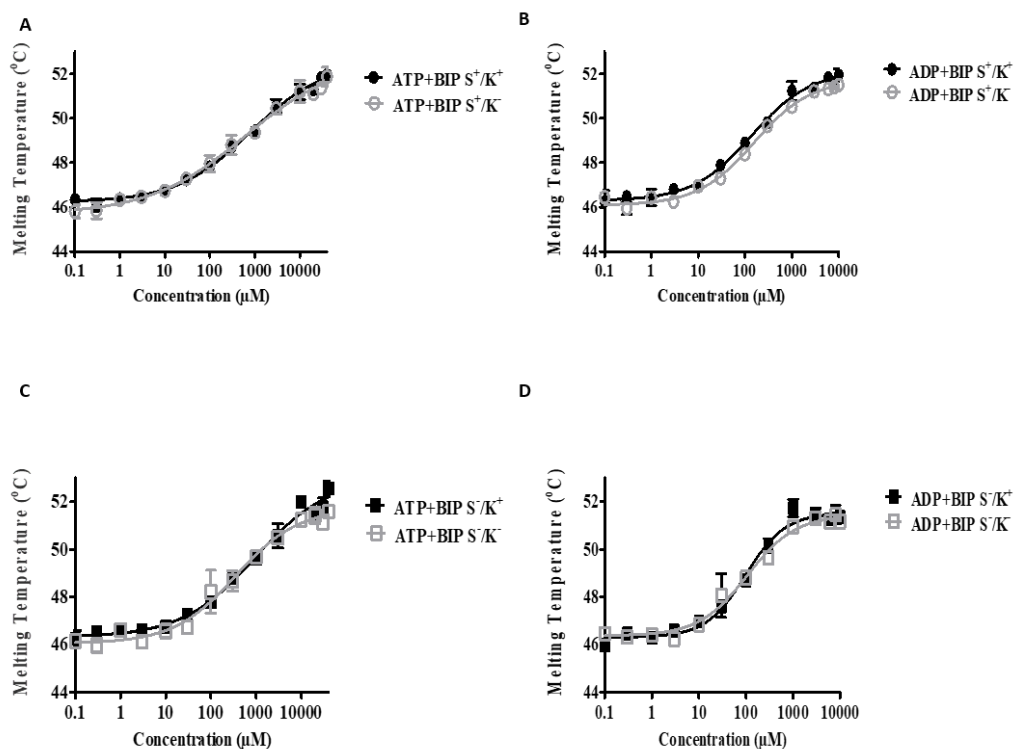
Figure 3.11: Nucleotide-binding of huBiP variants.

In DSF experiments presented here of 1 μM protein was incubated in 30 mM HEPES-KOH, pH 7.8, 150 mM NaCl, and 1x Sypro orange. The melting curve of the samples was measured from 25°C to 95°C with 1°C increments increase in temperature. (A) The interaction of BiP S^+/K^+ and BiP S^+/K^- with ATP were measured in the absence of divalent cations. The denaturation profiles of the proteins were studied in the presence of increasing amounts of ATP (0-40 mM). (B) The interaction of BiP S^+/K^+ and BiP S^+/K^- with ADP were determined without divalent cations. Denaturation profiles of the proteins were studied in the presence of increasing amounts of ADP (0-10 mM). (C) The interaction of BiP S^-/K^- and BiP S^-/K^+ with ATP were measured with no divalent cations present. The denaturation profiles of the proteins were studied in the presence of increasing amounts of ATP (0-40 mM). (D) The interaction of huBiP S^-/K^- and huBiP S^-/K^+ with ADP was determined without divalent cations. Denaturation profiles of the proteins were studied in the presence of increasing amounts of ADP (0-10 mM). In each diagram, the melting temperatures of the proteins as indicated (y-axis linear scale) dependent on the nucleotide concentrations (x-axis in logarithmic scale) are presented. The K_d values were calculated using Graph pad prism software under the assumption of a simple cooperative model.

3.5.6 Divalent cations modulate nucleotide-binding properties of BiP

The optimisation of the ATPase assay conditions showed a strict dependence on the presence of Mg^{2+} and Mn^{2+} divalent cations, whereas Ca^{2+} did not support ATPase activity (Figure 3.9A-C). To determine the effect of divalent cations on nucleotide-binding in more detail, we focused on the longest (S^+/K^+) and shortest (S^-/K^-) variants, as these represent the variants with the most significant differences in their enzyme activities.

Table 3.1: BiP Nucleotide-binding activity is modulated by the presence of divalent cations.

BiP variant	Nucleotide bound	Cation		K_d [µM]	Standard deviation [µM]
S^+/K^+	ATP	None		766	157
		$MgCl_2$	50 µM	14	2
			2 mM	44	5
		$MnCl_2$	25 µM	12	2
			2 mM	27	3
		$CaCl_2$	2 mM	30	4
	ADP	None		138	16
		$MgCl_2$	50 µM	100	18
			2 mM	59	7
		$MnCl_2$	25 µM	13	2
			2 mM	21	2
		$CaCl_2$	2 mM	19	2
S^-/K^-	ATP	None		352	75
		$MgCl_2$	50 µM	10	2
			2 mM	13	3
		$MnCl_2$	25 µM	2	0.5
			2 mM	5	3
		$CaCl_2$	2 mM	10	3
	ADP	None		107	17
		$MgCl_2$	50 µM	77	9
			2 mM	27	6
		$MnCl_2$	25 µM	15	2
			2 mM	15	4
		$CaCl_2$	2 mM	5	0.48
S^+/K^-	ATP	None		610	233
	ADP	None		188	15
S^-/K^+	ATP	None		945	262
	ADP	None		98	11

In the presence of divalent cations (Mg^{2+}, Mn^{2+}, Ca^{2+}) there was a several-fold increase in the affinities of ATP and ADP with both variants, at low (50 µM of Mg^{2+} and 25 of µM Mn^{2+}; Figures 3.12A and 3.12B; summarised in Table 3.1), and high divalent cation concentrations (2 mM each of Mg^{2+}, $Mn^{2+,}$ and $Ca^{2+,}$ Figures 3.12C and 3.12D, also see Table 3.1). Thus, the affinity of the two BiP variants for both nucleotides increased 2-to-10-fold in the presence of divalent cations (Table 3.1).
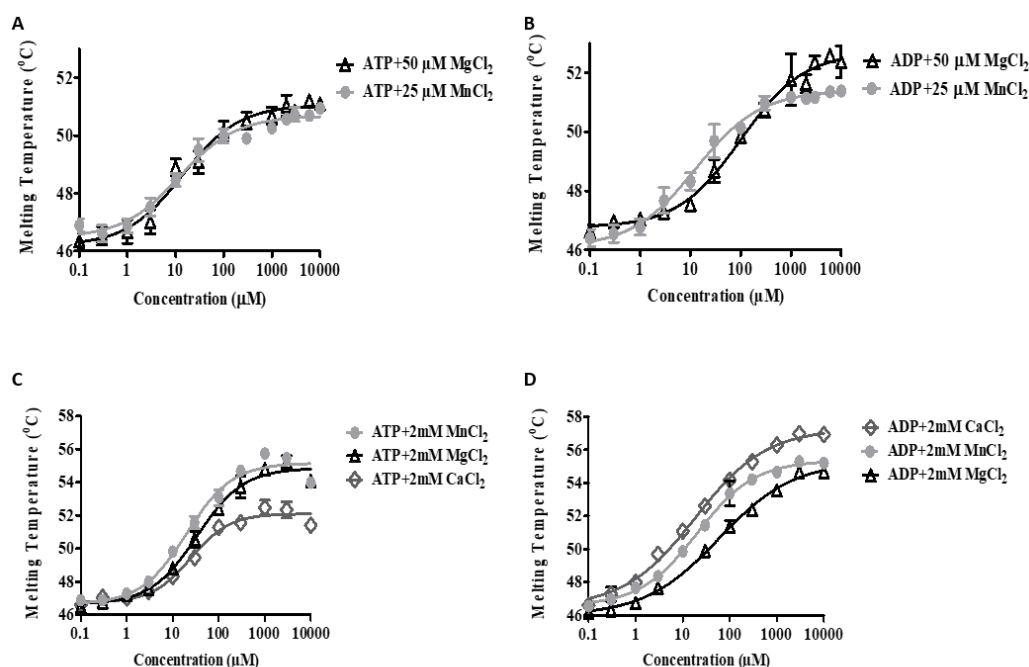
Figure 3.12: Effect of divalent cations on BiP S+/K+ and BiP S-/K-nucleotide-binding

In these DSF experiments, 1 µM protein was incubated in 30 mM HEPES-KOH, pH 7.8, 150 mM NaCl, and 1x Sypro orange. The melting curve of the samples was measured from 25°C to 95°C with 1°C increments increase in temperature. (**A**) The interaction of BiP S^+/K^+ in the presence of increasing amounts of ATP (0-10 mM) was studied using 50 µM Mg^{2+} and 25 µM Mn^2 as indicated. (**B**) Interaction of BiP S^+/K^+ with increasing concentrations of ADP (0-10 mM) in the presence 50 µM Mg^{2+} and 25 µM Mn^{2+} was measured. (**C**) The binding of BiP S^+/K^+ to increasing amounts of ATP (0-10 mM) having 2 mM of divalent cations (Mg^{2+}, $Mn^{2+,}$ and Ca^{2+} as indicated) present was measured. (**D**) The interaction of BiP S^+/K^+ with increasing amounts of ADP (0-10mM) in the presence of 2 mM of divalent cations (Mg^{2+}, Mn^{2+} and Ca^{2+}) was analysed. In each diagram, the melting temperatures of the proteins as indicated (y-axis linear scale) dependent on the nucleotide concentrations (x-axis in logarithmic scale) are presented. The K_d values were calculated using Graph pad prism software under the assumption of a simple cooperative model.

In the presence of 2 mM of Mg^{2+}, Mn^{2+} or Ca^{2+}, full-length BiP bound to ATP with K_d values of 44 µM, 27 µM or 30 µM, respectively, whereas BiP S⁻/K⁻ had at same divalent cation concentrations, K_d values of 13 µM, 5µM and 10 µM, respectively, suggesting that under these conditions, S⁻/K⁻ BiP has a greater affinity than S⁺/K⁺ BiP for ATP. The interaction of the two BiP variants with ADP was similarly influenced by divalent cations. S⁺/K⁺ BiP binds to ADP at concentrations of 2 mM of Mg^{2+}, Mn^{2+} or Ca^{2+} with K_d values of 59 µM, 21 µM, and 19 µM, respectively whereas ADP interacts with BiP S⁻/K⁻ in the presence of the same divalent cations with K_d values of 27 µM, 15 µM, and 5 µM, respectively. Interestingly, these data revealed that under the same cation conditions, full-length BiP had lower affinity for ATP and ADP than S⁻/K⁻ BiP.
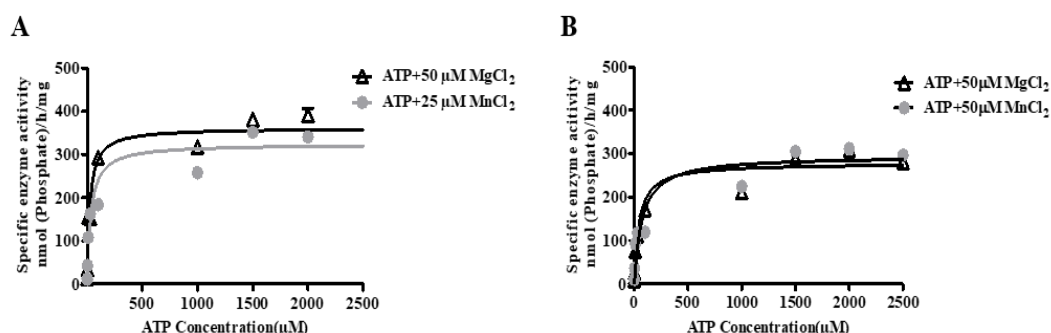
Figure 3.13: BiP ATPase activities in the presence of low concentrations of divalent cations.

ATPase activity of huBiP was measured in the presence of MgCl₂ (50 µM) and MnCl₂ (25 µM). Samples were prepared with a reaction volume of 160 µl containing 10 µg of protein, 30 mM HEPES-KOH, pH 7.8, 150 mM NaCl, either 50 µM MgCl₂ or 25 µM MnCl₂ and increasing concentrations of ATP (0 to 3 mM). Experiments were repeated twice in each case but only one representative set of experiments is presented. (A) BiP S⁺/K⁺ ATPase activity in the presence of 50 µM Mg^{2+} and 25 µM Mn^{2+}. (B) BiP S⁻/K⁻ ATPase activity in the presence of 50 µM of Mg^{2+} and 25 µM of Mn^{2+}. The K_m and V_{max} values were calculated using the Michaelis-Menten equation and Graph pad prism software.

In summary, these studies demonstrate that for both BiP variants tested, the ratio of K_d (ATP)/K_d (ADP) is larger than 1 in the presence of Ca^{2+} (ratio: 1.6 – 2), whereas the ratio of K_d (ATP)/K_d (ADP) is smaller than 1 with Mg^{2+} (ratio: 0.23 – 0.37). These findings suggest that in the presence of Ca^{2+}, BiP binds with

higher affinity to ADP than to ATP, while in the presence of Mg^{2+}, BiP shows stronger binding to ATP than to ADP. This could explain at least in part why Ca^{2+} does not support BiP's ATPase activity since in the presence of Ca^{2+} it is difficult for ATP to replace enzyme-bound ADP after hydrolysis, to allow its reloading in the following ATPase reaction. In contrast, the higher affinity of BiP for ATP than for ADP in the presence of Mg^{2+} would suggest that with this divalent cation, ATP can easily replace enzyme-bound ADP. The situation for Mn^{2+} is less clear and the ratio is about one for full-length BiP and BiP S^-/K^- (ratio: 1.3 and 0.86) suggesting that ATP might be able to replace enzyme-bound ADP in the presence of Mn^{2+} and that it would happen more easily than in the presence of Ca^{2+}. From these nucleotide-binding data, a ranking of the divalent cations for stimulating BiP enzyme activity would be $Mg^{2+} > Mn^{2+} > Ca^{2+}$, with the latter being most likely unable to support BiP ATPase activity.

3.5.7 Kinetic analysis of ATPase activity of BiP

We next addressed the question of whether or not the kinetics of ATPase activity was significantly different when S^+/K^+ and S^-/K^- BiP variants were compared. We were particularly interested in ATPase activities occurring at sub-millimolar concentrations of Mn^{2+}, as these represent normal physiological levels found within the human brain. Specifically, a concentration of 20.0-52.8 mM is recommended for the *in vitro* modelling of normal brain Mn^{2+}, while concentrations of 60.1-158.4 mM of Mn^{2+} can be considered to represent threshold pathological levels (Bowman and Aschner, 2014). Based on these findings and on our Mg^{2+} and Mn^{2+}-dependent ATPase activity data (Figure 3.9), we used 50 µM of Mg^{2+} and 25 µM of Mn^{2+} for kinetic profiling. In the presence of either cation, the ATPase reaction showed a hyperbolic function for both BiP variants (Figure 3.13). The V_{max} values of both BiP variants with both divalent cations were similar (see Table 3.2). However, in the presence of 50 µM Mg^{2+}, S^+/K^+ BiP had approximately a 20% higher V_{max} than S^-/K^- BiP under these conditions, whereas the three other V_{max} values were very consistent and they varied less than 5% from each other (Table 3.2).

In contrast, the K_M values differed by a factor of up to 3.7 (Figure 3.13 and Table 3.2). S^+/K^+ BiP had a K_M value of 18 µM in the presence of 50 µM of

Mg^{2+}, which was the lowest of all K_M values measured. Interestingly, this K_M is very similar to the K_d value of 14 µM for ATP suggesting that in the presence of 50 µM of Mg^{2+}, the binding of ATP to full-length BiP is the major contributing factor for its ATPase activity (compare respective data in Table 3.1 and Table 3.2). In the presence of 25 µM Mn^{2+}, the K_M of 38 µM of full-length BiP is twice as high as the K_M value with 50 µM of Mg^{2+}. Interestingly, the K_M of full-length BiP is also three times higher than the K_d of 12 µM for ATP under the same Mn^{2+} conditions (compare respective data in Table 3.1 and Table 3.2), revealing the possibility of another mechanism being the rate-limiting step in the ATPase reaction under this condition. For example, the formation of the transition complex, or the possibility that a secondary nucleotide-binding site may modulate the ATPase reaction.

Table 3.2: Kinetic analysis of BiP ATPase activity.

Protein	Divalent cation	K_M [µM]	Standard deviation (±)	V_{max} [nmol/h/mg]	Standard deviation (±)
S^+/K^+	$MgCl_2$ 50 µM	18	9.9	371	14
	$MnCl_2$ 25 µM	38	4.2	311	18
S^-/K^-	$MgCl_2$ 50 µM	61	21	293	21
	$MnCl_2$ 25 µM	66	9.9	307	18

For the S^-/K^- variant, at 50 µM of Mg^{2+} and 25 µM Mn^{2+}, the K_M values of 61 µM and 66 µM, respectively, are very similar, but both are higher (about 2 to 3 times) than the values found for full-length BiP, suggesting that the shorter BiP variant needs higher ATP concentrations than full-length BiP to reach V_{max}. Interestingly, the difference between the measured K_M values for BiP S^-/K^- and the apparent K_d values for ATP, are 6-fold and 33-fold higher in the presence of 50 µM Mg^{2+} or 25 µM Mn^{2+}, respectively. This suggests that in contrast to full-length BiP in the presence of Mg^{2+}, additional steps, especially in the case of

BiP S$^-$/K$^-$ with 25 µM Mn^{2+}, are controlling the ATPase activity of the shortest variant. On the other hand, in the presence of 25 µM Mn^{2+}, the determined V$_{max}$ (307 nmol/h/mg) of BiP S$^-$/K$^-$ is comparable to the V$_{max}$ (293 nmol/h/mg) of full-length BiP, indicating that at high ATP concentrations, ATP hydrolysis is no longer influenced by this apparent inhibitory mechanism, which usually would be regarded as a competitive inhibition.
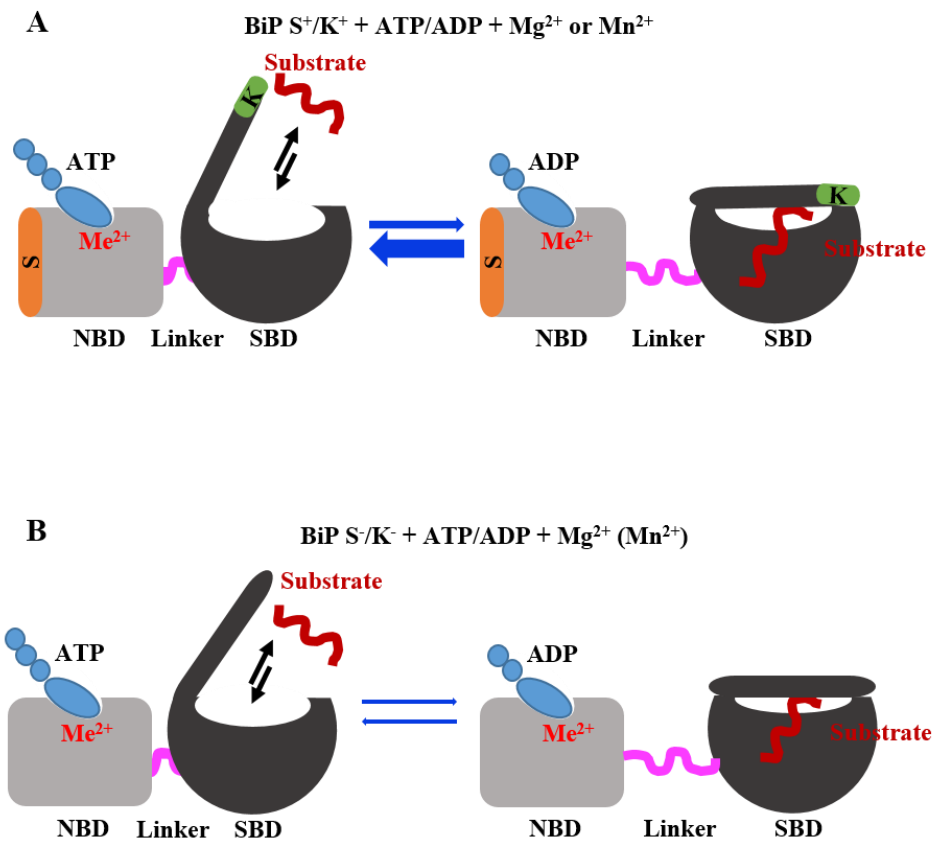
Figure 3.14: Model illustrating BiP-ATP- and BiP-ADP-bound conformation.

(A) Full-length BiP tends to be in open conformation in the ATP-bound state (indicated by the thick blue arrow) in the presence of metal ions (Me^{2+}), enabling easy exchange of ATP. (B) BiP S$^-$/K$^-$ tends to be in a closed conformation in the ADP-bound state in the presence of Ca^{2+} and the binding of ADP is tighter.

3.6 Discussion:

BiP is an ER-resident chaperone with several intra- and extracellular functions. The intracellular functions of BiP include calcium-binding, folding of unfolded protein, supporting transport of proteins into the ER, trafficking of misfolded proteins for degradation and regulating the unfolded protein response, whereas in its extracellular activities, it interacts with the immune cells and has anti-inflammatory properties in the context of Rheumatic Arthritis (Carvalho et al., 2014; Henderson and Martin, 2014; Wang et al., 2017). All or most of these functions require BiP-ATP or BiP-ADP interactions (Carvalho et al., 2014; Wang et al., 2017). Nucleotide-binding of BiP causes a conformational change of the protein and assists in its binding to newly-synthesised peptides to catalyse their proper folding. To study the basic functions of huBiP we expressed four variants, including the full-length protein and those lacking the signal peptide, the KDEL ER retention sequence, or both. The purified recombinant proteins show the correct size, varying slightly, depending on the presence or absence of signal/KDEL peptides. Here, it is important to note that the presence of six histidines has no effect on the biochemical properties of BiP, as previously reported (Wei and Hendershot, 1995). Native BiP exits as a monomer, dimer and in higher oligomeric forms (Čiplys et al., 2014; Preissler et al., 2015). All these forms were also determined for the full-length recombinant BiP and its variants studied here as shown by the native PAGE, which, with the DSF data, suggests that these recombinant proteins are properly folded. These higher oligomeric forms may act as a reservoir and can be instantly converted into active monomeric forms upon demand (Preissler et al., 2015). Binding of ATP can also convert BiP dimers to monomers (Carlino et al., 1992; Toledo et al., 1993). Full-length huBiP and the shortest version were tested using native gels for their oligomerisation in response to nucleotides and divalent cations and were shown to behave similarly in the presence of ATP alone or in the presence of ATP plus divalent cations and accumulation of monomeric BiP was found reproducing the previous finding. In contrast, the addition of ADP to recombinant BiP did not increase the appearance of monomeric forms in these preparations and the presence of divalent cations had no influence on the protein oligomerisation state.

Previous reports showed that ATPase activity and nucleotide-binding properties are conserved functions of heat shock proteins (Gauts and Hendershotsqv, 1993) and that divalent cations such as Mg^{2+}, Mn^{2+} and Ca^{2+} impact on the ATPase activity of non-human BiP (Kassenbrock and Kelly, 1989; Wang et al., 2017; Wei and Hendershot, 1995). To further characterise the purified recombinant huBiP variants, we investigated their melting temperatures including the melting temperature shift in the presence of nucleotides using DSF and their ATPase activities. We determined that all variants had a similar melting temperature and that the melting curves of all four variants were similar to those previously described for non-human S^-/K^+ BiP (Lamb et al., 2006). For the later, it has been reported that the thermal denaturing temperatures or melting temperatures of the N-terminal and the C-terminal were 46.2°C and 67°C, respectively. Both melting temperatures are comparable to those of the different huBiP variants reported here. It is important to note that unfolding of the N-terminal ATP-binding domain happens first followed by the unfolding of the C-terminal substrate-binding domains as previously described (Lamb et al., 2006).

BiP has a low Mg^{2+}-dependent ATPase activity (Flynn et al., 1989; Kassenbrock and Kelly, 1989). Various reports have described the influence of specific divalent cations on the functions of BiP and especially their impact on its ATPase activity (Kassenbrock and Kelly, 1989; Wei and Hendershot, 1995). Therefore, we decided to study the effect of cations on the ATPase activity of huBiP variants, focusing on full-length (S^+/K^+) BiP and the S^-/K^- variant. Interestingly, in our assays, both Magnesium and Manganese ions very efficiently and to a comparable extent stimulated the ATPase activity of full-length BiP and the S^-/K^- variant, at micromolar concentrations. In contrast, Ca^{2+} did not support the ATPase activity of full-length huBiP, which is in agreement with the results previously described for mammalian BiP (Lamb et al., 2006; Wei and Hendershot, 1995). This lack of stimulation in the presence of Calcium could be due to the inhibition of nucleotide exchange e.g., a higher affinity of BiP to ADP than to ATP in the presence of Ca^{2+}, which is consistent with our data and those previously described (Kassenbrock and Kelly, 1989; Lamb et al.,

2006; Wei and Hendershot, 1995). The efficiency of Mg^{2+} and Mn^{2+} to stimulate huBiP ATPase at low micromolar divalent ion concentrations was surprising, since previously the optimal Mg^{2+} concentration for mammalian BiP was described as 1 mM and it was reported that Mn^{2+} is significantly less efficient than Mg^{2+} at stimulating ATPase activity (Kassenbrock and Kelly, 1989; Wei and Hendershot, 1995). Perhaps previous studies missed the stimulation if sub-millimolar concentrations of cations were not examined closely (Kassenbrock and Kelly, 1989; Wei and Hendershot, 1995). However, it is important to note that the range of efficient stimulation of huBiP ATPase activity by Mn^{2+} mirrors the physiological concentrations found in the human brain. The concentration of Mg^{2+} in the ER has been described to be higher than that of Mn^{2+} and is in the range of 10 mM but only a fraction of this Mg^{2+} is available as a free cation (Romani, 2011). Although the concentration of free Mg^{2+} in the ER has not yet been determined it is thought to be similar as that in the cytoplasm and other cellular compartments where submillimolar concentrations of free Mg^{2+} were measured (Romani, 2011). It is important to note that the potential for either cation to influence BiP ATPase activity *in vivo* must depend on the particular tissue and cellular context (Bowman and Aschner, 2014).

Consistent with previous reports, DSF showed a two-phase melting-point profile of huBiP with the early melting point most likely being due to the melting of the N-terminal nucleotide-binding domain of hamster BiP (Lamb et al., 2006), which is consistent with the finding that divalent cations as well as ATP and ADP binding, stabilise this domain. Therefore, we also used DSF to study BiP-ligand interactions and to measure the dissociation constants (K_d) of all the variants of BiP for ATP and ADP including the effect of cations (Mg^{2+}, $Mn^{2+,}$ and Ca^{2+}) on the nucleotide-binding, as previously described (Niesen et al., 2007). In the absence of divalent cations, the K_d values of all the variants for ADP are lower than K_d for ATP, indicating that ADP has a higher binding affinity than ATP under these conditions. The addition of divalent cations Mg^{2+}, $Mn^{2+,}$ and Ca^{2+} reduced the K_d values of huBiP for both ATP and ADP by up to 80%, confirming that cations act as cofactors in the binding of BiP variants to these nucleotides (Lamb et al., 2006). However, the K_d values of BiP for ATP

and ADP appear to vary significantly, depending on the source of the protein and the methods used to determine the binding of BiP and other heat shock proteins to these nucleotides (Schmid et al., 1985). Heat shock cognate protein 71kDa (HSC70) prepared from the bovine brain or expressed in bacteria was reported to have K_d values for ADP or ATP ranging from 10^{-5} to 10^{-8} (Schmid et al., 1985). The values for huBiP variants, determined here, fall within that range. Importantly we report here for the first time, the influence of the concentration of divalent cations on the binding affinity of the BiP-nucleotide interactions.

A detailed analysis showed that at low concentrations of divalent cation (50 μM Mg^{2+}), the K_d value of S^+/K^+ and S^-/K^- for ADP is at least seven times higher than the K_d of S^+/K^+ and S^-/K^- for ATP, meaning that the affinity of these proteins for ATP is much greater than for ADP and that in the presence of Mg^{2+}, the exchange of ADP happens easily. In contrast, the presence of Manganese even at a low concentration results in ADP being tightly bound to huBiP, hindering its ATPase activity at least to some extent. However, as previously reported for higher cation concentrations, the affinity of BiP for ATP is still higher than it is for ADP, such that an exchange of ADP to ATP should still happen. Thus, the lower efficiency of huBiP activity at low ATP concentrations in the presence of Mn^{2+} (meaning higher K_M), can be explained by the affinities of huBiP for ATP or ADP, at least in part. However, the higher K_M of S^-/K^- cannot be explained simply by the binding model. Losing these two peptides may result in a conformational hindrance or a kinetic problem affecting the exchange between the two stages, i.e., the ATP- and the ADP-bound forms, or it may cause a conformational change that affects the hydrolysis of ATP, since the binding of ATP is not the limiting factor for the reaction of S^-/K^- variant of huBiP (see model in Figure 3.14). The stimulation of the ATPase activity could be caused by the signal sequence acting as an intramolecular D-type domain, or it may even act as a substrate and that this activity is enhanced by the C-terminal KDEL sequence. It is worth remembering that classically, BiP binds to polypeptides and is involved in their translocation into the ER. BiP interacts with the J-domain of the Sec63p, a component of the Sec complex that plays a

vital role in the translocation of polypeptides across the ER membrane (Misselwitz et al., 1999). BiP in the ADP-bound confirmation blocks the translocon and prevents protein translocation and Ca^{2+} leakage, whereas the ATP-bound state opens the translocon and assists in translocation (Alder et al., 2005). BiP has more preference for aliphatic amino acids Alanine, Valine, Leucine, and Proline. Leucine is the most preferred amino acid for binding to BiP (Flynn et al., 1991b). Due to the presence of six leucines in the signal sequence of BiP and the hydrophobic nature of the signal sequence itself, there exists a possibility of intermolecular or intramolecular binding via the signal sequence, perhaps leading to an enhanced ATPase activity of huBiP variants that retain the signal sequence.

Furthermore, when considering the enzyme reaction, the affinities of each flavour of huBiP for ATP and ADP is very important. The ATP-bound state has a weak affinity for substrates (peptides) and the ADP-bound state has a higher affinity for substrates, locking the peptides in the substrate-binding domain for folding (see model proposed in Figure 3.14). In the presence of Mg^{2+}, S^+/K^+ and S^-/K^- both prefer to be in the ATP-bound conformation while under Ca^{2+} conditions, S^-/K^- and S^+/K^+ both favour the ADP-bound state due to their higher affinity for ADP than for ATP. For Mn^{2+} the situation is less obvious, but it may depend on its concentration i.e., low (micromolar) and physiological, or high (millimolar) possibly pathological.

At concentrations, 50 µM of Mg^{2+} the K_d value of S^+/K^+ for ATP is similar to the K_M value obtained suggesting that ATP and ADP can freely exchange at the BiP nucleotide-binding site. The binding of ATP to S^+/K^+ does not hinder the enzyme activity. In contrast, at low concentration, 25 µM, of Mn^{2+} the K_d value of S^+/K^+ for ATP is lower compared to the K_m value obtained, revealing that ATP is tightly bound but that the hydrolysis of ATP to ADP might be slower. The increased K_M value suggests that the enzyme needs a higher concentration of nucleotide (ATP) to reach the same V_{max}. At low divalent cation concentration, 50 µM of Mg^{2+} and 25 µM of Mn^{2+}, the K_d values of S^-/K^- for ATP are lower compared to the K_M values obtained suggesting that ATP is tightly bound but that the hydrolysis of ATP to ADP is slow. This is also

consistent with ATPase assay data suggesting these variants without the signal sequence and KDEL are less active i.e., they need more nucleotide (ATP) to reach the same V_{max}. The enzyme activity might be hindered by the tight binding of ATP to S^-/K^- or kinetic hindrance of the formation of the ATP-containing transition complex or its changes towards an ADP-bound complex including the hydrolysis of ATP and the formation of ADP (see Figure 3.14).

The ATPase activity depends on the pH and the charge of the nucleotide-binding domain of BiP. To study the kinetical parameters of huBiP ATPase enzyme assays in the presence of increasing ATP concentration were performed and K_M and V_{max} values were determined. Interestingly the specific enzyme activity and V_{max} values of ~300 nmol/h/mg for huBiP S^-/K^-in comparison to the literature are very similar although different setups and choices of buffers were used. Wei and Hendershot measured the ATPase activity of recombinant hamster BiP purified from bacteria and reported a V_{max} of 5.2 pmol of ATP hydrolysed/min/µg (312 nmol/h/mg) whereas 4.7 pmol of ATP hydrolysed/min/µg (282 nmol/h/mg) was described for BiP purified from canine pancreas (Kassenbrock and Kelly, 1989), which are comparable to each other. In contrast, the K_M values for these purified enzymes seems to vary more, since published values of $K_M = 1.48 \pm 0.1$ µM (purified recombinant haBiP (Wei and Hendershot, 1995), $K_M = 0.1$ µM (BiP purified from canine pancreas (Kassenbrock and Kelly, 1989)), and K_M of 0.4 µM for ATP (recombinant murine BiP (Blond-Elguindi et al., 1993) have been previously reported whereas we found K_M of 18 to 66 µM depending on the Mg^{2+} and Mn^{2+} concentrations. The difference in these value could depend on the assays such as radioactive and non-radioactive assay system as well as the buffer conditions used but also that here, low µM concentrations of divalent cations and not mM concentrations of Mg^{2+}were present in the assays

3.7 Conclusion:

We have purified recombinant human BiP variants from *E. coli* and these variants behave similarly to previously analysed BiP in terms of size, melting temperatures and conformation. Consistent with previous reports, divalent

cations influence the binding of nucleotides and ATPase activity of purified huBiP variants and they showed similar V_{max} values to previously published studies. Interestingly, we found very efficient functional interactions of BiP with Mn^{2+} at low physiological concentration. However, these differed in some enzyme parameters such as K_d for nucleotides and K_M values. All variants bind ADP more tightly than ATP. Interestingly, the presence of the signal sequence significantly influences the enzyme characteristics of huBiP. Most of this work is already published (Bandla et al., 2019)(see Appendix 2.1).

Chapter 4 : Effect of exogenous BiP on spinal cord myelinating cultures

4.1 Introduction

Binding immunoglobulin protein/glucose-regulated protein (BiP/GRP78) is a chaperone protein that functions within a subcellular organelle called the endoplasmic reticulum (ER). Under certain disease conditions, for example in chronic neurodegenerative disorders such as Alzheimer's disease, Parkinson's disease and multiple sclerosis (MS), BiP may end up being secreted out of the cell, leading to its detection in body fluids. The Fitzgerald group has shown that ER stress-associated transcription factor ATF6 and downstream targets GRP94, GRP78 and PDI are significantly up-regulated during developmental myelination (Naughton et al., 2015). BiP is required for the survival of oligodendrocytes under inflammatory conditions (Hussien et al., 2015). Due to the significant upregulation of BiP during the production of myelin in the brain we speculated that BiP could be a 'super-therapeutic', or that it could act as an adjunct therapy, enhancing the effect of reparative compounds. Raised levels of BiP could positively impact remyelination by, for example, increasing the efficiency of the chaperoning of myelin proteins. Myelinating spinal cord cultures were used for testing whether the exogenous addition of recombinant BiP could accelerate or enhance myelin production by oligodendrocytes *in vitro*. The in-house-generated and characterised BiP S-/K- was utilised for these experiments as this variant was used by the Corrigall's group (Corrigall et al., 2004, 2001) for addressing the anti-inflammatory role of BiP when exogenously added to cultured dendritic cells.

4.2 Hypothesis

BiP intake by brain cells present in cultured spinal cord explants could increase the number of myelinated axons when compared to non-BiP-treated controls.

4.3 Aims

To determine the therapeutic potential or detrimental effects of BiP in *in- vitro* models of myelination

4.4 Specific aim

To determine if the exogenous recombinant BiP is taken up by different cell cultures.

To study the effect of exogenous BiP on myelination in spinal cord myelinating cultures.

4.5 Summary of methodology

4.5.1 Endotoxin quantification

A large batch (20 L) of recombinant BiP S^-/K^- protein was made endotoxin-free using endotoxin removal high-capacity kits (PUR030, Biorad) (for using in *in-vitro* experiments) according to manufacturer's instructions. The endotoxin levels were quantified using a competitive endotoxin quantification ELISA (OKEH02559, Aviva biological systems) according to manufacturer's instructions (see chapter 2). Additionally, we performed ELISA for chemokines as described in section (2.2.16). These experiments were carried in association with Dr Sean Mc Carthy and Dr Daniel O Toole, REMEDI, National University of Ireland, Galway.

4.5.2 Quantification of the effect of BiP S^-/K^- on spinal cord explant-based models of myelination *in-vitro*

A spinal cord explant model of myelination *in-vitro* was used to measure the effect of exogenous addition of BiP S^-/K^- on the ability of oligodendrocytes to myelinate. Since this work was being done for the first time, cultures were exposed to varying doses of BiP, to establish a suitable concentration of BiP to use for further treatments. A dose of 20 µg/ml BiP was selected for further experiments. The cultures were treated every other day with BiP S^-/K^- from DIV 18-28. Fixation and staining protocols were performed as described in Linder and Linington, (2014) to quantify the following features: axon density, myelination, number of microglia; number of cells of the oligodendrocyte lineage; number of astrocytes. Images were captured with an Olympus BX51 microscope (Olympus, Germany) and analysed using CellProfiler software. A

minimum of thirty images/parameter were analysed from three independent explant cultures for each of three biological replicates (n = 3) from at least three biological replicates per BiP concentration.

4.5.3 Uptake of labelled BiP S⁻/K⁻ protein by cell cultures

BiP S$^-$/K$^-$ was labelled with AnaTag™ 5 - FITC Protein Labelling Kit in order to confirm the ability of in-house-produced BiP to be taken up by cultured cells. Fluorescently labelled BiP S$^-$/K$^-$ was added to both B104 neuroblastoma cell line and spinal cord myelinating cultures cells fixed at various time-points before visualisation using a fluorescent and confocal microscope.

4.6 Results

4.6.1 Endotoxin quantification

The endotoxin quantities were found to be minimum in the recombinant BiP sample. The endotoxin quantification ELISA was performed thrice. However, we were able to generate values for endotoxin levels in only one experiment and this was found to be less than 0.00002 EU/µg protein (see Figure 4.1). When the experiment was repeated with different variants of BiP the endotoxins were below the detectable levels (see Table 4.1). As a competitive ELISA was being used for this experiment, it is worth noting that the higher the absorbance readings, the lower the amount of endotoxin that was present. Moreover, we attempted to study the cytokine IL-8 release from BEAS2B cells upon exposure to BiP. BEAS2B cells respond to LPS and secrete IL-8. The quantity of IL-8 secreted is 5-fold less than the 10 µg/ml LPS treated sample (see   Figure 4.2). The possibility that BiP is responsible for the secretion of IL-8 should not be ignored.
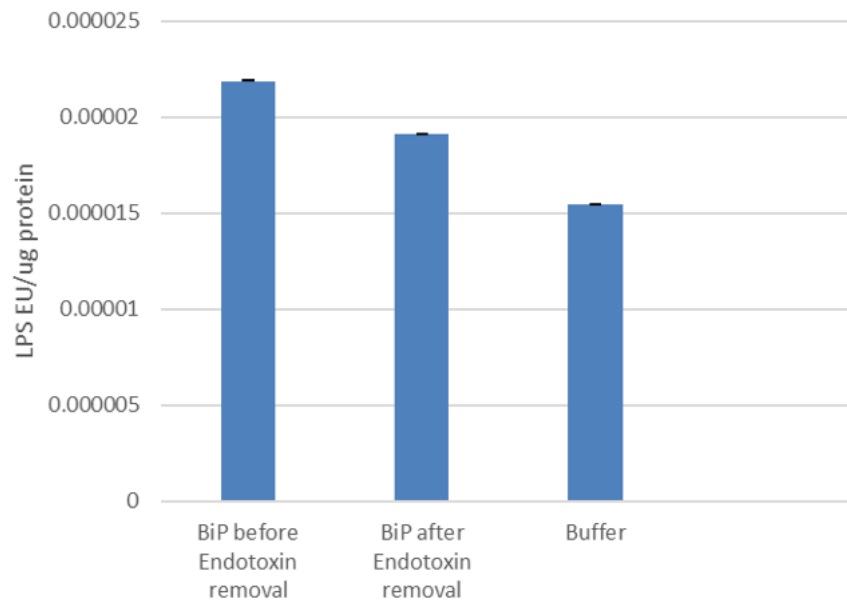
Figure 4.1: Quantification of endotoxin levels in BiP S⁻/K⁺ before and after purification with high capacity endotoxin removal kits.

A dose of 50 µg/ml of BiP was used to measure the amount of endotoxin present. A competitive endotoxin quantification ELISA was used to measure the levels of endotoxins. Data presented are the mean ± SD, n=1.

Table 4.1: Absorbance values of endotoxin quantification ELISA.

Standards	EU/mL	0.00001	0.015625	0.03125	0.0625	0.125	0.25	0.5	1
	A	0.43719	0.33382	0.271598	0.170636	0.113753	0.071442	0.046182	0.034513
	B	0.403776	0.332391	0.240676	0.186796	0.113303	0.070615	0.04793	0.03608
Samples		S^+/K^+	S^+/K^-	S^-/K^+	S^-/K^-	S^-/K^-	Endotoxin-free S^-/K^-	Buffer	
	ABS	1.545851	1.609156	1.649367	1.623972	1.688935	1.708398	1.744104	
		1.567326	1.665418	1.705626	1.651781	1.746378	1.739082	1.943663	
Standards	EU/mL	0	0.00001	0.03125	0.0625	0.125	0.25	0.5	1
	A	0.455562	0.401783	0.162793	0.115241	0.074382	0.051379	0.033672	0.02812
	B	0.616	0.352638	0.169254	0.093218	0.068729	0.051499	0.037308	0.029524
Samples		S^+/K^+	S^+/K^-	S^-/K^+	S^-/K^-	Endotoxin-free S^-/K^-	FITC labelled-Endotoxin free S^-/K^-		
	ABS	0.584315	0.706526	0.71384	0.758628	0.802779	0.474862		
		0.794298	0.702776	0.696333	0.581165	0.718386	0.466509		
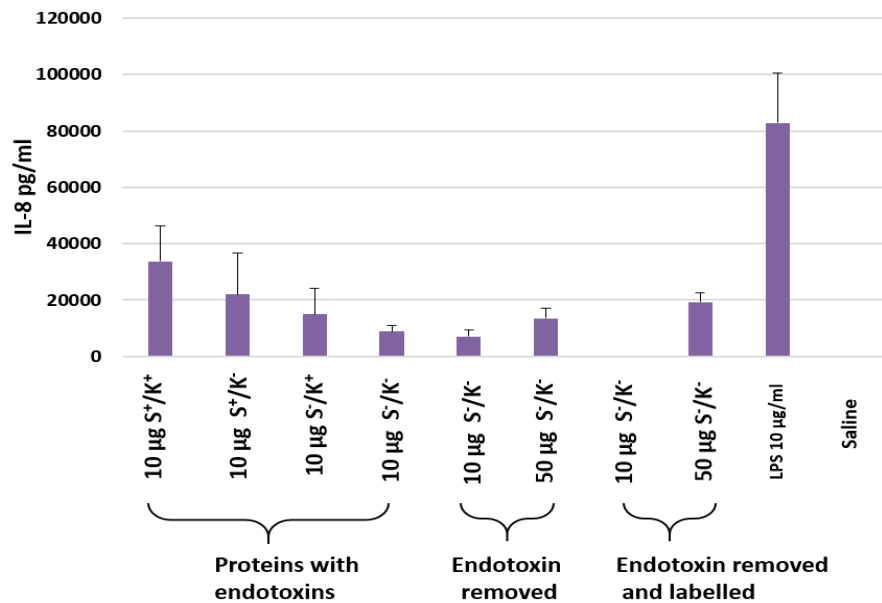
Figure 4.2: **Exogenous rBiP-induced upregulation of IL-8 in BEA2SB cells.**

BEAS-2B cells were cultured for 48 h. An initial seeding density of 100,000/ml was used. After 48 h, the cells were exposed to LPS or labelled and unlabelled BiP for 24 h. These cells proliferate and produce IL-8 in response to LPS (J. Verspohl and Podlogar, 2012). Quantification of IL-8 was carried out using ELISA kits (R and D Systems, DY208, Duoset, R and D systems. Wiesbaden, Germany. Data presented are the mean ± SD, n=1.

4.6.2 Dose-dependent uptake of fluorescently labelled BiP S⁻/K⁻ by B104 neuroblastoma cell line

BiP S⁻/K⁻ was fluorescently labelled as described in section 2.3.1. FITC-labelled BiP S⁻/K⁻ was taken up by cells in a dose-dependent manner. Doses of 1, 5, 10, 20, 30, 40 µg/ml were added to the cells and incubated for 24 hours. Preliminary observation indicated that the number of FITC-positive cells was directly proportional to the dose added. The lower doses such as 1 and 5 µg/ml had no FITC-positive cells or fewer numbers of FITC-positive cells when compared to higher doses (Figure 4.3 and Figure 4.4).
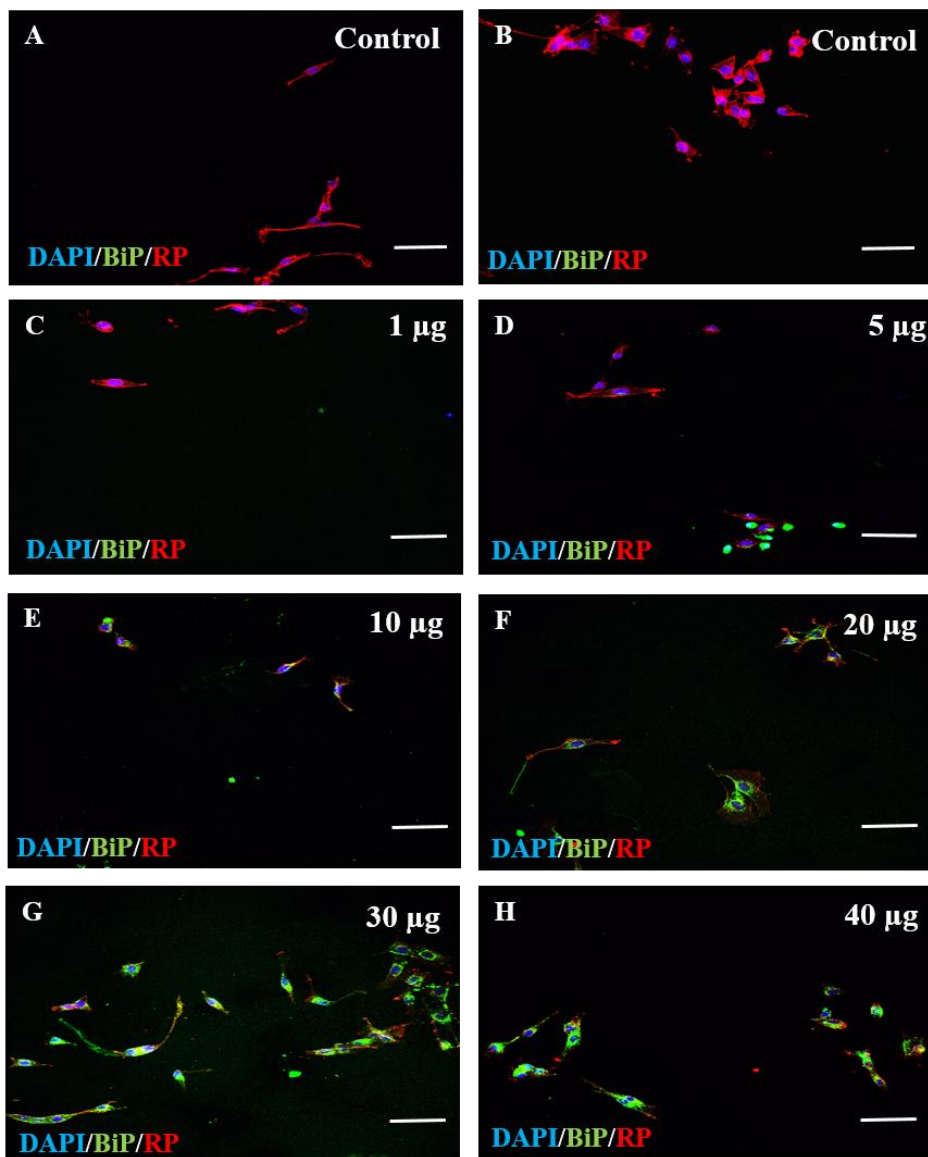
Figure 4.3: Dose-dependent uptake of FITC-labelled BiP by B104 cells.

B104 cultures were incubated with FITC-labelled BiP for 24 h at 37°C. Fixed cultures were stained with DAPI and Rhodamine phalloidin (RP). Images were captured using a 20x objective on a confocal microscope. A, B: untreated control, C, D, E, F, G, H: 1 µg, 5 µg, 10 µg, 20 µg, 30 µg, 40 µg FITC-labelled BiP, respectively. Scale bar=50 µM.
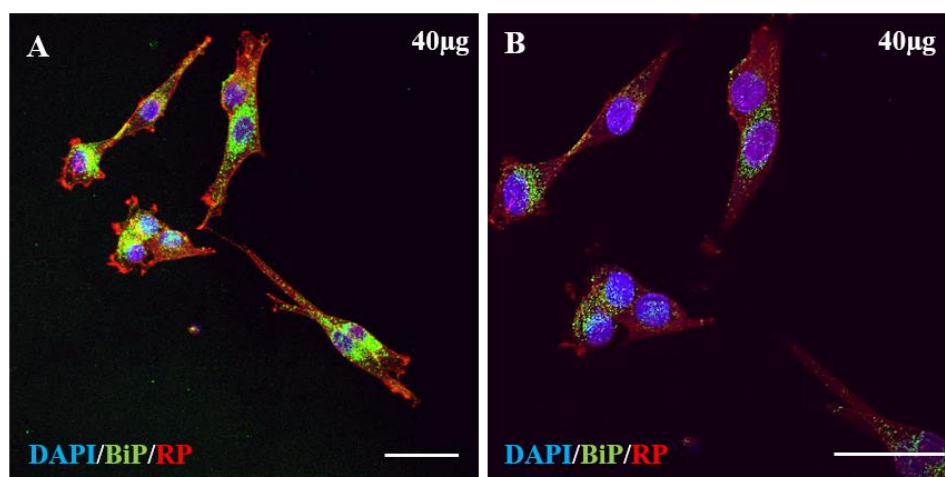
Figure 4.4: B104 cells treated with 40 µg FITC-labelled BiP.

Samples were incubated with FITC-labelled BiP for 24 h at 37ºC. B104 cultures were stained with DAPI and Rhodamine phalloidin (RP). Images captured using a confocal microscope. A: 40X magnification, scale bar=50 µm and B: 60X magnification, scale bar=50 µm.

4.6.3 Time-dependent uptake of labelled BiP S⁻/K⁻ by B104 cells

Additionally, the cells were fixed at different time points such as 3 h, 8 h, and 24 h to study the time-course of uptake. BiP S^-/K^- at a dose of 90 µg/ml was taken up by the cells as early as 30 min. There was a significant increase in the FITC positive cells at 3h ($p<0.01$), 8h ($p<0.001$) and 24 h ($p<0.001$) compared to 0 h time point. (Figure: 4.5 and 4.6).

The dose-dependent effect of unlabelled BiP was studied only using spinal cord myelinating cultures. As mentioned earlier, doses higher than 40 µg/ml of unlabelled BiP were toxic to these cultures. Therefore, a dose of 40 µg/ml of labelled BiP was added to study the uptake by spinal cord myelinating cultures. On the other hand, B104 cultures survived a dose of 90 µg/ml of labelled BiP. B104 cells were less sensitive to higher doses of labelled BiP compared to spinal cord myelinating cultures.

Initial dose-dependent uptake experiment of labelled BiP was carried out in a volume of 300 µl in 8 well chamber slide. Doses ranging from 20-40 µg had prominent FITC positive cells. When the experimental setup was modified to Petri dishes the dose of labelled BiP was increased to 90 µg/ml.

119
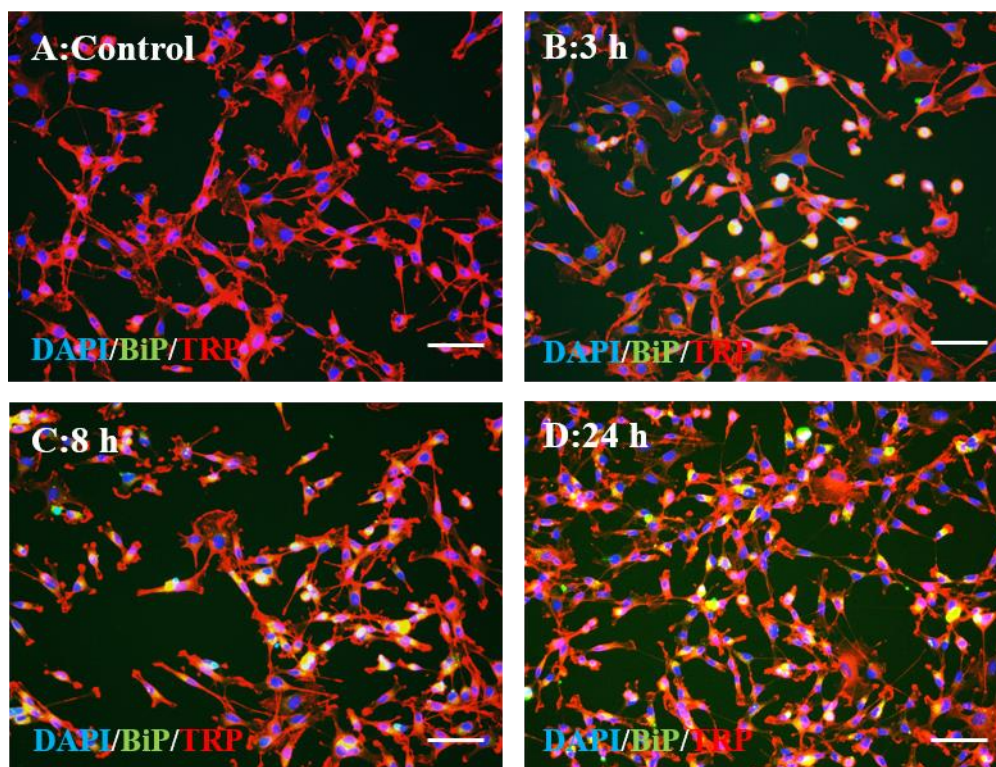
Figure 4.5: Time-dependent uptake of FITC-labelled BiP by B104 cells.

A dose of 90 μg/ml of FITC-labelled BiP was added to B104 cells. The uptake was noticed in a time-dependent manner. The maximum number of cells with FITC-labelled BiP were noticed at 8 h and 24 h. Images were taken at 20 X magnification using an Olympus BX15 microscope. Cultures were stained with Texas Red Phalloidin (TRP) and DAPI. Scale bar= 50 μm.
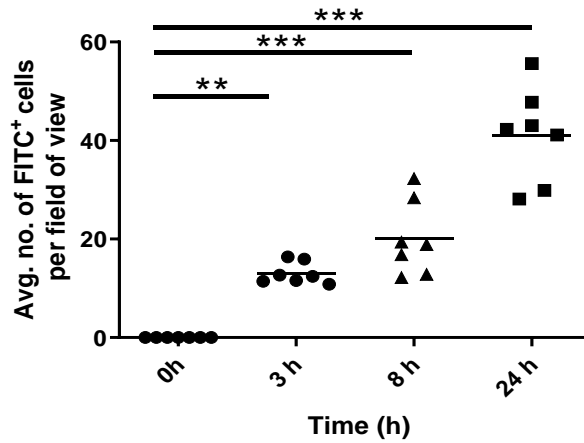
Figure 4.6: BIP-FITC-positive cells peak 24 h post-treatment.

A dose of 90 μg/ml of FITC-labelled BiP was added to B104 cells. The uptake was noticed in a time dependent manner. The maximum number of cells with FITC-labelled BiP were noticed at 24 h. Data presented are the mean ± SD, n=3, ***p< 0.001, (one-way Anova with Dunnett's Multiple comparison test).

4.6.4 Dose-dependent effect of labelled BiP S-/K- on myelinating cultures

Uptake of fluorescently labelled BiP S-/K- by myelinating cultures and microglia (Iba1), neural precursors (nestin) To study the cell-specific uptake of FITC-labelled BiP S-/K-, labelled BiP S-/K- was added to myelinating cultures and incubated for 3 h, 24 h, and 48 h. Later the cells were stained with antibodies specific for astrocytes (GFAP), neurons (MAP2), oligodendrocytes (Olig2). We noticed a time-dependent increase in the number of FITC positive cells (Figure 4.7) but we did not notice any cell type-specific uptake. High magnification images of double-positive cells for MAP2/FITC were provided in (Figure 4.8). We also attempted to stain these cultures with Iba1, Nestin, and sox2 on other occasions, but no cell-type-specific uptake was noticed.

121
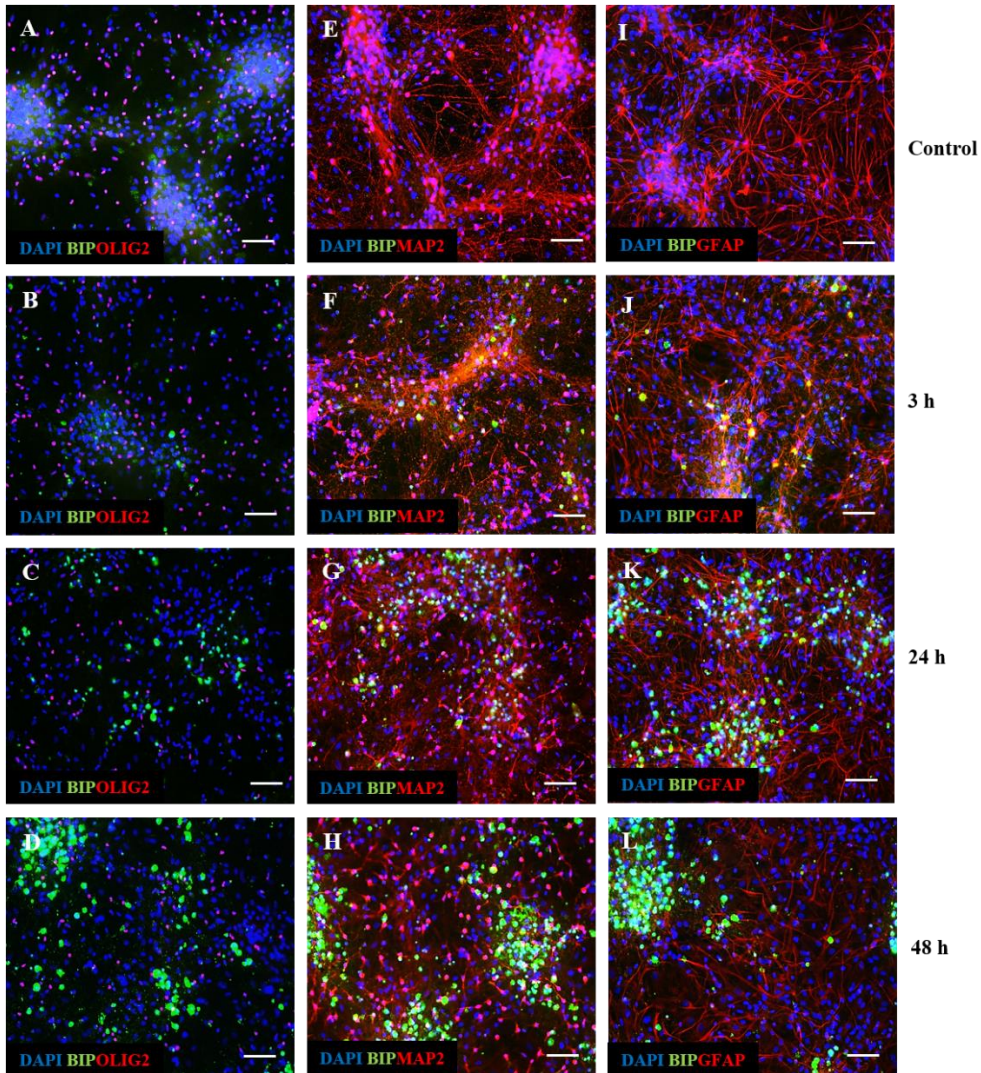
Figure 4.7: **Time-dependent uptake of FITC-labelled BiP by spinal cord myelinating cultures.**

FITC-labelled BiP (40 µg/ml) was added to the spinal cord myelinating cultures and incubated for 3h, 24h, and 48 h. A-D: Cultures were stained with Olig2, FITC-labelled BiP and DAPI. E-H: Cultures were stained with MAP2, FITC labelled BiP and DAPI. I-L: Cultures were stained with GFAP, FITC-labelled BiP and DAPI. Images were captured using Olympus BX15 microscope, Scale bar=50 µm, n=1.
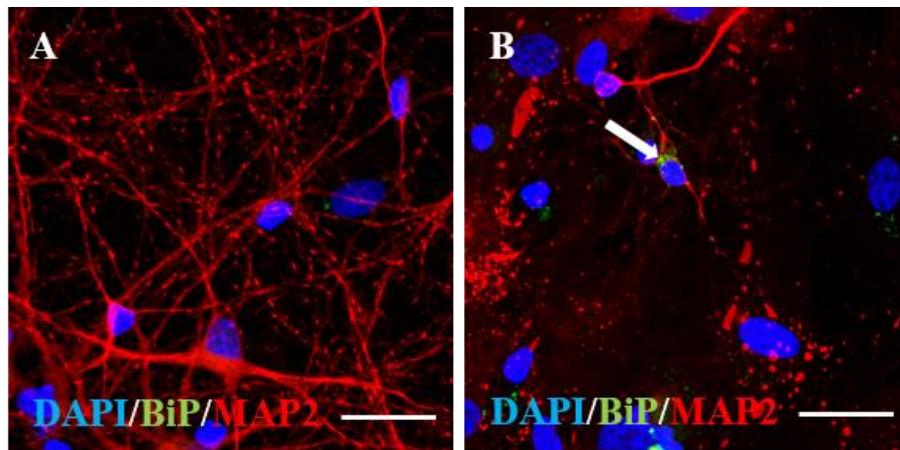
Figure 4.8: **FITC-labelled BiP taken up by neurons.**

FITC labelled BiP (40 µg/ml) was added to the spinal cord myelinating cultures and incubated for 8h. Images were taken at 60 X magnification using the confocal microscope. A, B: Cultures were stained with MAP2, FITC-labelled BiP and DAPI, Scale bar=25 µm.

4.6.5 Dose-dependent effect of BiP S⁻/K⁻ on myelinating cultures

Myelinating cultures were treated with BiP S⁻/K⁻ at a range of doses, between 10-80 µg/ml for 10 days. Controls were left untreated. BiP S⁻/K⁻ at doses higher than 40 µg /ml was toxic (Figure 4.9), and there was a trend towards a reduction in overall cell numbers, which is absent in doses up to and including 40 µg/ml (refer to 2.3.8) for details on quantification. A dose of 20 µg/ml of BiP S⁻/K⁻ was used for subsequent experiments.
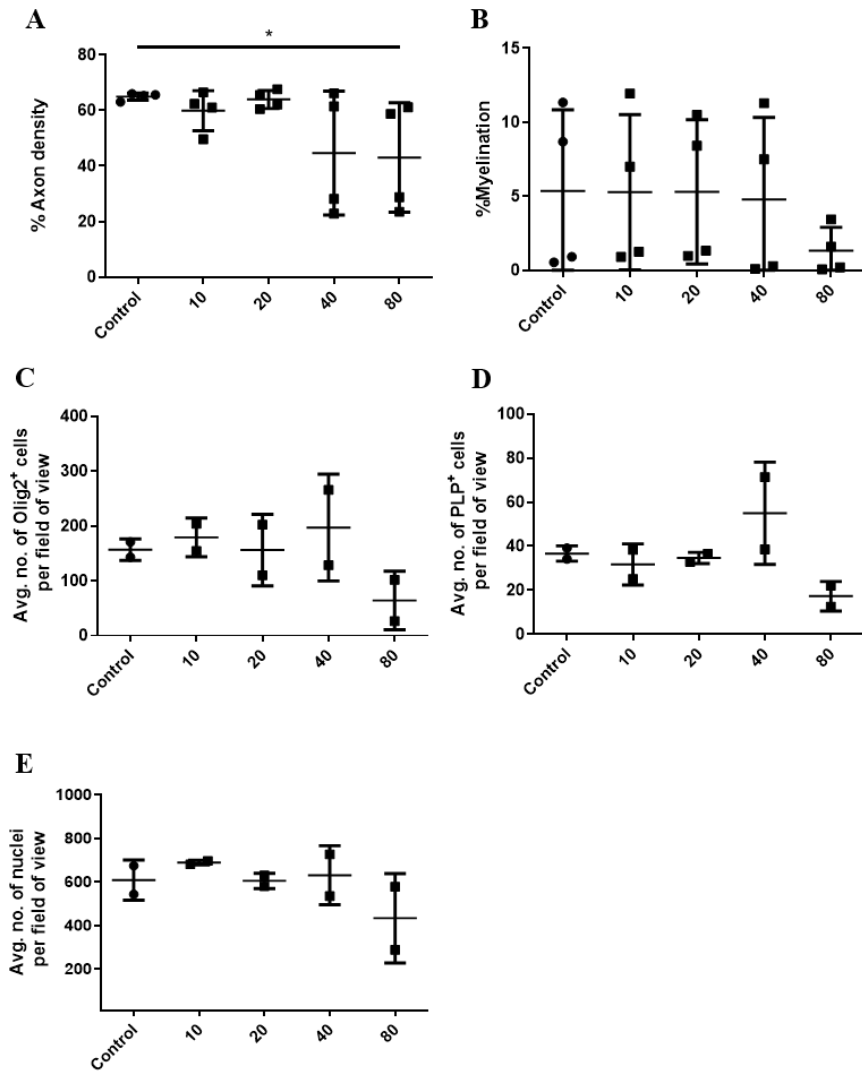
Figure 4.9: **Dose-dependent effect of BiP on myelinating cultures.**

The cultures DIV 18-28 were treated with different doses of BiP and controls were untreated. The cultures were fixed and stained with antibodies against axons (SMI31), MOG (Z2), nuclei (DAPI), Olig2 and PLP. DAPI positive nuclei, percentage of myelination, axon density, and olig2 positive cells were calculated using Cell Profiler software. PLP positive cells were counted manually. BiP induced cell death at concentrations higher than 40 μg/ml. Data presented are the mean ± SD, n=2, ***p< 0.001, (one-way ANOVA with Dunnett's multiple comparison test).

4.6.6 Increased microglial numbers in BiP-treated spinal cord myelinating culture

The cultures were treated with 20 µg/ml of BiP S⁻/K⁻ on alternative days for 10 days, from DIV 18-28 and the following parameters were quantified: axon density, myelination, microglia, and oligodendrocyte lineage cells. A significant increase ($p \leq 0.001$) in the microglia number (48.55 ± 14.90 in control cultures, versus, 123.1 ± 17.41 in BiP S⁻/K⁻ -treated cultures, Figure 4.10 and 4.11). BiP S⁻/K⁻ did not have any detectable effect on the other cell populations at this dose.
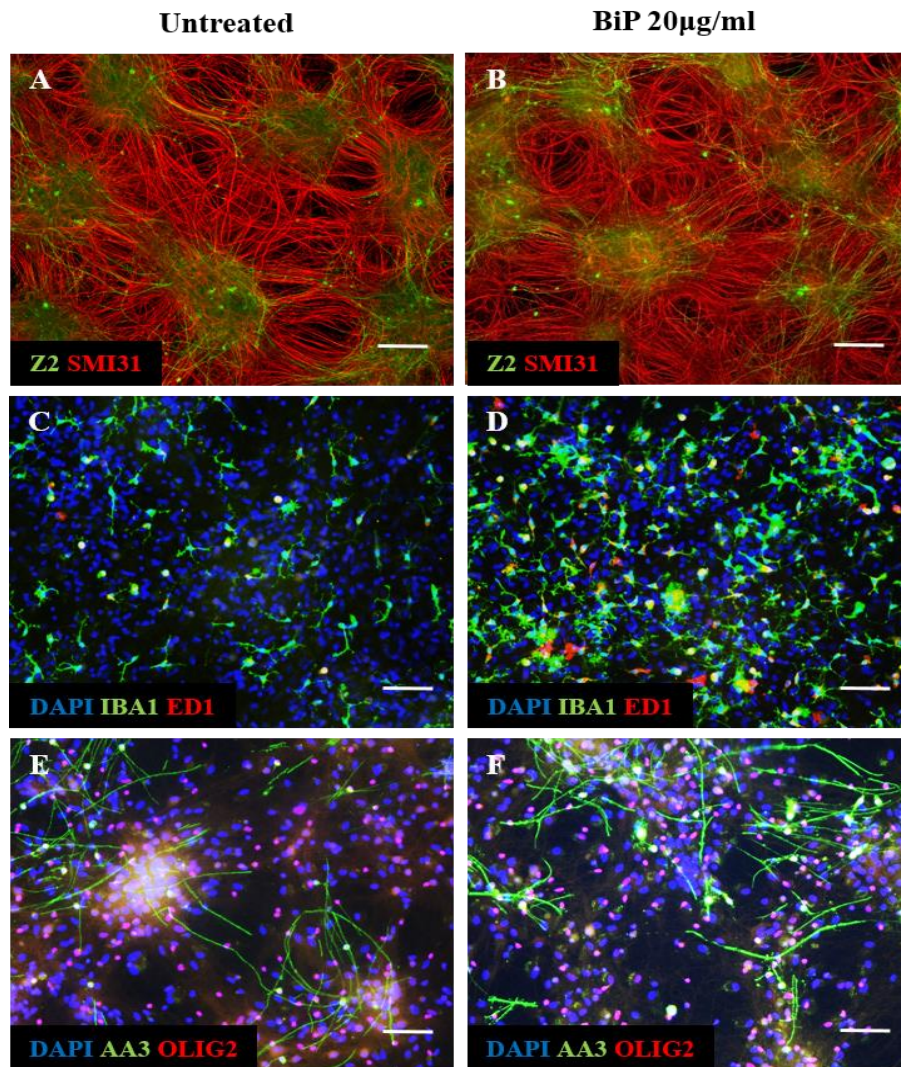
Figure 4.10: **Number of microglia increased in BiP-treated myelinating cultures.**

BiP did not have an effect on myelin, axonal density, Olig2-positive cells and AA3 (PLP)-positive cells. However, there was a significant increase in the microglia (Iba1 and ED1-positive cells) when compared to controls. Untreated and BiP 20 µg/ml treated cultures (A, B) stained with SMI31/Z2; (C, D) stained with DAPI/Iba1/ED1; (E, F) stained with DAPI/AA3/Olig2. Top row the images were taken at 10x magnification (Scale bar indicates 100 µm) and middle and the bottom row the images were taken at 20x magnification (Scale bar indicates 50 µm).
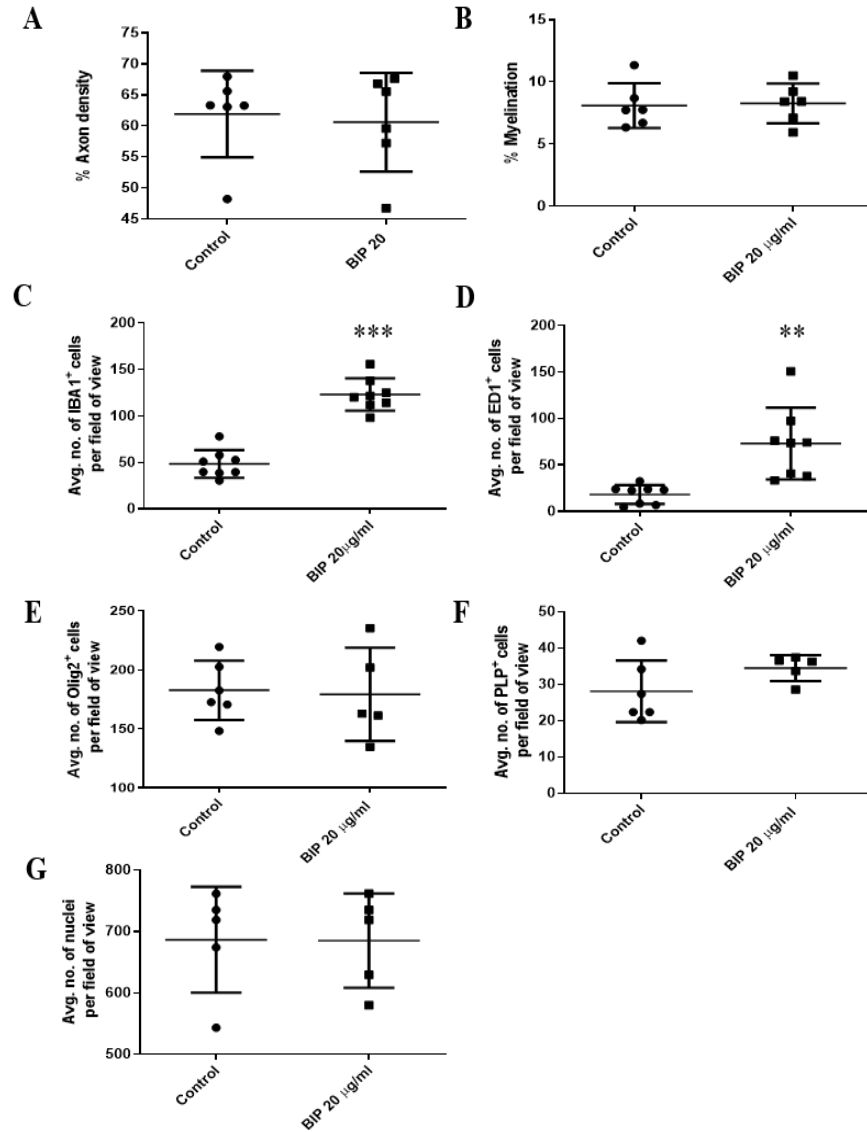
Figure 4.11: The effect of 20 μg/ml of BiP on microglia in myelinating cultures.

The cultures DIV 18-28 were treated with 20 μg/ml of BiP on alternative days during the treatment. The cultures were fixed and stained with antibodies against axons (SMI31), MOG (Z2), microglia (IBA1), activated microglia (ED1), Olig2 (oligodendrocyte lineage marker), PLP (proteolipid protein) and nuclei (DAPI). DAPI-positive nuclei, % myelination, % axons, olig2-positive cells, %GFAP, %MAP2 were calculated using Cell Profiler software. IBA1-positive, ED1-positive, and PLP-positive were counted manually. A, B. BiP did not have any significant effect on axonal density and myelination. C, D. BiP significantly increased microglial cell numbers positive for IBA1 and ED1. E, F. BiP did not have any significant effect on Olig-2 positive cells and PLP positive cells. G. BiP did not have any significant effect on overall cell number. Data is presented as mean ± SD (n =3). ***p< 0.001, (unpaired t-test).

Considering the lower values of endotoxin from the ELISA experiment, we decided to use the following doses of LPS in myelinating cultures (1 EU/ml= 0.1 ng/ml or 100 pg/ml, 0.1 EU/ml=10 pg/ml, 0.01 EU/ml=1 pg/ml, 0.001

EU/ml= 0.1 pg/ml). Since the BiP preparation had already been tested for the presence of endotoxins, an experiment was performed using known levels of endotoxins using lipopolysaccharides (0.1, 1, 10, 100 pg/ml) to compare the sensitivity of microglia in myelinating cultures to known amounts of endotoxin. Interestingly, even the cultures treated with 100 pg/ml of endotoxin had fewer microglia compared to BiP S^-/K^- 20 µg/ml treated cultures (Figure: 4.12). When compared to the controls, BiP S^-/K^- -treated cultures remarkably had a significantly higher number of microglia (DIV 28 Controls, 49.77 ± 9.930, DIV 28, BiP S^-/K^-, 119.5 ± 6.950, $p \leq 0.01$) than endotoxin treated groups. The morphology of the microglia of BiP S^-/K^- treated cultures appeared to be activated compared to endotoxin treated cultures (Figure: 4.13).
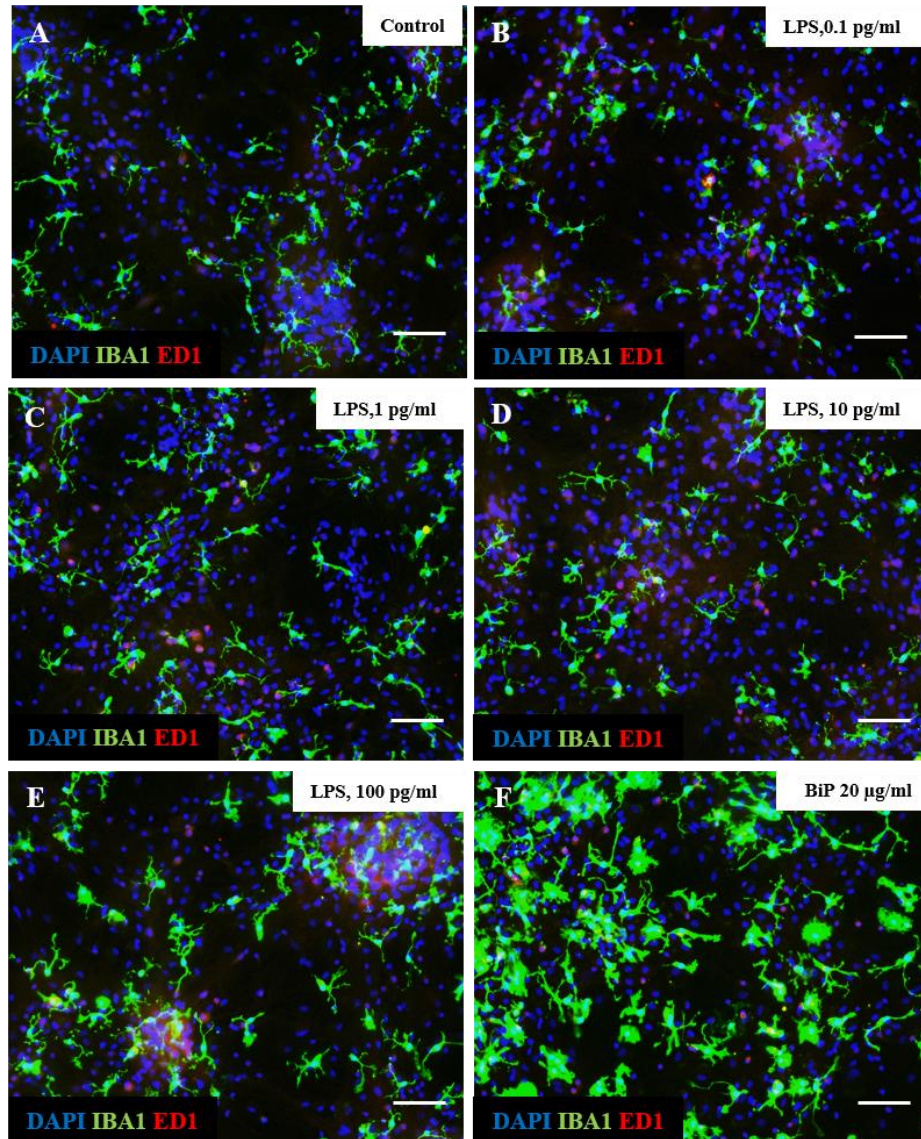
Figure 4.12: **LPS-treated myelinating cultures had less microglia compared to BiP-treated cultures.**

Spinal cord myelinating cultures were treated with varying doses of LPS ranging from (0.1 pg/ml to 100 pg/ml) or BiP 20 μg/ml. The cultures were fixed after 10 days of treatment and stained for microglia with Iba1 and ED1. BiP-treated cultures had a significant increase in the number of microglia compared to the LPS treated group. Images were taken at 20x magnification (Scale bar = 50 μm).
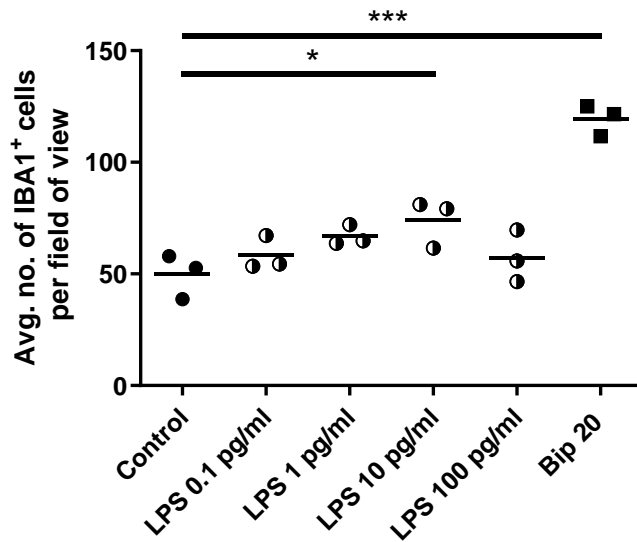
Figure 4.13: LPS treated myelinating cultures had less microglia compared to BiP treated cultures.

Spinal cord myelinating cultures were treated with varying doses of LPS ranging from (0.1 pg/m to 100 pg/ml) or BiP 20 μg/ml. The cultures were fixed after 10 days of treatment and stained for microglia with IBA1 and ED1. LPD 10pg/ml had a slight increase in the microglia numbe ($*p<0.005$). BiP treated cultures had a significant increase in the number of microglia compared to LPS treated groups ($***p<0.001$). n=1, (one-way ANOVA with Dunnett's multiple comparison test).

4.7 Discussion

FITC labelled BiP S⁻/K⁻ is uptaken by both B104 neuroblastoma cells and spinal cord myelinating cultures.

Eukaryotic cells uptake macromolecules and particles using endocytosis, leading to the formation of endocytic vesicles (Cooper, 2000). Endocytosis is classified into phagocytosis and pinocytosis based on the molecular mechanisms and the size of the endocytic vesicles. Vesicles with a diameter greater than 250 nm are referred to as phagocytic vesicles and vesicles with a diameter less than 150 nm are referred to as pinocytic vesicles. Pinocytosis is classified into clathrin-mediated endocytosis, caveolae-mediated endocytosis and micropinocytosis (Schmid, 2003). In the above-mentioned mechanisms, the endosomes act as the sorting stations for the internalised materials. The sorted materials are later transported to the cell organelles such as endoplasmic reticulum, Golgi complex, mitochondria, nuclei, and lysosomes.

The literature available on the exogenous addition of BiP to cell culture was limited. FITC-labelled BiP S$^-$/K$^-$ was used here to study BiP uptake by the B104 neuroblastoma cell line (Schubert et al., 1974) and spinal cord myelinating cultures (Thomson et al., 2008). The dose-response and time-course studies were carried out using the B104 cell line only. Uptake of the labelled BiP S$^-$/K$^-$ followed a dose-dependent and the time-dependent pattern. When labelled BiP S$^-$/K$^-$ was added to B104 cells, a few FITC positive cells were noticed as early as 3 h and the number doubled at 8 h and further doubled at 24 h, respectively. The localisation of FITC-BiP S$^-$/K$^-$ was around the nucleus, consistent with the endoplasmic reticulum. However, further investigation is required by dual labelling FITC and markers specific for endoplasmic reticulum, such as PDI or Calnexin. In a study conducted using microglia purified from mixed glial cultures made from the cerebral hemispheres of newborn Wistar rats, BiP increases the IL-6 and TNF alpha secretion from microglia. When microglial cells were treated with Aβ (1-42) in the presence of 64 nM of BiP the phagocytosis of Aβ (1-42) by the microglia increased. In the same study, when microglia were incubated with BiP, the extracellular BiP was thought to have translocated to the endoplasmic reticulum of the microglia as confirmed by the immunofluorescent staining, but this study failed to differentiate the intracellular BiP and exogenously added BiP (Kakimura et al., 2001). It could be possible that BiP might have interacted with one of the receptor partners on the cell surface thereby enhancing the expression of BiP within the ER. Please (refer to section 1.4.4) that describes the cell surface ligands and receptors that interact with BiP. In a study conducted using the RAW264.7 macrophage and THP-1 cell lines (human leukaemia monocytic cell line) (Chanput et al., 2014), tumour-secreted BiP was uptaken by the cells and the maximum uptake was noticed at 30 min (La et al., 2018). RAW264.7 macrophage cells were incubated with 40 nM FITC labelled BiP up to 6 h. Instead of being on the plasma membrane and mediating signals BiP enters macrophages through endocytosis, phagocytosis, and micropinocytosis. (La et al., 2018). Tumour-secreted BiP was taken up by cells via the Ajuba receptor in macrophages (La et al., 2018).

Having noticed the cellular uptake of FITC labelled BiP S⁻/K⁻ by B104 cells, we took advantage of the mixed population of the spinal cord myelinating cultures to determine if there could be preferential uptake of BiP in mixed cell cultures. Antibodies specific for astrocytes, microglia, oligodendrocytes, and neurons were used, however, uptake by a single specific cell type was not observed. The results suggest that the amount and time taken for uptake depend on the concentration and cell type.

Yurinskaya *et al* studied the uptake and uptake kinetics of labelled recombinant human HSP70 by different cells lines, THP-1 (human monocyte cell line), RAW 264.7, and human neuroblastoma cell line SK-N-SH. The difference in uptake of HSP70's by different cell lines is relative to the expression of toll-like receptors on the cell surface. SK-N-SH cell had a slow, gradual uptake as they do not have TLR on the cell surface and while THP-1 (human monocyte cell line) and RAW 264.7, that express TLR, had a faster uptake. The proteins were degraded instantly after uptake via the ubiquitin-proteasome system. The involvement of proteasomes was confirmed by the use of MG 132 a potent proteasome inhibitor. The inhibition of proteasome decreased the degradation of HSP70 in the cells. The uptake and the degradation of HSP70 are cell-specific (Yurinskaya et al., 2015). In the absence of TLR, the slow uptake of HSP70's by SK-N-SH could be due to simple diffusion. Along with TLRs, the adhesion receptors such as CD11-b and scavenging receptors also participate in the uptake of HSP70's (CALDERWOOD et al., 2007; Srivastava et al., 2000). In rat neuroblastoma B104 cell line, phospholipase D is involved in the uptake of synthetic prion peptide (PrP)$_{106-126}$ (Brandenburg et al., 2009). Use of another labelled protein such as bovine serum albumin could be interesting to use as a control to investigate whether it is trafficked to the same location as BiP. In the spinal cord myelination cultures and in B104 neuroblastoma cultures the possible mechanism of BiP uptake could be due to interaction with surface receptors or endocytosis.

Exogenous addition of unlabelled BiP S⁻/K⁻ to spinal cord myelinating cultures causes moderate activation of microglia

From the published literature it is known that BiP is required for the survival of oligodendrocytes under inflammatory conditions and it is upregulated during developmental myelination (Hussien et al., 2015; Naughton et al., 2015). To test the hypothesis that BiP enhances myelination *in-vitro,* BiP was added to spinal cord myelinating cultures. Prior to cell culture experiments, BiP produced from *E. coli* was passed through high capacity endotoxin removal columns to remove endotoxins. The amount of endotoxin present in the recombinant proteins after endotoxin removal was quantified using endotoxin quantification ELISA and as explained before the quantities of the endotoxins were very low.

BiP doses higher than 40 µg/ml were found to be toxic to these cultures and a dose of 20 µg/ml BiP S⁻/K⁻ did not have any effect on myelination, although a 2.5-fold increase in microglia was observed. As we did not perform the heat inactivation experiments, we could not differentiate whether the effect caused was due to recombinant BiP itself or due to the low levels of contaminating endotoxins.

BiP has been reported to induce microglial activation, enhance the release of IL-6 and TNF-α by microglia and also enhance the phagocytosis of Aβ (1-42) by microglia (Kakimura et al., 2001). Kitamura et al conducted a similar study where the exogenous addition of BiP caused activation of microglia and enhanced the cytokine production (Kitamura et al., 2002). In the study conducted by Kitamura et al, both BiP and endotoxin were heat-inactivated and exogenously added to cells (Kitamura et al., 2002). The cytokine production was not decreased in the heat-inactivated LPS cultures, whereas heat-inactivated BiP cultures produced reduced amounts of cytokines such as IL-6 and TNF-α. Therefore, microglial activation by BiP cannot be attributed to endotoxin alone (Kitamura et al., 2002). This supports our observation that the LPS treated cultures had reduced numbers of microglia compared to BiP treated cultures. Taken together, all the results, there is a trend towards reduced numbers of cells, axons, and myelin overall, which is absent in doses up to and

including 40 µg/ml. More experiments need to be done to draw any conclusions. We should perform heat inactivation experiments in the future, as endotoxins are heat stable and proteins are heat sensitive. Using a denatured protein control aids in differentiating the effects caused by protein and endotoxins. Based on the exisiting literature we assume that the increase in the number of microglia could be due to BiP itself.

4.8 Conclusion

B104 cells and cell types such as astrocytes, microglia and neurons uptake FITC labelled BiP S$^-$/K$^-$. The uptake could be via endocytosis dependent, phagocytosis, and micropinocytosis-mediated endocytosis pathways. BiP at a dose of 20 µg/ml did not have an effect on myelination or oligodendrocytes but increased the number of microglia. Alternative *E. coli* strains (LPS-free derivatives of *E. coli* K-12 and BL21 (DE3) strains) that produce only endotoxin precursor lipid 4_a, which does not cause an endotoxic response in humans (Mamat et al., 2015) could be used to fix any problems caused by endotoxin. Due to time constraints, heat inactivation experiments were not performed and should be considered while using recombinant proteins prepared from *E. coli* to differentiate the effects caused between endotoxins and the protein itself. BiP failed to answer the preliminary research question in terms of myelination, we utilised BIX (chemical inducer of BiP) for the later part of the project to induce the expression of BiP in the cells rather than exogenous addition of recombinant BiP and to study the effect on myelination.

Chapter 5 : **Effect of BiP chemical inducer-BIX on *in-vitro* and *ex-vivo* models of myelination**

5.1 Introduction

The details of BiP chemical inducer X (BIX, 1-(3, 4-dihydroxyphenyl) -2-thiocyanate-ethanone) were provided in the (section 1.4.7). BIX preferentially induces the expression of endoplasmic reticulum (ER) chaperone B cell-immunoglobulin-binding protein (BiP) through the activated transcription factor 6 (ATF6) arm of the unfolded protein response (UPR) (Kudo et al., 2008). BiP has also been shown to be significantly upregulated during normal myelination (Naughton et al., 2015) and its presence enhances the survival of myelinating oligodendrocytes in an EAE model of inflammatory demyelination (Hussien et al., 2015). Therefore, we sought to determine if myelination could be enhanced via the induction of the expression of BiP using BIX in two *in-vitro* models of myelination.

Spinal cord myelinating cultures were first used to study the effect of BIX on myelination. These mixed glial cell cultures partially replicate the CNS, enabling different types of CNS cells to interact with each other (see sections 1.5.1 for a more detailed description). These cultures produce myelin with a thickness that is consistent with that seen *in-vivo*, as shown by G ratio (axonal diameter to total myelinated fibre diameter) (Thomson et al., 2008, 2006). At 33 DIV the G ratio of myelinated axons was 0.81 ± 0.07 (mean ± SEM) (Thomson et al., 2006). To support the myelinating cultures, a neurosphere-derived astrocyte monolayer was first produced, and it acts a scaffold on which axonal development and myelination occur. The dense fibres form bridging networks between the adjacent 'nodes' and these dense sheets of myelinated fibres facilitate synapse formation and the development of electrical activity, which further promotes and supports myelination (Bijland et al., 2019; Demerens et al., 1996; Stassart et al., 2018; Thomson et al., 2006). The murine spinal myelinating cultures were also used to study the glial- axonal interactions (Ioannidou et al., 2012). Myelinating cultures were used to screen compounds such as a glycomolecules for CNS repair (McCanney et al., 2019) and study the role of stem cells (Lindsay et al., 2016, 2013).

Next, we exploited organotypic slice cultures, which offer an alternative experimental platform that preserves the 3D structural architecture of brain tissue (see section 1.5.2 for a more detailed description). These *ex-vivo* cultures have been established using different regions of the CNS, including the cerebellum, hippocampus, spinal cord, cortex and striatum (Gähwiler et al., 1997; Humpel, 2015a, 2015b; Lossi et al., 2009; Zhang et al., 2011). The age of the postnatal donors is vital for the survival of the tissue *ex-vivo*. Postnatal day 8-10 has been found to be an ideal period for setting up brain slice cultures on inserts, as tissue from most regions can survive for several months (Marksteiner and Humpel, 2008). The organotypic slices have been used successfully for the study of oligodendrocyte fate, proliferation and myelination (Healy et al., 2016; Llufriu-Dabén et al., 2019; Sekizar and Williams, 2019; Sherafat et al., 2018). Cerebellar tissue is a popular choice within the MS field, due to its prominent white matter tracts. When used in combination with chemicals such as lysophosphatidylcholine (Birgbauer et al., 2004) or immune myelin antibodies plus complement protein, (di Penta et al., 2013; Harrer et al., 2009), myelination, demyelination and remyelination can be examined in detail. (Zhang et al., 2011). For example, cerebellar slices were used for screening of drugs such as Fingolimod, progesterone, 5-methyl-7-methoxyisoflavone, edaravone, losartan and lovastatin for increased myelination (Eleuteri et al., 2017; Ghoumari et al., 2003; Huang et al., 2011; Miron et al., 2010). We used p10 rat cerebellar slice cultures to determine if data obtained using 2D myelinating cultures could be replicated in the more complex 3D system. The following sections summarise the methodology and results obtained.

5.1.1 Cerebellum

Vertebrate cerebella are located at the rostral roof of the fourth ventricle. The cerebellum has a consistent laminar organisation throughout, which includes the granular layer, Purkinje cell layer, and the molecular layer. The granular layer (GL) is the layer where mossy fibre afferents meet the Golgi cells and the granular cells and GL is internal to the Purkinje cell layer. The Purkinje cell layer (PCL) comprises the somata of the Purkinje cells and lies between the

granular layer and the molecular layer. The molecular layer (ML) is exterior to the PCL and consists of interneurons, Purkinje cells dendritic arbors, and parallel fibres. Internal to the molecular layer is the white matter layer (WML), which conveys the Purkinje fibres to the cerebellar nuclei (Voogd and Glickstein, 1998) (Figure 5.1).

Four main types of neurons form the building blocks of the cerebellar cortex, including granule cells (GCs), Purkinje cells (PCs), the Golgi cells and the stellate or basket cells, the latter two are inhibitory in nature. The extra-cerebellar afferents received by the cortex are the climbing fibres, mossy fibres and the mono-aminergic and cholinergic afferents (Voogd and Glickstein, 1998).
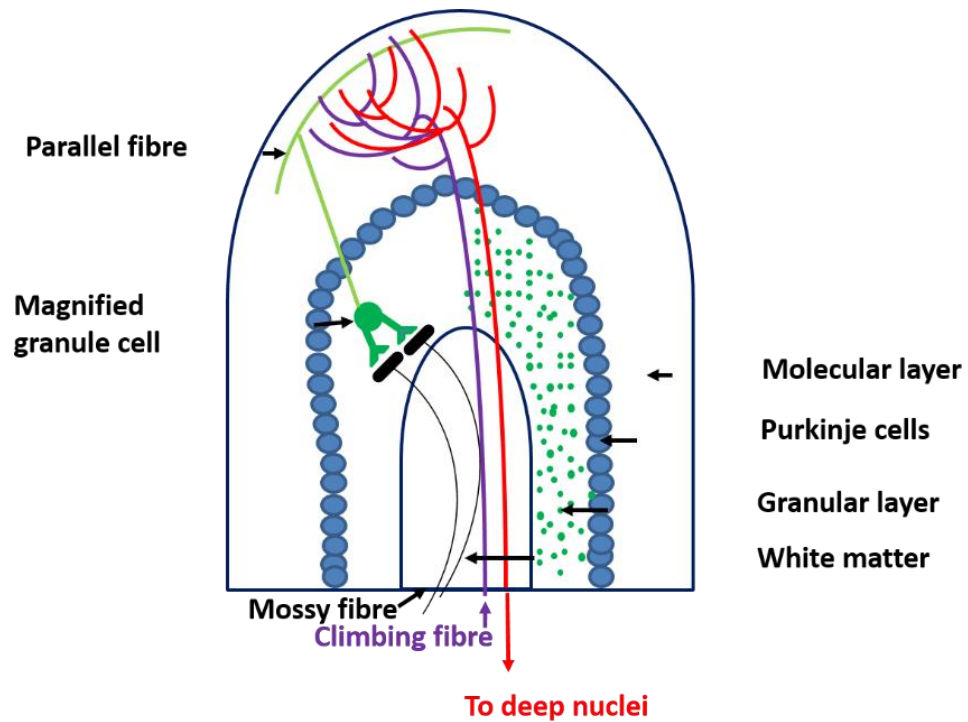
Figure 5.1: Enlarged view of single cerebellum folding.

The Purkinje layer lies between the molecular and granular layer. The axons in the white matter travel into and out of the folia. The afferents of the cerebellum are the mossy fibres and the climbing fibres. Granule cells axons divide into parallel fibres in the molecular layer and interact with the mossy fibre dendrites. Climbing fibres directly reach the Purkinje fibre and interact with the Purkinje dendrites. (Source: Sravanthi Bandla)

5.1.2 Glial Cells

Glial cells include astrocytes, oligodendrocytes and microglia. Similar to neurons some of the glial cells develop from the stem cells of the germinal matrix. Upon migrating to their designated locations they acquire a mature phenotype and physiological function. Glial cells are capable of proliferating after migrating to their final destinations (Molofsky and Deneen, 2015). Each of them has a specific function but also influences each other. Astrocytes participate in brain defence, creating the brain environment and architecture, regulating the development of neural cells, maintaining extracellular ion homeostasis, synaptic stability, supplying energy substrates, processing information and also offering functional connection with the surrounding circulation(Buffo et al., 2013)(De Zeeuw and Hoogland, 2015).

139

Oligodendrocytes are the major myelin-forming cells in the CNS. Some oligodendrocytes such as satellite oligodendrocytes present in the grey matter do not produce myelin. Oligodendrocytes also support the axon integrity apart from producing myelin. Astrocytes secrete promyelinating factors such as CNTF (ciliary neurotrophic factor) that promote myelination (Nash et al., 2011). Astrocytes, oligodendrocytes and neurons participate in myelination Microglia are the innate phagocytic cells which not only involves in cleaning the cellular debris but also participate in pruning synapses in the postnatal brain. Microglia also participate in the defence against pathogenic factors (Kettenmann et al., 2016). Microglia interact with neuronal and non-neuronal elements both structurally and functionally. Some of these interactions include phagocytosis of synaptic structures during postnatal development, alteration of the perisynaptic environment and phagocytosis of newly born neurons during adult neurogenesis. The neuronal plasticity and functions are influenced by these interactions. Microglia play vital role in pathological conditions as well as in healthy brain(Paolicelli et al.,2011)(Tremblay and Majewska, 2011)(Wake et al., 2009).

5.1.3 RNA sequencing

Next-generation sequencing of multiple RNA sequences also called RNA-seq or whole transcriptome shotgun sequencing gives information of the whole transcriptome. RNA-seq provides an advantage for identifying and quantifying the expression of genes at the same time (Conesa et al., 2016). It has several applications such as differential gene expression, pathway analysis, alternative splicing, co-expression network and data pre-processing (Han et al., 2015). Various studies have successfully applied pathway analysis to large-scale genetic datasets for Rheumatic arthritis, type-2 diabetes, Parkinson's disease and schizophrenia (Elbers et al., 2009; Giacomelli and Covani, 2010; Lesnick et al., 2007; Luo et al., 2010).

Identifying shared pathways between diseases is also a new area of interest, for example, rheumatic arthritis and systemic lupus erythematous (Lee et al., 2012), schizophrenia and type 2 diabetes (Liu et al., 2013). Initially, RNA sequencing generated differential gene expression data from bulk tissue covering a range of

organisms such as *Zea mays* (Emrich et al., 2007), *Arabidopsis thaliana* (Lister et al., 2008), *Saccharomyces cerevisae* (Nagalakshmi et al., 2008), *Mus musculus* (Mortazavi et al., 2008) and *Homosapiens* (Marioni et al., 2008). Sequencing of RNA molecules was originally developed by Sanger in the 1960s (Brownlee et al., 1967), since then it was used universally for several applications in molecular biology (Emrich et al., 2007; Lister et al., 2008). One of the most common applications of RNA-seq is differential gene expression and it has not changed much since its initial development. The standard workflow includes RNA extraction, removal of ribosomal RNA, cDNA synthesis, adapter-ligated sequencing library preparation. Between 10 and 30 million reads per sample depth is frequently used for sequencing the library on a high throughput platform such as Illumina. Alignment of sequences to a transcriptome, quantifying the reads that match the transcripts, normalising and filtering between samples and statistically modelling differentially expressed genes within the sample or between samples are the common steps followed in analysing RNA-seq data. To date, there are different methods derived from the RNA-seq protocol and most of them are based on Illumina short-read RNA-seq. The most common workflow is depicted in (Figure 5.2). Imperfections and biases can be introduced at several points during the sample preparation and computational analysis. This may limit the capacity of the RNA-seq experiments to answer biological questions (Djebali et al., 2012).
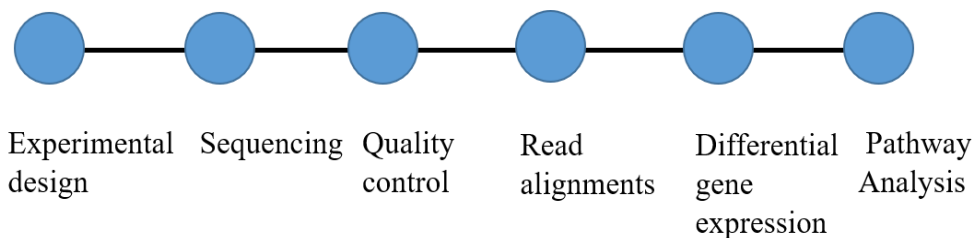
Figure 5.2: RNA sequencing workflow.

To summarise RNA isolated from the cells is converted into a library of cDNA fragments. Sequence adapters are added to each cDNA fragment. The short fragments are sequenced using high-throughput screening. Quality control was performed for RNA sequences. The sequenced reads are mapped to a reference genome. Followed by quantifying differential gene expression and pathway analysis.

5.2 Aims

1.   To determine if BIX is therapeutic or toxic in *in-vitro* models of myelination.

2.   To confirm whether the selective toxicity of BIX towards myelin, microglia, and oligodendrocytes observed in the spinal cord explant model is reproducible in an *ex-vivo* model of myelination.

5.3 Hypotheses

We hypothesis that BIX induces the expression of BiP, thereby enhancing myelination in *in-vitro* models of myelination

5.4 Summary of methodology

5.4.1 Myelinating spinal cord cultures

Myelinating spinal cord cultures were generated as described in Thomson *et al.,* (2008). The cultures were treated every other day with BIX or DMSO (vehicle control) at DIV18-28, or between DIV 28-38, based on the specific objectives of the experiments. Fixation and staining protocols were performed as described by Linder and Linington (2014), to quantify the following parameters: axonal density, myelination, microglia, cells of the oligodendrocyte lineage and astrocytes. Images were captured with an Olympus BX15 microscope and analysed using Ocular, CellProfiler software, (http://www.cellprofiler.org/) and ImageJ. A minimum of thirty images/parameter were analysed from three independent cultures for each biological replicate and from at least three biological replicates per condition ($n \geq 3$) (unless otherwise specified). For more details please refer to Sections (2.3.6, 2.3.7, 2.3.8)

5.4.2 Ex-vivo Myelinating cerebellar slice cultures

As described in section 2.4.2, cerebella were isolated from the brains of P10 Sprague Dawley rats and two or three slices of the sagittally-sectioned tissue were cultured per Millipore culture insert. The cultures were maintained at $37^{\circ}C$, 5 % CO_2 in culture media. Treatment with BIX was started on DIV-7 and

was continued on alternate days. The slice cultures were fixed on DIV12 or at other specified time-points with 10% formalin for 2 h, followed by 3X5 min washes with 1X PBS. The staining protocol was described in Section 2.4.3. Slices were imaged as indicated in section 2.4.4. To quantify tissue changes, four random images per slice were taken from 5-6 slices per condition, from three biological replicates per condition (n=3). The slices had an approx. diameter of 0.5 cm. The edges were avoided while capturing images to avoid the edge effect. The images include both grey matter and white matter. Oligodendrocyte lineage cells, microglia, and astrocytes were quantified in these cultures. We were not successful in staining and quantifying myelin in these cultures.

5.4.3 RNA sequencing and Bioinformatics

RNA samples were prepared from 5 µg/ml BIX-treated samples and 1 µl/ml DMSO-treated samples at 24 h time-point. RNA samples were analysed by Glasgow polyomics and the FASTQ files were sent to Siobhan Cleary, Bioinformatics group, National University of Galway, Ireland. Siobhan Cleary performed the quality analysis and differential gene expression analysis of the FASTQ files and Prof. Christopher Linington, University of Glasgow performed the pathway analysis using the Reactome Pathway Browser. The details were described in 2.3.11. In short, the FASTQ files provided by Glasgow Polyomics were analysed using the following software:

1. Prior to the alignment, the quality of the sequences within the FASTQs for read1 and read2 for each sample was analysed using FASTQC.

2. Alignment Statistics output was analysed using Hisat2 Aligner (Kim et al., 2015).

3. Qualimap was used to assess the quality of the alignment files (Okonechnikov et al., 2015).

4. Picard Mark Duplicates was used to analyse the read duplication rates (http://broadinstitute.github.io/picard/).
5. Feature Counts R package was used to assess the rRNA contamination (Liao et al., 2013).

6. MultiQC tool was used to produce a single report of the steps from 1-4.

7. Differential Gene expression analysis was carried out using the DeSeq2 R package.

8. Pathway analysis was carried out using the Reactome pathway browser version 3.6.

5.4.4 Statistical Analysis

Graph Pad Prism 5.0 (Graph Pad, San Diego, CA, USA) was used to analyse the data. A two-tailed unpaired t-test or one-way ANOVA with Dunnett's multiple comparison test or Two way ANOVA was used to determine the statistical difference and data is presented as mean ± SD. Significance was set at $P<0.05$. All the experiments were carried out in triplicates unless mentioned.

5.5 Results

5.5.1 BIX treatment of spinal cord myelinating cultures

In below description of results DIV refers to the number of days *in-vitro* and day1, day 5 or day 10 refers to the number of days post-treatment with DMSO or BIX. Myelinating cultures were treated with BIX at doses between 0.05 and 10 µg/ml and were evaluated for various parameters, as described in Section 2.3.7. Higher doses such as 10 µg/ml of BIX were toxic in general to the cultures. A dose of 1 µg/ml of BIX or lower did not have any significant effect on the cultures when compared to DMSO-treated controls (Figure 5.3, Figure 5.4, Figure 5.5 and Figure 5.6). Unexpectedly, in a pilot experiment, a dose of 5 µg/ml of BIX was shown to selectively inhibit myelination and selectively decrease the number of microglia dramatically (Figure 5.3). Therefore, a dose of 5 µg/ml of BIX was used for subsequent experiments.
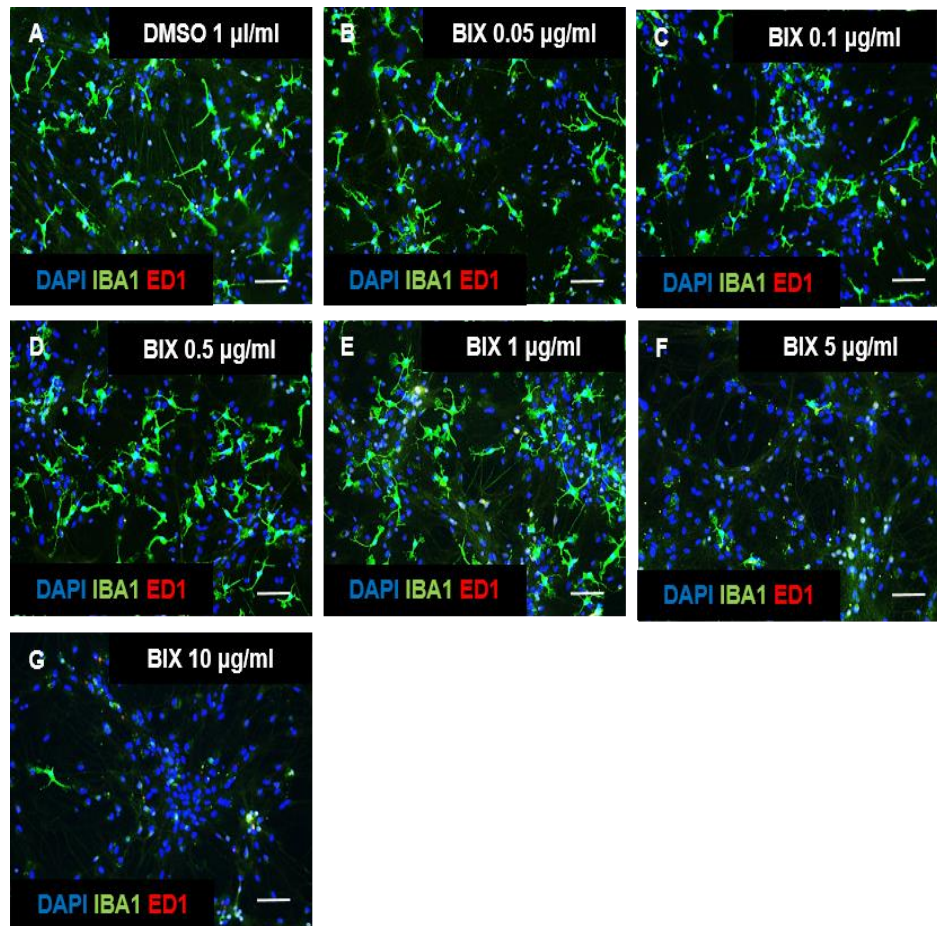
Figure 5.3: Dose-dependent reduction of microglial numbers in spinal cord myelinating cultures.

The cultures were treated with 5 µg/ml of BIX from DIV-18 to DIV-28. Cultures were fixed with 4% PFA on DIV-28 followed by immunofluorescent staining with Iba1 and ED1. Microglia were greatly reduced in 5 µg/ml BIX-treated cultures and higher doses. Cultures treated with DMSO (A), 0.05 µg/ml of BIX (B), 0.1 µg/ml of BIX (C), 0.5 µg/ml of BIX (D), 1 µg/ml of BIX (E), 5 µg/ml of BIX (F), 10 µg/ml of BIX (G), scale bar=50 µm.
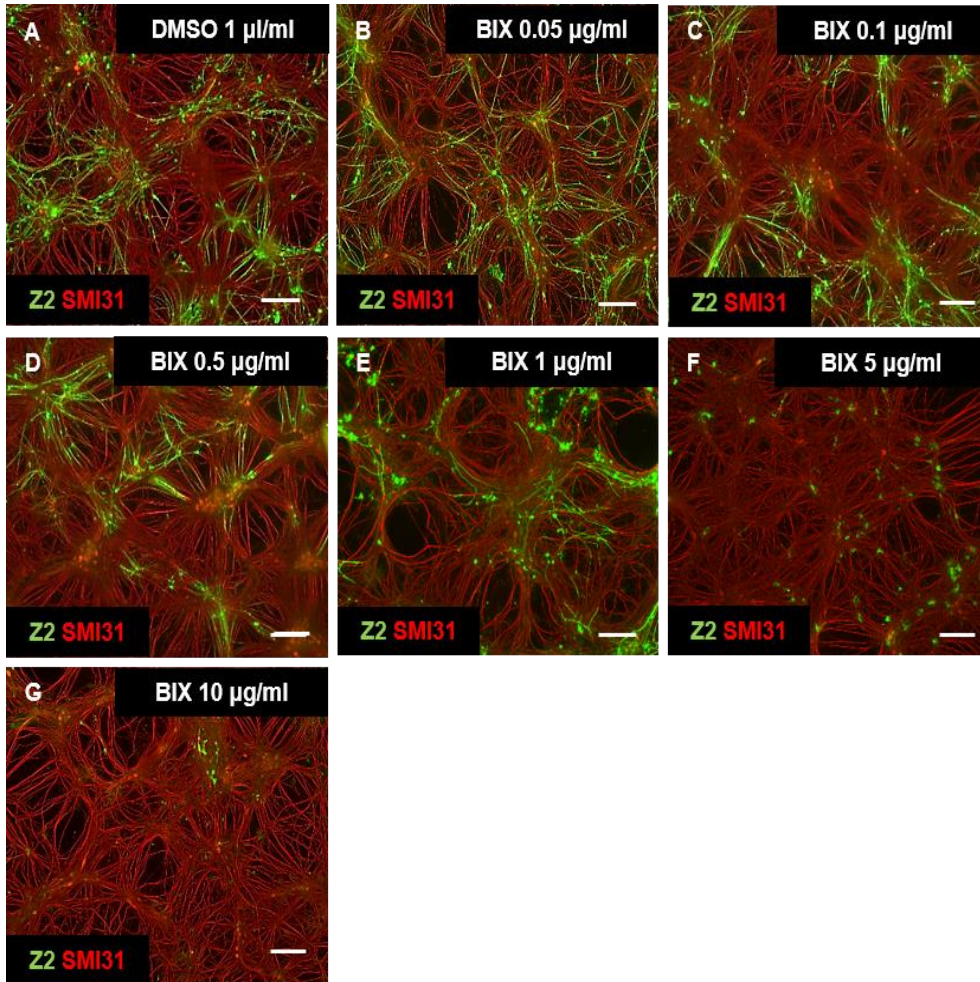
Figure 5.4: Dose-dependent reduction of myelin in the spinal cord myelinating cultures.

The cultures were treated with 5 µg/ml of BIX from DIV-18 to DIV-28. Cultures were fixed with 4% PFA on DIV-28 followed by immunofluorescent staining with SMI31 and Z2. Myelin was greatly reduced in 5 µg/ml BIX-treated cultures and higher doses whereas axons were less effected. Cultures treated with DMSO (A), 0.05 µg/ml of BIX (B), 0.1 µg/ml of BIX (C), 0.5 µg/ml of BIX (D), 1 µg/ml of BIX (E), 5 µg/ml of BIX (F), 10 µg/ml of BIX (G), scale bar=50 µm.
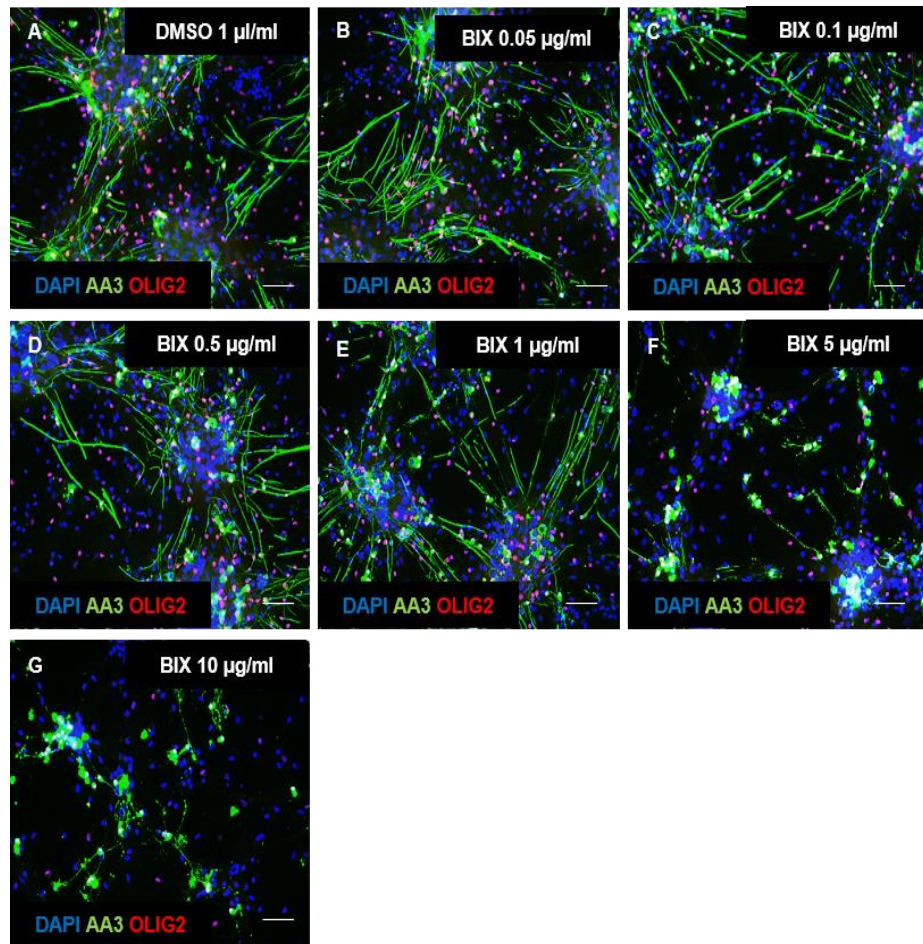
Figure 5.5: Dose-dependent reduction of oligodendrocyte lineage cells in spinal cord myelinating cultures.

The cultures were treated with 5 µg/ml of BIX from DIV-18 to DIV-28. Cultures were fixed with 4% PFA on DIV-28 followed by immunofluorescent staining with Olig2 and AA3 (PLP). Myelin was greatly reduced in 5 µg/ml BIX-treated cultures and higher doses whereas axons were less effected. Cultures treated with DMSO (A), 0.05 µg/ml of BIX (B), 0.1 µg/ml of BIX (C), 0.5 µg/ml of BIX (D), 1 µg/ml of BIX (E), 5 µg/ml of BIX (F), 10 µg/ml of BIX (G), scale bar=50 µm.
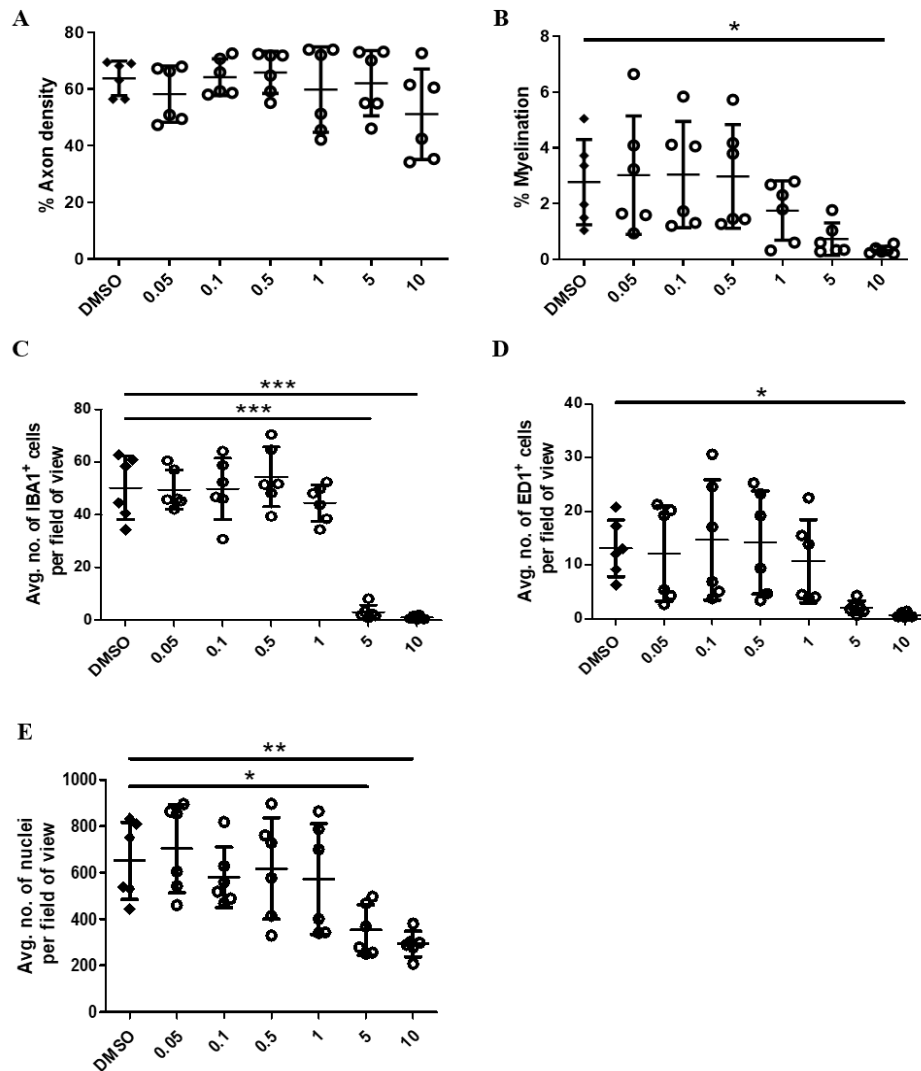
Figure 5.6: Dose-dependent effect of BIX on myelinating spinal cord myelinating cultures.

A pilot dose-response study (0.05-10 µg/ml) revealed that BIX (5 µg/ml) is selectively toxic with respect to myelination, microglia, oligodendrocyte-lineage cells. Data is presented as mean ± SD (n=2). *p< 0.05, **p< 0.01, ***p< 0.001, (one-way ANOVA with Dunnett's Multiple Comparison).

The cultures were treated with 1µl/ml of DMSO or 5 µg/ml of BIX on alternate days, from DIV 18 to DIV 28 and the following parameters were quantified: axonal density, myelination, microglia, oligodendrocyte-lineage cells and astrocytes. In the cultures treated with BIX, the axonal density was least effected (DMSO, 64.9 ± 4.2%; BIX, 63.3 ± 8.3%; *p*=0.5126), whereas the myelination significantly was reduced approximately 5-fold (DMSO, 5.9 ±

148

3.1%; BIX, 1.0 ± 0.5 %; $p \leq 0.001$). Additionally, 90% of IBA1$^+$microgolia were lost (DMSO, 49.3 ± 14.3; BIX, 5.3 ± 6.1; $p \leq 0.001$), and ED1$^+$ microglia were reduced by 80% (DMSO, 11.8 ± 4.4; BIX, 2.2 ± 1.5; $p \leq 0.001$). Olig2$^+$ cell numbers decreased by 50% (DMSO, 172.2 ± 23.7; BIX, 93.5 ± 35.4; $p \leq 0.001$). There was also a slight reduction in PLP$^+$ cells but this was not significant (DMSO, 40.3 ± 12.9; BIX, 32.8 ± 13.8; $p=0.2383$). Additionally, the percentage of GFAP$^+$ staining (DMSO, 55.1 ± 1.3%; BIX, 52.6 ± 2.7%, $p \leq 0.05$) and the percentage of MAP2$^+$ staining (DMSO, 45.2 ± 1.9%; BIX, 42.4 ± 3.4%; $p = 0.0764$) were not effected (Figure 5.7 and Figure 5.8). Representative images at higher magnification are provided in Figure 5.9.
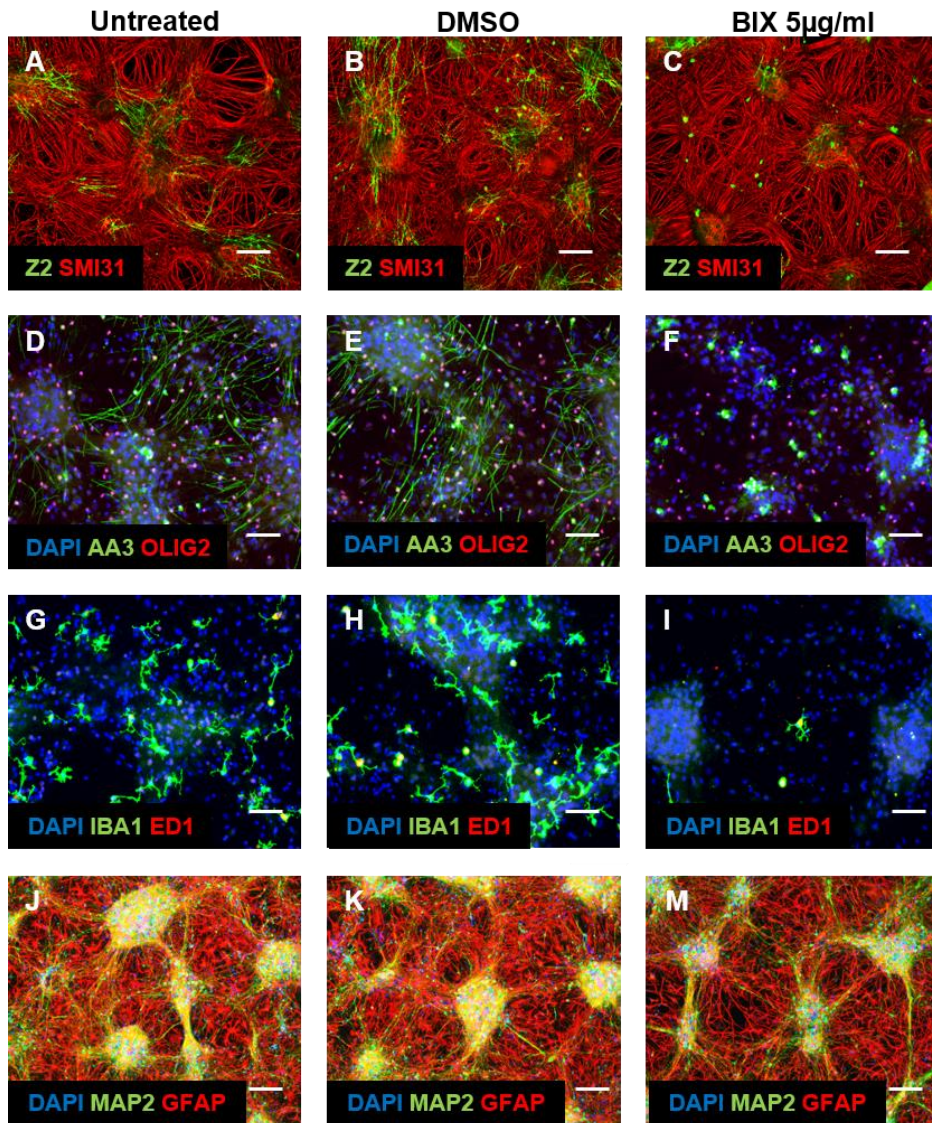
Figure 5.7: Representative images of BIX-treated spinal cord explant myelinating cultures on DIV-28.

The cultures were treated with 5 µg/ml of BIX from DIV-18 to DIV-28. Cultures were fixed with 4% PFA on DIV-28 followed by immunofluorescent staining. Myelin, Olig2-positive cells and microglia were greatly reduced in 5 µg/ml BIX-treated cultures. Axons, astrocytes and MAP2-positive neurons were less effected. Untreated, DMSO and 5 µg/ml of BIX-treated cultures stained with SMI31/Z2 (A-C), Olig2/AA3 (PLP) (D-F), IBA1/ED1 (G-I), GFAP/MAP2 (J-M). Top and bottom rows, scale bar=100 µm; middle rows, scale bar=50µm.
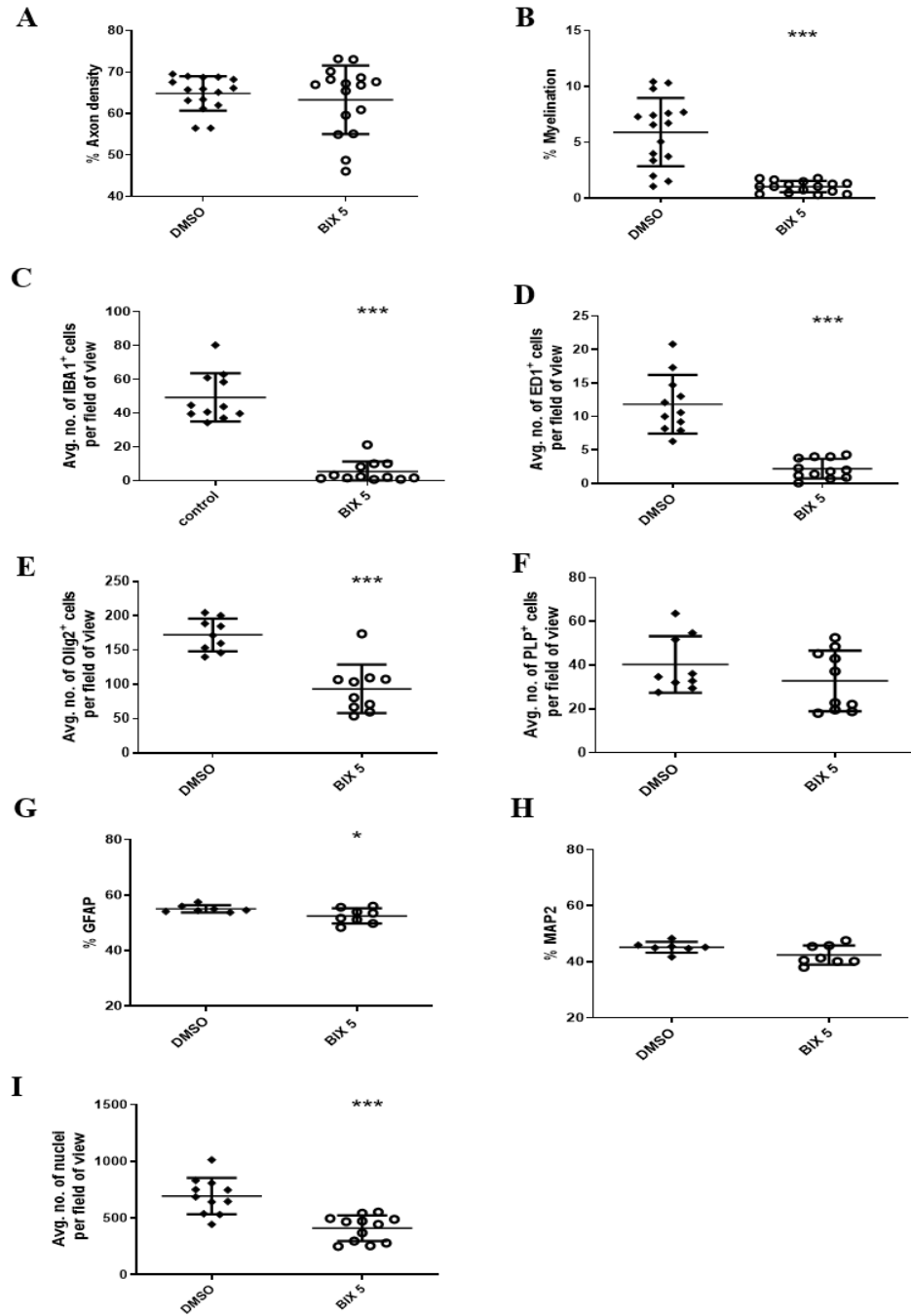
Figure 5.8: Selective toxicity of 5 μg/ml of BIX on myelin and microglia in spinal cord myelinating cultures.

BIX (open circles) did not have any significant effect on axonal density when compared to DMSO controls (solid diamonds) (A). BIX significantly reduced myelination (B), microglial cell numbers positive for IBA1 and ED1 (C, D) and Olig2-positive cells (E). PLP-positive cells are less effected (F). BIX did not have an effect on % GFAP and % MAP2 (G, H). Data are presented as mean ± SD (n ≥ 3). ***p< 0.001, (unpaired t-test).
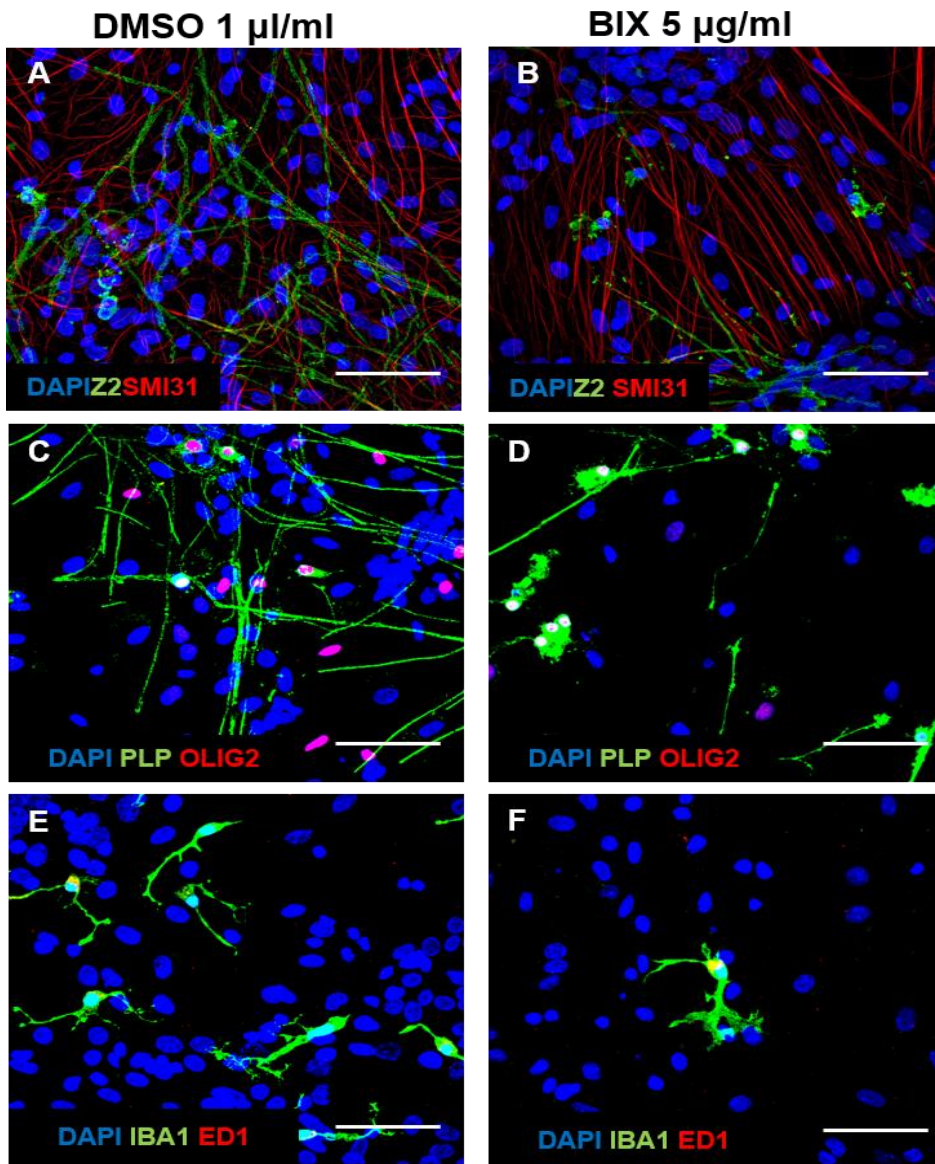
Figure 5.9: Representative images of BIX-treated myelinating cultures on DIV-28.

The cultures were treated with 5 μg/ml of BIX from DIV-18 to DIV-28. Cultures were fixed with 4% PFA on DIV-28 followed by immunofluorescent staining Myelin, Olig2-positive cells and microglia were greatly reduced in 5μg/ml BIX-treated cultures. DMSO and 5μg/ml of BIX-treated cultures stained with SMI31/Z2 (A-B), Olig2/AA3 (PLP) (C-D), and IBA1/ED1 (E-F). Scale bar=50μm.

Initial experiments were conducted for a duration of 10 days and the cells were

fixed on day 10. Later the effect of BIX on myelination and axonal density was

studied at different time points such as 1 day, 5 days, and 10 days post-treatment. This experiment was conducted only once. The effect of BIX on myelination was noticeable as early as 5 days post-exposure to BIX (Figure 5.10 and Figure 5.11). There was no significant effect of 5 µg/ml of BIX on myelination on day 1. Myelination only increased in DMSO- treated groups and not in BIX-treated groups on day 5 and day 10 compared to baseline day 0 (Figure 5.10 and Figure 5.11). There was no significant effect of 5 µg/ml of BIX on the axonal density on day 1 and day 5. A slight increase in the axonal density was noticed on day 10 in cultures treated with 1 µl/ml of DMSO and 5 µg/ml of BIX compared to baseline. They also have a significant difference between each other (DMSO, 62.6 ± 1.1; BIX, 67.1 ± 0.3; $p \leq 0.05$). However, this effect was not reproduced in other experiments carried out using the same conditions.
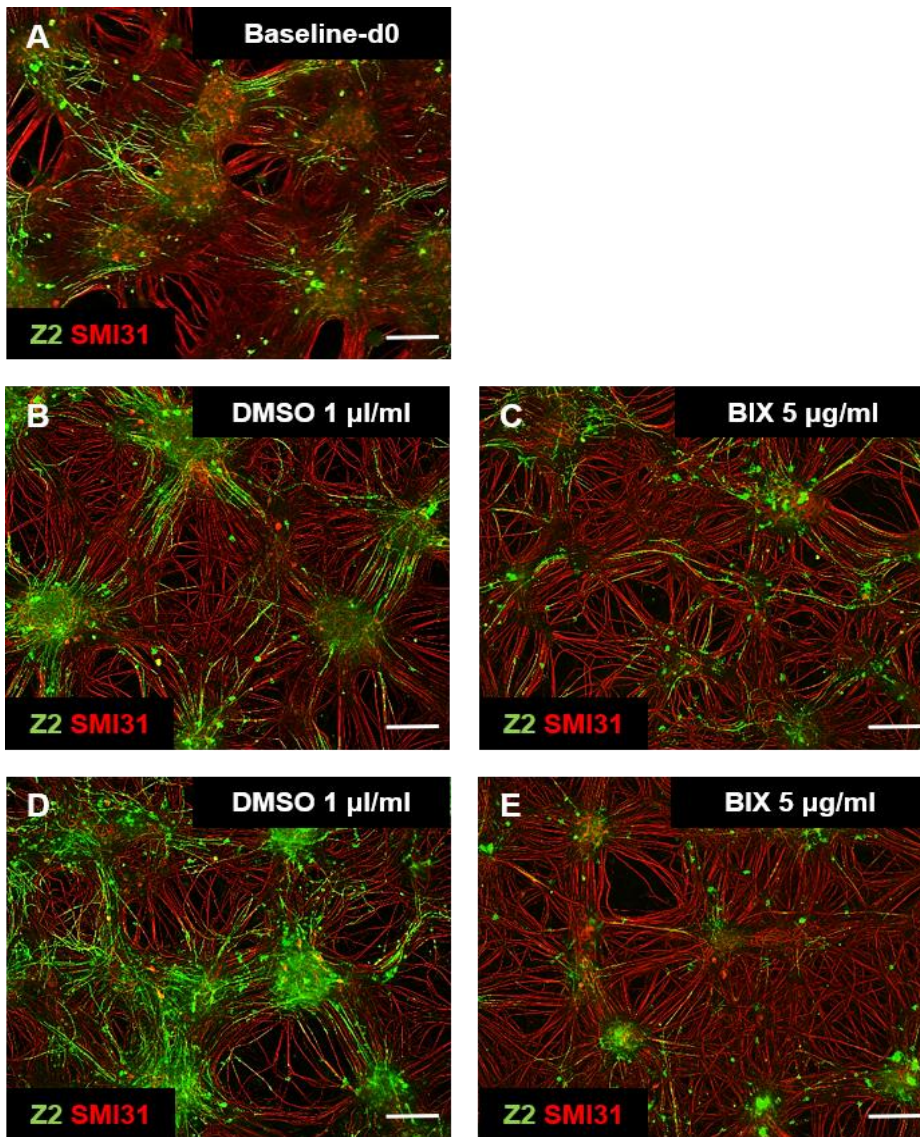
Figure 5.10: Effect of BIX on myelin in DIV28 spinal cord myelinating cultures.

Cultures were treated with 1 μl/ml of DMSO or 5 μg/ml of BIX on alternate days, between DIV28 and DIV38 and later fixed and stained for SMI31/Z2. Baseline (d0) conditions (A) and following 1d of DMSO treatment (B). The degree of myelination was not found to be different when images at 5d (C) and 10d (E) of BIX-treatment were compared. Myelin staining increased when DMSO-treated cultures at 10d were compared to those at 5d (B, D). Scale bar indicates 100 μm.
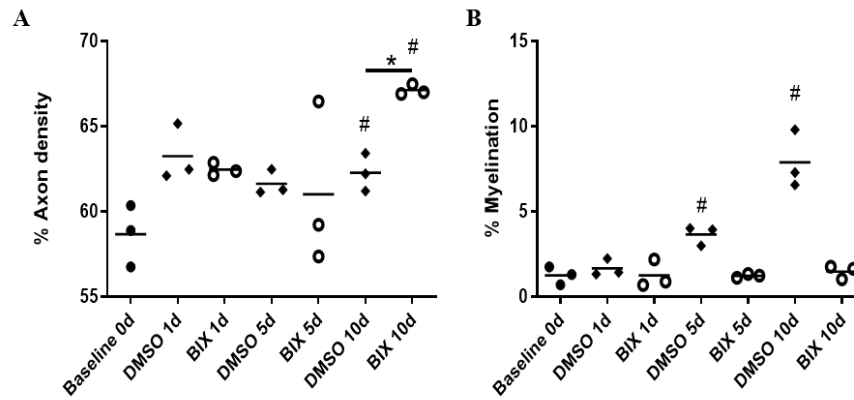
Figure 5.11: Time-course of the effect of BIX on myelin in DIV18 spinal cord explant cultures.

Cultures were treated with 1 μl/ml of DMSO (solid diamonds) or 5 μg/ml of BIX (open circles) for 1d, 5d or 10d and later stained for SMI31/Z2. (A) The axonal density significantly increased on day 10 in both DMSO and BIX-treated cultures compared to baseline and also significant difference was noticed between these two groups. (B) In the BIX-treated cultures, myelin did not increase significantly compared to DMSO at the same time points. BIX inhibited myelination and the vehicle-treated controls had a significantly higher percentage of myelin on day 5 and day 10. Data are presented as mean ± SD (n = 1).). Two way ANOVA was used. *p< 0.05 versus respective DMSO treatments; #p< 0.05 vs baseline 0d.

Following on from the initial experiments demonstrating that BIX inhibits myelination, an experiment was conducted to discover if it is capable of causing demyelination. To address this, the same 1 μl/ml of DMSO or 5 μg/ml of BIX treatment was repeated at a later time-point for 10 days, from DIV 28 to DIV 38, as the cultures on DIV 28 are already myelinated. The outcome of these experiments was in agreement with the previous results in terms of axonal density, myelination, and number of microglia. That is, on DIV 33 (day 5) and DIV 38 (day 10), there was no significant effect on the axonal density except that axonal density decreased in DMSO group at day 10 compared to baseline day 0. BIX did not cause demyelination but it was found to inhibit myelination, as before (Figure 5.12).
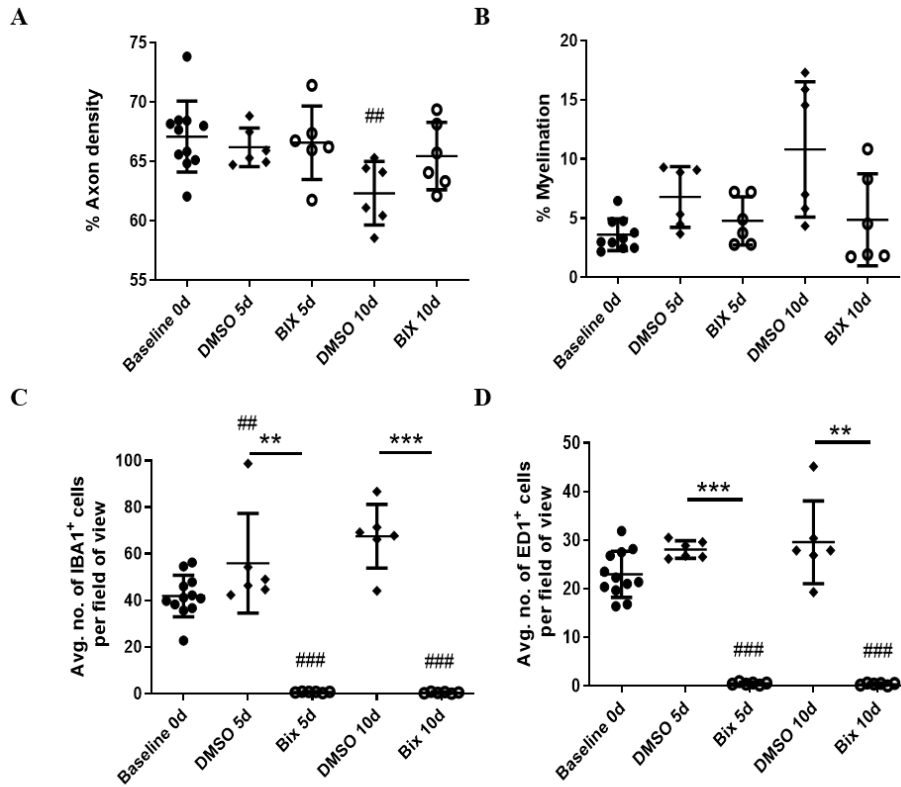
Figure 5.12: Effect of BIX on myelinated spinal cord explant cultures from DIV28-38.

Cultures were treated with 1 µl/ml of DMSO or 5µg/ml of BIX from DIV28-38 and later stained for SMI31/Z2 or IBA1/ED1. (A) DMSO on day 10 has significant low axonal density compared to baseline. (B) In the BIX-treated cultures myelin did not increase significantly and also BIX did not affect the pre-existing myelin compared to DMSO at the respective time points. (C, D). BIX treatment significantly reduced IBA1-positive and ED1-positive microglia at day 5 and 10 compared to baseline; BIX-treated cultures had less number of microglia compared to DMSO-treated cultures at respective time points. Data are presented as mean ± SD (n = 2). Two way ANOVA was used. **p< 0.01, ***p< 0.001 versus respective DMSO treatments; ##p< 0.01, ###p< 0.001 vs baseline 0d.

The degree of myelination in cultures differs between different biological preparations because of which the data from these experiments had huge error bars. In the controls, as anticipated, myelination continued to increase, while in the BIX-treated cultures, the amount of myelin remained the same as that seen at day 28, indicating that BIX did not cause demyelination but stops or reduces further myelination. Additionally, the effect of BIX on microglia was also studied at these time points. As expected, BIX reduced more than 95% of the microglia in the experiments conducted at a later stage (DIV 33-day 5, DMSO, 55.9 ± 21.4; BIX, 0.68 ± 0.2; $p \leq 0.001$) (DIV 38-day 10, DMSO, 67.57 ± 13.7;

156

BIX, 0.45 ± 0.3; $p \leq 0.001$), (Figure 5.12). Irrespective of the age of the culture DIV 18-28 or DIV 28-38, BIX treatment reduced the number of microglia to the same extent.

To further understand whether the effect of BIX on microglia and myelin were reversible, withdrawal experiments were performed. The cultures were treated from DIV 18-23 with BIX, followed by the transferal of the coverslips to fresh medium until DIV 28. The coverslips were washed in fresh medium a couple of times to remove any residual BIX. An 8-fold reduction in microglia number was observed in the BIX-treated groups at (DIV 23, DMSO, 52 ± 24.4; BIX, 6.7 ± 6.8; $p \leq 0.05$) and when the cultures were transferred to fresh medium for an additional 5 days, there was no significant increase in the number of microglia (DIV 23, BIX, 6.7 ± 6.8; DIV 28, BIX, 21.5 ± 19.0; $p=0.1485$). Under the same experimental conditions, the withdrawal effect on myelination and axonal density were also studied. As mentioned before, the axonal density was unaffected by BIX treatment and the percentage of myelination decreased on DIV 23 and did not improve on withdrawal of BIX, suggesting that BIX inhibits OPC proliferation and maturation (Figure 5.13).

Note: Long-term storage of BIX at 4$^\text{o}$C reduces its potency. Two batches of BIX were used in these experiments. The first batch, which was stored at 4$^\text{o}$ C for a few months, was less potent than the new batch.
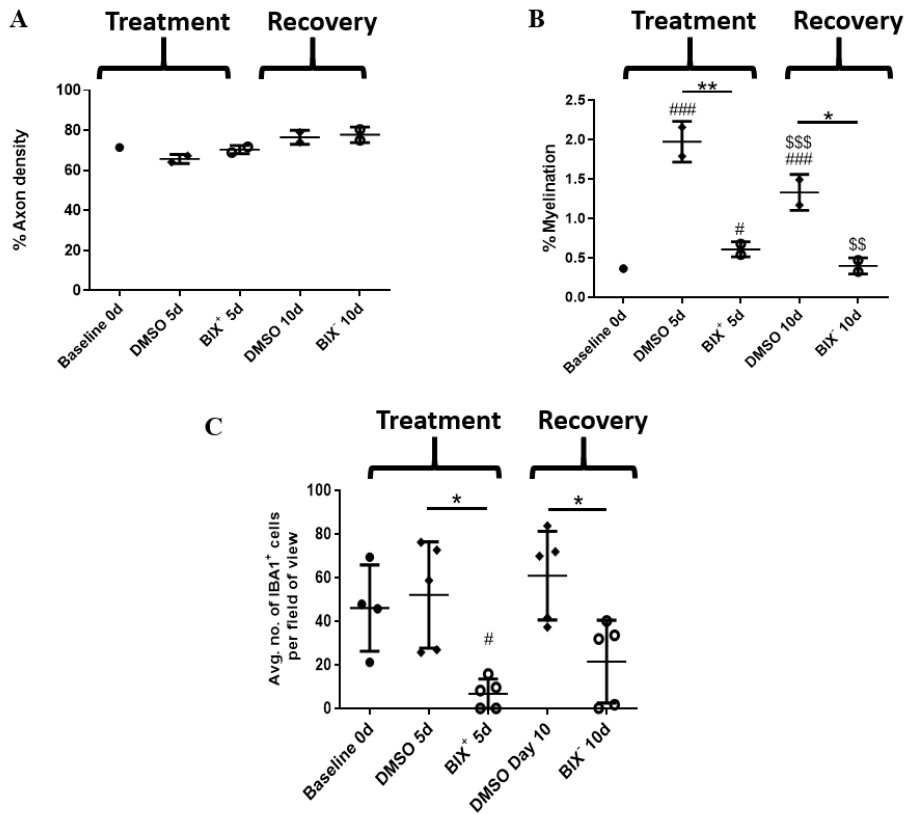
Figure 5.13: Selective and irreversible toxicity of 5 µg/ml of BIX on myelination and microglia in spinal cord explant myelinating cultures.

The DIV 18-23 cultures were treated with 5 µg/ml of BIX or 1 µl/ml of DMSO (vehicle control) on alternate days before being transferred to fresh media for another 5 days i.e., until DIV 28. **(A)** BIX did not have any significant effect on axonal density. **(B)** BIX inhibited myelination compared to DMSO-treated cultures at day 5, withdrawal of BIX did improve myelination **(C)** BIX treatment significantly reduced IBA1-positive at day 5 compared to baseline; BIX-treated cultures had less number of microglia compared to DMSO-treated cultures. Microglial cell numbers did not improve upon BIX withdrawal. Data are presented as mean ± SD (n ≥ 1). Two way ANOVA was used. *$p < 0.05$, **$p < 0.01$, ***$p < 0.001$ versus respective DMSO treatments; #$p < 0.05$, ##$p < 0.01$, ###$p < 0.001$ vs baseline 0d; $$$p < 0.01$, $$$$p < 0.001$, DMSO 5d versus DMSO 10d or BIX+ 5d versus BIX- 10d treated cultures.

5.5.2 BIX treatment of *ex-vivo* cerebellar slice cultures

Representative images of cerebellar slices were provided in Figure 5.14). A pilot experiment with different doses of BIX was performed using 1 μg/ml, 5 μg/ml and 10 μg/ml on cerebellar slice cultures (Figure 5.15). The higher doses were lethal, and the lower dose did not have any effect on any specific cell type. Hence, a dose of 5 μg/ml was used for subsequent experiments, which had selective toxicity towards microglia and oligodendrocytes. Changes between the doses were estimated by eye from a small number of imaged slices.

In the below description of results DIV refers to the number of days *in-vitro* and day 1, day 3 or day 5 refers to the number of days post-treatment with DMSO or BIX. Slices were treated with BIX or DMSO from DIV 7 to DIV 12. When BIX was added to slice cultures, there was almost 20 percent decrease in Iba1$^+$ cells following exposure to 5 μg/ml of BIX after day 3 (Figure 5.16 and Figure 5.18). Oligodendrocyte numbers reduced by 5-fold on day 1 (Figure 5.16 and Figure 5.18). However, astrocytes seem to be less effected (or not affected at all, Figure 5.17 and Figure 5.18). The percentage of GFAP$^+$ staining was not effected in BIX-treated cultures. These results agree with the results obtained from spinal cord myelinating cultures.

An attempt was made to stain neurons using MAP2$^+$ and myelinated axons using PLP, but this staining was not successful. Myelin staining was fragmented and was not useful quantification (see Appendix). Occasionally PLP$^+$ axons were noticed irrespective of the treatment group. This could be attributed to the survival of neurons in organotypic slice cultures. Various parameters can influence the survival of neurons in slice cultures, which include the age of the donor, growth factors in the media, serum, lack of thinning of slices, preparation speed, sterility and axotomy. (Humpel, 2015a).
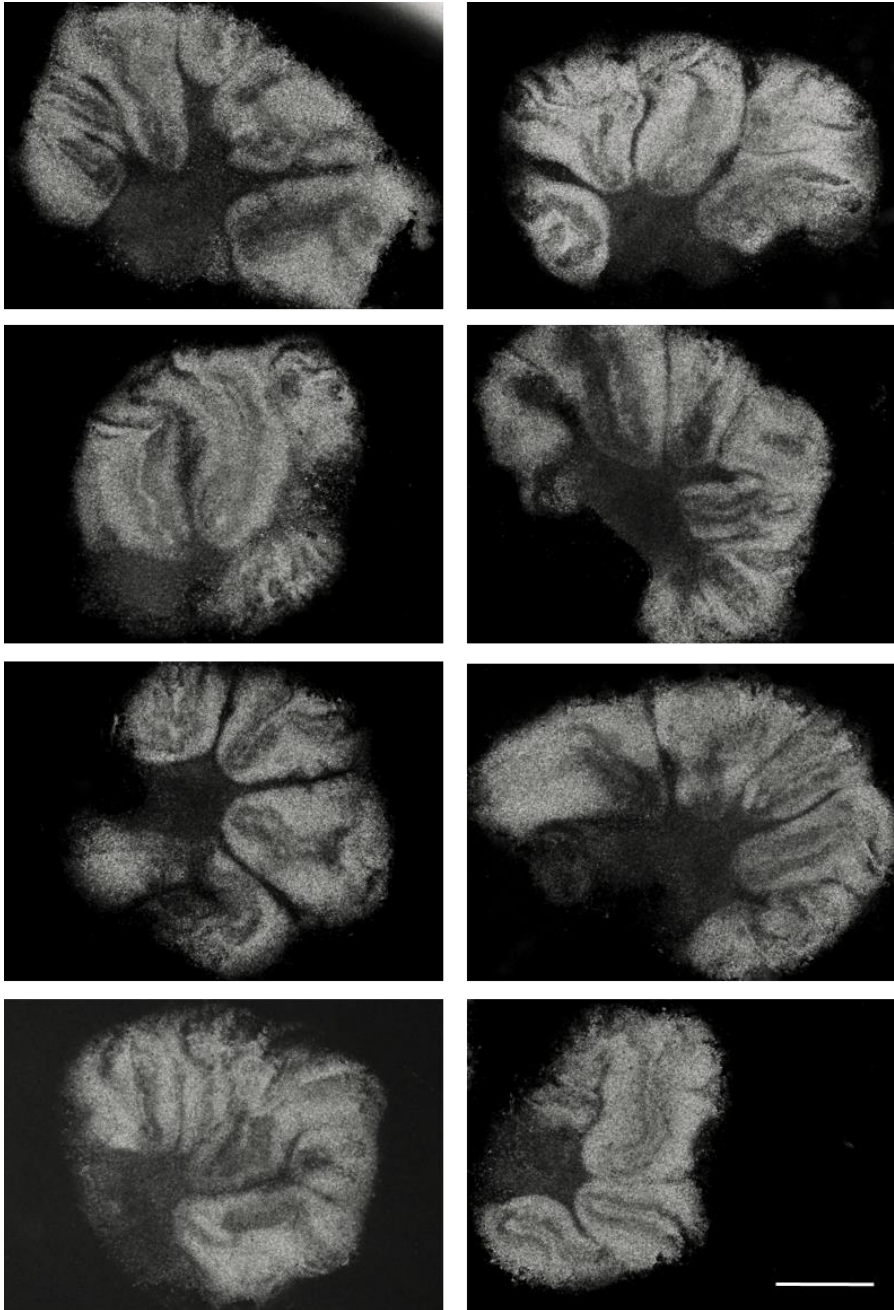
Figure 5.14: Representative images of organotypic cerebellar slice cultures on DIV-7.

Organotypic slice cultures were prepared from P10 Sprague Dawley rat pups and maintained on cell culture inserts in the slice culture medium. Images were captured using EVOS XL Core microscope, 4X magnification, Scale bar-1000 µm.
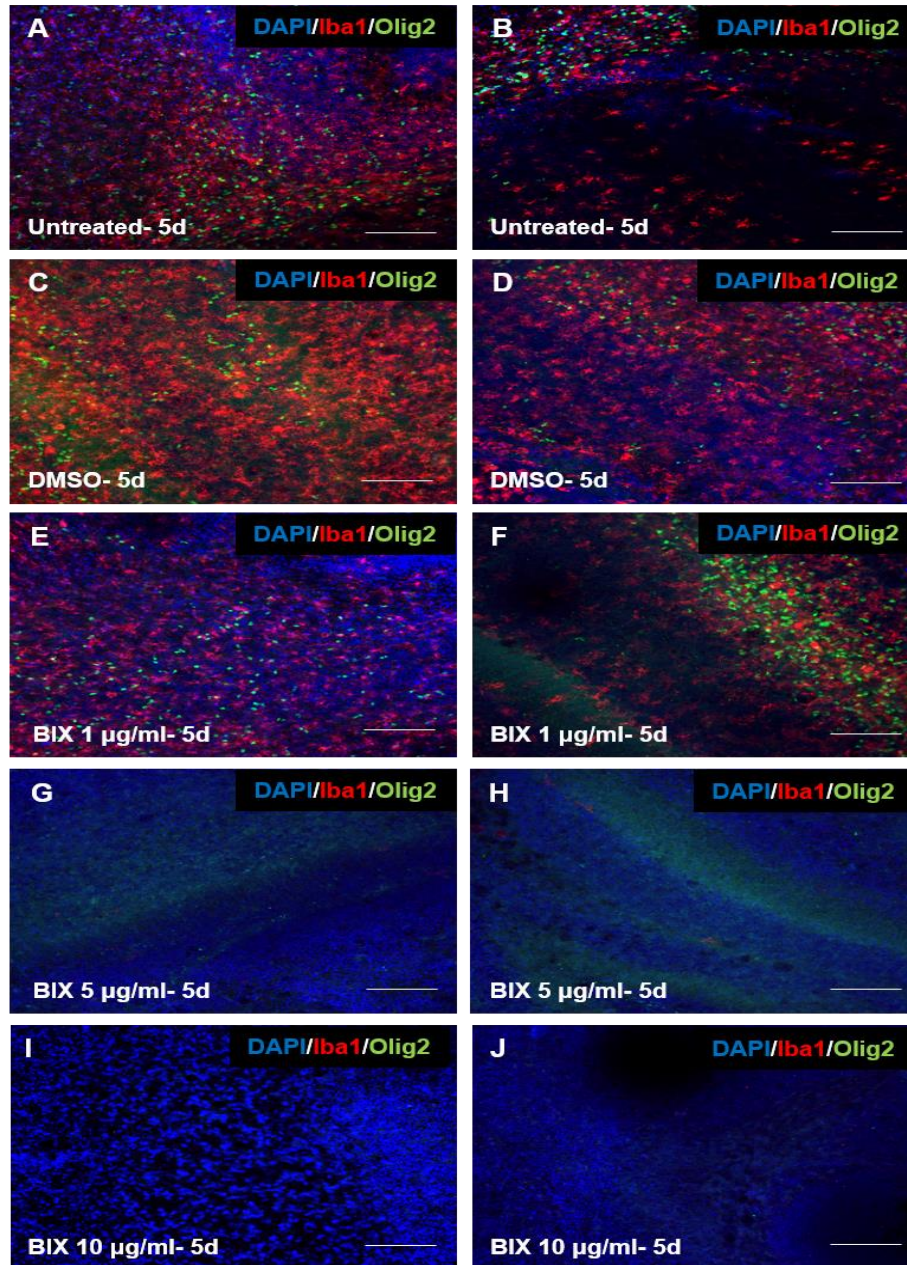
Figure 5.15: Dose-dependent effect of BIX on cerebellar slices stained for Iba1/Olig2.

The cultures were treated with 5 μg/ml of BIX from DIV-7 to DIV-11. Cultures were fixed with 10% neutral buffered formalin on DIV-12 followed by immunofluorescent staining with Iba1 and Olig2. No difference was observed between untreated and DMSO-treated cultures. However, Olig2$^+$ cells and Iba1$^+$ microglia were greatly reduced in 5 μg/ml and 10 μg/ml BIX-treated cultures. A-B. Untreated cultures. C-D. DMSO-treated cultures. E-F. Cultures treated with 1μg/ml of BIX. G-H. Cultures treated with 5 μg/ml of BIX. I-J. Cultures treated with 10 μg/ml of BIX. Images were taken at 20x magnification on the confocal microscope. Scale bar=100 μm.
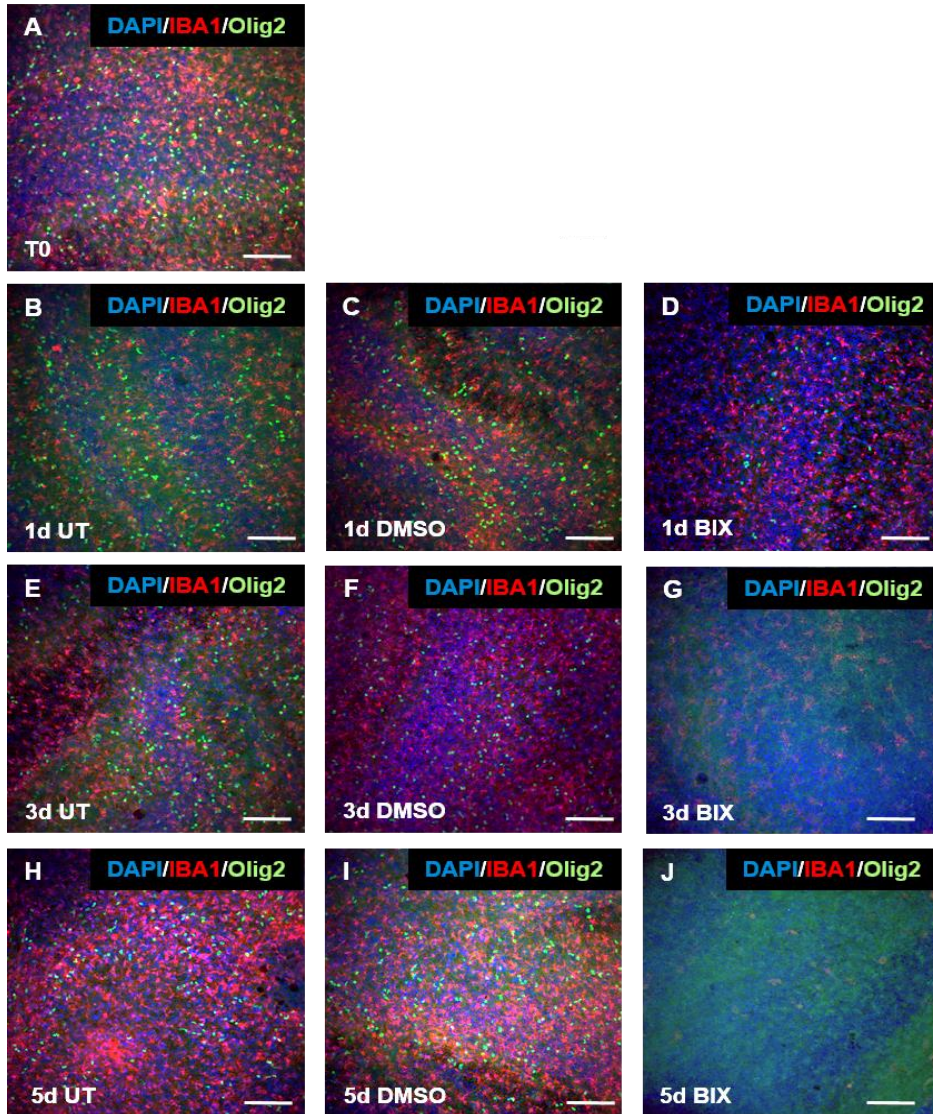
Figure 5.16: Time-course of BIX-treated cerebellar slices stained for Iba1/Olig2.

Cultures were treated with 1 µl/ml of DMSO or 5µg/ml of BIX and fixed at different time points (T0, day 1, day 3 and day 5). Reduction in oligodendrocytes number was observed after 1 d in treatment with BIX. Reduction in Iba+ cells was observed after 3 days of BIX treatment. A.T0 = day 0 of treatment. (B-D) Untreated, DMSO and 5 µg/ml of BIX-treated cultures on 1d of treatment. (E-G) Untreated, DMSO and 5 µg/ml of BIX-treated cultures on 3d of treatment. (H-J). Untreated, DMSO and 5 µg/ml of BIX-treated cultures on 5d of treatment. Images were taken at 20x magnification on confocal microscope. Scale bar=100 µm.
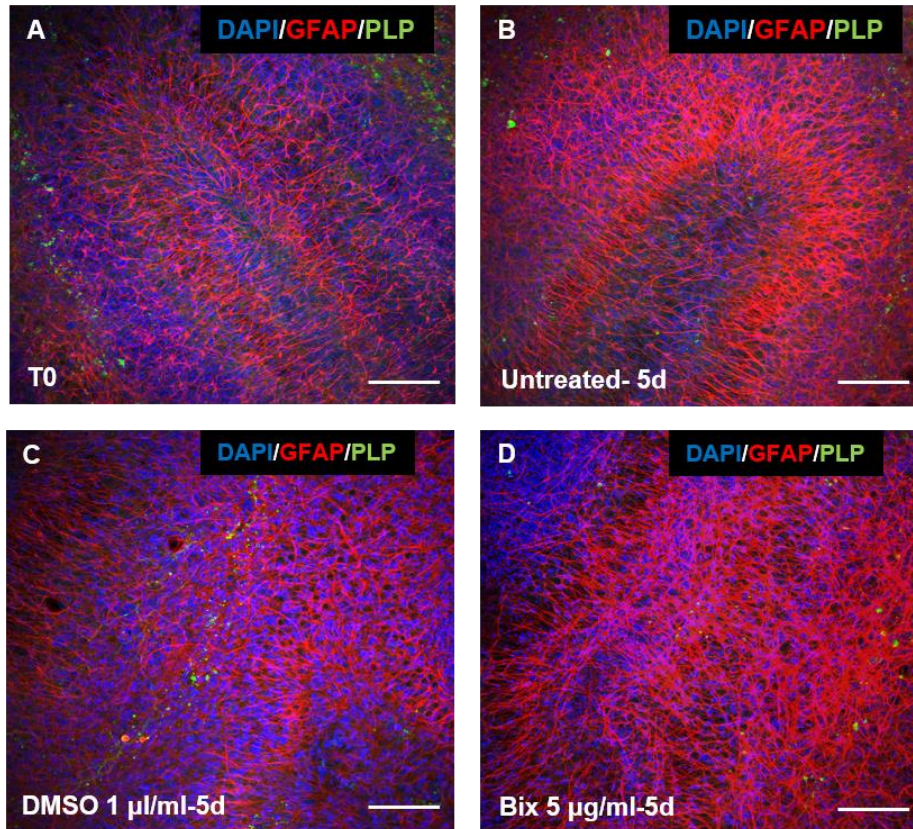
Figure 5.17: Representative images of BIX-treated cerebellar slices stained for GFAP/PLP.

Cultures were treated with 1 µl/ml of DMSO or 5µg/ml for 5 days and later stained for GFAP (astrocytes) /PLP (proteolipid protein present in myelin). No difference was observed between untreated, DMSO-treated cultures or BIX-treated cultures. A.T0 = day 0 of treatment. B. Untreated cultures. C. DMSO-treated cultures. D. Cultures treated with 5µg/ml of BIX. Images were taken at 20x magnification on the confocal microscope. Scale bar=100 µm.
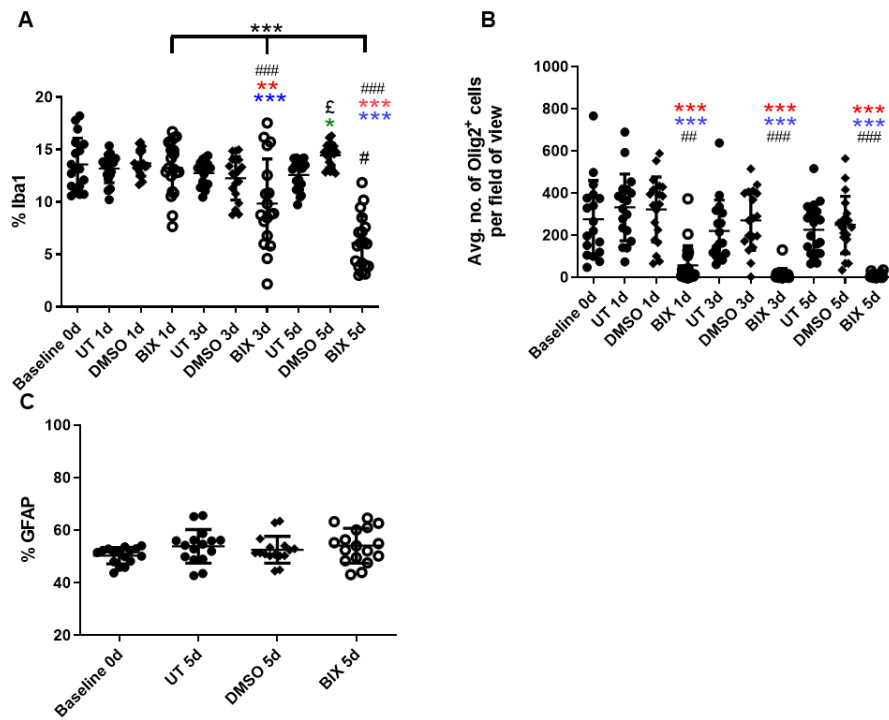
Figure 5.18: Selective toxicity of 5 µg/ml of BIX to microglia and oligodendrocyte in organotypic slice cultures.

Each dot indicates an independent slice. **(A)** BIX significantly reduced IBA1^{+} microglia after 3d of treatment. **(B)** BIX significantly reduced Olig2^{+} cells after 1d of treatment. **(C)** BIX did not have any significant effect on GFAP^{+} cells. Data is presented as mean ± SD (n= 3). Two way ANOVA was used. [##]$p< 0.01$, [###]$p< 0.001$ vs baseline 0d; [£]$p< 0.05$ versus DMSO 3d, [*]$p< 0.05$ versus untreated 5d; [**] $p< 0.01$, [***] $p< 0.001$ versus untreated at respective time points; [***] $p< 0.001$ versus DMSO at respective time points.

Note: %Iba1 and %GFAP were quantified using Cell profiler software and Olig2^{+} cells were quantified using Fiji (Image J).

164

Table 5.1: Summarising the effects of BIX-treatment in *in-vitro* models.

Myelinating cultures	Markers	Effect of BIX treatment
Oligodendrocyte lineage cells	Olig2/PLP (AA3)	Reduced
Microglia	Iba1 and ED1	Reduced
Myelin	Z2 (MOG)	Reduced
Astrocytes	GFAP	Less effected
Neurons	MAP2	Not effected
Axons	SMI31	Not effected
Total cell numbers	DAPI	Reduced
Organotypic slice culture		
Oligodendrocytes	Olig2	Reduced
Microglia	Iba1	Reduced
Astrocytes	GFAP	Not effected
Myelin	MOG and PLP	Not quantified

5.5.3 RNA sequencing-based analysis of pathways activated by BIX in the spinal cord myelinating cultures

RNA samples were prepared from 5 µg/ml BIX treated cultures and 1 µl/ml DMSO treated cultures at 24 h time point and the summary of the results is provided here.

Sequence counts

Sequence counts for each sample are provided. The duplicate level in the whole file was estimated by analysing the first 100,000 sequences in each file. An exact match over the whole length of the sequence is required for duplication detection (Figure 5.19 A).

Mean Phred score

The quality of the sequences is good and therefore used for further analysis. The per sequence quality score gives information about the quality of the read instead of individual bases. The histogram is skewed to the right for good quality data (Figure 5.19B and Figure 5.19C). The mean Phred score remains above the cutoff of 30 which indicates good quality data sequences.

Per Base Sequence Content

The proportion of individual bases (A, T, G, C) was drawn as a line across the length of the read. All 12 FASTQ files were marked as a failure. This occurred due to the priming step of the library preparation. During the reverse transcription of mRNA to cDNA, hexamer primers are used and due to the usage of these hexamer primers in the library preparation, bias towards certain bases in the sequences within the samples arises (Conesa et al., 2016). This is a common feature in RNA sequencing experiments. The sequences did not require any additional processing and were used for downstream analysis. An example plot is provided in (Figure 5.19 D).
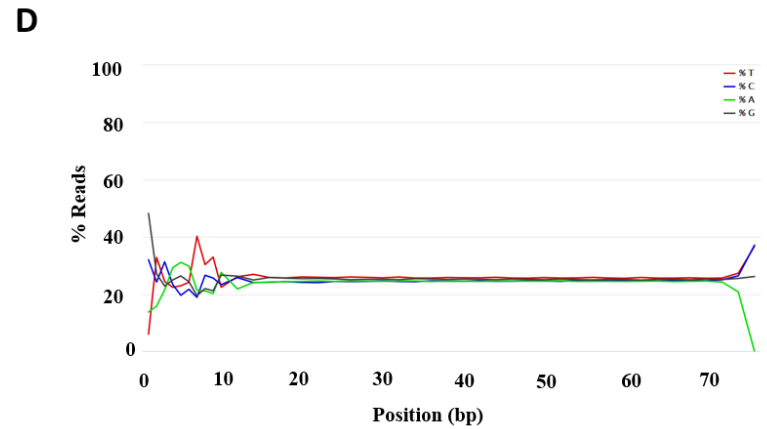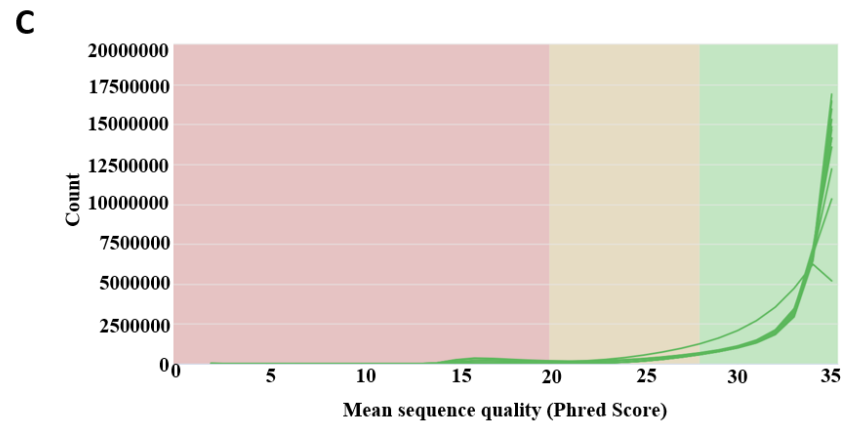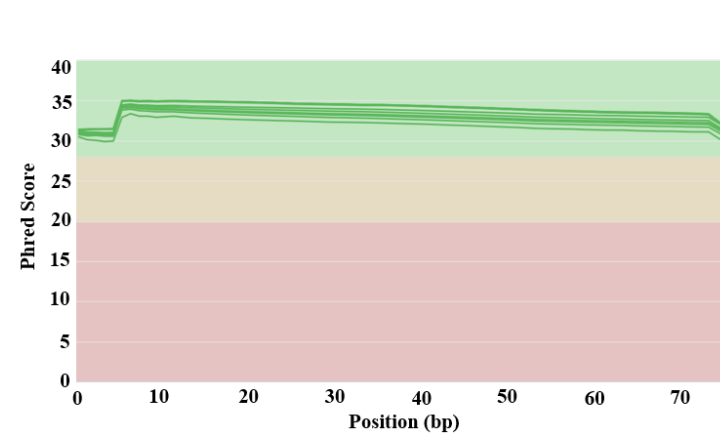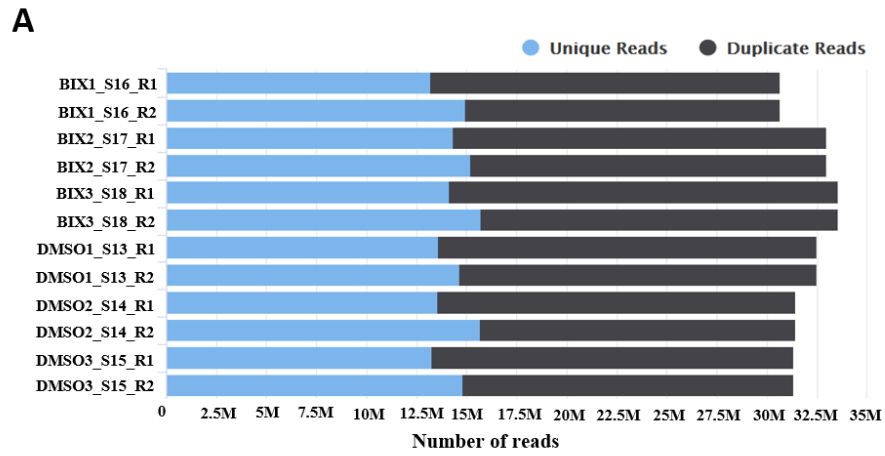
Figure 5.19: Quality control analysis of RNA-seq data

A. Sequence count chart represents the total number of reads divided into unique reads and duplicate reads. **B.** Mean quality score represents the mean quality value across each base position in the read, the higher the score the better the base call **C.** Per sequence quality score chart. The confidence with which a base is called is given a score and higher the score the better the quality of the read (Ewing et al., 1998). The mean Phred quality score for the entire sequences remains above 30. The accuracy of the base call is 99.9% when the mean Phred score is 30. This graph facilitates in identifying subsets of sequences with poor quality **D.** Per base sequence content chart. The proportion of each base position in a file for which each of the bases has been called. Example graph of percentages of bases (BIX-S16-R1) file.

Per base GC content

Among all the files provided (BIX Read2) failed and 4 other files had a warning, the slight deviation from the normal GC content is less likely due to contamination and more likely to be due to the uneven distribution of GC content (Figure 5.20 A). The samples deviated slightly from the GC content. There was an issue with only one file and did not cause any problems with alignment. The slight peak at 100% could be due to contamination.

N content

When a sequencer fails to call a particular base with sufficient confidence, the base is substituted with N. This graph represents the percentage of base calls at each position for which an N was called (Figure 5.20 B).

Over-represented sequences

A couple of files BIX1 Read2 and DMSO3 Read 2 had a high number of over-represented sequences (Figure 5.20 C). There was no adaptor contamination in these files as confirmed by the adaptor content analysis. The possible reason could be over-representation of these sequences in the overall library.

Sequence length distribution

All the files were flagged indicating that some fragments differed in read length. Most of the fragments had 75 bp, and some fragments had 71-74 bp. The FASTQ files were already trimmed to exclude bad quality bases at the end of the fragment (Figure 5.20 D).

Sequence Duplication levels

FASTQC assumes all the reads are equally distributed in the library which is a feature of DNA sequencing experiments. But RNA sequencing experiments differ from this based on the low expressed and highly expressed genes. In general, high duplication level is expected for sequences that belong to highly expressed genes (Figure 5.20 E). In this data, all the 12 files are flagged for high duplication rate and this could be due to PCR artefacts but not due to highly expressed transcripts.

169

t
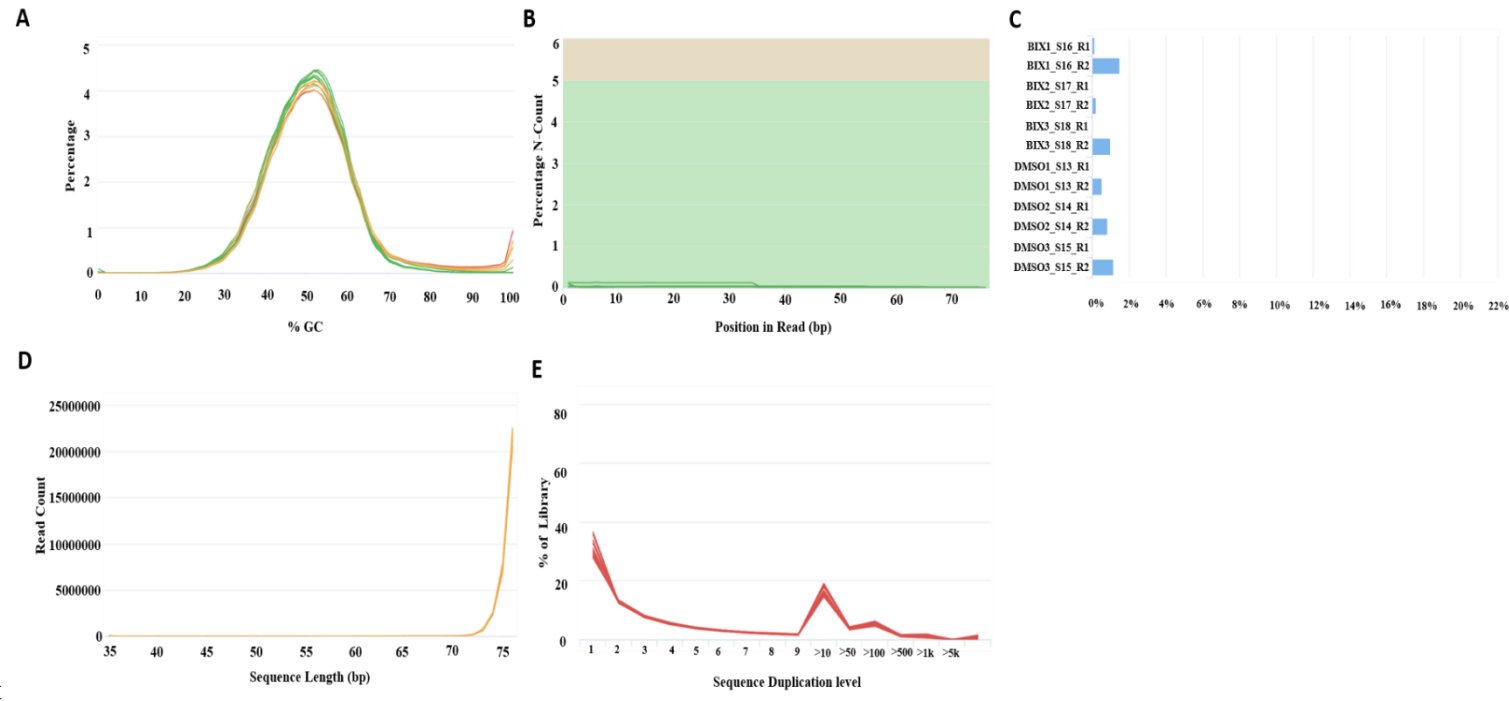
Figure 5.20 : Quality control analysis of RNA-seq data.

A. Per sequence GC content plot depicts the distribution of GC content per read. Under ideal conditions the GC distribution of the samples should be similar to the theoretical distribution. **B.** Per base N content plot shows indistinguishable bases as a function of base position of the read. In a good quality data, the values are expected to be close to zero. **C.** Overrepresented sequences in FASTQC refer to the extremely high frequency reads. **D.** Sequence length distribution plot depicts the length distribution of the reads. **E.** Sequence duplication level in FASTQC reflects the extent of repeated

sequences in the library. All the 12 files were flagged for high duplication rate and this could be more due to PCR artifacts than highly expressed transcripts being overexpressed.

Alignment:

Uniquely mapped reads for the samples exist between 78.2% and 83.8%, which is characteristic of RNA sequencing experiment. Qualimap requires files as the gene transfer format and it reconstructs the exon structure of the known transcripts. This allows the mapped reads to group them based on their origin as exonic, intronic or intergenic (Figure 5.21 A). Qualimaps computes the coverage depth at each base position of each annotated transcript and plots a graph between coverage depth and transcript position. The number of high quality reads that map to the transcript at that position (Sims et al., 2014). Among the mapped reads 78.2-79.6% reads are classified as exonic and 6.5%-7% were classified as intronic. The number of reads mapped to the intronic regions is due to the nascent or unspliced transcripts (Hansen et al., 2010). These values are typical for RNA-seq experiment. Gene coverage profile indicates that the samples have a uniform covering pattern across transcripts (Figure 5.21 B).
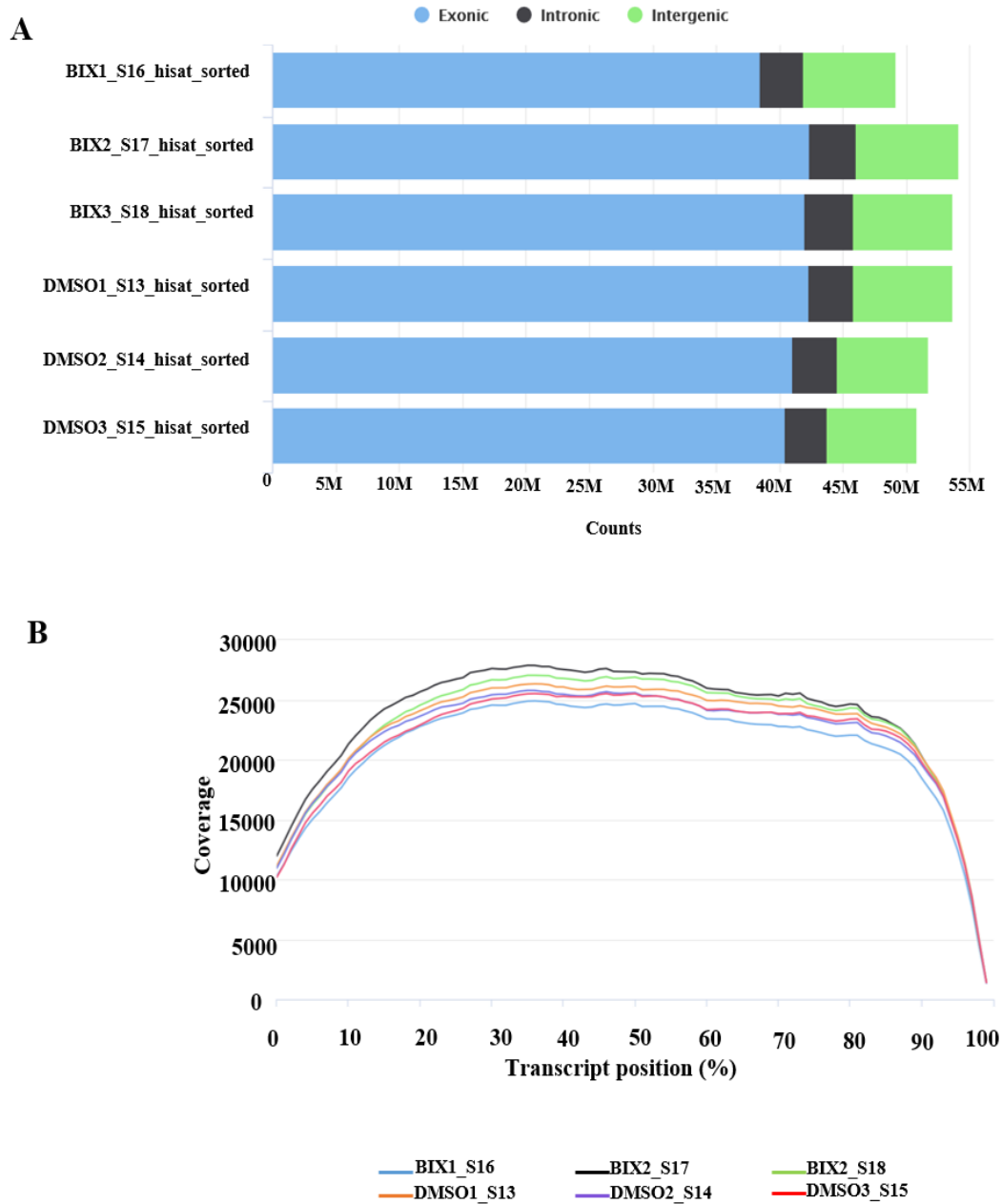
Figure 5.21: Quality control of alignment sequencing data using Qualimap.

A. This plot depicts the positional biases that occur due to poor quality RNA such as accumulation of mapped reads at 3ʹ end. Based on the origin of reads, the reads can be classified into exonic, intronic and intergenic. The graph shows the proportion of mapped reads assigned to different regions and the amount of useful RNA data. **B.** The mean distribution of coverage depth across the length of all mapped transcripts is uniform.

Bowtie 2 is used for aligning the sequencing reads to the reference sequence. The percentage of unique reads ranges from 78.2-83.8% (Figure 5.22 A). Picard Mark Duplicates identifies the duplication rate in samples. Library construction during PCR can cause duplicates and highly expressed genes are usually a source of read duplicates as well. It is an important parameter to check as low-quality RNA with few transcripts can be amplified in PCR causing read duplicates. The duplication rate in the samples is between 13.9 %-16.4% (Figure 5.22 B).
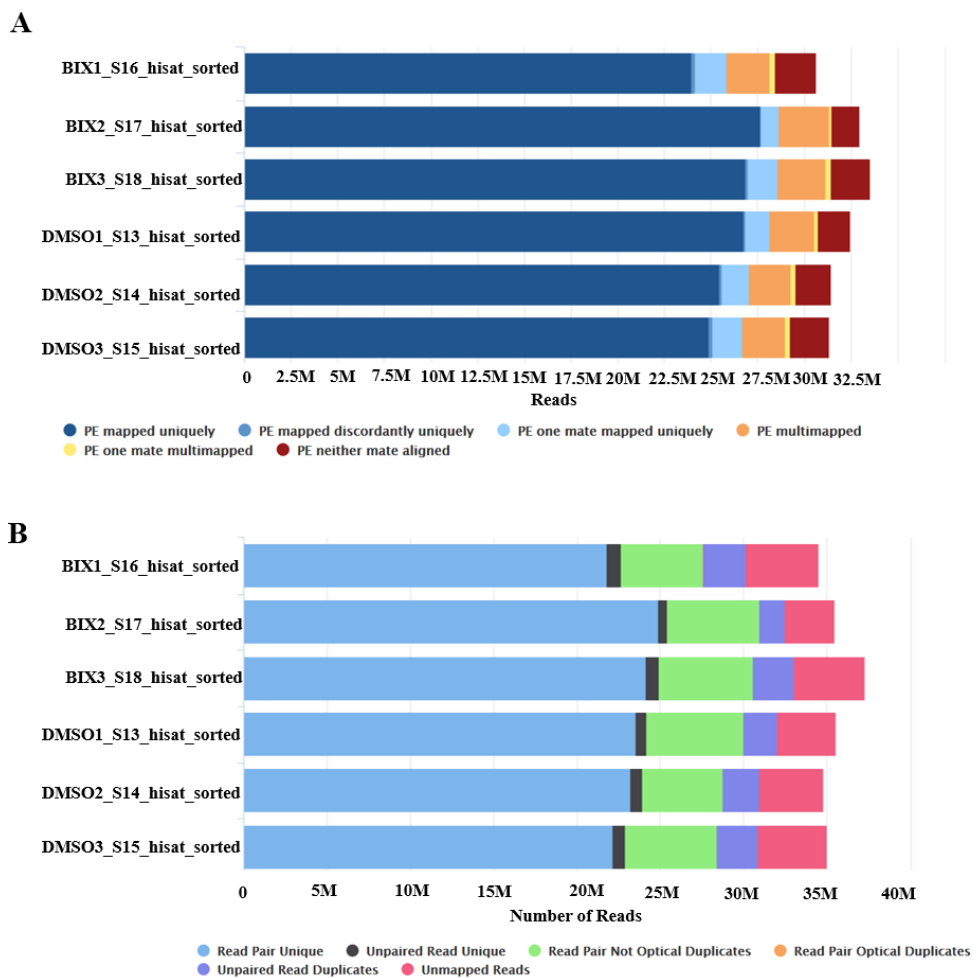
Figure 5.22: Sequence alignment to the reference and duplication rates.

A. Paired-end (PE) alignment score developed using Bowtie 2. The 6 possible outcomes of alignment include PE mapped uniquely: Pair has only one occurrence in the reference genome; PE one mate mapped: one read of a pair occurs once; PE mapped discordantly uniquely: The pair has one occurrence, but not with a proper pair; PE multimapped: The pair has several occurrences; PE one mate multimapped. One of a pair occurs several times in the genome. PE neither mate aligned: Neither of the pair has occurred in the genome. **B.** Picard mark deduplication stats shows the duplication rate in samples. Read pair unique: The number of reads that are not marked as duplicates; Unpaired read unique: Reads that are unique but not paired; Read pair not optic duplicates: The number of read pairs that were caused not due to

optic duplication; Read pair optic duplicates: The number of read pairs that were caused due to optic duplication; Unpaired read duplicates: The number of fragments marked as duplicates; Unmapped reads: Total number of unmapped reads.

Principle component analysis

Based on the clusters formed, the PCA plot shows that the difference between the groups is due to the treatment type (BIX treated group vs DMSO treated group) (Figure 5.23).
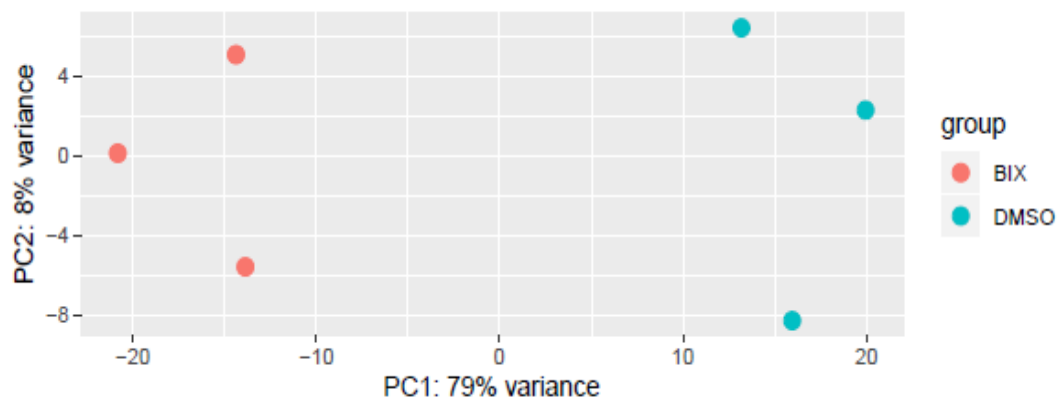
Figure 5.23: PCA plot of all samples.

The samples cluster based on the treatment type and the source of variation is caused due to treatment type.

Table 5.2: General Statistics data of RNA sequencing data.

Sample Name	5'-3' bias	M Aligned	% Dups	% Aligned	% Dups	% GC	Length	M Seqs
BIX1_S16_R1_001					56.9%	50%	75 bp	30.6
BIX1_S16_R2_001					51.2%	52%	76 bp	30.6
BIX1_S16__hisat.stdout				92.8%				
BIX1_S16__hisat_sorted	1.50	56.9	21.8%					
BIX2_S17_R1_001					56.6%	49%	76 bp	33.0
BIX2_S17_R2_001					54.0%	50%	75 bp	33.0
BIX2_S17__hisat.stdout				95.4%				
BIX2_S17__hisat_sorted	1.47	62.9	20.1%					
BIX3_S18_R1_001					58.0%	49%	75 bp	33.5
BIX3_S18_R2_001					53.2%	51%	75 bp	33.5
BIX3_S18_hisat.stdout				93.7%				
BIX3_S18_hisat_sorted	1.51	62.8	21.8%					
DMSO1_S13_R1_001					58.2%	50%	76 bp	32.5
DMSO1_S13_R2_001					54.9%	51%	75 bp	32.5
DMSO1_S13_hisat.stdout				94.5%				
DMSO1_S13_hisat_sorted	1.45	61.4	22.3%					
Sample Name	5'-3' bias	M Aligned	% Dups	% Aligned	% Dups	% GC	Length	M Seqs

Sample							
DMSO2_S14_R1_001				56.9%	50%	76 bp	31.4
DMSO2_S14_R2_001				50.2%	52%	76 bp	31.4
DMSO2_S14_hisat.stdout			93.9%				
DMSO2_S14_hisat_sorted	1.53	59.0	20.1%				
DMSO3_S15_R1_001				57.7%	50%	76 bp	31.3
DMSO3_S15_R2_001				52.8%	52%	75 bp	31.3
DMSO3_S15_hisat.stdout			93.4%				
DMSO3_S15_hisat_sorted	1.50	58.5	22.9%				

General statistics summarise all the data for each sample from different modules. 5'-3' bias (Qualimap); M-Aligned stands for reads aligned in millions (Qualimap); % Dup stands for percentage duplicate reads (Picard mark duplicates); % Aligned stands for overall alignment rate (Bowtie 2); % GC average percentage GC content (FastQC); length indicates the average length of the sequences (FastQC); M sequences indicates total sequences in millions (FastQC).

Differential gene expression analysis

To study the differentially expressed genes between the DMSO treated group and BIX treated group, differential gene expression analysis was carried out using the DESeq2 R package. Upon applying an adjusted p-value of 0.05, 6077 genes were either upregulated or downregulated between the BIX-treated groups or the DMSO treated groups. The 10 most upregulated and downregulated genes are listed in (Table 5.3 and Table 5.4).

Table 5.3: Top-10 most upregulated genes based on the adjusted p-value.

	baseMean	log2FoldChange	lfcSE	stat	pvalue	padj
Aldh1a1	775	-4.02	0.172	-23.3	1.63e-120	2.95e-116
Ppm1j	442	-4.86	0.246	-19.8	4.15e-87	3.76e-83
AC128848.1	2781	-2.15	0.130	-16.5	5.55e-61	2.01e-57
Lpin3	357	-2.59	0.171	-15.1	1.15e-51	2.97e-48
Tesc	278	-3.99	0.265	-15.1	1.90e-51	4.31e-48
Chrna5	463	-3.75	0.252	-14.9	4.38e-50	8.81e-47
Comp	184	-4.52	0.321	-14.1	3.81e-45	6.27e-42
Gchfr	281	-2.55	0.182	-14.0	1.24e-44	1.73e-41
Abcg2	251	-3.79	0.273	-13.9	8.08e-44	1.05e-40
Mt1	627	-2.44	0.181	-13.5	1.57e-41	1.78e-38

Based on the adjusted p-value 0.05 the top 10 upregulated genes were listed. *Aldh1a1*: Aldehyde dehydrogenase 1 family member A1; *Ppm1j*: Protein Phosphatase, Mg^{2+}/ Mn^{2+} dependent 1J; *Lpin3*: Lipin family member; *Tesc*: Tescalcin; *Chrna5*: Cholinergic Receptor Nicotinic Alpha 5 subunit; Comp: Cartilage Oligomeric matrix protein; *Gchfr*: GTP Cyclohydrolase 1 feedback regulator; *Abcg2*: Binding cassette subfamily G member 2; *Mt1*: Metallothionein 1

Table 5.4: Top-10 most downregulated genes based on the adjusted p-value.

	baseMean	log2FoldChange	lfcSE	stat	pvalue	padj
Top2a	650	4.11	0.221	18.6	3.86e-77	2.33e-73
Gpr17	781	4.71	0.260	18.1	2.00e-73	9.06e-70
Lims2	436	3.68	0.233	15.8	1.68e-56	5.08e-53
Kif11	231	3.66	0.256	14.3	2.17e-46	3.93e-43
Aqp4	27828	2.60	0.185	14.0	9.12e-45	1.38e-41
Smc2	543	2.08	0.152	13.7	1.50e-42	1.81e-39
Nusap1	170	4.18	0.310	13.5	1.79e-41	1.91e-38
Ldlr	734	2.71	0.203	13.3	1.68e-40	1.70e-37
Ccna2	149	4.46	0.347	12.9	7.83e-38	7.09e-35
Tacc3	249	3.43	0.268	12.8	1.44e-37	1.24e-34

Based on the adjusted p-value 0.05 the top 10 downregulated genes were listed. *Top2*: DNA topoisomerase II alpha; *Gpr17*: G protein-coupled receptor 17; *Lims2*: LIM zinc finger domain containing 2; *Kif11*: Kinesin family member 11; *Aqp4*: Aquaporin 4; *Smc2*: Structural maintenance of chromosomes protein 2; Nusap1: Nucleolar and spindle associated protein 1; *Ldlr*: low density lipoprotein; *Ccna2*: Cyclin A2; *Tacc3*: Transforming acidic coiled-coil containing protein 3.

Reactome pathway browser

As the topmost upregulated or down-regulated genes do not reflect the overall picture, due to the diversity of the genes. We continued our further analysis using the Reactome pathway browser to study the pathways involved. To reduce

185

the 6077 differential genes to a more manageable number, transcripts with a log fold change $\pm$ 2 were used as an input for the Reactome pathway browser. The most significant pathways based on p-values were listed below (Table 5.5 and Table 5.6).

Table 5.5: Top 25 significant pathways (Log$_2$ Fold change > -2).

Pathway name	#Entities found	#Entities total	Entities ratio	Entities pValue	Entities FDR	#Reactions found	#Reactions total	Reactions ratio
Cell Cycle	51	682	0.048	1.41E-08	5.98E-06	194	410	0.034
Resolution of Sister Chromatid Cohesion	20	134	0.009	1.76E-08	5.98E-06	7	8	6.55E-04
Signaling by Rho GTPases	39	457	0.032	2.88E-08	6.52E-06	41	117	0.010
Cell Cycle, Mitotic	44	570	0.040	6.24E-08	8.10E-06	180	322	0.026
Mitotic Prometaphase	24	207	0.015	7.51E-08	8.10E-06	14	15	0.001
Amplification of signal from the kinetochores	16	94	0.007	8.35E-08	8.10E-06	4	4	3.28E-04
Amplification of signal from unattached kinetochores via a MAD2 inhibitory signal	16	94	0.007	8.35E-08	8.10E-06	4	4	3.28E-04
Mitotic Spindle Checkpoint	17	110	0.008	1.28E-07	1.09E-05	7	7	5.74E-04
RHO GTPase Effectors	29	326	0.023	8.08E-07	6.06E-05	36	112	0.009
RHO GTPases Activate Formins	18	149	0.011	1.82E-06	1.24E-04	10	27	0.002
Separation of Sister Chromatids	20	194	0.014	5.21E-06	3.18E-04	7	8	6.55E-04
Polo-like kinase mediated events	7	23	0.002	1.04E-05	5.78E-04	13	15	0.001
Cell Cycle Checkpoints	24	279	0.020	1.24E-05	5.78E-04	13	56	0.005

Pathway name	#Entities found	#Entities total	Entities ratio	Entities pValue	Entities FDR	#Reactions found	#Reactions total	Reactions ratio
Neutrophil degranulation	34	480	0.034	1.26E-05	5.78E-04	10	10	8.19E-04
Innate Immune System	70	1324	0.093	1.28E-05	5.78E-04	206	685	0.056
Mitotic Anaphase	20	208	0.015	1.41E-05	5.92E-04	7	11	9.01E-04
Mitotic Metaphase and Anaphase	20	211	0.015	1.72E-05	6.90E-04	8	12	9.83E-04
Immune System	124	2803	0.198	2.52E-05	9.34E-04	351	1586	0.130
Immunoregulatory interactions between a Lymphoid and a non-Lymphoid cell	25	316	0.022	3.22E-05	0.001	15	43	0.004
G0 and Early G1	8	38	0.003	3.40E-05	0.001	12	27	0.002
Transcription of E2F targets under negative control by p107 (RBL1) and p130 (RBL2) in complex with HDAC1	6	20	0.001	4.86E-05	0.002	6	8	6.55E-04
Phosphorylation of Emi1	4	8	5.65E-04	1.34E-04	0.004	2	2	1.64E-04
Trafficking and processing of endosomal TLR	5	16	0.001	1.73E-04	0.005	7	7	5.74E-04
Adaptive Immune System	52	998	0.070	2.65E-04	0.007	73	261	0.021
M Phase	26	390	0.028	3.34E-04	0.009	44	66	0.005

Reactome pathway browser v3.6 was used to identify the 25 most significant downregulated pathways. Entities found: the number of curated molecules of the type selected with results type that are common between the submitted data set and the pathway named; Entities total: The total number of curated molecules of the type selected with results type within the pathway named; Entities ratio: It is the ratio of entities from this pathway that are molecules of the type selected with results type vs. all entities of the type selected with results type; Entities *p*-value: The result of the statistical test for over-representation, for molecules of

the results type selected; Entities FDR : False discovery rate values corrected over-representation probability; Reactions found: The number of reactions in the pathway that are represented by at least one molecule in the submitted data set, for the molecule type selected with results type; Reactions Total: The number of reactions in the pathway that contain molecules of the type selected with results type; Reactions ratio: It is computed as the ratio of reactions from this pathway that contain molecules of the type selected with results type vs. all Reactome reactions that contain molecules of the type selected with results type.

Table 5.6: Top 25 significant pathways (Log$_2$ Fold change > +2).

Pathway name	#Entities found	#Entities total	Entities ratio	Entities pValue	Entities FDR	#Reactions found	#Reactions total	Reactions ratio
Calcitonin-like ligand receptors	4	11	7.76E-04	0.002	0.705	3	4	3.28E-04
Cellular hexose transport	6	28	0.002	0.002	0.705	4	17	0.001
Tight junction interactions	6	30	0.002	0.003	0.705	2	3	2.46E-04
YAP1- and WWTR1 (TAZ)-stimulated gene expression	4	18	0.001	0.01	0.767	2	9	7.37E-04
Activation of TRKA receptors	3	10	7.06E-04	0.011	0.767	8	8	6.55E-04
Butyrophilin (BTN) family interactions	3	12	8.47E-04	0.018	0.767	3	8	6.55E-04
TP53 Regulates Transcription of Genes Involved in Cytochrome C Release	5	33	0.002	0.019	0.767	9	25	0.002
TRKA activation by NGF	2	5	3.53E-04	0.022	0.767	4	4	3.28E-04
TFAP2 (AP-2) family regulates transcription of other transcription factors	2	5	3.53E-04	0.022	0.767	2	2	1.64E-04
Activation of NOXA and translocation to mitochondria	2	6	4.23E-04	0.031	0.767	5	5	4.10E-04
Cell-cell junction organization	7	67	0.005	0.036	0.767	4	21	0.002
Oncogene Induced Senescence	5	42	0.003	0.045	0.767	12	18	0.001
TNFs bind their physiological receptors	4	30	0.002	0.05	0.767	5	13	0.001
NGF-independant TRKA activation	2	8	5.65E-04	0.052	0.767	4	4	3.28E-04

Pathway name	#Entities found	#Entities total	Entities ratio	Entities pValue	Entities FDR	#Reactions found	#Reactions total	Reactions ratio
Relaxin receptors	2	8	5.65E-04	0.052	0.767	4	4	3.28E-04
Voltage gated Potassium channels	5	44	0.003	0.053	0.767	1	1	8.19E-05
PIWI-interacting RNA (piRNA) biogenesis	4	31	0.002	0.055	0.767	13	15	0.001
RUNX3 regulates YAP1-mediated transcription	2	9	6.35E-04	0.064	0.767	2	3	2.46E-04
Regulation of gene expression in endocrine committed (NEUROG3+) progenitor cells	2	9	6.35E-04	0.064	0.767	1	4	3.28E-04
Cell junction organization	8	94	0.007	0.069	0.767	8	37	0.003
POU5F1 (OCT4), SOX2, NANOG activate genes related to proliferation	3	21	0.001	0.072	0.767	3	16	0.001
Class B/2 (Secretin family receptors)	8	99	0.007	0.086	0.767	5	20	0.002
MGMT-mediated DNA damage reversal	1	2	1.41E-04	0.087	0.767	2	2	1.64E-04

Reactome pathway browser v3.6 was used to identify the 25 most significant upregulated pathways. Entities found: the number of curated molecules of the type selected with results type that are common between the submitted data set and the pathway named; Entities total: The total number of curated molecules of the type selected with results type within the pathway named; Entities ratio: It is the ratio of entities from this pathway that are molecules of the type selected with results type vs. all entities of the type selected with results type; Entities *p*-value: The result of the statistical test for over-representation, for molecules of the results type selected; Entities FDR : False discovery rate values corrected over-representation probability; Reactions found: The number of reactions in the pathway that are represented by at least one molecule in the submitted data set, for the molecule type selected with results type; Reactions Total: The number of reactions in the pathway that contain molecules of the type selected with results type; Reactions ratio: It is computed as the ratio of reactions from this pathway that contain molecules of the type selected with results type vs. all Reactome reactions that contain molecules of the type selected with results type.

Further to the immunofluorescent analysis, we proceeded to perform RNA-seq to understand the genes and pathways that are associated with the toxic effects of BIX. A 24 h time point was selected to capture the early transcriptome changes upon exposure to BIX. The quality of the sequence provided by Glasgow Polyomics was good and did not require any further processing for downstream analysis.

Initial analysis of the differential gene expression with an adjusted p-value 0.05 had few genes related to the ATF6 pathway such as *Bip*, *Pdia5, Calr3, Atf4*, *Asns*, *Atf6b*, *Xbp,* the expression of these genes was slightly altered (Table 5.7). UPR related genes such as *Wfs1*, *Nck1*, *Nck2, Bax*, *Bak1, Asns, Bax, Bid, Fas,* and *Bad* were slightly altered (Table 5.7). To exclude the genes with minimal fold change, the Log$_2$ fold change cutoff was increased to $\pm$ 2, these genes except *Bik* no longer appeared in the list indicating that the change in expression level was minimal. The effects of these genes could be masked by the effects of other genes which are highly expressed. Some of the UPR genes altered were proapoptotic, for example, *Bax*, *Bid*, *Bad*, *Bik, and Fas* (Table 5.7). The change in the expression level of genes related to UPR in response to BIX treatment was minimal.

From the immunofluorescence data, we noticed a significant reduction in Oligodendrocytes, Myelin, and microglia. Therefore, we looked at the change in expression of cell-specific genes in astrocytes, neurons, oligodendrocytes, oligodendrocyte precursor cells, and microglia. Astrocyte markers such as *Aqp4*, *Slc25a18*, *Gfap*, *Gjb6* were downregulated. The following neuron-specific genes *Reln*, *Vip*, *Gad2*, *Dlx1*, *Penk*, *Syt1*, *Gad1*, *Synpr*, *Stmn2*, *Gpr83*, *Sst*, *Zmat4*, *Snap25*, *Rab3c*, *Scg2* were absent in the log$_2$ fold change $\pm$ 2 gene list, however, *Tac3*, *Tmem130*, *Nell1*, *Gabrg2* genes were below log$_2$ fold change $\pm$ 2. A large number of Oligodendrocyte specific genes *Mbp*, *Plp1*, *Mag*, *Opalin*, *Klk6*, *Fa2h*, *Enpp6, Tmem125, Anln* were downregulated. And a few Oligodendrocyte precursor marker genes *Pnlip, Fam180a, Gpr17* were also downregulated. A large number of Microglial marker gene *Ccl3, Ccl4, C1qb*, *Trem2, Gpr183, C1qc, Csf1r, Cd300a, Laptm5, C3ar1, Cx3cr1, Ptafr, C1qa* were also downregulated (see Table: 5.8). The information from the gene

expression along with the pathway analysis fits well with our immunofluorescence data.

BIX effects several pathways, the top 25 upregulated and downregulated pathways were provided in the table (5.5 and 5.6). Pathways related to cell cycle, mitotic division, cytoskeletal reorganisation, cellular transport, trafficking via Rho GTPases, innate and adaptive immune systems are downregulated (See Table 5.5). Upregulated pathways include hexose metabolism, potassium voltage channels, cellular junction organisation, oxidative stress. (See Table 5.6).

Table 5.7: Genes related to unfolded protein response.

baseMean	log2FoldChange	lfcSE	stat	pvalue	padj	Gene
2548.291966	0.765592168	0.149548103	-5.119370643	3.06557E-07	4.25562E-06	*Asns*
4427.585408	-0.530711188	0.101665045	5.22019329	1.78736E-07	2.64479E-06	*Atf4*
10179.50996	-0.489070807	0.158241456	3.090661696	0.00199711	0.008783601	*Hspa5*
1464.256436	0.635194775	0.123013652	-5.16361203	2.42229E-07	3.45318E-06	*Bax*
744.9200112	0.55137962	0.142453984	-3.870580537	0.000108576	0.000748467	*Bid*
568.6347361	1.114094454	0.255807504	-4.355206304	1.32942E-05	0.00012072	*Fas*
1079.147301	-0.69151514	0.106412619	6.498431745	8.11616E-11	2.48786E-09	*Bad*
1080.975146	-0.725077404	0.144307418	5.02453315	5.04659E-07	6.53962E-06	*Xbp1*
1425.099487	1.918905476	0.160932054	-11.92369967	8.90638E-33	5.56372E-30	*Wfs1*
959.5041313	0.396661877	0.126087419	-3.145927484	0.00165561	0.00749826	*Nck1*
681.8609603	0.613647103	0.204273437	-3.00404747	0.002664138	0.011115503	*Nck2*
1464.256436	0.635194775	0.123013652	-5.16361203	2.42229E-07	3.45318E-06	*Bax*
750.8618853	-0.559296698	0.150942681	3.705358189	0.000211092	0.001322776	*Bak1*
2279.301678	-0.283425375	0.097358523	2.911151133	0.003600998	0.014268521	*Atf6b*
98.62476738	1.942305695	0.256014672	-7.586696794	3.28164E-14	1.8695E-12	*Pdia5*
143.3278475	1.236239113	0.390880748	-3.162701465	0.001563125	0.007137902	*Calr3*
8.810017365	3.212289203	1.093683678	-2.937128228	0.003312671	0.013339041	*Bik*

Genes related to unfolded protein response. *Asns*: Asparagine Synthetase; *Atf4*: Activated transcription factor 4; *Hspa5*: Heat Shock 70kDa protein 5; *Bax*: Bcl2 associated X; *Bid*: BH3 interacting domain death agonist; *Bad*: Bcl2 associated agonist of cell death; *Xbp1*: X-box Binding Protein-1; *Wfs1*: Wolframin ER transmembrane glycoprotein; *Nck1*: NCK adapter protein 1; *Nck2*: NCK adapter protein 2; *Bax*: Bcl2 associated X; *Bak1*: Bcl2 antagonist/killer 1; *Atf6b*: Activating transcription factor 6 beta;*Pdia5*: Protein disulphide isomerase family A member 5; *Calr3*: Calreticulin 3.

Table 5.8: Genes downregulated in the different cell populations (Log$_2$ Fold change > -2).

baseMean	log2FoldChange	lfcSE	stat	pvalue	padj	gene	Cell type
27828.14	-2.60	0.19	14.04	9.12046E-45	1.37689E-41	*aqp4*	Astrocytes
4837.75	-2.14	0.25	8.62	6.58159E-18	6.97263E-16	*slc25a18*	Astrocytes
64242.19	-2.22	0.27	8.12	4.60272E-16	3.77298E-14	*gfap*	Astrocytes
165.86	-2.04	0.52	3.93	8.33817E-05	0.000591905	*gjb6*	Astrocytes
33323.55	-2.63	0.67	3.90	9.57671E-05	0.001	*mbp*	Oligodendrocytes
33894.09	-2.75	0.62	4.46	8.30689E-06	7.91624E-05	*plp1*	Oligodendrocytes
598.16	-2.77	0.83	3.34	0.001	0.004	*opalin*	Oligodendrocytes
2674.80	-4.08	0.40	10.26	1.08632E-24	2.98178E-22	*mag*	Oligodendrocytes
9.26	-3.71	1.15	3.24	0.001186769	0.005711879	*klk6*	Oligodendrocytes
226.14	-2.81	0.36	7.84	4.48168E-15	3.01822E-13	*fa2h*	Oligodendrocytes
63.99	-2.79	0.59	4.76	1.97949E-06	2.20544E-05	*enpp6*	Oligodendrocytes
265.58	-2.08	0.50	4.20	2.69003E-05	0.000222523	*tmem125*	Oligodendrocytes
109.19	-2.16	0.42	5.11	3.18785E-07	4.40511E-06	*anln*	Oligodendrocytes
169.06	-3.09	0.37	8.30	1.07797E-16	9.47984E-15	*pnlip*	Oligodendrocyte precursor cells
36.94	-2.40	0.68	3.54	0.0004	0.002	*fam180a*	Oligodendrocyte precursor cells
781.47	-4.71	0.26	18.13	1.9999E-73	9.05756E-70	*gpr17*	Oligodendrocyte precursor cells
23.20	-2.80	0.61	4.61	4.11658E-06	4.26636E-05	*ccl4*	microglia
2743.16	-2.30	0.26	8.68	4.0011E-18	4.41975E-16	*c1qb*	microglia
333.51	-3.60	0.33	11.05	2.17336E-28	8.74947E-26	*trem2*	microglia
105.50	-3.46	0.43	8.10	5.6704E-16	4.58593E-14	*gpr183*	microglia

baseMean	log2FoldChange	lfcSE	stat	pvalue	padj	gene	Cell type
74.31	-2.55	0.43	5.92	3.18071E-09	6.94238E-08	*cd300a*	microglia
969.67	-2.81	0.32	8.81	1.22112E-18	1.47479E-16	*laptm5*	microglia
2414.79	-2.24	0.25	8.88	6.52272E-19	8.4404E-17	*c1qc*	microglia
2875.76	-2.86	0.29	9.74	2.00207E-22	3.89996E-20	*csf1r*	microglia
142.61	-3.00	0.33	9.04	1.50406E-19	2.07996E-17	*c3ar1*	microglia
300.39	-3.08	0.40	7.66	1.83208E-14	1.07759E-12	*cx3cr1*	microglia
129.82	-2.82	0.46	6.07	1.30565E-09	3.12048E-08	*ptafr*	microglia
2558.94	-2.56	0.26	9.85	7.05579E-23	1.5038E-20	*c1qa*	microglia
8753.41	-0.86	0.27	3.23	0.001	0.006	*tmem130*	Neurons
1046.41	-0.74	0.29	2.57	0.010	0.033	*nell1*	Neurons
1075.34	-1.03	0.31	3.31	0.0009	0.004	*gabrg2*	Neurons
72.44	-0.94	0.36	2.63	0.008	0.029	*tac3*	Neurons

Differentially expressed genes with $\log_2$ fold change ± 2 were listed in the table. *Aqp4*: Aquaporin 4; *Slc25a18*: Solute carrier family 25 member 18 protein encoding gene; *Gfap*: Glial Fibrillary acid protein; *Gjb6*: Gap junction protein beta 6; *Mbp*: Myelin basic protein; *Plp1*: Proteo lipid protein 1; *Opalin*: Oligodendrocyte myelin paranodal and inner loop protein; *Mag*: Myelin associated glycoprotein; *Klk6*: Kallikrein related peptidase 6; *Fa2h*: Fatty acid 2-hydroxylase; *Enpp6*: Ectonucleotide pyrophosphatase/phosphodiesterase 6; *Tmem125*: Transmembrane protein125; *Anln*: Anillin actin binding protein; *Pnlip*: Pancreatic lipase; *Fam180a*: Family with sequence similarity 180 member; *Gpr17*: G protein-coupled receptor 17; *Ccl4*: C-C Motif chemokine ligand 4; *C1qb*: Compliment C1q B chain; *Trem2*: Triggering receptor expressed on myeloid cells 2; *Gpr183*: G protein-coupled receptor 183; *C1qc*: Compliment C1q C chain; *Csf1r*: Colony stimulating factor 1 receptor; *Cd300a*: Cluster of differentiation 300a; *Laptm5*: Lysosomal protein transmembrane 5; *C3ar1*: Complement C3a receptor 1; *Cx3cr1*: CXC3 chemokine receptor 1; *Ptafr*: Platelet activating factor receptor; *C1qa*: Compliment C1q A chain; *Tmem130*: Transmembrane protein 130; *Nell1*: Neural EGFL like 1; *Gabrg2*: Gamma-aminobutyric acid type A receptor gamma2 subunit; *Tac3*: Tachykin

5.6 Discussion

It is challenging to compare our data regarding BIX treatments to those reported in the literature because most published studies were performed *in-vivo* in acute models of disease, such that long-term effects were not considered. In our hands, the chronic treatment with BIX has proved to be fatal for microglia and oligodendrocyte lineage-cells in spinal cord myelinating cultures and organotypic cerebellar slice cultures. Myelin-producing oligodendrocytes produce large amounts of myelin through the secretory pathway during the active myelination phase. Therefore, any factors that interrupt the endoplasmic reticulum homeostasis could be playing a vital role in cell survival. The toxic effects observed after BIX treatment were could be due to the imbalance in the ER homeostasis caused by BIX.

BIX was identified in a chemical high throughput screening performed in a search for compounds that selectively induce BiP mRNA (Kudo et al., 2008). Several studies describe BIX as a therapeutic agent and tested this compound *in-vitro* and *in-vivo*, but the outcome of our experiments was different from the published literature. Different doses of BIX were used in different cell lines. A dose of 1-50 µM BIX was added to SK-N-SH (human neuroblastoma cell line) to study the expression of BiP, this study was focused on the ER stress-induced neuronal death. The highest induction of BiP was noticed at 50 µM with little toxicity, however, doses higher than 50 µm were proved to be cytotoxic (Kudo et al., 2008). A dose of BIX 5 µg/ml falls within this range and it is equivalent to 23 µm BIX. A dose 1-5 µm of BIX was used in experiments conducted using SH SY5Y cells (Oida et al., 2008). Doses as high as 150 µm were also utilised in RGC-5 (a rat ganglion cell line) to study BiP induction and effects on other chaperones, such as GRP94, Calreticulin, protein kinase inhibitor of 58 kDa and asparagine synthetase (Inokuchi et al., 2009). It seems likely that the sensitivity of the cultures to BIX is cell- and tissue-specific. The duration of the treatment should also be considered. In both the spinal cord myelinating cultures and the organotypic slice culture BIX had specific toxicity towards microglia and

oligodendrocytes at a dose of 5 µg/ml. This effect has yet to be reported by any other groups.

The therapeutic potential of BIX has been tested in several animal models of disease (Inokuchi et al., 2009; Nakanishi et al., 2013; Oida et al., 2010). The BIX doses, routes of administration and the disease models utilised are diverse. Nevertheless, BIX was always characterized and found to have a beneficial effect.

Oida et al studied the effect of BIX on tunicamycin-induced cell death in SH-SY5Y cells and forebrain ischemia in Gerbils. Pre-treatment with a dose of 2 or 5 µg of BIX reduced the cell death in SH-SY5Y cells and a dose of 10 or 40 µg injected via intracerebroventricular injection reduced the number of TUNEL-positive cells in the hippocampal CA1 subfield (Oida et al., 2008). Inokuchi et al studied the effect of BIX against tunicamycin-induced cell death in RGC-5 and tunicamycin or N-methyl-D-aspartate (NMDA)-induced retinal damage in mice. A dose of 1 or 5 µM protected against tunicamycin induced cell death. Intravitreal injection of BIX (5 nmol) induced BiP expression in the mouse retina. Administration of BIX (5 nmol) along with tunicamycin or NMDA reduced CHOP expression and cell death in the ganglion cell layer (Inokuchi et al., 2009). Nakanishi *et al* studied the effect of BIX against photoreceptor cell death in light-exposed retinas. Treatment with BIX (3 µM) induced BiP expression, reduced CHOP expression, and reduced the photoreceptor cell death in light-exposed 661W cells (photoreceptor cell line) (Nakanishi et al., 2013). Middle cerebral artery occlusion induces ER stress-induced apoptosis in the penumbra and pre-treatment with BIX decreased this ER stress-induced apoptosis. The area of infarction in the penumbra was also reduced in the BIX pre-treated group. BIX has proved to be therapeutic in ER stress-induced neuronal cell death (Kudo et al., 2008). Pre-treatment with BIX reduced cell death and reduced TUNEL-positive cells in the hippocampus CA1 subfield and ischemia-induced neuronal cell death in forebrains of gerbils (Oida et al., 2008). Also, post-treatment with BIX after middle cerebral artery occlusion in mice had a protective effect against neuronal damage caused by acute ischemia and reduced the number of TUNEL-positive cells in the ischemic penumbra (Oida

et al., 2010). Pre-treatment with BIX significantly reduced the renal ischemia/reperfusion injury (Prachasilchai et al., 2009). BIX increased the osteoblast induced bone formation and prevented bone loss in a model of osteoporosis (Hino et al., 2010).

Most of the published literature had a similar pattern of experiments. BIX was co-administered or given prior to induction of ER of stress in *in-vitro* and *in-vivo* models, followed by measurement of expression of BiP gene expression and other UPR upregulated genes such as *Eif2α, Edem, Pdi, Chop, Grp94, P58[ipk], Calr*, and *Asns*. All these published works had a BIX exposure time of 24 h or less and most of them were single doses for their *in-vitro* experiments. The published literature has always focused on apoptotic markers such as CHOP, caspase 3/4/7 and Hoechst and TUNEL staining was employed to measure cell viability. Our study is unique due to the complexity of the culture system and treatment duration in which the organotypic slice cultures and spinal cord myelinating cultures received 3-5 doses of 5 µg/ml of BIX over the treatment period 7-10 days, respectively. The published work used cell lines (see Table 5.9) to study the effect of BIX and did not explore the effect of BIX on oligodendrocytes, astrocytes, microglia, and neurons derived from primary cultures. The information regarding the stability of BIX at 37 °C was also left out in the published literature.

Table 5.9: Studies conducted using BIX

Disease model	Cell type	Duration	Dose	Route of Admin.	Animal model	Outcome	Other information	Reference
Tunicamycin or N-methyl D-aspartate induced retinal damage in mice	RGC-5 Rat ganglion cell line	12 h *in-vitro* 7 days *in-vivo* experiments	1-150 µM *in-vitro* 0.5 *or* 5 nmol *in-vivo* experiments	Intra vitreous injection	Male adult ddY mice Thy-1-cyan fluorescent protein (CFP) transgenic mice ER stress-activated indicator (ERAI) -transgenic mice	BIX 5 nmol preferentially induced BIP expression *in-vivo* Coadministration of BIX 5nmol with tunicamycin or NMDA significantly reduced the CHOP expression levels in the ganglion cell layer and also reduced the retinal cell death	BIX also affects the expression of other ER stress-associated genes such as Calreticulin, GRP94, and protein kinase inhibitor of 58 kDa and asparagine synthetase. Used 5% DMSO in PBS as vehicle control for *in -vivo* experiments.	(Inokuchi et al., 2009)
Neuronal cell death caused by Tunicamycin induced-ER stress *(in vitro)* or ischemia *(in vivo)*	SK-N-SH Neuroblastoma cell line	12 h *in-vitro* 24 h *in-vivo* experiments	1-50 µM *in-vitro* 5 or 20 µg *in-vivo* experiments	Intra cerebroventricular injection (ICV)	Focal Cerebral ischemia model (male adult ddY mice) (24-34 g weight)	Middle cerebral artery occlusion induces ER stress-induced apoptosis in the penumbra and Pre-treatment with BIX decreased this ER stress-induced apoptosis. The area of infarction in the penumbra was also reduced in the BIX pre-treated group	Focal cerebral ischemia was caused by middle cerebral artery occlusion. Animals were given BIX 30 min before the start of ischaemia. Controls did not receive any BIX pretreatment. BIX mainly induces BiP along with	(Kudo et al., 2008)

Disease model	Cell type	Duration	Dose	Route of Admin.	Animal model	Outcome	Other information	Reference
							slight induction of GRP94, Calreticulin, and CHOP.	
Neuronal cell death caused by forebrain ischemia in gerbil	SH-SY5Y cell line Neuroblastoma cell line SK-N-SH cell Neuroblastoma cell line	24 h *in-vitro* experiments 7 days *in-vivo* experiments	1-5 µM *in-vitro* experiments 10 or 40 µg *in-vivo* experiments	Single stereotaxic injection into the lateral ventricle (ICV)	Male adult Mongolian Gerbils (60-80 g weight)	Pre-treatment with BIX reduced cell death and reduced the TUNEL positive cells in the hippocampus CA1 subfield	Both carotid arteries were occluded using Sugita No.50 temporary aneurysm clips. 5 µl of 10% DMSO in saline was used as vehicle control. Animals were treated 30 min before the occlusion.	(Oida et al., 2008)
Permanent middle cerebral artery occlusion (MCAO)	NA	24 h *in-vivo* experiments	1, 5 or 20 µg	Intra cerebroventricular injection (post-MCAO)	Male adult ddY mice (26 -32 g weight)	Post-treatment with BIX is protective against ischemic neuronal damage and reduced the number of TUNEL positive cells in the ischemic penumbra	2 µl of 10% DMSO in saline. BIX was administered at 5 min, 3 h, and 6 h after ischemia.	(Oida et al., 2010)
Renal ischemia/reperfusion injury	NA	24 h *in-vivo* experiments	2 mg/kg 15 mg/kg *in-vivo* experiments	Sub renal capsule injection Intraperitoneal injection	Male ddY mice (7-week-old)	Pre-treatment with BIX significantly reduced the ischemia/reperfusion injury. Co-treatment	Drugs were administered in a volume of 100 µl	(Prachasilchai et al., 2009)

Disease model	Cell type	Duration	Dose	Route of Admin.	Animal model	Outcome	Other information	Reference
						of tunicamycin with BIX did not have any additional protection.		
Bone loss in a murine model of osteoporosis	Primary Osteoblasts culture	24 h *in-vitro* experiments 24 h *in-vivo* experiments	5 µM *in-vitro* experiments 10 or 30 mg/kg/day	Oral administration	Female ICR mice (20-36-week-old)	BIX increases osteoblast induced bone formation and prevents bone loss	0.5% sodium carboxymethyl cellulose was used as a vehicle control	(Hino et al., 2010)
Paclitaxel induced ER stress	SK-N-SH Neuroblastoma cells or MCF cells	24 h *in-vitro* experiments	0.5-10 µM *in-vitro* experiments	NA	NA	BIX attenuated the ER stress caused by Paclitaxel thereby preventing apoptosis	DMSO was used as a vehicle	(Tanimukai et al., 2013)
Light-induced retinal cell death	661W cells Photoreceptor cell line	3, 6 or 30 h	3 µM *in-vitro* experiments	NA	NA	BIX attenuated the ER stress caused by exposure to light	BIX was dissolved in DMSO and later diluted with FBS	(Nakanishi et al., 2013)

The RNA sequences met the quality requirements and were used for downstream analysis. As mentioned in the results section 5.5.3 the genes related to UPR such as *Xbp1, Atf6b, Wfs1*, *Nck1*, *Nck2, Bax*, *Bak1, Asns, Atf4, Hspa5, Bax, Bid, Fas, Bad* are slightly altered, the selective induction of BiP through ATF6 pathway is questionable at least in spinal cord myelinating cultures. The downregulation of cell-specific genes partially explains the BIX effects on microglia and oligodendrocytes. A few number of astrocyte and neuron-specific genes were also downregulated but they seem to be more resistant to BIX related toxicity.

There is no single pathway that is upregulated in response to BIX treatment. There are several pathways related to cell cycle, mitotic division, cytoskeletal reorganisation, cellular transport, trafficking via Rho GTPases, innate and adaptive immune systems that are downregulated, we conclude that BIX is targeting rapidly diving cells, such as microglia and oligodendrocytes precursor cells and cell with high metabolic rate such as oligodendrocytes (see Table 5.6). The pathways derived from upregulated genes include hexose metabolism, potassium voltage channels, cellular junction organisation, oxidative stress (See Table 5.5). Taken together the gene expression analysis and pathway analysis, BIX proves to be toxic. The reproducibility of BIX effects in cerebellar slice cultures makes the toxic effects of BIX trustworthy.

5.7 Conclusion

Significant inhibition of myelination and loss of microglia was observed after 5 days (5 µg/ml) in the absence of any significant effect on axonal density or astrocytes. Withdrawal experiments demonstrated that these effects on myelination and microglia were irreversible. Although BIX inhibited myelination we found it was unable to mediate primary demyelination. BIX, therefore, appeared to have selective toxicity towards oligodendrocyte-lineage cells and microglia. Therapeutic use of BIX to protect against ER stress should be considered with caution. BIX significantly downregulates various genes related to oligodendrocytes and microglia. We conclude that BIX is targeting

rapidly diving cells, such as microglia and oligodendrocytes precursor cells and cell with high metabolic rate such as oligodendrocytes (see Table 5.4 and 5.5 for details of the pathways)

Chapter 6 : Discussion

BiP, a highly conserved ER chaperone, belongs to the HSP70 family of proteins. It is an ER chaperone with a multitude of diverse biological functions. BiP on the cancer cells involves in the cell signalling and viability and produces a chemotherapeutic resistant phenotype. BiP also facilitates the entry of viruses into the cells. In rheumatic arthritis, increased levels of BiP and BiP auto-antibodies were reported (Corrigall et al., 2001; Park et al., 2014). Cardiac dysfunction is attributed to BiP and Ca^{2+} dysregulation in the ER (Roe and Ren, 2013). Additionally, BiP can suppress the formation of the atherosclerotic plaque (Ni and Lee, 2007). BiP may play a role in the pathogenesis of various neurodegenerative disorders such as Huntington's disease (Lajoie and Snapp, 2011), Parkinson's disease (Hara et al., 2011), Multiple Sclerosis (Hussien et al., 2015) and Alzheimer's (Sakono and Kidani, 2017). It is associated with metabolic disease such as diabetes mellitus (Synofzik et al., 2014). The association of BiP with several diseases and the underlying mechanism are depicted in (Figure 6.1). Among the plethora of BiP functions, we attempted to explore the effects of BiP on myelination by exogenous addition of BiP to myelinating cells and slice cultures and by chemically inducing BiP with BIX in the same models.
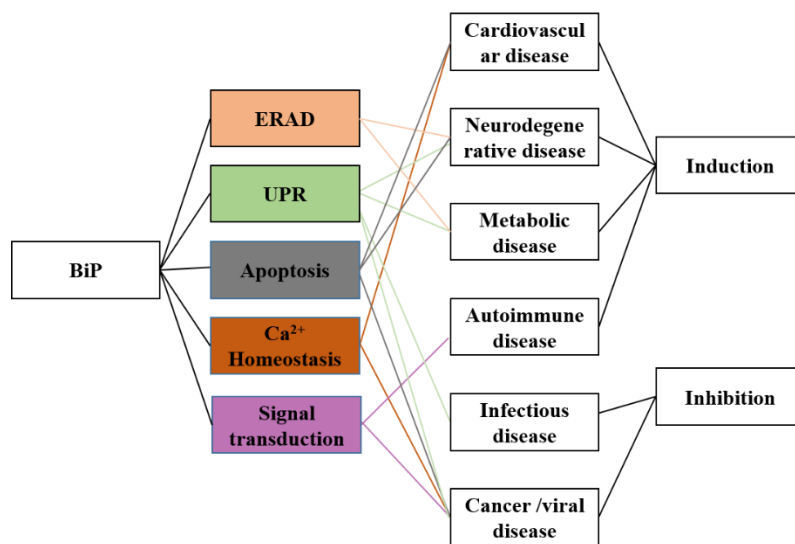
Figure 6.1: Clinical importance of BiP (source: S. Bandla).

The involvement of BiP in disease: Cardiovascular diseases, mainly heart failure; neurodegenerative diseases such as, Alzheimer's and prion disease; autoimmune disorders such as rheumatic arthritis and multiple sclerosis; metabolic disease such as diabetes mellitus and obesity; infectious disease including prokaryotic and eukaryotic pathogens utilizing BiP homologs; Cancer and viral diseases that depend on host's BiP expression. The underlying mechanisms, including unfolded protein response, ER-associated degradation (ERAD), Ca^{2+}

homeostasis and other signalling pathways involved are shown. Inhibition or induction of BiP expression can be used as a treatment. Inhibition affects the survival of the cancerous and infected cells, whereas induction protects the cells from misfolded proteins, ER-stress, and apoptosis. (Adapted from (Wang et al., 2017)).

The unfolded protein response is regulated by the three molecular sensors IRE1, ATF6 and PERK (section 1.3) and activation of these pathways cause the induction of proteins and chaperones that assist in restoring normal ER function. The UPR can be either beneficial or detrimental based on whether it is supporting survival or apoptosis. When prolonged ER stress overtakes the protective mechanisms, signals may become proapoptotic (Oyadomari and Mori, 2004). Inflammatory demyelination and neurodegeneration in MS are related to ER stress (Deslauriers et al., 2011).

Accumulating evidence hints that ER stress-associated signalling pathways could be a therapeutic target in neurodegenerative disorders such as MS. For example, our group reported the upregulation of ER stress molecules such a CHOP, XBP-1 and BiP within MS lesions. Increased expression of BiP, CHOP, and XBP1 was observed in acute lesions of MS patients and at the edges of the chronic active lesions (Mháille et al., 2008). Increased expression of CHOP, BiP and ATF4 transcripts was also observed by our group in the normal-appearing white matter (NAWM), compared to non-MS controls. The presence of increased levels of CHOP transcript was observed in the peri-lesional area of the active lesions (Cunnea et al., 2011). We also detected ER stress molecule upregulation in grey matter MS lesions and in NAGM (McMahon et al., 2012). Other groups showed via microarray analysis upregulated HSP genes in active MS lesions (Graumann et al., 2006; Mycko et al., 2012). Also, exogenous addition of HSP70/90 chaperones was proved to be therapeutic in a model of Alzheimer's disease (Dou et al., 2003; Magrane et al., 2004).

Elimination of BiP during development and adulthood was shown to have a detrimental effect on myelinating cells, such as oligodendrocytes and Schwann cells, causing hypomyelination in the central and peripheral nervous system (Hussien et al., 2015). During myelination, the secretory pathway plays an important role in the glial cells. BiP regulates the unfolded protein response and elimination of BiP actually leaves the stress sensors of the unfolded protein response in an activated state. For example, the PERK and ATF6 arms were

proved to be activated in the absence of BiP in OL-BiP$^{ko/ko}$ mice. Chronic ER stress causes apoptosis by upregulating the transcription factor CHOP (Hussien et al., 2015). Inadequate availability of BiP can also cause ER stress (Vitale et al., 2019). Amongst the upregulated UPR genes, we focused on BiP as it is required for the survival of oligodendrocytes and Schwann cells. Our group had also reported the upregulation of BiP during rat developmental myelination (Naughton et al., 2015).

As mentioned earlier, BiP is present in different cellular organelles such as the ER, cytoplasm, nucleus, mitochondria, and on the cell surface and it can be released into extracellular space (Casas, 2017). Chaperoning and regulating the UPR are considered the main functions of BiP (Pobre et al., 2019). However, the interactions of BiP with cell-surface ligands and receptors (described in section 1.4.4) and the functions of BiP in the cytoplasm, mitochondria and nucleus should not be underestimated (Cook, 2019; Ni et al., 2011; Quinones et al., 2008). The normal physiological or pathological functions of BiP have been thought to be related to its intracellular function. However, detection of BiP within body fluids of healthy and diseased individuals (Giusti et al., 2010a; Ni et al., 2011; Tsunemi et al., 2010) and its secretion from cells under stress hints that BiP has extracellular functions, as a receptor, immune modulator and cell signalling molecule. Several possible mechanisms for extracellular localisation of BiP have been proposed that include cleavage or masking of the KDEL retention motif, surpassing the KDEL receptor function (Zhang et al., 2013), alternative splicing of BiP that escapes from the ER (Corrigall et al., 2004; Zhang et al., 2010), or association with membrane proteins (Ni et al., 2011; Wiest et al., 1997; Xiao et al., 1999; Zhang et al., 2010) (refer to section 1.4.3 for more details).

Cell-Surface BiP interacts with several ligands and receptors (refer section 1.4.4). Some of these ligands and receptors such as alpha 2 macroglobulin (α_2-M), MHC-1 class-related gene A (MICA), low density lipoprotein receptor-related protein 1 (LRP1), urokinase plasminogen activator surface receptor (UPAR), insulin-like growth factor-1 (IGF-1), epidermal growth factor receptor (EGFR) have been linked to MS (see Table 6.1). The possibility that

BiP interacts with these molecules in the context of MS still exists and warrants further study.

Table 6.1: Role of BiP interacting molecules in the context of MS.

Molecule	Role in MS	Reference
α_2-M	Native and transformed α_2-M levels were increased in patients with MS	(Jensen et al., 2004)
MICA	Clinical behaviour of MS in patients is regulated by MHC-1 class-related gene	(Fdez-Morera et al., 2006)
Transthyretin	Post-translational modification of transthyretin at cysteine in the position ten are connected with multiple sclerosis	(Pieragostino et al., 2013)
Low-density lipoprotein receptor-related protein 1	LRP1 is expressed on all the cell types and mediate uptake of myelin vesicles	(Gaultier et al., 2009)
Urokinase plasminogen activator surface receptor (UPAR)	UPAR was expressed on monocytes in relapsing-remitting patients.	(Balabanov et al., 2001)
Insulin-like Growth factor 1 (IGF-1)	IGF-1-1 increases myelin production and the number of oligodendrocytes.	(Costales and Kolevzon, 2016).
Epidermal growth factor receptor (EGFR)	The EGFR is expressed in astrocytes present in the glial scar in multiple sclerosis	(Holley et al., 2003)
T-cadherin	Endothelial barrier function	(Andreeva et al., 2009)

The published literature is quite ambiguous in defining the presence or absence of signal or KDEL sequences in circulating BiP. As there was no clear evidence regarding peripheral BiP having a signal and/or ER retention sequence, here we produced and biochemically characterised four variants of BiP (S^+/K^+, S^+/K^-, S^-/K^+, and S^-/K^-). S refers to signal sequence and K refers to KDEL. The most commonly used bacteria in biotechnology for gene cloning is *E. coli*. Protein expression using *E. coil* is one of the cheapest methods (Baneyx, 1999). Because

of the well-explored genome (approximately 4400 genes), simple growth conditions and replication rate, working with *E.coli* is very convenient (Blattner et al., 1997; Rosano and Ceccarelli, 2014). *E. coli* is available in a wide variety of strains and it is important to select the suitable expression hosts in order to achieve required protein expression.

The optimisation of protein expression was carried out using Rosetta 2 (DE3) pLysS and BL21- CodonPlus (DE3)-RIL strains at 26°C and 37°C. Based on the level of protein expression (Figure 3.4), all four variants were purified from the BL21-CodonPlus (DE3)-RIL strain. Expressed proteins had a C-terminal histidine-tag; all variants were purified using affinity (nickel) chromatography. The physicochemical characterization proved the proteins to be of the right size (approximately 78 KDa) as confirmed by SDS PAGE gels. The proteins were present as monomers, dimers and oligomers, in keeping with published literature. We found that oligomers and dimers were converted to monomers in the presence of nucleotides (ATP and ADP) or nucleotides and cations (Ca^{2+}, Mg^{2+}, Mn^{2+}). The ATPase assay was used to measure the enzyme activity of these proteins and the S^+/K^+ had the highest ATPase activity. As a part of the protein characterisation, the influence of cations Ca^{2+}, Mg^{2+} and Mn^{2+} (millimolar and submillimolar concentrations) on the enzyme kinetics and binding affinity of nucleotides (ATP and ADP) was assessed (see sections 3.5.4-3.5.7). Using Differential Scanning Flourimetry, the melting temperatures of these proteins were measured and found to be 45.1 - 45.8°C. Binding affinities of ATP and ADP were measured in the using Differential Scanning Flouirmetry. In the absence of cations, all the variants had a higher affinity for ADP than ATP. In the presence of cations, the K_d values decreased by up to 80% indicating that cations act as cofactors in the binding of nucleotides to BiP. The K_d values reported in the literature vary within a range of 10^{-5} to 10^{-8} based on the source of the protein or the methods used for measuring K_d (Schmid et al., 1985). We found that in the presence of 50 μM Mg^{2+} the K_d values were higher for ADP than ATP for S^+/K^+ and S^-/K^-. These results suggest that in the presence of Mg^{2+} the binding affinity is higher for ATP and the exchange of ATP to ADP happens easily. In the presence of Mn^{2+}, the binding affinity was higher for ADP than ATP. The reduced activity could be due to the tighter binding of ADP than ATP

or the presence of a second mechanism. The K_M and V_{max} values obtained from the kinetics experiments support this observation.

Mg^{2+} and Mn^{2+} had a stimulating effect on the ATPase activity, whereas Ca^{2+} did not have any stimulatory effect. The lack of stimulation in the presence of calcium could be due to the stronger binding of ADP when compared to ATP. In the published literature, the effect of Mg^{2+} and Mn^{2+} at sub-millimolar concentrations were not examined. The concentration of Mg^{2+} in the ER was around 10 millimolar but only a fraction of it is freely available (Romani, 2011). At sub-millimolar concentrations such as 10 µM and 30 µM, Mg^{2+} effectively stimulated BiP S^+/K^+ ATPase activity. Mn^{2+} was more efficient at these lower concentrations at stimulating ATPase activity than Mg^{2+}. At concentration above 100 µM, Mn^{2+} was less effective than Mg^{2+} (See figure: 3.9). The physiological concentration of Mn^{2+} in the brain is 20-50 µM, while higher concentrations of 60-150 µM are considered pathological (Bowman and Aschner, 2014). Mg^{2+} had stimulatory effect at concentrations as high as 10 mM which was not noticed with Mn^{2+}.

In summary, cations do influence the ATPase activity and binding affinity of nucleotides to BiP variants (refer section 3.6). Further characterisation of BiP using mass spectrometry would aid in the understanding of the folding and function. X-ray diffraction, CD spectroscopy could be performed to study the crystal structure of BiP variants.

On completion of the biochemical characterisation of all BiP variants, we studied the effect of exogenous addition of BiP S^-/K^- on myelination. Considering the cost involved in making four large batches of endotoxin-free protein, we narrowed down the focus to one variant (BiP S^-/K^-). The decision to make the S^-/K^- variant in large quantities for cell culture experiments was made based on the Corrigall's group published literature in which BiP lacking the signal and KDEL sequences was added exogenously to peripheral blood monocyte cell cultures (Corrigall et al., 2004, 2001). In a clinical trial conducted on patients with Rheumatic arthritis, a range of doses were administered systemically (1, 5 and 15 mg). Administration of a single dose of BiP (5 or15 mg) was proved to be therapeutic and safe (Kirkham et al., 2016). On the other

hand, BiP is essential for the angiogenesis and proliferation of synoviocytes which are the hallmarks of rheumatic arthritis (Yoo et al., 2012). BiP also promotes the proliferation of T cells, antibody secretion and the production of proinflammatory cytokines (Ehrenreich et al., 2007; Park et al., 2014). Therefore, it appears that the location of the BiP and its association with other molecules dictates BiP's role as a 'friend' or a 'foe'.

We eluted BiP S^-/K^- in endotoxin-free PBS and passed it through endotoxin removal high-capacity columns to make it endotoxin-free for cell culture experiments. The FITC-labelled BiP was made from the same batch. (see section 2.3.1) for more details). Both B104 neuroblastoma and spinal cord myelinating cultures demonstrated the uptake of FITC-labelled BiP in a time- and dose-dependent manner. FITC-labelled protein aggregates were also noticed in spinal cord myelinating cultures which is one of the reasons for not quantifying these FITC positive cells in spinal cord myelinating cultures. These are preliminary observations and further investigation is required to study the mechanism of uptake.

The endotoxin amounts were quantified and found to be less than 0.015 EU/ml in our BiP preparation (see section 4.6.1), but we could not determine if the effect on microglia was due to BiP or endotoxins or small amounts of co-purified proteins. To rule out the possibility that the increase in microglia was due to the presence of endotoxins, we suggest performing the protein heat inactivation experiments. As endotoxin is heat-resistant and proteins are heat-sensitive, the impact of the endotoxins can be differentiated from that of the protein, once the protein is denatured. Others have shown that commercial compounds having residual endotoxin less than 1 EU is sufficient to drive immune response (Schwarz et al., 2014). Most commercially available recombinant protein products have residual endotoxin amounts of less than 1 Endotoxin Unit, which is equivalent to 100 pg (Dawson et al 1988). CD 1c$^+$ Dendritic cells are sensitive to endotoxin levels as low as 0.002 ng/ml which is equivalent to the residual endotoxin in commercial preparations (<1 EU) (Schwarz et al., 2014). Corrigall et al reported endotoxin levels less than 5 ng per 20 g/ml of BiP protein (Corrigall et al., 2004). Brownlie et al reported an

endotoxin value of less than 95 EU/mg (Brownlie et al., 2006). Very low concentration, such as 0.1 ng-0.001 ng of endotoxins are enough to elicit cytotoxicity in monocytes (Ziegler-Heitbrock et al., 1986). To avoid problems associated with endotoxin we suggest using alternative methods of protein expression such as human embryonic kidney cells -HEK293 cells (Subedi et al., 2015) (non-bacterial protein expression systems) or *E. coli* strains (LPS-free derivatives of *E. coli* K-12 and BL21 (DE3) strains) that produce only endotoxin precursor lipid 4_a, which does not cause an endotoxin response in humans (Mamat et al., 2015). The possibility of BiP proteins getting contaminated with bacterial components such as peptidoglycans or lipoproteins also exists (Gorbet and Sefton, 2005). The half-life of BiP varies across different species and different tissue from few hours -15 days (Wang et al., 2017). The stability of the recombinant BiP variants in the *in-vitro* experiments is another factor to investigate.

Because of the possible unpredictable effects of recombinant BiP on microglia present in our explant cultures, we decided to discontinue the use of recombinant BiP. Instead, we studied the effect of chemical induction of BiP on myelination by using BIX.

As described before BIX is 1-(3, 4-dihydroxyphenyl) -2-thiocyanate-ethanone or 2-(3, 4-dihydroxyphenyl)-2-oxoethyl thiocyanate which is a member of thiocyanates that is 3, 4-dihydroxyacetophenone.

Disappointingly, when spinal cord myelinating cultures were treated, BIX was found to be severely toxic towards myelin, oligodendrocytes, and microglia. In it unclear whether the microglial activation comes first, or if the microglia are activated by myelin debris. As microglia take up debris it is possible that the myelin debris is uptaken by microglia causing their activation. Alternatively, BIX might have activated microglia that exerts toxic effects on myelination.

Microglia develop from the yolk sac and enter the CNS during embryonic development. They participate in neurodegenerative disorders such as Alzheimer's, Nasu-Hakola, neuropathic pain, Rett syndrome. Elimination of microglia seems to be appealing for certain disorders, but these cells are also

important for synaptic pruning, plasticity, the clearing of cellular debris and in programmed cell death.

In our models, the least-affected cell types were astrocytes and neurons. To-date, BIX has been portrayed as a protective agent in the published literature (see Table 5.7). BIX was proved to be therapeutic in models of brain ischemia (Kudo et al., 2008; Oida et al., 2008), retinal damage (Inokuchi et al., 2009), photoreceptor death (Nakanishi et al., 2013), bone loss (Hino et al., 2010) and acute kidney injury (Prachasilchai et al., 2009). Most of the published *in-vitro* experiments were designed around tunicamycin or ER stress-induced apoptosis. Possible chronic effects were ignored. However, we demonstrated that BIX is toxic for chronic treatments, at least at the 5µg/ml dose. The usage of BIX for chronic treatments should be carried out with caution. The stability of this chemical should also be investigated. There is no evidence that BIX is transported to the ER to induce the ATF6 pathway. This has not been described in the literature.

The molecular mechanisms underlying BIX toxicity were explored using RNA sequencing. RNA was isolated from BIX-treated cultures or DMSO control cultures after 24 h of treatment. The sequencing was carried out by Glasgow polyomics. The sequences passed the quality test and were used for differential gene expression analyses. The top 10 upregulated and downregulated genes (see Tables 5.2 and 5.3). were filtered with a log-fold threshold of 1.5 and an adjusted p-value of 0.05. The diversity of the genes did not lead us towards any conclusions. The generation of differentially expressed genes is only the beginning of an understanding of the biological context. The appropriate interpretation of differentially expressed genes is vital to draw conclusions. Genes always function collectively in a biological context by involving inter-dependent signalling pathways. Occasionally, a minute expression change of a few genes participating in a pathway might create a phenomenal change in the biological processes. Therefore, the Reactome pathway browser was used to understand the pathways involved. The differentially expressed genes with a $\log_2$ fold change of ± 2 were used for identifying the pathways involved. The top 25 upregulated pathways and downregulated pathways were listed in (see Tables 5.4 and 5.5). The downregulated pathways include cell cycle, cell cycle

mitotic division, resolution of sister chromatic cohesion, mitotic spindle checkpoints, separation of sister chromatids, cell cycle checkpoints, mitotic anaphase, and metaphase, which clearly indicate that BIX interferes the cell cycle and cell division. The rapidly diving cells such as microglia and oligodendrocytes which have a heavy burden of making myelin were most effected. The upregulated pathways include cellular hexose transport, yes associated protein one (YAP1) - and WW domain-containing transcription regulator one-WWTR1 (TAZ) gene expression. These are transcriptional coactivators with downstream targets involving the control of proliferation and apoptosis; Tumour p53 activates the proapoptotic target genes such as p53 upregulated modulator of apoptosis (PUMA), proapoptotic member of Bcl2 family (NOXA), Bcl-2 like protein 4 (BAX), BH3 interacting domain death agonist (BID) (Maritsi et al., 2006). Other up-regulated signals include those associated with nerve growth factor, which mediates neuroprotective activities by binding Tropomyosin receptor kinase A (TRKA) receptor. The cell-cell junctions (tight junctions, adhesion junctions, and desmosomes), which participate in forming barriers, paracellular transport and signalling were also affected by BIX. The tight junctions also participate in cell proliferation (Garcia et al., 2018). Other pathways include oncogene-induced senescence which can be obtained via retinoblastoma protein and p53-pathway activation (Chandeck and Mooi, 2010). Inhibition of proliferation, interference with the cell cycle, cell division, metabolism and activation of proapoptotic genes justifies the cell death caused by BIX.

There are alternative chemicals that could be used to induce the expression of BiP. Exendin-4 and Forskolin are agonists of Glucagon-like peptide (GLP-1) and have been shown to protect pancreatic β cells from free fatty acid-induced ER stress. Exendin-4 and Forskolin also protect the pancreatic β cells from Salubrinal-induced stress and apoptosis by upregulating protective mechanism (eg. BiP, Bcl-2, and JunB) (Cunha et al., 2009). Other chemicals such as Salubrinal, Bortizomib also upregulate the expression of BiP (Boyce, 2005; LeBlanc et al., 2002) In a high throughput screen conducted for ER stress inducers Spiperone and AMI-193 activated all the three arms of the UPR, while amlodipine and Roxindole upregulated the ATF6 and PERK pathways.

Primaquine and 6-thioguanine only induced the ATF6 pathway (Bi et al., 2015). All six molecules induced the expression BiP (Bi et al., 2015). The selective upregulation of BiP is questionable as all these chemicals upregulate BiP via the UPR. Chaperones such as GRP94, CHOP, PDI are often upregulated, along with BiP (Kudo et al., 2008). The therapeutic activity of these chemicals is yet to be explored.

In conclusion, functionally active recombinant proteins can be produced from *E. coli* in a cost-effective manner, but the risk associated with endotoxins should be considered. The existing literature on BIX did not shed light on the long-term and chronic effects of this compound in *in-vivo* or *in-vitro* disease models. Factors such as dose, duration and the type of model influence the therapeutic characteristics of BIX. These factors should be stringently optimised prior to the therapeutic application of BIX. Spinal cord myelinating cultures revealed the unforeseen toxic effects of BIX and BiP thereby contributing to the principles of 3R's.

References

Alder, N.N., Shen, Y., Brodsky, J.L., Hendershot, L.M., Johnson, A.E., 2005. The molecular mechanisms underlying BiP-mediated gating of the Sec61 translocon of the endoplasmic reticulum, J cell Biol.168, 389–400.

Alexandra, S., Nakaki, T., Vanhamme, L., Lee, A.S., 1991. A Binding Site for the Cyclic Adenosine 3', 5'-Monophosphate-Response Element-Binding Protein as a Regulatory Element in the grp78 Promoter, Molecular Endocrinology. 5(12):1862-72

Andreeva, A. V., Han, J., Kutuzov, M.A., Profirovic, J., Tkachuk, V.A., Voyno-Yasenetskaya, T.A., 2009. T-cadherin modulates endothelial barrier function. J. Cell. Physiol. 223(1):94-102

Ashwell, K., 1990. Microglia and cell death in the developing mouse cerebellum. Dev. Brain Res. 55, 219–230.

Awad, W., Estrada, I., Shen, Y., Hendershot, L.M., 2008. BiP mutants that are unable to interact with endoplasmic reticulum DnaJ proteins provide insights into interdomain interactions in BiP. Proc. Natl. Acad. Sci. 105, 1164–1169.

Balabanov, R., Lisak, D., Beaumont, T., Lisak, R.P., Dore-Duffy, P., 2001. Expression of urokinase plasminogen activator receptor on monocytes from patients with relapsing-remitting multiple sclerosis: effect of glatiramer acetate (copolymer 1). Clin. Diagn. Lab. Immunol. 8, 1196–203.

Bandla, S., Diaz, S., Nasheuer, H.P., FitzGerald, U., 2019. ATPase activity of human binding immunoglobulin protein (BiP) variants is enhanced by signal sequence and physiological concentrations of Mn 2+. FEBS Open Bio 9, 1355–1369.

Baneyx, F., 1999. Recombinant protein expression in Escherichia coli. Curr. Opin. Biotechnol. 10, 411–421.

Barria, A., 2019. Preparation of Organotypic Slice Cultures for the Study of Glutamate Receptor Function. pp. 57–64.

Baumann, O., Walz, B., 2001. Endoplasmic reticulum of animal cells and its organization into structural and functional domains. Int. Rev. Cytol. 205, 149–214.

Bellani, S., Mescola, A., Ronzitti, G., Tsushima, H., Tilve, S., Canale, C., Valtorta, F., Chieregatti, E., 2014. GRP78 clustering at the cell surface of neurons transduces the action of exogenous alpha-synuclein. Cell Death Differ. 21, 1971–1983.

Berghoff, S.A., Gerndt, N., Winchenbach, J., Stumpf, S.K., Hosang, L., Odoardi, F., Ruhwedel, T., Böhler, C., Barrette, B., Stassart, R., Liebetanz, D., Dibaj, P., Möbius, W., Edgar, J.M., Saher, G., 2017. Dietary cholesterol promotes repair of demyelinated lesions in the adult brain. Nat. Commun. 8, 14241.

Bergmans, H.E., van Die, I.M., Hoekstra, W.P., 1981. Transformation in Escherichia coli: stages in the process. J. Bacteriol. 146, 564–70.

Bernales, S., McDonald, K.L., Walter, P., 2006. Autophagy counterbalances endoplasmic reticulum expansion during the unfolded protein response. PLoS Biol. 4, 2311–2324.

Bertelsen, E.B., Chang, L., Gestwicki, J.E., Zuiderweg, E.R.P., 2009. Solution conformation of wild-type E. coli Hsp70 (DnaK) chaperone complexed with ADP and substrate. Proc. Natl. Acad. Sci. 106, 8471–8476.

Bhattacharjee, G., 2005. Regulation of Tissue Factor-Mediated Initiation of the Coagulation Cascade by Cell Surface Grp78. Arterioscler. Thromb. Vasc. Biol. 25, 1737–1743.

Bi, K., Nishihara, K., Machleidt, T., Hermanson, S., Wang, J., Sakamuru, S., Huang, R., Xia, M., 2015. Identification of known drugs targeting the endoplasmic reticulum stress response. Anal. Bioanal. Chem. 407, 5343–5351.

Biancotti, J.C., Kumar, S., de Vellis, J., 2008. Activation of Inflammatory Response by a Combination of Growth Factors in Cuprizone-Induced Demyelinated Brain Leads to Myelin Repair. Neurochem. Res. 33, 2615–2628.

Bijland, S., Thomson, G., Euston, M., Michail, K., Thümmler, K., Mücklisch, S., Crawford, C.L., Barnett, S.C., McLaughlin, M., Anderson, T.J., Linington, C., Brown, E.R., Kalkman, E.R., Edgar, J.M., 2019. An in vitro model for studying CNS white matter: functional properties and experimental approaches. F1000Research 8, 117.

Birgbauer, E., Rao, T.S., Webb, M., 2004. Lysolecithin induces demyelination in vitro in a cerebellar slice culture system. J. Neurosci. Res. 78, 157–166.

Bläss, S., Union, A., Raymackers, J., Schumann, F., Ungethüm, U., Müller-Steinbach, S., De Keyser, F., Engel, J.-M., Burmester, G.R., 2001. The stress protein BiP is overexpressed and is a major B and T cell target in rheumatoid arthritis. Arthritis Rheum. 44, 761–771.

Blattner, F.R., Plunkett, G., Bloch, C.A., Perna, N.T., Burland, V., Riley, M., Collado-Vides, J., Glasner, J.D., Rode, C.K., Mayhew, G.F., Gregor, J., Davis, N.W., Kirkpatrick, H.A., Goeden, M.A., Rose, D.J., Mau, B., Shao, Y., 1997. The complete genome sequence of Escherichia coli K-12. Science 277, 1453–62.

Blond-Elguindi, S., Fourie, A.M., Sambrook, J.F., Gething, M.J.H., 1993. Peptide-dependent stimulation of the ATPase activity of the molecular chaperone BiP is the result of conversion of oligomers to active monomers. J. Biol. Chem. 268, 12730–12735.

Bowman, A.B., Aschner, M., 2014. Considerations on manganese (Mn) treatments for in vitro studies. Neurotoxicology 41, 141–142.

Boyce, M., 2005. A Selective Inhibitor of eIF2 Dephosphorylation Protects Cells from ER Stress. Science. 307, 935–939.

Braakman, I., Bulleid, N.J., 2011. Protein Folding and Modification in the Mammalian Endoplasmic Reticulum. Annu. Rev. Biochem. 80, 71–99.

Bracher, A., Hayer-Hartl, M., 2011. Molecular chaperones in protein folding and proteostasis. 475(7356):324-32

Brandenburg, L.-O., Lucius, R., Tameh Abolfazl, A., Kipp, M., Wruck, C.J., Koch, T., Beyer, C., Pufe, T., 2009. Internalization and signal transduction of PrP106−126 in neuronal cells. Ann. Anat. - Anat. Anzeiger 191, 459–468.

Brodsky, J.L., Schekman, R., 1993. A Sec63p-BiP complex from yeast is required for protein translocation in a reconstituted proteoliposome. J. Cell Biol. 123, 1355–63.

Brown, I.R., Sharp, F.R., 1999. The Cellular Stress Gene Response in Brain. Springer, Berlin, Heidelberg, pp. 243–263.

Brown, M., Figge, J., Hansen, U., Wright, C., Jeang, K.-T., Khoury, G., Livingston, D.M., Roberts, T.M., 1987. Lac repressor can regulate expression from a hybrid SV40 early promoter containing a lac operator in animal cells. Cell 49, 603–612.

Browne, P., Chandraratna, D., Angood, C., Tremlett, H., Baker, C., Taylor, B. V., Thompson, A.J., 2014. Atlas of multiple sclerosis 2013: A growing global problem with widespread inequity. Neurology 83, 1022–1024.

BROWNLEE, G.G., SANGER, F., BARRELL, B.G., 1967. Nucleotide Sequence of 5S-ribosomal RNA from Escherichia coli. Nature 215, 735–736.

Brownlie, R.J., Myers, L.K., Wooley, P.H., Corrigall, V.M., Bodman-Smith, M.D., Panayi, G.S., Thompson, S.J., 2006. Treatment of murine collagen-induced arthritis by the stress protein BiP via interleukin-4-producing regulatory T cells: a novel function for an ancient protein. Arthritis Rheum. 54, 854–63.

Buffo, A., Rossi, F., 2013. Origin, lineage and function of cerebellar glia. Prog. Neurobiol. 109, 42–63.

Buffo, A., Rossi, F., Levi-Montalcini, R., 2013. Origin, lineage and function of cerebellar glia. Prog. Neurobiol. 109, 42–63.

Burikhanov, R., Zhao, Y., Goswami, A., Qiu, S., Schwarze, S.R., Rangnekar, V.M., 2009. The tumor suppressor Par-4 activates an extrinsic pathway for apoptosis. Cell 138, 377–88.

Calderwood, S.K., Mambula, S.S., Gray, P.J., 2007. Extracellular Heat Shock Proteins in Cell Signaling and Immunity. Ann. N. Y. Acad. Sci. 1113, 28–39.

Cao, S.S., Kaufman, R.J., Weissman, J.S., 2012. Unfolded protein response. Curr. Biol. 22, R622-6.

Carassiti, D., Altmann, D.R., Petrova, N., Pakkenberg, B., Scaravilli, F., Schmierer, K., 2018. Neuronal loss, demyelination and volume change in the multiple sclerosis neocortex. Neuropathol. Appl. Neurobiol. 44, 377–390.

Carlino, A., Toledo, H., Skaleris, D., DeLisio, R., Weissbach, H., Brot, N., 1992. Interactions of liver Grp78 and Escherichia coli recombinant Grp78 with

ATP: multiple species and disaggregation. Proc. Natl. Acad. Sci. U. S. A. 89, 2081–5.

Carroll, R., Yellon, D.M., 1999. Heat Stress Proteins and Their Relationship to Myocardial Protection. Springer, Berlin, Heidelberg, pp. 265–279.

Carvalho, H.H., Silva, P.A., Mendes, G.C., Brustolini, O.J.B., Pimenta, M.R., Gouveia, B.C., Valente, M.A.S., Ramos, H.J.O., Soares-Ramos, J.R.L., Fontes, E.P.B., 2014. The endoplasmic reticulum binding protein BiP displays dual function in modulating cell death events. Plant Physiol. 164, 654–70.

Casas, C., 2017. GRP78 at the centre of the stage in cancer and neuroprotection. Front. Neurosci. 11, 1–15.

Chandeck, C., Mooi, W.J., 2010. Oncogene-induced cellular senescence. Adv. Anat. Pathol. 17, 42–8.

Chang, A.Y., Chau, V.W., Landas, J.A., Yvonne, 2017. Preparation of calcium competent Escherichia coli and heat-shock transformation.Jemi Methods. Vol. 1:22-25

Chanput, W., Mes, J.J., Wichers, H.J., 2014. THP-1 cell line: An in vitro cell model for immune modulation approach. Int. Immunopharmacol. 23, 37–45.

Chen, K.-D., Hung, J.-J., Huang, H.-L., Dah-Tysr CHANG, M., 1997. Rapid induction of the Grp78 gene by cooperative actions of okadaic acid and heat-shock in 9L rat brain tumor cells Involvement of a CAMP responsive element-like promoter sequence and a protein kinase A signaling pathway, Eur. J. Biochem. 248(1):120-9

Čiplys, E., Aučynaite, A., Slibinskas, R., 2014. Generation of human ER chaperone BiP in yeast Saccharomyces cerevisiae. Microb. Cell Fact. 13:22.

Coelho, D.S., Domingos, P.M., 2014. Physiological roles of regulated Ire1 dependent decay. Front. Genet. 5:76

Cohen, B.A., Oger, J., Gagnon, A., Giovannoni, G., 2008. The implications of immunogenicity for protein-based multiple sclerosis therapies. J. Neurol. Sci. 275, 7–17.

Compston, A., Coles, A., 2008. Multiple sclerosis. Lancet 372, 1502–1517.

Conesa, A., Madrigal, P., Tarazona, S., Gomez-Cabrero, D., Cervera, A., McPherson, A., Szcześniak, M.W., Gaffney, D.J., Elo, L.L., Zhang, X., Mortazavi, A., 2016. A survey of best practices for RNA-seq data analysis. Genome Biol. 17, 13.

Cook, K.L., 2019. Outside the Endoplasmic Reticulum: Non-Canonical GRP78 Signaling. Humana Press, Cham, pp. 181–195.

Cooper GM. The Cell: A Molecular Approach. 2nd edition. Sunderland (MA): Sinauer Associates; 2000

Corrigall, V.M., Bodman-Smith, M.D., Brunst, M., Cornell, H., Panayi, G.S., 2004. Inhibition of antigen-presenting cell function and stimulation of human peripheral blood mononuclear cells to express an antiinflammatory cytokine profile by the stress protein BiP: Relevance to the treatment of inflammatory arthritis. Arthritis Rheum. 50, 1164–1171.

Corrigall, V.M., Bodman-Smith, M.D., Fife, M.S., Canas, B., Myers, L.K., Wooley, P.H., Soh, C., Staines, N.A., Pappin, D.J.C., Berlo, S.E., van Eden, W., van der Zee, R., Lanchbury, J.S., Panayi, G.S., 2001. The Human Endoplasmic Reticulum Molecular Chaperone BiP Is an Autoantigen for Rheumatoid Arthritis and Prevents the Induction of Experimental Arthritis. J. Immunol. 166, 1492–1498.

Corrigall, V.M., Vittecoq, O., Panayi, G.S., 2009. Binding immunoglobulin protein-treated peripheral blood monocyte-derived dendritic cells are refractory to maturation and induce regulatory T-cell development. Immunology 128, 218–226.

Costales, J., Kolevzon, A., 2016. The therapeutic potential of insulin-like growth factor-1 in central nervous system disorders. Neurosci. Biobehav. Rev. 63, 207–22.

Crayton, H.J., Rossman, H.S., 2006. Managing the symptoms of multiple sclerosis: A multimodal approach. Clin. Ther. 28, 445–460.

Croft, C.L., Noble, W., 2018. Preparation of organotypic brain slice cultures for the study of Alzheimer's disease. F1000Research 7, 592.

Cumberworth, S.L., Barrie, J.A., Cunningham, M.E., de Figueiredo, D.P.G., Schultz, V., Wilder-Smith, A.J., Brennan, B., Pena, L.J., Freitas de Oliveira

França, R., Linington, C., Barnett, S.C., Willison, H.J., Kohl, A., Edgar, J.M., 2017. Zika virus tropism and interactions in myelinating neural cell cultures: CNS cells and myelin are preferentially affected. Acta Neuropathol. Commun. 5, 50.

Cummings, C.J., Mancini, M.A., Antalffy, B., DeFranco, D.B., Orr, H.T., Zoghbi, H.Y., 1998. Chaperone suppression of aggregation and altered subcellular proteasome localization imply protein misfolding in SCA1. Nat. Genet. 19, 148–154.

Cunnea, P., Mháille, A.N., McQuaid, S., Farrell, M., McMahon, J., Fitzgerald, U., 2011. Expression profiles of endoplasmic reticulum stress-related molecules in demyelinating lesions and multiple sclerosis. Mult. Scler. J. 17, 808–818.

Dargahi, N., Katsara, M., Tselios, T., Androutsou, M.-E., De Courten, M., Matsoukas, J., Apostolopoulos, V., 2017. Brain sciences Review Multiple Sclerosis: Immunopathology and Treatment Update. 7(7). pii: E78.

Das Sarma, J., Ciric, B., Marek, R., Sadhukhan, S., Caruso, M.L., Shafagh, J., Fitzgerald, D.C., Shindler, K.S., Rostami, A.M., 2009. Functional interleukin-17 receptor A is expressed in central nervous system glia and upregulated in experimental autoimmune encephalomyelitis. J. Neuroinflammation 6, 1–12.

DasGupta, R., Fowler, C.J., 2003. Bladder, Bowel and Sexual Dysfunction in Multiple Sclerosis. Drugs 63, 153–166.

Davidson, D.J., Haskell, C., Majest, S., Kherzai, A., Egan, D.A., Walter, K.A., Schneider, A., Gubbins, E.F., Solomon, L., Chen, Z., Lesniewski, R., Henkin, J., 2005. Kringle 5 of Human Plasminogen Induces Apoptosis of Endothelial and Tumor Cells through Surface-Expressed Glucose-Regulated Protein 78. Cancer Res. 65, 4663–4672.

Dawson, M.E., Novitsky, T.J., Gould, M.J., 1998. Microbes, endotoxins and water. Pharm.Engineering, 8 (2), 145-148.

De Zeeuw, C.I., Hoogland, T.M., 2015. Reappraisal of Bergmann glial cells as modulators of cerebellar circuit function. Front. Cell. Neurosci. 9, 246.

De Zeeuw, C.I., Hoogland, T.M., 2015. Reappraisal of Bergmann glial cells as modulators of cerebellar circuit function. Front. Cell. Neurosci. 9, 246.

Dekki, N., Refai, E., Holmberg, R., Köhler, M., Jörnvall, H., Berggren, P.-O., Juntti-Berggren, L., 2012. Transthyretin binds to glucose-regulated proteins and is subjected to endocytosis by the pancreatic β-cell. Cell. Mol. Life Sci. 69, 1733–1743.

Della Chiesa, M., Romagnani, C., Thiel, A., Moretta, L., Moretta, A., 2006. Multidirectional interactions are bridging human NK cells with plasmacytoid and monocyte-derived dendritic cells during innate immune responses. Blood 108, 3851–8.

Delpino, A., Castelli, M., 2002. The 78 kDa Glucose-regulated Protein (GRP78 / BIP) is expressed on the cell membrane, is released into cell culture medium and is also present in human peripheral circulation 22, 407–420.

Demerens, C., Stankoff, B., Logak, M., Angladet, P., Allinquantt, B., Couraud, F., Zalc, B., Lubetzki, C., Linington, C., 1996. Induction of myelination in the central nervous system by electrical activity, Neurobiology.

Deora, A.B., Kreitzer, G., Jacovina, A.T., Hajjar, K.A., 2004. An Annexin 2 Phosphorylation Switch Mediates p11-dependent Translocation of Annexin 2 to the Cell Surface*. 279(42):43411-8.

Deslauriers, A.M., Afkhami-Goli, A., Paul, A.M., Bhat, R.K., Acharjee, S., Ellestad, K.K., Noorbakhsh, F., Michalak, M., Power, C., 2011. Neuroinflammation and Endoplasmic Reticulum Stress Are Coregulated by Crocin To Prevent Demyelination and Neurodegeneration. J. Immunol. 187, 4788–4799.

Di Penta, A., Moreno, B., Reix, S., Fernandez-Diez, B., Villanueva, M., Errea, O., Escala, N., Vandenbroeck, K., Comella, J.X., Villoslada, P., 2013. Oxidative stress and proinflammatory cytokines contribute to demyelination and axonal damage in a cerebellar culture model of neuroinflammation. PLoS One 8, e54722.

Diebold, M., Derfuss, T., 2016. Immunological treatment of multiple sclerosis. Semin. Hematol. 53, S54–S57.

Djebali, S., Davis, C.A., Merkel, A., Dobin, A., Lassmann, T., Mortazavi, A., Tanzer, A., Lagarde, J., Lin, W., Schlesinger, F., Xue, C., Marinov, G.K., Khatun, J., Williams, B.A., Zaleski, C., Rozowsky, J., Röder, M., Kokocinski,

F., Abdelhamid, R.F., Alioto, T., Antoshechkin, I., Baer, M.T., Bar, N.S., Batut, P., Bell, K., Bell, I., Chakrabortty, S., Chen, X., Chrast, J., Curado, J., Derrien, T., Drenkow, J., Dumais, E., Dumais, J., Duttagupta, R., Falconnet, E., Fastuca, M., Fejes-Toth, K., Ferreira, P., Foissac, S., Fullwood, M.J., Gao, H., Gonzalez, D., Gordon, A., Gunawardena, H., Howald, C., Jha, S., Johnson, R., Kapranov, P., King, B., Kingswood, C., Luo, O.J., Park, E., Persaud, K., Preall, J.B., Ribeca, P., Risk, B., Robyr, D., Sammeth, M., Schaffer, L., See, L.-H., Shahab, A., Skancke, J., Suzuki, A.M., Takahashi, H., Tilgner, H., Trout, D., Walters, N., Wang, H., Wrobel, J., Yu, Y., Ruan, X., Hayashizaki, Y., Harrow, J., Gerstein, M., Hubbard, T., Reymond, A., Antonarakis, S.E., Hannon, G., Giddings, M.C., Ruan, Y., Wold, B., Carninci, P., Guigó, R., Gingeras, T.R., 2012. Landscape of transcription in human cells. Nature 489, 101–108.

Dou, F., Netzer, W.J., Tanemura, K., Li, F., Hartl, F.U., Takashima, A., Gouras, G.K., Greengard, P., Xu, H., 2003. Chaperones increase association of tau protein with microtubules. Proc. Natl. Acad. Sci. U. S. A. 100, 721–6.

Dutta, R., McDonough, J., Yin, X., Peterson, J., Chang, A., Torres, T., Gudz, T., Macklin, W.B., Lewis, D.A., Fox, R.J., Rudick, R., Mirnics, K., Trapp, B.D., 2006. Mitochondrial dysfunction as a cause of axonal degeneration in multiple sclerosis patients. Ann. Neurol. 59, 478–489.

Dutta, R., Trapp, B.D., 2011. Mechanisms of neuronal dysfunction and degeneration in multiple sclerosis. Prog. Neurobiol. 93, 1–12.

Ebers, G.C., 2000. The natural history of multiple sclerosis. Neurol. Sci. 21, S815–S817.

Ebers, G.C., 2001. Natural history of multiple sclerosis. J Neurol Neurosurg Psychiatry. 71. Suppl_2.ii16

Ebers, G.C., 2004. Natural history of primary progressive multiple sclerosis. Mult. Scler. J. 10, S8–S15.

Edgar, J.M., McCulloch, M.C., Thomson, C.E., Griffiths, I.R., 2008. Distribution of mitochondria along small-diameter myelinated central nervous system axons. J. Neurosci. Res. 86, 2250–2257.

Ehrenreich, H., Fischer, B., Norra, C., Schellenberger, F., Stender, N., Stiefel, M., Sirén, A.-L., Paulus, W., Nave, K.-A., Gold, R., Bartels, C., 2007. Exploring

recombinant human erythropoietin in chronic progressive multiple sclerosis. Brain 130, 2577–2588.

El Bitar, F., Dastugue, B., Meiniel, A., 1999. Neuroblastoma B104 cell line as a model for analysis of neurite outgrowth and neuronal aggregation induced by Reissner's fiber material. Cell Tissue Res. 298, 233–42.

Elbers, C.C., van Eijk, K.R., Franke, L., Mulder, F., van der Schouw, Y.T., Wijmenga, C., Onland-Moret, N.C., 2009. Using genome-wide pathway analysis to unravel the etiology of complex diseases. Genet. Epidemiol. 33, 419–431.

Eleuteri, C., Olla, S., Veroni, C., Umeton, R., Mechelli, R., Romano, S., Buscarinu, M., Ferrari, F., Calò, G., Ristori, G., Salvetti, M., Agresti, C., 2017. A staged screening of registered drugs highlights remyelinating drug candidates for clinical trials. Sci. Rep. 7, 45780.

Ellis, R.J., 1993. The general concept of molecular chaperones. Philos Trans R Soc Lond B Biol Sci.339 (1289):257-61.

Emrich, S.J., Barbazuk, W.B., Li, L., Schnable, P.S., 2007. Gene discovery and annotation using LCM-454 transcriptome sequencing. Genome Res. 17, 69–73.

English, A.R., Zurek, N., Voeltz, G.K., 2009. Peripheral ER structure and function. Curr. Opin. Cell Biol. 21, 596–602.

Ericsson, U.B., Hallberg, B.M., Detitta, G.T., Dekker, N., Nordlund, P., 2006. Thermofluor-based high-throughput stability optimization of proteins for structural studies. Anal Biochem.357 (2):289-98.

Ewing, B., Hillier, L., Wendl, M.C., Green, P., 1998. Base-calling of automated sequencer traces using phred. I. Accuracy assessment. Genome Res. 8, 175–85.

Fdez-Morera, J.L., Tunon, A., Rodriguez-Rodero, S., Rodrigo, L., Martinez-Borra, J., Gonzalez, S., Lopez-Vazquez, A., Lahoz, C.H., Lopez-Larrea, C., 2006. Clinical behavior of multiple sclerosis is modulated by the MHC class I-chain-related gene A. Tissue Antigens 67, 409–414.

Fewell S.W., Brodsky J.L. 2009.Entry into the Endoplasmic Reticulum: Protein Translocation, Folding and Quality Control. In: Trafficking Inside Cells. Molecular Biology Intelligence Unit. Springer, New York, NY. pp 119-142

Filippi, M., Rocca, M.A., Calabrese, M., Sormani, M.P., Rinaldi, F., Perini, P., Comi, G., Gallo, P., 2010. Intracortical lesions: relevance for new MRI diagnostic criteria for multiple sclerosis. Neurology 75, 1988–94.

Filippi, M., Rocca, M.A., Ciccarelli, O., De Stefano, N., Evangelou, N., Kappos, L., Rovira, A., Sastre-Garriga, J., Tintorè, M., Frederiksen, J.L., Gasperini, C., Palace, J., Reich, D.S., Banwell, B., Montalban, X., Barkhof, F., 2016. MRI criteria for the diagnosis of multiple sclerosis: MAGNIMS consensus guidelines. Lancet Neurol. 15, 292–303.

Fillatreau, S., Sweenie, C.H., McGeachy, M.J., Gray, D., Anderton, S.M., 2002. B cells regulate autoimmunity by provision of IL-10. Nat. Immunol. 3, 944–950.

Flynn, G.C., Chappell, T.G., Rothman, J.E., 1989. Peptide binding and release by proteins implicated as catalysts of protein assembly. Science 245, 385–90.

Flynn, G.C., Pohl, J., Flocco, M.T., Rothman, J.E., 1991a. Peptide-binding specificity of the molecular chaperone BiP. Nature 353, 726–730.

Flynn, G.C., Pohl, J., Flocco, M.T., Rothman, J.E., 1991b. Peptide-binding specificity of the molecular chaperone BiP. Nature 353, 726–730.

Friedman, J.R., Voeltz, G.K., 2012. The ER in 3-D: a multifunctional dynamic membrane network Overview of ER shape 21, 709–717.

Fu, H., Kesari, S., Cai, J., 2012. Tcf7l2 is Tightly Controlled During Myelin Formation. Cell. Mol. Neurobiol. 32, 345–352.

Gähwiler, B.., Capogna, M., Debanne, D., McKinney, R.., Thompson, S.., 1997. Organotypic slice cultures: a technique has come of age. Trends Neurosci. 20, 471–477.

Garcia, M.A., Nelson, W.J., Chavez, N., 2018. Cell-Cell Junctions Organize Structural and Signaling Networks. Cold Spring Harb. Perspect. Biol. 10, a029181.

Gaultier, A., Wu, X., Le Moan, N., Takimoto, S., Mukandala, G., Akassoglou, K., Campana, W.M., Gonias, S.L., 2009. Low-density lipoprotein receptor-related protein 1 is an essential receptor for myelin phagocytosis. J. Cell Sci. 122, 1155–62.

Gauts, J.R., Hendershotsqv, L.M., 1993. Mutations within the Nucleotide Binding Site of Immunoglobulin- binding Protein Inhibit ATPase Activity and Interfere with Release of Immunoglobulin Heavy Chain * 7248–7255.

Gensicke, H., Leppert, D., Yaldizli, Ö., Lindberg, R.L.P., Mehling, M., Kappos, L., Kuhle, J., 2012. Monoclonal Antibodies and Recombinant Immunoglobulins for the Treatment of Multiple Sclerosis. CNS Drugs 26, 11–37.

Ghoumari, A.M., Ibanez, C., El-Etr, M., Leclerc, P., Eychenne, B., O'Malley, B.W., Baulieu, E.E., Schumacher, M., 2003. Progesterone and its metabolites increase myelin basic protein expression in organotypic slice cultures of rat cerebellum. J. Neurochem. 86, 848–859.

Giacomelli, L., Covani, U., 2010. Bioinformatics and data mining studies in oral genomics and proteomics: new trends and challenges. Open Dent. J. 4, 67–71.

Giorgio, A., Stromillo, M.L., Rossi, F., Battaglini, M., Hakiki, B., Portaccio, E., Federico, A., Amato, M.P., De Stefano, N., 2011. Cortical lesions in radiologically isolated syndrome. Neurology 77, 1896–9.

Giusti, L., Baldini, C., Ciregia, F., Giannaccini, G., Giacomelli, C., de Feo, F., Sedie, A.D., Riente, L., Lucacchini, A., Bazzichi, L., Bombardieri, S., 2010a. Is GRP78/BiP a potential salivary biomarker in patients with rheumatoid arthritis? Proteomics - Clin. Appl. 4, 315–324.

Giusti, L., Baldini, C., Ciregia, F., Giannaccini, G., Giacomelli, C., de Feo, F., Sedie, A.D., Riente, L., Lucacchini, A., Bazzichi, L., Bombardieri, S., 2010b. Is GRP78/BiP a potential salivary biomarker in patients with rheumatoid arthritis? Proteomics - Clin. Appl. 4, 315–324.

Gonzalez–Gronow, M., Selim, M.A., Papalas, J., Pizzo, S. V., 2009. GRP78: A Multifunctional Receptor on the Cell Surface. Antioxid. Redox Signal. 11, 2299–2306.

Gorbet, M.B., Sefton, M. V., 2005. Endotoxin: The uninvited guest. Biomaterials 26, 6811–6817.

Grajchen, E., Hendriks, J.J.A., Bogie, J.F.J., 2018. The physiology of foamy phagocytes in multiple sclerosis. Acta Neuropathol. Commun. 6, 124.

Graumann, U., Reynolds, R., Steck, A.J., Schaeren-Wiemers, N., 2006. Molecular Changes in Normal Appearing White Matter in Multiple Sclerosis are Characteristic of Neuroprotective Mechanisms against Hypoxic Insult. Brain Pathol. 13, 554–573.

Grieve, A.G., Rabouille, C., 2011. Golgi bypass: skirting around the heart of classical secretion. Cold Spring Harb. Perspect. Biol. 3, a005298.

Grigoriadis, N., van Pesch, V., 2015. A basic overview of multiple sclerosis immunopathology. Eur. J. Neurol. 22, 3–13.

Grimaldi, P., Parras, C., Guillemot, F., Rossi, F., Wassef, M., 2009. Origins and control of the differentiation of inhibitory interneurons and glia in the cerebellum. Dev. Biol. 328, 422–433.

Gveric, D., KaltschmidT, C., Cuzner, M.L., Newcombe, J., 1998. Transcription Factor NF-kB and Inhibitor kBα are localized in Macrophages in Active Multiple Sclerosis Lesions. J. Neuropathol. Exp. Neurol. 57, 168–169.

Haider, L., Simeonidou, C., Steinberger, G., Hametner, S., Grigoriadis, N., Deretzi, G., Kovacs, G.G., Kutzelnigg, A., Lassmann, H., Frischer, J.M., 2014. Multiple sclerosis deep grey matter: the relation between demyelination, neurodegeneration, inflammation and iron. J. Neurol. Neurosurg. Psychiatry 85, 1386–95.

Han, Y., Gao, S., Muegge, K., Zhang, W., Zhou, B., 2015. Advanced Applications of RNA Sequencing and Challenges. Bioinform. Biol. Insights 9s1, BBI.S28991.

Hansen, K.D., Brenner, S.E., Dudoit, S., 2010. Biases in Illumina transcriptome sequencing caused by random hexamer priming. Nucleic Acids Res. 38, e131–e131.

Hara, H., Kamiya, T., Adachi, T., 2011. Endoplasmic reticulum stress inducers provide protection against 6-hydroxydopamine-induced cytotoxicity. Neurochem. Int. 58, 35–43.

Harding, H.P., Zhang, Y., Bertolotti, A., Zeng, H., Ron, D., 2000. Perk is essential for translational regulation and cell survival during the unfolded protein response. Mol. Cell 5, 897–904.

Harding, H.P., Zhang, Y., Ron, D., 1999. Protein translation and folding are coupled by an endoplasmic-reticulum-resident kinase. [see comments.] [erratum appears in Nature 1999 Mar 4;398(6722):90.]. Nature 397, 271–274.

Harrer, M.D., von Büdingen, H.-C., Stoppini, L., Alliod, C., Pouly, S., Fischer, K., Goebels, N., 2009. Live imaging of remyelination after antibody-mediated demyelination in an ex-vivo model for immune mediated CNS damage. Exp. Neurol. 216, 431–438.

Hartl, F.U., 1996. Molecular chaperones in cellular protein folding. Nature 381, 571–580.

Hartl, F.U., Hayer-Hartl, M., 2002. Molecular Chaperones in the Cytosol: from Nascent Chain to Folded Protein. Science (80-). 295, 1852–1858.

Hashimoto, R., Hori, K., Owa, T., Miyashita, S., Dewa, K., Masuyama, N., Sakai, K., Hayase, Y., Seto, Y., Inoue, Y.U., Inoue, T., Ichinohe, N., Kawaguchi, Y., Akiyama, H., Koizumi, S., Hoshino, M., 2016. Origins of oligodendrocytes in the cerebellum, whose development is controlled by the transcription factor, Sox9. Mech. Dev. 140, 25–40.

Healy, S., McMahon, J., Owens, P., FitzGerald, U., 2016. Significant glial alterations in response to iron loading in a novel organotypic hippocampal slice culture model. Sci. Rep. 6, 36410.

Hefti, M.H., Van Vugt-Van Der Toorn, C.J.G., Dixon, R., Vervoort, J., 2001. A Novel Purification Method for Histidine-Tagged Proteins Containing a Thrombin Cleavage Site. Anal Biochem. 295(2):180-5

Hemmer, B., Nessler, S., Zhou, D., Kieseier, B., Hartung, H.P., 2006. Immunopathogenesis and immunotherapy of multiple sclerosis. Nat. Clin. Pract. Neurol. 2, 201–211.

Henderson, B., Martin, A.C.R., 2014. Protein moonlighting: a new factor in biology and medicine. Biochem. Soc. Trans. 42, 1671–1678.

Higgins, G.C., Beart, P.M., Shin, Y.S., Chen, M.J., Cheung, N.S., Nagley, P., 2010. Oxidative stress: emerging mitochondrial and cellular themes and variations in neuronal injury. J. Alzheimers. Dis. 20 Suppl 2, S453-73.

Hino, S.I., Kondo, S., Yoshinaga, K., Saito, A., Murakami, T., Kanemoto, S., Sekiya, H., Chihara, K., Aikawa, Y., Hara, H., Kudo, T., Sekimoto, T., Funamoto, T., Chosa, E., Imaizumi, K., 2010. Regulation of ER molecular chaperone prevents bone loss in a murine model for osteoporosis. J. Bone Miner. Metab. 28, 131–138.

Hochuli, E., Döbeli, H., Schacher, A., 1987. New metal chelate adsorbent selective for proteins and peptides containing neighbouring histidine residues. J. Chromatogr. 411, 177–84.

Holley, J.E., Gveric, D., Newcombe, J., Cuzner, M.L., Gutowski, N.J., 2003. Astrocyte characterization in the multiple sclerosis glial scar. Neuropathol. Appl. Neurobiol. 29, 434–444.

Honda, T., Horie, M., Daito, T., Ikuta, K., Tomonaga, K., 2009. Molecular Chaperone BiP Interacts with Borna Disease Virus Glycoprotein at the Cell Surface † Downloaded from. J. Virol. 83, 12622–12625.

Hsu, A.-L., Murphy, C.T., Kenyon, C., 2003. Regulation of Aging and Age-Related Disease by DAF-16 and Heat-Shock Factor. Science (80-.). 300, 1142–1145.

Huang, D., 2015. Challenges in randomized controlled trials and emerging multiple sclerosis therapeutics. Neurosci. Bull. 31, 745–754.

Huang, J.K., Jarjour, A.A., Nait Oumesmar, B., Kerninon, C., Williams, A., Krezel, W., Kagechika, H., Bauer, J., Zhao, C., Evercooren, A.B.-V., Chambon, P., ffrench-Constant, C., Franklin, R.J.M., 2011. Retinoid X receptor gamma signaling accelerates CNS remyelination. Nat. Neurosci. 14, 45–53.

Huang, Y.M., Xiao, B.G., Ozenci, V., Kouwenhoven, M., Teleshova, N., Fredrikson, S., Link, H., 1999. Multiple sclerosis is associated with high levels of circulating dendritic cells secreting pro-inflammatory cytokines. J. Neuroimmunol. 99, 82–90.

Huergo-Zapico, L., Gonzalez-Rodriguez, A.P., Contesti, J., Gonzalez, E., López-Soto, A., Fernandez-Guizan, A., Acebes-Huerta, A., de los Toyos, J.R., Lopez-Larrea, C., Groh, V., Spies, T., Gonzalez, S., 2012. Expression of ERp5 and GRP78 on the membrane of chronic lymphocytic leukemia cells:

association with soluble MICA shedding. Cancer Immunol. Immunother. 61, 1201–1210.

Hughes, S.J., Antoshchenko, T., Chen, Y., Lu, H., Pizarro, J.C., Park, H.-W., 2016. Probing the ATP Site of GRP78 with Nucleotide Triphosphate Analogs. PLoS One 11, e0154862.

Humpel, C., 2015a. Neuroscience forefront review organotypic brain slice cultures: A review. Neuroscience 305, 86–98.

Humpel, C., 2015b. Organotypic brain slice cultures: A review. Neuroscience 305, 86–98.

Huppert, J., Closhen, D., Croxford, A., White, R., Kulig, P., Pietrowski, E., Bechmann, I., Becher, B., Luhmann, H.J., Waisman, A., Kuhlmann, C.R.W., 2010. Cellular mechanisms of IL-17-induced blood-brain barrier disruption. Faseb J. 24, 1023–1034.

Hussien, Y., Podojil, J.R., Robinson, A.P., Lee, A.S., Miller, S.D., Popko, B., 2015. ER Chaperone BiP/GRP78 Is Required for Myelinating Cell Survival and Provides Protection during Experimental Autoimmune Encephalomyelitis. J. Neurosci. 35, 15921–15933.

Ifergan, I., Kébir, H., Bernard, M., Wosik, K., Dodelet-Devillers, A., Cayrol, R., Arbour, N., Prat, A., 2008. The blood-brain barrier induces differentiation of migrating monocytes into Th17-polarizing dendritic cells. Brain 131, 785–799.

Inokuchi, Y., Nakajima, Y., Shimazawa, M., Kurita, T., Kubo, M., Saito, A., Sajiki, H., Kudo, T., Aihara, M., Imaizumi, K., Araie, M., Hara, H., 2009. Effect of an inducer of BiP, a molecular chaperone, on endoplasmic reticulum (ER) stress-induced retinal cell death. Investig. Ophthalmol. Vis. Sci. 50, 334–344.

Ioannidou, K., Anderson, K.I., Strachan, D., Edgar, J.M., Barnett, S.C., 2012. Time-Lapse Imaging of the Dynamics of CNS Glial-Axonal Interactions *In-Vitro* and *Ex-Vivo*. PLoS One 7, e30775.

J. Verspohl, E., Podlogar, J., 2012. LPS-Induced Proliferation and Chemokine Secretion from BEAS-2B Cells. Pharmacol. & Pharm. 03, 166–177.

Jäättelä, M., 1999. Heat shock proteins as cellular lifeguards. Ann. Med. 31, 261–71.

Jahng, A., Maricic, I., Aguilera, C., Cardell, S., Halder, R.C., Kumar, V., 2004. Prevention of autoimmunity by targeting a distinct, noninvariant CD1d-reactive T cell population reactive to sulfatide. J. Exp. Med. 199, 947–57.

Jana, N.R., Tanaka, M., Wang, G. h, Nukina, N., 2000. Polyglutamine length-dependent interaction of Hsp40 and Hsp70 family chaperones with truncated N-terminal huntingtin: their role in suppression of aggregation and cellular toxicity. Hum. Mol. Genet. 9, 2009–2018.

Jensen, P.E.H., Humle Jørgensen, S., Datta, P., Sørensen, P.S., 2004. Significantly increased fractions of transformed to total α2-macroglobulin concentrations in plasma from patients with multiple sclerosis. Biochim. Biophys. Acta - Mol. Basis Dis. 1690, 203–207.

Kakimura, J., Kitamura, Y., Taniguchi, T., Shimohama, S., Gebicke-Haerter, P.J., 2001. BiP/GRP78-Induced Production of Cytokines and Uptake of Amyloid-β (1-42) Peptide in Microglia. Biochem. Biophys. Res. Commun. 281, 6–10.

Kassenbrock, C.K., Kelly, R.B., 1989. Interaction of heavy chain binding protein (BiP/GRP78) with adenine nucleotides. EMBO J. 8, 1461–7.

Kawanokuchi, J., Shimizu, K., Nitta, A., Yamada, K., Mizuno, T., Takeuchi, H., Suzumura, A., 2008. Production and functions of IL-17 in microglia. J. Neuroimmunol. 194, 54–61.

Kelber, J.A., Panopoulos, A.D., Shani, G., Booker, E.C., Belmonte, J.C., Vale, W.W., Gray, P.C., 2009. Blockade of Cripto binding to cell surface GRP78 inhibits oncogenic Cripto signaling via MAPK/PI3K and Smad2/3 pathways. Oncogene 28, 2324–2336.

Kern, J., Untergasser, G., Zenzmaier, C., Sarg, B., Gastl, G., Gunsilius, E., Steurer, M., 2009. GRP-78 secreted by tumor cells blocks the antiangiogenic activity of bortezomib. Blood 114, 3960–3967.

Kettenmann, H., Verkhratsky, A. Glial Cells: Neuroglia 18.

Kim, D., Langmead, B., Salzberg, S.L., 2015. HISAT: a fast spliced aligner with low memory requirements. Nat. Methods 12, 357–60.

Kinnunen, T., Chamberlain, N., Morbach, H., Cantaert, T., Lynch, M., Preston-Hurlburt, P., Herold, K.C., Hafler, D.A., O'Connor, K.C., Meffre, E., 2013. Specific peripheral B cell tolerance defects in patients with multiple sclerosis. J. Clin. Invest. 123, 2737–2741.

Kirkham, B., Chaabo, K., Hall, C., Garrood, T., Mant, T., Allen, E., Vincent, A., Vasconcelos, J.C., Prevost, A.T., Panayi, G.S., Corrigall, V.M., 2016. Safety and patient response as indicated by biomarker changes to binding immunoglobulin protein in the phase I/IIA RAGULA clinical trial in rheumatoid arthritis. Rheumatol. (United Kingdom) 55, 1993–2000.

Kivisäkk, P., Healy, B.C., Viglietta, V., Quintana, F.J., Hootstein, M.A., Weiner, H.L., Khoury, S.J., 2009. Natalizumab treatment is associated with peripheral sequestration of proinflammatory T cells. Neurology 72, 1922–1930.

Kjer-Nielsen, L., Patel, O., Corbett, A.J., Le Nours, J., Meehan, B., Liu, L., Bhati, M., Chen, Z., Kostenko, L., Reantragoon, R., Williamson, N.A., Purcell, A.W., Dudek, N.L., McConville, M.J., O'Hair, R.A.J., Khairallah, G.N., Godfrey, D.I., Fairlie, D.P., Rossjohn, J., McCluskey, J., 2012. MR1 presents microbial vitamin B metabolites to MAIT cells. Nature 491, 717–723.

Klaver, R., Popescu, V., Voorn, P., Galis-De Graaf, Y., Van Der Valk, P., De Vries, H.E., Schenk, G.J., Geurts, J.J.G., 2015. Neuronal and Axonal Loss in Normal-Appearing Gray Matter and Subpial Lesions in Multiple Sclerosis. J Neuropathol Exp Neurol. 74(5), 453-8.

Kobayashi, Y., Kume, A., Li, M., Doyu, M., Hata, M., Ohtsuka, K., Sobue, G., 2000. Chaperones Hsp70 and Hsp40 Suppress Aggregate Formation and Apoptosis in Cultured Neuronal Cells Expressing Truncated Androgen Receptor Protein with Expanded Polyglutamine Tract. J. Biol. Chem. 275, 8772–8778.

Kudo, T., Kanemoto, S., Hara, H., Morimoto, N., Morihara, T., Kimura, R., Tabira, T., Imaizumi, K., Takeda, M., 2008. A molecular chaperone inducer protects neurons from ER stress. Cell Death Differ. 15(2), 364-75

La, X., Zhang, L., Li, H., Li, Z., Song, G., Yang, P., Yang, Y., 2018. Ajuba receptor mediates the internalization of tumor-secreted GRP78 into macrophages through different endocytosis pathways. Oncotarget 9, 15464–15479.

Lajoie, P., Snapp, E.L., 2011. Changes in BiP availability reveal hypersensitivity to acute endoplasmic reticulum stress in cells expressing mutant huntingtin. J. Cell Sci. 124, 3332–43.

Lamb, H. K., Mee, C., Xu, W., Liu, L., Blond, S., Cooper, A., Charles, I.G., Hawkins, A.R., 2006. The affinity of a major Ca2+ binding site on GRP78 is differentially enhanced by ADP and ATP. J. Biol. Chem. 281, 8796–805.

Lassmann, H., 2014. Mechanisms of white matter damage in multiple sclerosis. Glia 62, 1816–1830.

LeBlanc, R., Catley, L.P., Hideshima, T., Lentzsch, S., Mitsiades, C.S., Mitsiades, N., Neuberg, D., Goloubeva, O., Pien, C.S., Adams, J., Gupta, D., Richardson, P.G., Munshi, N.C., Anderson, K.C., 2002. Proteasome inhibitor PS-341 inhibits human myeloma cell growth in vivo and prolongs survival in a murine model. Cancer Res. 62, 4996–5000.

Lebrun, C., Bensa, C., Debouverie, M., Wiertlevski, S., Brassat, D., Seze, J. de, Rumbach, L., Pelletier, J., Labauge, P., Brochet, B., Tourbah, A., Clavelou, P., 2009. Association between Clinical Conversion to Multiple Sclerosis in Radiologically Isolated Syndrome and Magnetic Resonance Imaging, Cerebrospinal Fluid, and Visual Evoked Potential. Arch. Neurol. 66, 841.

Lee, A.S., 1987. Coordinated regulation of a set of genes by glucose and calcium ionophores in mammalian cells. Trends Biochem. Sci. 12, 20–23.

Lee, A.S., 2007. GRP78 Induction in Cancer: Therapeutic and Prognostic Implications. Cancer Res. 67, 3496–3499.

Lee, K., Tirasophon, W., Shen, X., Michalak, M., Prywes, R., Okada, T., Yoshida, H., Mori, K., Kaufman, R.J., 2002. IRE1-mediated unconventional mRNA splicing and S2P-mediated ATF6 cleavage merge to regulate XBP1 in signaling the unfolded protein response. Genes Dev. 16, 452–466. 2

Lee, Y.H., Bae, S.-C., Choi, S.J., Ji, J.D., Song, G.G., 2012. Genome-wide pathway analysis of genome-wide association studies on systemic lupus erythematosus and rheumatoid arthritis. Mol. Biol. Rep. 39, 10627–10635.

Lenz, N., Engler, O., Grandgirard, D., Leib, S.L., Ackermann-Gäumann, R., 2018. Evaluation of antivirals against tick-borne encephalitis virus in organotypic brain slices of rat cerebellum. PLoS One 13, e0205294.

Lesnick, T.G., Papapetropoulos, S., Mash, D.C., Ffrench-Mullen, J., Shehadeh, L., de Andrade, M., Henley, J.R., Rocca, W.A., Ahlskog, J.E., Maraganore, D.M., 2007. A Genomic Pathway Approach to a Complex Disease: Axon Guidance and Parkinson Disease. PLoS Genet. 3, e98.

Li, Q., Verma, I.M., 2002. NF-κB regulation in the immune system. Nat. Rev. Immunol. 2, 725–734.

Li, W.W., Hsiung, Y., Zhou, Y., Roy, B., Lee, A.S., 1997. Induction of the Mammalian GRP78/BiP Gene by Ca 2 Depletion and Formation of Aberrant Proteins: Activation of the Conserved Stress-Inducible grp Core Promoter Element by the Human Nuclear Factor YY1. Mol Cell Biol. 17(1), 54-60.

Li, Y., Guo, Y., Tang, J., Jiang, J., Chen, Z., 2014. New insights into the roles of CHOP-induced apoptosis in ER stress. Acta Biochim. Biophys. Sin. (Shanghai). 46, 629–640.

Li, Zongwei, Zhang, L., Zhao, Y., Li, H., Xiao, H., Fu, R., Zhao, C., Wu, H., Li, Zhuoyu, 2013. Cell-surface GRP78 facilitates colorectal cancer cell migration and invasion. Int. J. Biochem. Cell Biol. 45, 987–994.

Liao, Y., Smyth, G.K., Shi, W., 2013. The Subread aligner: fast, accurate and scalable read mapping by seed-and-vote. Nucleic Acids Res. 41, e108–e108.

Lindsay, S.L., Johnstone, S.A., McGrath, M.A., Mallinson, D., Barnett, S.C., 2016. Comparative miRNA-Based Fingerprinting Reveals Biological Differences in Human Olfactory Mucosa- and Bone-Marrow-Derived Mesenchymal Stromal Cells. Stem Cell Reports 6, 729–742.

Lindsay, S.L., Johnstone, S.A., Mountford, J.C., Sheikh, S., Allan, D.B., Clark, L., Barnett, S.C., 2013. Human mesenchymal stem cells isolated from olfactory biopsies but not bone enhance CNS myelination in vitro. Glia 61, 368–382.

Lister, R., O'Malley, R.C., Tonti-Filippini, J., Gregory, B.D., Berry, C.C., Millar, A.H., Ecker, J.R., 2008. Highly Integrated Single-Base Resolution Maps of the Epigenome in Arabidopsis. Cell 133, 523–536.

Liu, Y., Li, Z., Zhang, M., Deng, Y., Yi, Z., Shi, T., 2013. Exploring the pathogenetic association between schizophrenia and type 2 diabetes mellitus diseases based on pathway analysis. BMC Med. Genomics 2013 61 6, 1–14.

Llufriu-Dabén, G., Meffre, D., Massaad, C., Jafarian-Tehrani, M., 2019. A novel model of trauma-induced cerebellar injury and myelin loss in mouse organotypic cerebellar slice cultures using live imaging. J. Neurosci. Methods 311, 385–393.

Lossi, L., Alasia, S., Salio, C., Merighi, A., 2009. Cell death and proliferation in acute slices and organotypic cultures of mammalian CNS. Prog. Neurobiol. 88, 221–245.

Lu, F., Selak, M., O'Connor, J., Croul, S., Lorenzana, C., Butunoi, C., Kalman, B., 2000. Oxidative damage to mitochondrial DNA and activity of mitochondrial enzymes in chronic active lesions of multiple sclerosis. J. Neurol. Sci. 177, 95–103.

Lubetzki, C., Demerens, C., Angladet, P., Villarroya, H., Frankfurtert, A., Lee, M.-Y., Zalc, B., 1993. Even in culture, oligodendrocytes myelinate solely axons, Proc. Natl. Acad. Sci. USA. 90(14), 6820–6824.

Lucchinetti, C., Brück, W., Parisi, J., Scheithauer, B., Rodriguez, M., Lassmann, H., Heterogeneity, L.H., 2000. Heterogeneity of Multiple Sclerosis Lesions: Implications for the Pathogenesis of Demyelination. Ann Neurol. 47(6), 707-17.

Luo, L., Peng, G., Zhu, Y., Dong, H., Amos, C.I., Xiong, M., 2010. Genome-wide gene and pathway analysis. Eur. J. Hum. Genet. 18, 1045.

Luo, S., Baumeister, P., Yang, S., Abcouwer, S.F., Lee, A.S., 2003. Induction of Grp78/BiP by Translational Block Activation of the Grp78 promoter by Atf4 through an upstream Atf/Cre site independent of the endoplasmic reticulum stress elements*. J Biol Chem.278 (39), 37375-85.

Määttänen, P., Gehring, K., Bergeron, J.J.M., Thomas, D.Y., 2010. Protein quality control in the ER: The recognition of misfolded proteins. Semin. Cell Dev. Biol. 21, 500–511.

Macejak, D.G., Sarnow, P., 1991. Internal initiation of translation mediated by the 5′ leader of a cellular mRNA. Nature 353, 90–94.

Madhavan, M., Nevin, Z.S., Shick, H.E., Garrison, E., Clarkson-Paredes, C., Karl, M., Clayton, B.L.L., Factor, D.C., Allan, K.C., Barbar, L., Jain, T., Douvaras, P., Fossati, V., Miller, R.H., Tesar, P.J., 2018. Induction of myelinating oligodendrocytes in human cortical spheroids. Nat. Methods 15, 700–706.

Maggi, P., Cummings Macri, S.M., Gaitán, M.I., Leibovitch, E., Wholer, J.E., Knight, H.L., Ellis, M., Wu, T., Silva, A.C., Massacesi, L., Jacobson, S., Westmoreland, S., Reich, D.S., 2014. The formation of inflammatory demyelinated lesions in cerebral white matter. Ann. Neurol. 76, 594–608.

Magliozzi, R., Howell, O.W., Reeves, C., Roncaroli, F., Nicholas, R., Serafini, B., Aloisi, F., Reynolds, R., 2010. A Gradient of neuronal loss and meningeal inflammation in multiple sclerosis. Ann. Neurol. 68, 477–493.

Magrane, J., Smith, R.C., Walsh, K., Querfurth, H.W., 2004. Heat Shock Protein 70 Participates in the Neuroprotective Response to Intracellularly Expressed-Amyloid in Neurons. J. Neurosci. 24, 1700–1706.

Mahad, D., Ziabreva, I., Lassmann, H., Turnbull, D., 2008. Mitochondrial defects in acute multiple sclerosis lesions. Brain 131, 1722–1735.

Mahad, D.H., Trapp, B.D., Lassmann, H., 2015. Pathological mechanisms in progressive multiple sclerosis. Lancet Neurol. 14, 183–193.

Mamat, U., Wilke, K., Bramhill, D., Schromm, A.B., Lindner, B., Kohl, T.A., Corchero, J.L., Villaverde, A., Schaffer, L., Head, S.R., Souvignier, C., Meredith, T.C., Woodard, R.W., 2015. Detoxifying Escherichia coli for endotoxin-free production of recombinant proteins. Microb Cell Fact. 16, 14-57.

Mandel, M., Higa, A., 1970. Calcium-dependent bacteriophage DNA infection. J. Mol. Biol. 53, 159–162.

Mandolesi, G., Gentile, A., Musella, A., Fresegna, D., De Vito, F., Bullitta, S., Sepman, H., Marfia, G.A., Centonze, D., 2015. Synaptopathy connects inflammation and neurodegeneration in multiple sclerosis. Nat. Rev. Neurol. 11, 711–724.

Marín-Briggiler, C.I., González-Echeverría, M.F., Munuce, M.J., Ghersevich, S., Caille, A.M., Hellman, U., Corrigall, V.M., Vazquez-Levin, M.H., 2010a. Glucose-regulated protein 78 (Grp78/BiP) is secreted by human oviduct epithelial cells and the recombinant protein modulates sperm–zona pellucida binding. Fertil. Steril. 93, 1574–1584.

Marín-Briggiler, C.I., González-Echeverría, M.F., Munuce, M.J., Ghersevich, S., Caille, A.M., Hellman, U., Corrigall, V.M., Vazquez-Levin, M.H., 2010b. Glucose-regulated protein 78 (Grp78/BiP) is secreted by human oviduct epithelial cells and the recombinant protein modulates sperm-zona pellucida binding. Fertil. Steril. 93, 1574–1584.

Marín-Teva, J.L., Dusart, I., Colin, C., Gervais, A., van Rooijen, N., Mallat, M., 2004. Microglia promote the death of developing Purkinje cells. Neuron 41, 535–47.

Marioni, J.C., Mason, C.E., Mane, S.M., Stephens, M., Gilad, Y., 2008. RNA-seq: An assessment of technical reproducibility and comparison with gene expression arrays. Genome Res. 18, 1509–1517.

Maritsi, D., Stagikas, D., Charalabopoulos, K., Batistatou, A., 2006. What's new in p53? Hippokratia 10, 116–9.

Marksteiner, J., Humpel, C., 2008. Beta-amyloid expression, release and extracellular deposition in aged rat brain slices. Mol. Psychiatry 13, 939–952.

Matsushita, T., Yanaba, K., Bouaziz, J.-D., Fujimoto, M., Tedder, T.F., 2008. Regulatory B cells inhibit EAE initiation in mice while other B cells promote disease progression. J. Clin. Invest.118 (10), 3420-30.

Mayer, M.P., Bukau, B., 2005. Hsp70 chaperones: Cellular functions and molecular mechanism. Cell. Mol. Life Sci. 62, 670–684.

McCanney, G.A., Lindsay, S.L., McGrath, M.A., Willison, H.J., Moss, C., Bavington, C., Barnett, S.C., McCanney, G.A., Lindsay, S.L., McGrath, M.A., Willison, H.J., Moss, C., Bavington, C., Barnett, S.C., 2019. The Use of

Myelinating Cultures as a Screen of Glycomolecules for CNS Repair. Biology (Basel). 8, 52.

McMahon, J.M., McQuaid, S., Reynolds, R., Fitzgerald, U.F., 2012. Increased expression of ER stress- and hypoxia-associated molecules in grey matter lesions in multiple sclerosis. Mult. Scler. J. 18, 1437–1447.

Mecklenburg, N., Garcia-López, R., Puelles, E., Sotelo, C., Martinez, S., 2011. Cerebellar oligodendroglial cells have a mesencephalic origin. Glia 59, 1946–1957.

Melville, M.W., Tan, S.L., Wambach, M., Song, J., Morimoto, R.I., Katze, M.G., 1999. The cellular inhibitor of the PKR protein kinase, P58 (IPK), is an influenza virus-activated co-chaperone that modulates heat shock protein 70 activity. J. Biol. Chem. 274, 3797–803.

Meusser, B., Hirsch, C., Jarosch, E., Sommer, T., 2005. ERAD: The long road to destruction. Nat. Cell Biol. 7, 766–772.

Mháille, A.N., McQuaid, S., Windebank, A., Cunnea, P., McMahon, J., Samali, A., FitzGerald, U., 2008. Increased expression of endoplasmic reticulum stress-related signaling pathway molecules in multiple sclerosis lesions. J. Neuropathol. Exp. Neurol. 67, 200–211.

Michels, A.A., Kanon, B., Konings, A.W., Ohtsuka, K., Bensaude, O., Kampinga, H.H., 1997. Hsp70 and Hsp40 chaperone activities in the cytoplasm and the nucleus of mammalian cells. J. Biol. Chem. 272, 33283–9.

Miller, D., Barkhof, F., Montalban, X., Thompson, A., Filippi, M., 2005. Review clinically isolated syndromes suggestive of multiple sclerosis, part I: natural history, pathogenesis, diagnosis, and prognosis. Lancet Neurol. 4, 281–288.

Minami, Y., Höhfeld, J., Ohtsuka, K., Hartl, F.-U., 1996. Regulation of the Heat-shock Protein 70 Reaction Cycle by the Mammalian DnaJ Homolog, Hsp40. J. Biol. Chem. 271, 19617–19624.

Miron, V.E., Ludwin, S.K., Darlington, P.J., Jarjour, A.A., Soliven, B., Kennedy, T.E., Antel, J.P., 2010. Fingolimod (FTY720) Enhances Remyelination Following Demyelination of Organotypic Cerebellar Slices. Am. J. Pathol. 176, 2682–2694.

Misra, U.K., Deedwania, R., Pizzo, S.V., 2005. Binding of activated alpha2-macroglobulin to its cell surface receptor GRP78 in 1-LN prostate cancer cells regulates PAK-2-dependent activation of LIMK. J. Biol. Chem. 280, 26278–86.

Misselwitz, B., Staeck, O., Matlack, K.E.S., Rapoport, T.A., 1999. Interaction of BiP with the J-domain of the Sec63p component of the endoplasmic reticulum protein translocation complex. J. Biol. Chem. 274, 20110–20115.

Mizuno, Y., Fisher, A., Hanin, I., 2002. Mapping the progress of Alzheimer's and Parkinson's disease. Kluwer Academic/Plenum Publishers-Springer US. Ed-1, 51

Molofsky, A.V., Deneen, B., 2015. Astrocyte development: A Guide for the Perplexed. Glia. 63, 1320-1329

Morinaga, N., Yahiro, K., Matsuura, G., Moss, J., Noda, M., 2008. Subtilase cytotoxin, produced by Shiga-toxigenic Escherichia coli, transiently inhibits protein synthesis of Vero cells via degradation of BiP and induces cell cycle arrest at G1 by downregulation of cyclin D1. Cell. Microbiol. 10, 921–929.

Mortazavi, A., Williams, B.A., McCue, K., Schaeffer, L., Wold, B., 2008. Mapping and quantifying mammalian transcriptomes by RNA-Seq. Nat. Methods 5, 621–628.

Munro, S., Pelham, H.R., 1986. An Hsp70-like protein in the ER: identity with the 78 kd glucose-regulated protein and immunoglobulin heavy chain binding protein. Cell 46, 291–300.

Murphy, Á.C., Lalor, S.J., Lynch, M.A., Mills, K.H.G., 2010. Infiltration of Th1 and Th17 cells and activation of microglia in the CNS during the course of experimental autoimmune encephalomyelitis. Brain. Behav. Immun. 24, 641–651.

Murray, T.J., 2006. Diagnosis and treatment of multiple sclerosis. BMJ 332, 525–7.

Mycko, M.P., Brosnan, C.F., Raine, C.S., Fendler, W., Selmaj, K.W., 2012. Transcriptional profiling of microdissected areas of active multiple sclerosis lesions reveals activation of heat shock protein genes. J. Neurosci. Res. 90, 1941–1948.

Myhr, K.-M., Torkildsen, Ø., Lossius, A., Bø, L., Holmøy, T., 2019. B cell depletion in the treatment of multiple sclerosis. Expert Opin. Biol. Ther. 19, 261–271.

Nagalakshmi, U., Wang, Z., Waern, K., Shou, C., Raha, D., Gerstein, M., Snyder, M., 2008. The Transcriptional Landscape of the Yeast Genome Defined by RNA Sequencing. Science (80-). 320, 1344–1349.

Nakanishi, T., Shimazawa, M., Sugitani, S., Kudo, T., Imai, S., Inokuchi, Y., Tsuruma, K., Hara, H., 2013. Role of endoplasmic reticulum stress in light-induced photoreceptor degeneration in mice. J. Neurochem. 125, 111–124.

Nakatsuka, A., Wada, J., Iseda, I., Teshigawara, S., Higashio, K., Murakami, K., Kanzaki, M., Inoue, K., Terami, T., Katayama, A., Hida, K., Eguchi, J., Horiguchi, C.S., Ogawa, D., Matsuki, Y., Hiramatsu, R., Yagita, H., Kakuta, S., Iwakura, Y., Makino, H., 2012. Vaspin is an adipokine ameliorating ER stress in obesity as a ligand for cell-surface GRP78/MTJ-1 complex. Diabetes 61, 2823–32.

Napier, R.J., Adams, E.J., Gold, M.C., Lewinsohn, D.M., 2015. The Role of Mucosal Associated Invariant T Cells in Antimicrobial Immunity. Front. Immunol. 6, 344.

Napoli, I., Neumann, H., 2010. Protective effects of microglia in multiple sclerosis. Exp. Neurol. 225, 24–28.

Nash, B., Thomson, C.E., Linington, C., Arthur, A.T., McClure, J.D., McBride, M.W., Barnett, S.C., 2011. Functional Duality of Astrocytes in Myelination. J. Neurosci. 31, 13028–13038.

Naughton, M.C., McMahon, J.M., FitzGerald, U., 2015. Differential activation of ER stress pathways in myelinating cerebellar tracts. Int. J. Dev. Neurosci. 47, 347–360.

Nguyen, T.H., Law, D.T., Williams, D.B., 1991. Binding protein BiP is required for translocation of secretory proteins into the endoplasmic reticulum in Saccharomyces cerevisiae. Proc Natl Acad Sci USA 88, 1565–1569.

Ni, M., Lee, A.S., 2007. ER chaperones in mammalian development and human diseases. FEBS Lett. 581, 3641–3651.

Ni, M., Zhang, Y., Lee, A.S., 2011. Beyond the endoplasmic reticulum: atypical GRP78 in cell viability, signalling and therapeutic targeting. Biochem. J. 434, 181–188.

Niesen, F.H., Berglund, H., Vedadi, M., 2007. The use of differential scanning fluorimetry to detect ligand interactions that promote protein stability. Nat. Protoc. 2, 2212–2221.

Nishikawa, S.I., Fewell, S.W., Kato, Y., Brodsky, J.L., Endo, T., 2001. Molecular chaperones in the yeast endoplasmic reticulum maintain the solubility of proteins for retrotranslocation and degradation. J. Cell Biol. 153, 1061–1069.

Ochoa-Repáraz, J., Kirby, T.O., Kasper, L.H., 2018. The Gut Microbiome and Multiple Sclerosis. Cold Spring Harb. Perspect. Med. 8, a029017.

Odani, N., Negishi, M., Takahashi, S., Kitano, Y., Kozutsumi, Y., Ichikawa, A., 1996. Regulation of BiP gene expression by cyclopentenone prostaglandins through unfolded protein response element. J. Biol. Chem. 271, 16609–16613.

Oida, Y., Hamanaka, J., Hyakkoku, K., Shimazawa, M., Kudo, T., Imaizumi, K., Yasuda, T., Hara, H., 2010. Post-treatment of a BiP inducer prevents cell death after middle cerebral artery occlusion in mice. Neurosci. Lett. 484, 43–46.

Oida, Y., Izuta, H., Oyagi, A., Shimazawa, M., Kudo, T., Imaizumi, K., Hara, H., 2008. Induction of BiP, an ER-resident protein, prevents the neuronal death induced by transient forebrain ischemia in gerbil. Brain Res. 1208, 217–224.

Okonechnikov, K., Conesa, A., García-Alcalde, F., 2015. Qualimap 2: advanced multi-sample quality control for high-throughput sequencing data. Bioinformatics. 15, 32(2), 292-4.

Oksenberg, J.R., Baranzini, S.E., 2010. Multiple sclerosis geneticsĝ€"is the glass half full, or half empty? Nat. Rev. Neurol. 6, 429–439.

Okuda, D. T., Mowry, E. M., Cree, B. A., Crabtree, E. C., Goodin, D. S., Waubant, E., & Pelletier, D. (2011). Asymptomatic spinal cord lesions predict disease progression in radiologically isolated syndrome. Neurology, 76(8), 686–692.

Okuda, D.T., Mowry, E.M., Beheshtian, A., Waubant, E., Baranzini, S.E., Goodin, D.S., Hauser, S.L., Pelletier, D., 2009. Incidental MRI anomalies suggestive of multiple sclerosis: The radiologically isolated syndrome. Neurology 72, 800–805.

Otero, J.H., Lizák, B., Hendershot, L.M., 2010. Life and death of a BiP substrate. Semin. Cell Dev. Biol. 21, 472–8.

Oyadomari, S., Mori, M., 2004. Roles of CHOP/GADD153 in endoplasmic reticulum stress. Cell Death Differ. 11, 381–389.

Panayi, G.S., Corrigall, V.M., 2006. BiP regulates autoimmune inflammation and tissue damage. Autoimmun. Rev. 5, 140–142.

Paolicelli, R.C., Bolasco, G., Pagani, F., Maggi, L., Scianni, M., Panzanelli, P., Giustetto, M., Ferreira, T.A., Guiducci, E., Dumas, L., Ragozzino, D., Gross, C.T., 2011. Synaptic pruning by microglia is necessary for normal brain development. Science. 333, 1456–1458.

Park, Y.-J., Yoo, S.-A., Kim, W.-U., 2014. Role of Endoplasmic Reticulum Stress in Rheumatoid Arthritis Pathogenesis. J. Korean Med. Sci. 29, 2.

Parker Harp, C.R., Archambault, A.S., Sim, J., Ferris, S.T., Mikesell, R.J., Koni, P.A., Shimoda, M., Linington, C., Russell, J.H., Wu, G.F., 2015. B-Cell Antigen Presentation Is Sufficient To Drive Neuroinflammation in an Animal Model of Multiple Sclerosis. J. Immunol. 194, 5077–5084.

Parker, R., Phan, T., Baumeister, P., Roy, B., Cheriyath, V., Roy, A.L., Lee, A.S., 2001. Identification of TFII-I as the Endoplasmic Reticulum Stress Response Element Binding Factor ERSF: Its Autoregulation by Stress and Interaction with ATF6. Mol. Cell. Biol. 21, 3220–3233.

Parsell, D.A., Lindquist, S., 1993. The Function of Heat-Shock Proteins in Stress Tolerance: Degradation and Reactivation of Damaged Proteins. Annu. Rev. Genet. 27, 437–496.

Pashenkov, M., Huang, Y.M., Kostulas, V., Haglund, M., Söderström, M., Link, H., 2001. Two subsets of dendritic cells are present in human cerebrospinal fluid. Brain 124, 480–492.

Patil, C., Walter, P., 2001. Intracellular signaling from the endoplasmic reticulum to the nucleus: The unfolded protein response in yeast and mammals. Curr. Opin. Cell Biol. 13, 349–356.

Paton, A.W., Beddoe, T., Thorpe, C.M., Whisstock, J.C., Wilce, M.C.J., Rossjohn, J., Talbot, U.M., Paton, J.C., 2006. AB5 subtilase cytotoxin inactivates the endoplasmic reticulum chaperone BiP. Nature 443, 548–552.

Peters, A., Pitcher, L.A., Sullivan, J.M., Mitsdoerffer, M., Acton, S.E., Franz, B., Wucherpfennig, K., Turley, S., Carroll, M.C., Sobel, R.A., Bettelli, E., Kuchroo, V.K., 2011. Th17 Cells Induce Ectopic Lymphoid Follicles in Central Nervous System Tissue Inflammation. Immunity 35, 986–996.

Petrova, K., Oyadomari, S., Hendershot, L.M., Ron, D., 2008. Regulated association of misfolded endoplasmic reticulum lumenal proteins with P58/DNAJc3. EMBO J. 27, 2862–2872.

Piccioli, D., Sbrana, S., Melandri, E., Valiante, N.M., 2002. Contact-dependent Stimulation and Inhibition of Dendritic Cells by Natural Killer Cells. J. Exp. Med. 195, 335–341.

Pidoux, A.L., Armstrong, J., 1993. The BiP protein and the endoplasmic reticulum of Schizosaccharomyces pombe: fate of the nuclear envelope during cell division. J. Cell Sci. 1115–20.

Pieragostino, D., Del Boccio, P., Di Ioia, M., Pieroni, L., Greco, V., De Luca, G., D'Aguanno, S., Rossi, C., Franciotta, D., Centonze, D., Sacchetta, P., Di Ilio, C., Lugaresi, A., Urbani, A., 2013. Oxidative modifications of cerebral transthyretin are associated with multiple sclerosis. Proteomics 13, 1002–1009.

Pitt, D., Werner, P., Raine, C.S., 2000. Glutamate excitotoxicity in a model of multiple sclerosis. Nat. Med. 6, 67–70.

Pobre, K.F.R., Poet, G.J., Hendershot, L.M., 2019. The endoplasmic reticulum (ER) chaperone BiP is a master regulator of ER functions: Getting by with a little help from ERdj friends. J. Biol. Chem. 294, 2098–2108.

Popoff, V., Adolf, F., Brügger, B., Wieland, F., 2011. COPI budding within the Golgi stack. Cold Spring Harb. Perspect. Biol. 3, a005231.

Potentiates, E., Of, I., Hsieh, K., Wilke, N., Harris, A., Miles, M.F., 1996. Interaction of Ethanol with Inducers of Glucose-regulated 271, 2709–2716.

Prachasilchai, W., Sonoda, H., Yokota-Ikeda, N., Ito, K., Kudo, T., Imaizumi, K., Ikeda, M., 2009. The Protective Effect of a Newly Developed Molecular Chaperone–Inducer Against Mouse Ischemic Acute Kidney Injury. J. Pharmacol. Sci. 109, 311–314.

Preissler, S., Rato, C., Chen, R., Antrobus, R., Ding, S., Fearnley, I.M., Ron, D., 2015. AMPylation matches BiP activity to client protein load in the endoplasmic reticulum. Elife 4, 1–33.

Preziosa, P., Rocca, M.A., Mesaros, S., Meani, A., Montalban, X., Drulovic, J., Droby, A., Zipp, F., Calabrese, M., Sastre-Garriga, J., Dujmovic-Basuroski, I., Rovira, A., Filippi, M., 2018. Diagnosis of multiple sclerosis: a multicentre study to compare revised McDonald-2010 and Filippi-2010 criteria. J. Neurol. Neurosurg. Psychiatry 89, 316–318.

Price, B.D., Mannheim-Rodman, L.A., Calderwood, S.K., 1992. Brefeldin A, thapsigargin, and AlF4- stimulate the accumulation of GRP78 mRNA in a cycloheximide dependent manner, whilst induction by hypoxia is independent of protein synthesis. J. Cell. Physiol. 152, 545–552.

Printsev, I., Curiel, D., Carraway, K.L., 2017. Membrane Protein Quantity Control at the Endoplasmic Reticulum. J. Membr. Biol. 250, 379–392.

Qin, K., Ma, S., Li, H., Wu, M., Sun, Y., Fu, M., Guo, Z., Zhu, H., Gong, F., Lei, P., Shen, G., 2017. GRP78 impairs production of lipopolysaccharide-induced cytokines by interaction with CD14. Front. Immunol. 8, 1–11.

Quick, E.D., Seitz, S., Clarke, P., Tyler, K.L., 2017. Minocycline Has Anti-inflammatory Effects and Reduces Cytotoxicity in an Ex Vivo Spinal Cord Slice Culture Model of West Nile Virus Infection. J. Virol. 91, e00569-17.

Quinones, Q.J., de Ridder, G.G., Pizzo, S. V, 2008. GRP78: a chaperone with diverse roles beyond the endoplasmic reticulum. Histol. Histopathol. 23, 1409–16.

Rakic, P., 1971. Neuron-glia relationship during granule cell migration in developing cerebellar cortex. A Golgi and electonmicroscopic study in Macacus rhesus. J. Comp. Neurol. 141, 283–312.

Rauschert, N., Brändlein, S., Holzinger, E., Hensel, F., Müller-Hermelink, H.-K., Vollmers, H.P., 2008. A new tumor-specific variant of GRP78 as target for antibody-based therapy. Lab. Investig. 88, 375–386.

Ray, R., 2018. Escherichia coli Subtilase Cleaves Cell Surface GRP78 Preventing COOH-Terminal Domain Signaling. Cell Surf. GRP78, a New Paradig. Signal Transduct. Biol. 111–126.

Reddy, R.K., Mao, C., Baumeister, P., Austin, R.C., Kaufman, R.J., Lee, A.S., 2003. Endoplasmic reticulum chaperone protein GRP78 protects cells from apoptosis induced by topoisomerase inhibitors. Role of ATP binding site in suppression of caspase-7 activation. J. Biol. Chem. 278, 20915–20924.

Reich, D.S., Lucchinetti, C.F., Calabresi, P.A., 2018. Multiple Sclerosis. N. Engl. J. Med. 378, 169–180.

Reindl, M., Kuenz, B., Berger, T., 2009. B Cells and Antibodies in MS. Results Probl Cell Differ. 51, 99-113.

Resendez, E., Attenello, J.W., Grafsky, A., Chang, C.S., Lee, A.S., 1985. Calcium Ionophore A23187 Induces Expression of Glucose-Regulated Genes and Their Heterologous Fusion Genes. Mol Cell Biol. 5(6), 1212–1219

Resendez, E., Wooden, S.K., Lee, A.S., 1988. Identification of Highly Conserved Regulatory Domains and Protein-Binding Sites in the Promoters of the Rat and Human Genes Encoding the Stress-Inducible 78-Kilodalton Glucose-Regulated Protein. Mol Cell Biol. 8(10), 4579-84.

Reynders, T., D'haeseleer, M., De Keyser, J., Nagels, G., D'hooghe, M.B., 2017. Definition, prevalence and predictive factors of benign multiple sclerosis. eNeurologicalSci 7, 37–43.

Rodriguez, M., Pavelko, K.D., McKinney, C.W., Leibowitz, J.L., 1994. Recombinant human IL-6 suppresses demyelination in a viral model of multiple sclerosis. J. Immunol. 153, 3811–21.

Roe, N.D., Ren, J., 2013. Oxidative activation of Ca 2+ /calmodulin-activated kinase II mediates ER stress-induced cardiac dysfunction and apoptosis. Am. J. Physiol. Circ. Physiol. 304, H828–H839.

Romani, A.M.P., 2011. Cellular magnesium homeostasis. Arch. Biochem. Biophys. 512, 1–23.

Rosano, G.L., Ceccarelli, E.A., 2014. Recombinant protein expression in Escherichia coli: advances and challenges. Front. Microbiol. 5, 172.

Roy, B., Lee, A.S., 1995. Transduction of Calcium Stress through Interaction of the Human Transcription Factor CBF with the Proximal CCAAT Regulatory Element of the grp78/BiP Promoter, Mol Cell Biol. 15(4), 2263-74.

Sakono, M., Kidani, T., 2017. ATP-independent inhibition of amyloid beta fibrillation by the endoplasmic reticulum resident molecular chaperone GRP78. Biochem. Biophys. Res. Commun. 493, 500–503.

Schmid, S.L., 2003. Regulated portals of entry into the cell. Nature 422, 37–44.

Schmid, S.L., Braell, W.A., Rothman, J.E., 1985. ATP catalyzes the sequestration of clathrin during enzymatic uncoating. J. Biol. Chem. 260, 10057–10062.

Schmitt, J., Hess, H., Stunnenberg, H.G., 1993. Affinity purification of histidine-tagged proteins, Mol Biol Rep. 18, 223.

Schreiber, K., Magyari, M., Sellebjerg, F., Iversen, P., Garde, E., Madsen, C.G., Börnsen, L., Romme Christensen, J., Ratzer, R., Siebner, H.R., Laursen, B., Soelberg Sorensen, P., 2017. High-dose erythropoietin in patients with progressive multiple sclerosis: A randomized, placebo-controlled, phase 2 trial. Mult. Scler. J. 23, 675–685.

Schubert, D., Heinemann, S., Carlisle, W., Tarikas, H., Kimes, B., Patrick, J., Steinbach, J.H., Culp, W., Brandt, B.L., 1974. Clonal cell lines from the rat central nervous system. Nature 249, 224–227.

Schwarz, H., Schmittner, M., Duschl, A., Horejs-Hoeck, J., 2014. Residual endotoxin contaminations in recombinant proteins are sufficient to activate human CD1c+ dendritic cells. PLoS One 9, e113840.

Sekizar, S., Williams, A., 2019. Ex Vivo Slice Cultures to Study Myelination, Demyelination, and Remyelination in Mouse Brain and Spinal Cord. Humana Press, New York, NY, pp. 169–183.

Serafini, B., Rosicarelli, B., Magliozzi, R., Stigliano, E., Capello, E., Mancardi, G.L., Aloisi, F., 2006. Dendritic cells in multiple sclerosis lesions: Maturation stage, myelin uptake, and interaction with proliferating T cells. J. Neuropathol. Exp. Neurol. 65, 124–141.

Shani, G., Fischer, W.H., Justice, N.J., Kelber, J.A., Vale, W., Gray, P.C., 2008. GRP78 and Cripto Form a Complex at the Cell Surface and Collaborate To Inhibit Transforming Growth Factor Signaling and Enhance Cell Growth. Mol. Cell. Biol. 28, 666–677.

Sharma, R., Fischer, M.-T., Bauer, J., Felts, P.A., Smith, K.J., Misu, T., Fujihara, K., Bradl, M., Lassmann, H., 2010. Inflammation induced by innate immunity in the central nervous system leads to primary astrocyte dysfunction followed by demyelination. Acta Neuropathol. 120, 223–236.

Shen, P., Roch, T., Lampropoulou, V., O'Connor, R.A., Stervbo, U., Hilgenberg, E., Ries, S., Dang, V.D., Jaimes, Y., Daridon, C., Li, R., Jouneau, L., Boudinot, P., Wilantri, S., Sakwa, I., Miyazaki, Y., Leech, M.D., McPherson, R.C., Wirtz, S., Neurath, M., Hoehlig, K., Meinl, E., Grützkau, A., Grün, J.R., Horn, K., Kühl, A.A., Dörner, T., Bar-Or, A., Kaufmann, S.H.E., Anderton, S.M., Fillatreau, S., 2014. IL-35-producing B cells are critical regulators of immunity during autoimmune and infectious diseases. Nature 507, 366–370.

Shen, Y., Meunier, L., Hendershot, L.M., 2002. Identification and Characterization of a Novel Endoplasmic Reticulum (ER) DnaJ Homologue, Which Stimulates ATPase Activity of BiP in Vitro and Is Induced by ER Stress. J. Biol. Chem. 277, 15947–15956.

Sherafat, A., Hill, R.A., Nishiyama, A., 2018. Organotypic Slice Cultures to Study Oligodendrocyte Proliferation, Fate, and Myelination. Humana Press, New York, NY, pp. 145–156.

Shi, Y., Vattem, K.M., Sood, R., An, J., Liang, J., Stramm, L., Wek, R.C., 1998. Identification and Characterization of Pancreatic Eukaryotic Initiation Factor 2 alpha-Subunit Kinase, PEK, Involved in Translational Control. Mol. Cell. Biol. 18, 7499–7509.

Shibata, Y., Voeltz, G.K., Rapoport, T.A., 2006. Rough Sheets and Smooth Tubules. Cell 126, 435–439.

Shields, A.M., Panayi, G.S., Corrigall, V.M., 2011. Resolution-associated molecular patterns (RAMP): RAMParts defending immunological homeostasis? Clin. Exp. Immunol. 165, 292–300.

Shields, A.M., Panayi, G.S., Corrigall, V.M., 2012. A new-age for biologic therapies: Long-term drug-free therapy with BiP? Front Immunol. 3, 17.

Sidrauski, C., Walter, P., 1997. The transmembrane kinase Ire1p is a site-specific endonuclease that initiates mRNA splicing in the unfolded protein response. Cell 90, 1031–1039.

Sims, D., Sudbery, I., Ilott, N.E., Heger, A., Ponting, C.P., 2014. Sequencing depth and coverage: key considerations in genomic analyses. Nat. Rev. Genet. 15, 121–132.

Siva, A., Saip, S., Altintas, A., Jacob, A., Keegan, B., Kantarci, O., 2009. Multiple sclerosis risk in radiologically uncovered asymptomatic possible inflammatory-demyelinating disease. Mult. Scler. J. 15, 918–927.

Sorensen, A., Moffat, K., Thomson, C., Barnett, S.C., 2008. Astrocytes, but not olfactory ensheathing cells or Schwann cells, promote myelination of CNS axons in vitro. Glia 56, 750–763.

Sörgjerd, K., Ghafouri, B., Jonsson, B.-H., Kelly, J.W., Blond, S.Y., Hammarström, P., 2006. Retention of Misfolded Mutant Transthyretin by the Chaperone BiP/GRP78 Mitigates Amyloidogenesis. J. Mol. Biol. 356, 469–482.

Sospedra, M., Martin, R., 2005. Immunology of Multiple Sclerosis. Annu. Rev. Immunol. 23, 683–747.

Spaan, C.N., Smit, W.L., van Lidth de Jeude, J.F., Meijer, B.J., Muncan, V., van den Brink, G.R., Heijmans, J., 2019. Expression of UPR effector proteins ATF6 and XBP1 reduce colorectal cancer cell proliferation and stemness by activating PERK signaling. Cell Death Dis. 10, 490.

Srivastava, P.K., Binder, R.J., Harris, M.L., Ménoret, A., 2000. Saturation, competition, and specificity in interaction of heat shock proteins (hsp) gp96, hsp90, and hsp70 with CD11b+ cells. J Immunol. 165(5), 2582-7.

Stadelmann, C., Kerschensteiner, M., Misgeld, T., Brück, W., Hohlfeld, R., Lassmann, H., 2002. BDNF and gp145trkB in multiple sclerosis brain lesions: Neuroprotective interactions between immune and neuronal cells? Brain 125, 75–85.

Stassart, R.M., Möbius, W., Nave, K.-A., Edgar, J.M., 2018. The Axon-Myelin Unit in Development and Degenerative Disease. Front. Neurosci. 12, 467.

Subedi, G.P., Johnson, R.W., Moniz, H.A., Moremen, K.W., Barb, A., 2015. High Yield Expression of Recombinant Human Proteins with the Transient Transfection of HEK293 Cells in Suspension. J. Vis. Exp. e53568.

Suzuki, C.K., Bonifacino, J.S., Lin, A.Y., Davis, M.M., Klausner, R.D., 1991. Regulating the retention of T-cell receptor alpha chain variants within the endoplasmic reticulum: Ca(2+)-dependent association with BiP. J. Cell Biol. 114, 189–205.

Svenningsen, Å.F., Shan, W.-S., Colman, D.R., Pedraza, L., 2003. Rapid method for culturing embryonic neuron-glial cell cocultures. J. Neurosci. Res. 72, 565–573.

Synofzik, M., Haack, T.B., Kopajtich, R., Gorza, M., Rapaport, D., Greiner, M., Schönfeld, C., Freiberg, C., Schorr, S., Holl, R.W., Gonzalez, M.A., Fritsche, A., Fallier-Becker, P., Zimmermann, R., Strom, T.M., Meitinger, T., Züchner, S., Schüle, R., Schöls, L., Prokisch, H., 2014. Absence of BiP Co-chaperone DNAJC3 Causes Diabetes Mellitus and Multisystemic Neurodegeneration. Am. J. Hum. Genet. 95, 689–697.

Takemoto, H., Yoshimori, T., Yamamoto, A., Miyata, Y., Yahara, I., Inoue, K., Tashiro, Y., 1992. Heavy chain binding protein (BiP/GRP78) and endoplasmin are exported from the endoplasmic reticulum in rat exocrine pancreatic cells, similar to protein disulfide-isomerase. Arch. Biochem. Biophys. 296, 129–136.

Takeuchi, H., Kobayashi, Y., Yoshihara, T., Niwa, J., Doyu, M., Ohtsuka, K., Sobue, G., 2002. Hsp70 and Hsp40 improve neurite outgrowth and suppress intracytoplasmic aggregate formation in cultured neuronal cells expressing mutant SOD1. Brain Res. 949, 11–22.

Tan, G.A., Furber, K.L., Thangaraj, M.P., Sobchishin, L., Doucette, J.R., Nazarali, A.J., 2018. Organotypic Cultures from the Adult CNS: A Novel

Model to Study Demyelination and Remyelination Ex Vivo. Cell. Mol. Neurobiol. 38, 317–328.

Tang, Y., Jiang, Q., Ou, Y., Zhang, F., Qing, K., Sun, Y., Lu, W., Zhu, H., Gong, F., Lei, P., Shen, G., 2016. BIP induces mice CD19hi regulatory B cells producing IL-10 and highly expressing PD-L1, FasL. Mol. Immunol. 69, 44–51.

Tanimukai, H., Kanayama, D., Omi, T., Takeda, M., Kudo, T., 2013. Paclitaxel induces neurotoxicity through endoplasmic reticulum stress. Biochem. Biophys. Res. Commun. 437, 151–155.

Tao, J., Sha, B., 2011. Structural Insight into the Protective Role of P58 (IPK) during Unfolded Protein Response. Methods Enzymol. 490, 259–270.

Tatar, M., Khazaeli, A.A., Curtsinger, J.W., 1997. Chaperoning extended life. Nature 390, 30–30.

Terasaki, M., Shemesh, T., Kasthuri, N., Klemm, R.W., Schalek, R., Hayworth, K.J., Hand, A.R., Yankova, M., Huber, G., Lichtman, J.W., Rapoport, T.A., Kozlov, M.M., 2013. XStacked endoplasmic reticulum sheets are connected by helicoidal membrane motifs. Cell 154, 285–296.

Thetiot, M., Ronzano, R., Aigrot, M.-S., Lubetzki, C., Desmazières, A., 2019. Preparation and Immunostaining of Myelinating Organotypic Cerebellar Slice Cultures. J. Vis. Exp. e59163.

Thompson, A.J., Banwell, B.L., Barkhof, F., Carroll, W.M., Coetzee, T., Comi, G., Correale, J., Fazekas, F., Filippi, M., Freedman, M.S., Fujihara, K., Galetta, S.L., Hartung, H.P., Kappos, L., Lublin, F.D., Marrie, R.A., Miller, A.E., Miller, D.H., Montalban, X., Mowry, E.M., Sorensen, P.S., Tintoré, M., Traboulsee, A.L., Trojano, M., Uitdehaag, B.M.J., Vukusic, S., Waubant, E., Weinshenker, B.G., Reingold, S.C., Cohen, J.A., 2018. Diagnosis of multiple sclerosis: 2017 revisions of the McDonald criteria. Lancet Neurol. 17, 162–173.

Thomson, C.E., Griffiths, I.R., McCulloch, M.C., Kyriakides, E., Barrie, J.A., Montague, P., 1993. In vitro studies of axonally-regulated Schwann cell genes during Wallerian degeneration. J. Neurocytol. 22, 590–602.

Thomson, C.E., Hunter, A.M., Griffiths, I.R., Edgar, J.M., McCulloch, M.C., 2006. Murine spinal cord explants: A model for evaluating axonal growth and myelination in vitro. J. Neurosci. Res. 84, 1703–1715.

Thomson, C.E., McCulloch, M., Sorenson, A., Barnett, S.C., Seed, B. V., Griffiths, I.R., McLaughlin, M., 2008. Myelinated, synapsing cultures of murine spinal cord - validation as an in vitro model of the central nervous system. Eur. J. Neurosci. 28, 1518–1535.

Toledo, H., Carlino, A, Vidal, V., Redfield, B., Nettleton, M.Y., Kochan, J.P., Brot, N., Weissbach, H., 1993. Dissociation of glucose-regulated protein Grp78 and Grp78-IgE Fc complexes by ATP. Proc. Natl. Acad. Sci. U. S. A. 90, 2505–8.

Trebst, C., Sørensen, T.L., Kivisäkk, P., Cathcart, M.K., Hesselgesser, J., Horuk, R., Sellebjerg, F., Lassmann, H., Ransohoff, R.M., 2001. CCR1+/CCR5+ mononuclear phagocytes accumulate in the central nervous system of patients with multiple sclerosis. Am. J. Pathol. 159, 1701–1710.

Tremblay, M.È., Majewska, A.K., 2011. A role for microglia in synaptic plasticity? Commun. Integr. Biol. 4, 220–222.

Triantafilou, K., Fradelizi, D., Wilson, K., Triantafilou, M., 2002. GRP78, a coreceptor for coxsackievirus A9, interacts with major histocompatibility complex class I molecules which mediate virus internalization. J. Virol. 76, 633–43.

Tsai, Y.L., Lee, A.S., 2018. Cell Surface GRP78: Anchoring and Translocation Mechanisms and Therapeutic Potential in Cancer, in: Cell Surface GRP78, a New Paradigm in Signal Transduction Biology. 41-62

Tsai, Y.-L., Zhang, Y., Tseng, C.-C., Stanciauskas, R., Pinaud, F., Lee, A.S., 2015. Characterization and Mechanism of Stress-induced Translocation of 78-Kilodalton Glucose-regulated Protein (GRP78) to the Cell Surface. J Biol Chem. 290(13), 8049-64

Tsunemi, S., Nakanishi, T., Fujita, Y., Bouras, G., Miyamoto, Y., Miyamoto, A., Nomura, E., Takubo, T., Tanigawa, N., 2010. Proteomics-based identification of a tumor-associated antigen and its corresponding autoantibody in gastric cancer. Oncol. Rep. 23, 949–56.

Van Kaer, L., Wu, L., Parekh, V. V., 2015. Natural killer T cells in multiple sclerosis and its animal model, experimental autoimmune encephalomyelitis. Immunology 146, 1–10.

Vela, J.M., Dalmau, I., González, B., Castellano, B., 1995. Morphology and distribution of microglial cells in the young and adult mouse cerebellum. J. Comp. Neurol. 361, 602–616.

Veto, S., Acs, P., Bauer, J., Lassmann, H., Berente, Z., Setalo, G., Borgulya, G., Sumegi, B., Komoly, S., Gallyas, F., Illes, Z., 2010. Inhibiting poly (ADP-ribose) polymerase: a potential therapy against oligodendrocyte death. Brain 133, 822–834.

Vig, S., Buitinga, M., Rondas, D., Crèvecoeur, I., van Zandvoort, M., Waelkens, E., Eizirik, D.L., Gysemans, C., Baatsen, P., Mathieu, C., Overbergh, L., 2019. Cytokine-induced translocation of GRP78 to the plasma membrane triggers a pro-apoptotic feedback loop in pancreatic beta cells. Cell Death Dis. 10.

Vitale, M., Bakunts, A., Orsi, A., Lari, F., Tadè, L., Danieli, A., Rato, C., Valetti, C., Sitia, R., Raimondi, A., Christianson, J.C., van Anken, E., 2019. Inadequate BiP availability defines endoplasmic reticulum stress. eLife, 8,e41168

Vitale, M., Della Chiesa, M., Carlomagno, S., Pende, D., Aricò, M., Moretta, L., Moretta, A., 2005. NK-dependent DC maturation is mediated by TNFα and IFNγ released upon engagement of the NKp30 triggering receptor. Blood 106, 566–571.

Vivoli, M., Novak, H.R., Littlechild, J.A., Harmer, N.J., 2014. Determination of Protein-ligand Interactions Using Differential Scanning Fluorimetry. J. Vis. Exp. e51809–e51809.

Voeltz, G.K., Rolls, M.M., Rapoport, T.A., 2002. Structural organization of the endoplasmic reticulum. EMBO Rep. 3, 944–50.

Vogel, J.P., Misra, L.M., Rose, M.D., 1990. Loss of BiP/GRP78 function blocks translocation of secretory proteins in yeast. J. Cell Biol. 110, 1885–1895.

von Büdingen, H.C., Gulati, M., Kuenzle, S., Fischer, K., Rupprecht, T.A., Goebels, N., 2010. Clonally expanded plasma cells in the cerebrospinal fluid of

patients with central nervous system autoimmune demyelination produce "oligoclonal bands." J. Neuroimmunol. 218, 134–139.

Voogd, J., Glickstein, M., 1998. The anatomy of the cerebellum. Trends Neurosci. 21, 370–5.

Wake, H., Moorhouse, A.J., Jinno, S., Kohsaka, S., Nabekura, J., 2009. Resting microglia directly monitor the functional state of synapses in vivo and determine the fate of ischemic terminals. J. Neurosci. 29, 3974–3980.

Walter, P., 2011. The Unfolded Protein Response : 1081.

Wang, J., Lee, J., Liem, D., Ping, P., 2017. HSPA5 Gene encoding Hsp70 chaperone BiP in the endoplasmic reticulum. Gene 618, 14–23.

Wei, J., Hendershot, L.M., 1995. Cell Biology and Metabolism : Characterization of the Nucleotide Binding Properties and ATPase Activity of Recombinant Hamster BiP Purified from Bacteria Characterization of the Nucleotide Binding Properties and ATPase Activity of Recombinant Hamster BiP 270, 26670–26676.

Wiest, D.L., Bhandoola, A., Punt, J., Kreibich, G., McKean, D., Singer, A., 1997. Incomplete endoplasmic reticulum (ER) retention in immature thymocytes as revealed by surface expression of " ER-resident" molecular chaperones. Proc. Natl. Acad. Sci. U. S. A. 94, 1884–9.

Witte, M.E., Mahad, D.J., Lassmann, H., van Horssen, J., 2014. Mitochondrial dysfunction contributes to neurodegeneration in multiple sclerosis. Trends Mol. Med. 20, 179–187.

Wu, G.F., Alvarez, E., 2011. The immunopathophysiology of multiple sclerosis. Neurol. Clin. 29, 257–78.

Xiang, W., Ke, Z., Zhang, Y., Ho-Yuet Cheng, G., Irwan, I.D., Sulochana, K.N., Potturi, P., Wang, Z., Yang, H., Wang, J., Zhuo, L., Kini, R.M., Ge, R., 2011. Isthmin is a novel secreted angiogenesis inhibitor that inhibits tumour growth in mice. J. Cell. Mol. Med. 15, 359–374.

Xiao, D., Ohlendorf, J., Chen, Y., Taylor, D.D., Rai, S.N., Waigel, S., Zacharias, W., Hao, H., McMasters, K.M., 2012. Identifying mRNA, MicroRNA and Protein Profiles of Melanoma Exosomes. PLoS One 7, e46874.

Xiao, G., Chung, T.-F., Pyun, H.Y., Fine, R.E., Johnson, R.J., 1999. KDEL proteins are found on the surface of NG108-15 cells. Mol. Brain Res. 72, 121–128.

Xie, C., Li, Z., Zhang, G.-X., Guan, Y., 2014. Wnt Signaling in Remyelination in Multiple Sclerosis: Friend or Foe? Mol. Neurobiol. 49, 1117–1125.

Yamamoto, Y., Gaynor, R.B., 2004. IκB kinases: key regulators of the NF-κB pathway. Trends Biochem. Sci. 29, 72–79.

Yan, J., Greer, J.M., 2008. NF-kappa B, a potential therapeutic target for the treatment of multiple sclerosis. CNS Neurol. Disord. Drug Targets 7, 536–57.

Yang, J., Nune, M., Zong, Y., Zhou, L., Liu, Q., 2015. Close and Allosteric Opening of the Polypeptide-Binding Site in a Human Hsp70 Chaperone BiP. Structure 23, 2191–2203.

Yang, M., Zhang, F., Qin, K., Wu, M., Li, H., Zhu, H., Ning, Q., Lei, P., Shen, G., 2016. Glucose-Regulated Protein 78-Induced Myeloid Antigen-Presenting Cells Maintained Tolerogenic Signature upon LPS Stimulation. Front. Immunol. 7, 552.

Yin, Y., Chen, C., Chen, J., Zhan, R., Zhang, Q., Xu, X., Li, D., Li, M., 2017. Cell surface GRP78 facilitates hepatoma cells proliferation and migration by activating IGF-IR. Cell. Signal. 35, 154–162.

Ying Liu, †, Sebastian C. J. Steiniger, †, YoungSoo Kim, †, Gunnar F. Kaufmann, †, Brunhilde Felding-Habermann, ‡ and, Kim D. Janda*, †,§, 2007. Mechanistic Studies of a Peptidic GRP78 Ligand for Cancer Cell-Specific Drug Delivery. Mol Pharm. 4(3), 435-47.

Yoo, S.-A., You, S., Yoon, H.-J., Kim, D.-H., Kim, H.-S., Lee, K., Ahn, J.H., Hwang, D., Lee, A.S., Kim, K.-J., Park, Y.-J., Cho, C.-S., Kim, W.-U., 2012. A novel pathogenic role of the ER chaperone GRP78/BiP in rheumatoid arthritis. J. Exp. Med. 209, 871–86.

Yoshida, H., Matsui, T., Yamamoto, A., Okada, T., Mori, K., 2001a. XBP1 mRNA is induced by ATF6 and spliced by IRE1 in response to ER stress to produce a highly active transcription factor. Cell 107, 881–891.

Yoshida, H., Matsui, T., Yamamoto, A., Okada, T., Mori, K., 2001b. XBP1 mRNA Is Induced by ATF6 and Spliced by IRE1 in Response to ER Stress to Produce a Highly Active Transcription Factor. Cell 107, 881–891.

Yoshida, H., Okada, T., Haze, K., Yanagi, H., Yura, T., Negishi, M., Mori, K., 2001c. Endoplasmic Reticulum Stress-Induced Formation of Transcription Factor Complex ERSF Including NF-Y (CBF) and Activating Transcription Factors 6 and 6 That Activates the Mammalian Unfolded Protein Response. Mol. Cell. Biol. 21, 1239–1248.

Yu, M., Haslam, R.H.A., Haslam, D.B., 2000. HEDJ, an Hsp40 Co-chaperone Localized to the Endoplasmic Reticulum of Human Cells. J. Biol. Chem. 275, 24984–24992.

Yurinskaya, M., Zatsepina, O.G., Vinokurov, M.G., Bobkova, N. V, Garbuz, D.G., Morozov, A. V, Kulikova, D.A., Mitkevich, V.A., Makarov, A.A., Funikov, S.Y., Evgen'ev, M.B., 2015. The Fate of Exogenous Human HSP70 Introduced into Animal Cells by Different Means. Curr. Drug Deliv. 12, 524–32.

Zhang, H., Jarjour, A.A., Boyd, A., Williams, A., 2011. Central nervous system remyelination in culture -A tool for multiple sclerosis research. Exp. Neurol. 230, 138–148.

Zhang, Y., Liu, R., Ni, M., Gill, P., Lee, A.S., 2010. Cell surface relocalization of the endoplasmic reticulum chaperone and unfolded protein response regulator GRP78/BiP. J. Biol. Chem. 285, 15065–15075.

Zhang, Y., Tseng, C.-C., Tsai, Y.-L., Fu, X., Schiff, R., Lee, A.S., 2013. Cancer Cells Resistant to Therapy Promote Cell Surface Relocalization of GRP78 Which Complexes with PI3K and Enhances PI (3, 4, 5) P3 Production. PLoS One 8, e80071.

Ziabreva, I., Campbell, G., Rist, J., Zambonin, J., Rorbach, J., Wydro, M.M., Lassmann, H., Franklin, R.J.M., Mahad, D., 2010. Injury and differentiation following inhibition of mitochondrial respiratory chain complex IV in rat oligodendrocytes. Glia 58, 1827–1837.

Ziegler-Heitbrock, H.W., Möller, A., Linke, R.P., Haas, J.G., Rieber, E.P., Riethmüller, G., 1986. Tumor necrosis factor as effector molecule in monocyte mediated cytotoxicity. Cancer Res. 46, 5947–52.

Zimmermann, R., Eyrisch, S., Ahmad, M., Helms, V., 2011. Protein translocation across the ER membrane. Biochim. Biophys. Acta - Biomembr. 1808, 912–924.

Zozulya, A.L., Wiendl, H., 2008. The role of regulatory T cells in multiple sclerosis. Nat. Clin. Pract. Neurol. 4, 384–398.

Appendix

Score	Expect	Method	Identities	Positives	Gaps
1308 bits(3385)	0.0	Compositional matrix adjust.	644/654(98%)	648/654(99%)	0/654(0%)

```
Query   1    MKLSLVAAMLLLLSAARAEEEDKKEDVGTVVGIDLGTTYSCVGVFKNGRVEIIANDQGNR   60
Sbjct   1    ..FTV...A....C.V............................................   60

Query   61   ITPSYVAFTPEGERLIGDAAKNQLTSNPENTVFDAKRLIGRTWNDPSVQQDIKFLPFKVV   120
Sbjct   61   ............................................................   120

Query   121  EKKTKPYIQVDIGGGQTKTFAPEEISAMVLTKMKETAEAYLGKKVTHAVVTVPAYFNDAQ   180
Sbjct   121  ............................................................   180

Query   181  RQATKDAGTIAGLNVMRIINEPTAAAIAYGLDKREGEKNILVFDLGGGTFDVSLLTIDNG   240
Sbjct   181  ............................................................   240

Query   241  VFEVVATNGDTHLGGEDFDQRVMEHFIKLYKKKTGKDVRKDNRAVQKLRREVEKAKRALS   300
Sbjct   241  ............................................................   300

Query   301  SQHQARIEIESFYEGEDFSETLTRAKFEELNMDLFRSTMKPVQKVLEDSDLKKSDIDEIV   360
Sbjct   301  ...........F................................................   360

Query   361  LVGGSTRIPKIQQLVKEFFNGKEPSRGINPDEAVAYGAAVQAGVLSGDQDTGDLVLLDVC   420
Sbjct   361  ............................................................   420

Query   421  PLTLGIETVGGVMTKLIPRNTVVPTKKSQIFSTASDNQPTVTIKVYEGERPLTKDNHLLG   480
Sbjct   421  ............................................................   480

Query   481  TFDLTGIPPAPRGVPQIEVTFEIDVNGILRVTAEDKGTGNKNKITITNDQNRLTPEEIER   540
Sbjct   481  ............................................................   540

Query   541  MVNDAEKFAEEDKKLKERIDTRNELESYAYSLKNQIGDKEKLGGKLSSEDKETMEKAVEE   600
Sbjct   541  .......................................P............         600

Query   601  KIEWLESHQDADIEDFKAKKKELEEIVQPIISKLYGSAGPPPTGEEDTAEKDEL   654
Sbjct   601  .......................................G.........S.....   654
```

Figure A 1.1: A comparision of the amino acid sequence of the Homosapiens BiP (https://www.uniprot.org/uniprot/P11021) and the Rattus Norvegicus BiP (https://www.uniprot.org/uniprot/P06761). Query (Homosapiens-Human BiP), Sbjct (Rattus Norvegicus-Rat BiP) were aligned using BlastP and identities are shown as dots, mismatches are shown in red.

Score		Expect	Identities	Gaps	Strand
2654 bits(1437)		0.0	1789/1965(91%)	0/1965(0%)	Plus/Plus

```
Query  1     ATGAAGCTCTCCCTGGTGGCCGCGATGCTGCTGCTGCTCAGCGCGGCGCGGGCCGAGGAG  60
Sbjct  1     ......T..A.TG.......G...GC............GT.T....T......G......  60

Query  61    GAGGACAAGAAGGAGGACGTGGGCACGGTGGTCGGCATCGACCTGGGGACCACCTACTCC  120
Sbjct  61    .................T..A.........T.........T............T...   120

Query  121   TGCGTCGGCGTGTTCAAGAACGGCCGCGTGGAGATCATCGCCAACGATCAGGGCAACCGC  180
Sbjct  121   ........T..A..............................A...............   180

Query  181   ATCACGCCGTCCTATGTCGCCTTCACTCCTGAAGGGGAACGTCTGATTGGCGATGCCGCC  240
Sbjct  181   .....A.....G.....G................G...................G...   240

Query  241   AAGAACCAGCTCACCTCCAACCCCGAGAACACGGTCTTTGACGCCAAGCGGCTCATCGGC  300
Sbjct  241   ........A.....G........G.....C.....C...........C.......A   300

Query  301   CGCACGTGGAATGACCCGTCTGTGCAGCAGGACATCAAGTTCTTGCCGTTCAAGGTGGTT  360
Sbjct  301   .....T...........T..C.....................A...............   360

Query  361   GAAAAGAAAACTAAACCATACATTCAAGTTGATATTGGAGGTGGGCAAACAAAGACATTT  420
Sbjct  361   .....................T.........C...........C............   420

Query  421   GCTCCTGAAGAAATTTCTGCCATGGTTCTCACTAAAATGAAAGAAACCGCTGAGGCTTAT  480
Sbjct  421   ..C..A.........T.................G.....T.C.....G...   480

Query  481   TTGGGAAAGAAGGTTACCCATGCAGTTGTTACTGTACCAGCCTATTTTAATGATGCCCAA  540
Sbjct  481   ...............C...........G.........T..C..C.........A..G   540

Query  541   CGCCAAGCAACCAAAGACGCTGGAACTATTGCTGGCCTAAATGTTATGAGGATCATCAAC  600
Sbjct  541   ..G..........G..T.....C..........A..G.....C.............T   600

Query  601   GAGCCTACGGCAGCTGCTATTGCTTATGGCCTGGATAAGAGGGAGGGGGAGAAGAACATC  660
Sbjct  601   .....A..A...........A............A.....A...............   660

Query  661   CTGGTGTTTGACCTGGGTGGCGGAACCTTCGATGTGTCTCTTCTCACCATTGACAATGGT  720
Sbjct  661   ..C...............T...............................   720

Query  721   GTCTTCGAAGTTGTGGCCACTAATGGAGATACTCATCTGGGTGGAGAAGACTTTGACCAG  780
Sbjct  721   .....T.....G.................C.................G.........T...  780

Query  781   CGTGTCATGGAACACTTCATCAAACTGTACAAAAAGAAGACGGGCAAAGATGTCAGGAAA  840
Sbjct  781   ..G.......G..........G.................T..G...........A..G   840

Query  841   GACAATAGAGCTGTGCAGAAACTCCGGCGCGAGGTAGAAAAGGCCAAACGGGCCCTGTCT  900
Sbjct  841   .....C...................T...............GA.A.........   900

Query  901   TCTCAGCATCAAGCAAGAATTGAAATTGAGTCCTTCTATGAAGGAGAAGACTTTTCTGAG  960
Sbjct  901   ..............G..G..................TC...............C..A...  960

Query  961   ACCCTGACTCGGGCCAAATTTGAAGAGCTCAACATGGATCTGTTCCGGTCTACTATGAAG  1020
Sbjct  961   .....T.....................G........C.......C.....C.....A  1020

Query  1021  CCCGTCCAGAAAGTGTTGGAAGATTCTGATTTGAAGAAGTCTGATATTGATGAAATTGTT  1080
Sbjct  1021  ..T...............C.....C.....A............G.....  1080

Query  1081  CTTGTTGGTGGCTCGACTCGAATTCCAAAGATTCAGCAACTGGTTAAAGAGTTCTTCAAT  1140
Sbjct  1081  ..G.....C..A..T.............GT....G.............  1140

Query  1141  GGCAAGGAACCATCCCGTGGCATAAACCCAGATGAAGCTGTAGCGTATGGTGCTGCTGTC  1200
Sbjct  1141  ........G..G..........C.........G.......A.......C.....  1200

Query  1201  CAGGCTGGTGTGCTCTCTGGTGATCAAGATACAGGTGACCTGGTACTGCTTGATGTATGT  1260
Sbjct  1201  ..........C...........................T.........G...  1260

Query  1261  CCCCTTACACTTGGTATTGAAACTGTGGGAGGTGTCATGACCAAACTGATTCCAAGGAAC  1320
Sbjct  1261  ..T.............................A...........G......  1320

Query  1321  ACAGTGGTGCCTACCAAGAAGTCTCAGATCTTTTCTACAGCTTCTGATAATCAACCAACT  1380
Sbjct  1321  ..T........C...................C..C...........G..C..C  1380

Query  1381  GTTACAATCAAGGTCTATGAAGGTGAAAGACCCCTGACAAAAGACAATCATCTTCTGGGT  1440
Sbjct  1381  ..A.............C........C...............C.........  1440

Query  1441  ACATTTGATCTGACTGGAATTCCTCCTGCTCCTCGTGGGGTCCCACAGATTGAAGTCACC  1500
Sbjct  1441  ....................C...........C.......A..C.............  1500
```

259

```
Query  1501  TTTGAGATAGATGTGAATGGTATTCTTCGAGTGACAGCTGAAGACAAGGGTACAGGGAAC  1560
Sbjct  1501  .................................................A..G.....A...  1560

Query  1561  AAAAATAAGATCACAATCACCAATGACCAGAATCGCCTGACACCTGAAGAAATCGAAAGG  1620
Sbjct  1561  .....C..A....C..............A..C........C...........T.....  1620

Query  1621  ATGGTTAATGATGCTGAGAAGTTTGCTGAGGAAGACAAAAAGCTCAAGGAGCGCATTGAT  1680
Sbjct  1621  .....C.....C..C.................................A...........C  1680

Query  1681  ACTAGAAATGAGTTGGAAAGCTATGCCTATTCTCTAAAGAATCAGATTGGAGATAAAGAA  1740
Sbjct  1681  ..G..G.....A..............T..C.....T.....C.....C...........G  1740

Query  1741  AAGCTGGGAGGTAAACTTTCCTCTGAAGATAAGGAGACCATGGAAAAAGCTGTAGAAGAA  1800
Sbjct  1741  ..............G..G..TC.........A.........G...........G...  1800

Query  1801  AAGATTGAATGGCTGGAAAGCCACCAAGATGCTGACATTGAAGACTTCAAAGCTAAGAAG  1860
Sbjct  1801  .....C...............G.....A.............T........A...  1860

Query  1861  AAGGAACTGGAAGAAATTGTTCAACCAATTATCAGCAAACTCTATGGAAGTGCAGGCCCT  1920
Sbjct  1861  .......A........G...........................G.......  1920

Query  1921  CCCCCAACTGGTGAAGAGGATACAGCAGAAAAAGATGAGTTGTAG  1965
Sbjct  1921  .....................T...................  1965
```

Figure A 2.1: A comparison of the nucleotide sequence of the Homosapiens BiP (https://www.ncbi.nlm.nih.gov/nuccore/NM_005347.5) and the Rattus Norvegicus BiP (https://www.ncbi.nlm.nih.gov/nuccore/NM_013083.2) Query (Homosapiens-Human BiP), Subject (Sbjct :Rattus Norvegicus-Rat BiP) were aligned using BlastP and identities are shown as dots, mismatches are shown in red.

A 3.1 Scientific communications

Publication

Bandla, S., Diaz, S., Nasheuer, H.P., FitzGerald, U., 2019. **ATPase activity of human binding immunoglobulin protein (BiP) variants is enhanced by signal sequence and physiological concentrations of Mn $^{2+}$.** FEBS Open Bio 9, 1355–1369.

Presentation

- British Neuroscience Association conference, Dublin-Poster presentation, '**Microglia and Myelin are susceptible to BiP inducer x (BIX)-induced damage in spinal cord explant culture model'** Sravanthi Bandla, Paula Arseni, Lorna Hayden, Christopher Linington, Una FitzGerald (2019).

- Young Neuroscience Ireland Conference, Dublin-Oral presentation, '**Microglia and Myelin are susceptible to BiP inducer x (BIX)-induced damage in spinal cord explant culture model'**. Sravanthi Bandla, Paula Arseni, Lorna Hayden, Christopher Linington, Una FitzGerald (2018).
- Neuroscience Ireland Conference, Galway, Ireland-Poster presentation, **'Production and Biochemical Characterisation of Wild-type and variant Forms of the ER Chaperone - Binding Immunoglobulin Protein/Glucose-Regulated Protein 78'.** Sravanthi Bandla, Suraya Diaz, Jill McMahon, Heinz Peter Nasheuer and Una Fitzgerald (2017).